

TOWARDS THE MODELLING OF BLAST LOADS ON STRUCTURES

by

Philip Miller

A thesis submitted in conformity with the requirements
for the degree of Master of Applied Science
Graduate Department of Civil Engineering
University of Toronto

© Copyright by Philip Miller (2004)

ABSTRACT

TOWARDS THE MODELLING OF BLAST LOADS ON STRUCTURES.

Master of Applied Science

Philip Miller 2004

Department of Civil Engineering

University of Toronto

This research examines the physics behind blast waves and their interaction with structures. A computer program, *VecTor-Blast*, is developed based on the blast wave characteristics of TNT. Energy methods are used to scale TNT properties to other explosives. *VecTor-Blast* calculates the pressure-time history at specified points on a 3-dimensional cuboid structure.

The performance of the numerical tool was verified with experimental data. Verification showed that *VecTor-Blast* is capable of accurately calculating pressure-time histories on the front and rear faces of the structure. Performance on the sides of the structure was shown to be highly conservative due to an over-simplification of diffractive effects. Complex wave phenomena such as a mach stem formation could not be adequately tested due to limitations in available data.

It has been recommended that future expansion of *VecTor-Blast* include an improvement in the calculations involved in diffraction and that an experimental program be developed to produce more data.

ACKNOWLEDGEMENTS

My greatest appreciation goes to my supervisor, Professor Frank J. Vecchio, for all his support, expert advice, patience, and understanding throughout my graduate studies. The technical recommendations and counsel from Professor Bibhu Mohanty has also been invaluable.

Sincere thanks to Iqbal Mohomed for all his expertise and programming assistance with Visual C++.

The Ontario Graduate Scholarship Program (OGS) is acknowledged for its financial contribution.

The advice and friendship from numerous students, Anas Diab, Kien Vinh Duong, Dan Laine, Dave Ho, Karen Liu, Nabil Mansour, Esneyder Montoya, and Adam Zhou, made this experience truly enjoyable and rewarding.

Last but not least, I want to thank my family and Caroline Wigley for their support and encouragement throughout the duration of my studies.

TABLE OF CONTENTS

ABSTRACT.....	II
ACKNOWLEDGEMENTS.....	III
LIST OF FIGURES.....	VII
LIST OF TABLES	X
NOTATION.....	XI
CHAPTER 1 INTRODUCTION	1
1.1 BACKGROUND	1
1.2 OBJECTIVES	2
1.3 ORGANIZATION.....	2
CHAPTER 2 LITERATURE REVIEW.....	4
2.1 THEORETICAL BACKGROUND.....	4
2.1.1 <i>External Blast Wave Characteristics</i>	4
2.1.1.1 Ideal Blast Waves.....	4
2.1.1.2 Non-Ideal Blast Waves	7
2.1.2 <i>Blast Scaling Laws</i>	8
2.1.3 <i>TNT Equivalence</i>	11
2.1.4 <i>Atmospheric and Ground Affects</i>	12
2.1.5 <i>Types of Blast Loads</i>	13
2.1.5.1 Air Bursts.....	13
2.1.5.1.1 Quantifying Air Bursts	13
2.1.5.1.2 Nuclear Burst.....	14
2.1.5.1.3 Chemical Burst.....	15
2.1.5.2 Surface Bursts	17
2.1.6 <i>Dynamic Pressure</i>	20
2.1.7 <i>Wave Reflection and Reflected Overpressure</i>	20
2.1.8 <i>Structural Loading</i>	25
2.1.8.1 Blast Face	26
2.1.8.2 Roof and Side Faces	30
2.1.8.3 Rear Face	31
2.2 PREVIOUS EXPERIMENTAL WORK	33
2.2.1 <i>Airblast Experimentation</i>	33
2.2.1.1 Air Bursts.....	33
2.2.1.2 Surface Bursts	35
2.2.1.3 Mach and Reflected Waves	37
2.2.2 <i>Blast Experiments on Concrete Structures</i>	38
2.2.2.1 Hoffman and Mills (1956).....	39
2.2.2.2 Feldman, Kennan, and Seiss (1962).....	41
2.2.2.3 Slawson (1984)	44
2.2.2.4 Smith et al. (1999).....	48
2.2.2.5 Dennis, Baylot, and Woodson (2002)	51
2.2.2.6 Rickman and Murrell (2004).....	53
2.2.2.7 Ripley et al. (2004)	55
2.3 ANALYTICAL WORK	58

TABLE OF CONTENTS

2.3.1	<i>Numerical Formulations</i>	58
2.3.2	<i>Computer Codes</i>	59
2.3.2.1	CONWEP	59
2.3.2.2	LS-DYNA.....	60
2.3.2.3	SHAMRC.....	60
2.3.3	<i>Analytical Analysis</i>	60
2.3.3.1	Krauthammer et al. (1994).....	60
2.3.3.2	Dharaneepathy et al. (1995).....	62
2.3.3.3	Krauthammer and Ottani (1997).....	63
2.3.3.4	Armstrong et al. (2002).....	65
CHAPTER 3 THEORETICAL BASIS FOR PROGRAM VECTOR-BLAST		68
3.1	INTRODUCTION	68
3.2	EXPLOSIVES	68
3.3	STRUCTURES	69
3.4	FREE FIELD BLAST PARAMETER DATA.....	70
3.5	THE ORIGIN.....	70
3.6	RAY PATHS	71
3.6.1	<i>Ray Paths on the Blast Face</i>	71
3.6.1.1	Ground Burst or Free Air Bursts	71
3.6.1.2	Air Bursts.....	72
3.6.1.3	Mach Stem.....	79
3.6.1.3.1	Mach Stem Formation	79
3.6.1.3.2	Mach Stem Parameters	80
3.6.1.4	Flow Chart for Blast Face	81
3.6.2	<i>Ray paths on Sides, Roof, and Rear</i>	82
3.6.2.1	Diffraction.....	82
3.6.2.2	Calculating Ray Paths.....	84
3.7	WAVE-STRUCTURE INTERACTION	87
3.7.1	<i>Wave Reflection</i>	87
3.7.1.1	Positive Pressure and Impulse.....	87
3.7.1.2	Negative Pressure and Impulse.....	88
3.7.2	<i>Wave Diffraction</i>	88
3.8	PRESSURE-TIME HISTORIES.....	89
3.8.1	<i>Blast-Face Time Histories</i>	90
3.8.2	<i>Other Faces</i>	91
CHAPTER 4 VERIFICATION.....		93
4.1	HOFFMAN AND MILLS (1956).....	93
4.1.1	<i>Modelling</i>	93
4.1.2	<i>Results and Conclusions</i>	94
4.2	SMITH ET AL. (1999).....	98
4.2.1	<i>Modelling</i>	98
4.2.2	<i>Results and Conclusions</i>	98
4.3	ARMSTRONG ET AL. (2002)	104
4.3.1	<i>Experimental Characterization</i>	104
4.3.2	<i>Results and Conclusions</i>	105
4.3.2.1	Free Field Results	105
4.3.2.2	Results from the Structure.....	107
4.4	TM 5-1300 (1969) EXAMPLE 4A-7	110
4.4.1	<i>Problem Definition</i>	110
4.4.2	<i>Results and Conclusion</i>	110

TABLE OF CONTENTS

4.5	TM 5-1300 (1990) EXAMPLE 2A-10	113
4.5.1	<i>Problem Definition</i>	113
4.5.2	<i>Results and Conclusion</i>	114
4.6	GENERAL CONCLUSIONS	116
CHAPTER 5	DISCUSSION AND RECOMMENDATIONS	118
5.1	APPLICATION TO FINITE ELEMENT ANALYSIS OF CONCRETE STRUCTURES	118
5.1.1	<i>VecTor-Blast and VecTor2</i>	118
5.1.2	<i>VecTor-Blast and the remaining VecTor suite of programs</i>	121
5.2	TRENDS IN THE ANALYTICAL WORK	121
5.2.1	<i>Direct Loading</i>	121
5.2.2	<i>Diffraction Events</i>	121
5.3	LIMITATIONS OF ANALYTICAL WORK	123
5.4	RECOMMENDATIONS FOR FUTURE ANALYTICAL WORK	124
5.4.1	<i>Recommendations for VecTor</i>	124
5.4.2	<i>Recommendations for VecTor-Blast</i>	124
CHAPTER 6	CONCLUSIONS	126
REFERENCES	127
APPENDIX A	VECTOR-BLAST USER'S MANUAL	132
APPENDIX B	EQUATIONS AND CURVES	160
APPENDIX C	VECTOR-BLAST PROGRAM	188
APPENDIX D	SAMPLE PROBLEMS	220
APPENDIX E	SAMPLE INPUTS/OUTPUTS	261

LIST OF FIGURES

FIGURE 2.1 IDEAL BLAST WAVE (AFTER BAKER (1973)).	5
FIGURE 2.2 PRESSURE TIME CURVE PRODUCED BY A CASED CHARGE (AFTER BAKER (1973)).	7
FIGURE 2.3 NON-IDEAL PRESSURE-TIME CURVE (AFTER BAKER (1973)).	8
FIGURE 2.4 HOPKINSON SCALING (AFTER BAKER (1973)).	10
FIGURE 2.5 OVERPRESSURE FROM CHEMICAL AND NUCLEAR WEAPONS (AFTER KINNEY (1985)).	14
FIGURE 2.6 SHOCK WAVE PARAMETERS FOR SPHERICAL TNT EXPLOSION IN FREE AIR AT SEA LEVEL (AFTER TM 5-1300 (1969)).	16
FIGURE 2.7 SHOCK WAVE PARAMETERS FOR HEMISPHERICAL TNT EXPLOSION IN FREE AIR AT SEA LEVEL (AFTER TM 5-1300 (1969)).	19
FIGURE 2.8 INCIDENCE ANGLE VS. REFLECTION ANGLE FOR SHOCKS UNDERGOING REGULAR REFLECTION (AFTER BAKER (1983)).	22
FIGURE 2.9 LIMIT OF MACH STEM FORMATION UNDER IDEAL GAS CONDITIONS (AFTER BAKER (1983)).	22
FIGURE 2.10 VARIATION IN REFLECTION COEFFICIENT WITH INCIDENCE ANGLE (AFTER TM 5-1300 (1990)).	23
FIGURE 2.11 MACH FORMATION AND REGULAR REFLECTION FROM (AFTER BULSON (1997)).	24
FIGURE 2.12 PLANE-WAVE PROPAGATION OVER A RECTANGULAR STRUCTURE (SIDE VIEW) (AFTER BAKER (1973)).	26
FIGURE 2.13 PLANE-WAVE PROPAGATION OVER A RECTANGULAR STRUCTURE (TOP VIEW) (AFTER BAKER (1973)).	26
FIGURE 2.14 IDEALIZED TRIANGULAR FRONT FACE LOADING.	29
FIGURE 2.15 AIR BLAST LOADING ON THE FRONT FACE OF A STRUCTURE.	30
FIGURE 2.16 DIFFRACTION OF A SHOCK WAVE.	31
FIGURE 2.17 SIDE-ON AND NORMALLY REFLECTED PRESSURE VS. SCALED DISTANCE (AFTER BAKER (1973)).	34
FIGURE 2.18 SIDE-ON AND NORMALLY REFLECTED IMPULSE VS. SCALED DISTANCE (AFTER BAKER (1973)).	34
FIGURE 2.19 SCALED ARRIVAL TIME VS. GROUND RANGE (AFTER BAKER (1973)).	36
FIGURE 2.20 SCALED POSITIVE DURATION VS. GROUND RANGE (AFTER BAKER (1973)).	36
FIGURE 2.21 COMPARISONS OF PEAK PARTICLE VELOCITIES FOR SURFACE BURST TNT (AFTER BAKER (1973)).	36
FIGURE 2.22 MEASURED ARRIVAL TIMES FOR SURFACE BURST TNT COMPARED TO PREDICTION (AFTER BAKER (1973)).	37
FIGURE 2.23 OPTIMUM HEIGHT FOR MAXIMUM IMPULSE (AFTER BAKER (1973)).	38
FIGURE 2.24 HOFFMAN AND MILLS EXPERIMENT (AFTER HOFFMAN AND MILLS (1956)).	40
FIGURE 2.25 BEAM SERIES (AFTER FELDMAN ET AL. (1962)).	42
FIGURE 2.26 LOADING APPARATUS (AFTER FELDMAN ET AL. (1962)).	43
FIGURE 2.27 (FY81) DS1-DS5 CONSTRUCTION DETAILS (AFTER SLAWSON (1984)).	44
FIGURE 2.28 (FY82) DS2-1 TO DS2-6 CONSTRUCTION DETAIL (AFTER SLAWSON (1984)).	45
FIGURE 2.29 (FY82) SHEAR REINFORCEMENT FOR DS2-1 TO DS2-6 (AFTER SLAWSON (1984)).	46
FIGURE 2.30 EXPERIMENT SETUP (AFTER SLAWSON (1984)).	47
FIGURE 2.31 EXPERIMENTAL SET-UP (DIMENSIONS IN MM) (AFTER SMITH ET AL. (1999)).	49
FIGURE 2.32 NORMAL PRESSURE VS. SCALED DISTANCE (AFTER SMITH ET AL. (1999)).	50
FIGURE 2.33 NORMAL IMPULSE VS. SCALED DISTANCE (AFTER SMITH ET AL. (1999)).	50
FIGURE 2.34 IMPULSE VS. SCALED DISTANCE FOR VARYING ANGLES INCIDENCE (AFTER SMITH ET AL. (1999)).	51
FIGURE 2.35 EXPERIMENTAL SETUP (AFTER DENNIS ET AL. (2002)).	52
FIGURE 2.39 EXPERIMENTAL SETUP (AFTER RICKMAN AND MURRELL (2004)).	53
FIGURE 2.40 COMPARISON OF A BLAST WAVE FORM (AFTER RICKMAN AND MURRELL (2004)).	54
FIGURE 2.41 EFFECT OF CHARGE-TO-WALL STANDOFF ON PEAK REFLECTED PRESSURE (AFTER RICKMAN AND MURRELL (2004)).	54
FIGURE 2.36 (A) PRESSURE AND CHARGE LOCATIONS (B) BLAST TABLE (AFTER RIPLEY ET AL. (2004)).	56
FIGURE 2.37 (A) DIFFRACTION ANGLE (B) SHOCK FOCUSING (SOLID LINES – EXPERIMENTAL; BROKEN LINES – NUMERICAL) (AFTER RIPLEY ET AL. (2004)).	57

LIST OF FIGURES

FIGURE 2.38 EFFECT OF SCENARIO CONFIGURATION (GAUGE 14) (SOLID LINES – EXPERIMENTAL; BROKEN LINES – NUMERICAL) (AFTER RIPLEY ET AL. (2004)).	57
FIGURE 2.42 COMPARISON OF EXPERIMENTAL WITH NUMERICAL RESULTS (AFTER KRAUTHAMMER ET AL. (1994)).	62
FIGURE 2.43 BLAST CONTAINMENT STRUCTURE (AFTER KRAUTHAMMER AND OTTANI (1997)).	64
FIGURE 2.44 FINE AND COARSE MESH (AFTER KRAUTHAMMER AND OTTANI (1997)).	65
FIGURE 2.45 FREE-FIELD RESULTS COMPARING SHARMC, CONWEP, AND DATA (AFTER ARMSTRONG ET AL. (2002)).	66
FIGURE 2.46 SHARMC RESULTS WITH A STRUCTURE (AFTER ARMSTRONG ET AL. (2002)).	67
FIGURE 3.1 ORIGIN.	71
FIGURE 3.2 SIMPLE RAY PATH CALCULATION.	72
FIGURE 3.3 GROUND REFLECTED RAY PATH CALCULATIONS.	73
FIGURE 3.4 STEADY FLOW COUNTERPART OF OBLIQUE REFLECTION (AFTER KINNEY (1985)).	74
FIGURE 3.5 FLOW CHART OF THE ITERATION PROCEDURE.	77
FIGURE 3.6 GEOMETRY OF MACH STEM FORMATION.	80
FIGURE 3.7 FLOW CHART DEPICTING THE PROCESS FOR DETERMINING THE LOADING ON THE BLAST FACE.	81
FIGURE 3.8 DIFFRACTION AT A CORNER.	82
FIGURE 3.9 DIFFRACTION LOADING ON THE ANALYSIS POINT (AP).	83
FIGURE 3.10 RAY PATH CALCULATIONS.	84
FIGURE 3.11 RAY PATH CALCULATIONS FOR AN AP ON THE REAR FACE.	86
FIGURE 3.12 COMPONENT PRESSURE-TIME HISTORY FOR THE BLAST FACE.	92
FIGURE 4.1 <i>VECTOR-BLAST</i> MODEL OF A CONCRETE SLAB.	94
FIGURE 4.2 OVERPRESSURE COMPARISONS: <i>VECTOR-BLAST</i> AND HOFFMAN AND MILLS.	96
FIGURE 4.3 IMPULSE COMPARISONS: <i>VECTOR-BLAST</i> AND HOFFMAN AND MILLS.	97
FIGURE 4.4 POSITIVE DURATION COMPARISONS: <i>VECTOR-BLAST</i> AND HOFFMAN AND MILLS.	97
FIGURE 4.14 REFLECTED OVERPRESSURE T2-A1.	99
FIGURE 4.15 REFLECTED OVERPRESSURE T3-A2.	99
FIGURE 4.16 REFLECTED OVERPRESSURE T2-A3.	100
FIGURE 4.17 REFLECTED OVERPRESSURE T3-A4.	100
FIGURE 4.18 NORMAL OVERPRESSURE.	101
FIGURE 4.19 REFLECTED SCALED IMPULSE T2-A1.	101
FIGURE 4.20 REFLECTED SCALED IMPULSE T3-A2.	102
FIGURE 4.21 REFLECTED SCALED IMPULSE T2-A3.	102
FIGURE 4.22 REFLECTED SCALED IMPULSE T3-A4.	103
FIGURE 4.23 NORMAL SCALED IMPULSE.	103
FIGURE 4.5 EXPERIMENT SET UP (AFTER (ARMSTRONG, 2002)).	104
FIGURE 4.6 FREE-FIELD SCALE ARRIVAL TIME COMPARISONS.	105
FIGURE 4.7 FREE-FIELD PRESSURE COMPARISONS.	106
FIGURE 4.8 FREE-FIELD IMPULSE COMPARISONS.	106
FIGURE 4.9 PEAK REFLECTED IMPULSE AT CENTER OF FRONT WALL.	107
FIGURE 4.10 PEAK IMPULSE AT CENTER OF SIDE WALL.	108
FIGURE 4.11 PEAK OVERPRESSURE AT CENTER OF SIDE WALL.	108
FIGURE 4.12 PEAK IMPULSE AT CENTER OF REAR WALL.	109
FIGURE 4.13 PEAK OVERPRESSURE AT CENTER OF REAR WALL.	109
FIGURE 4.24 LOADING AND STRUCTURE DIMENSIONS OF EXAMPLE 4A-7 (AFTER (TM 5-1300, 1969)).	110
FIGURE 4.25 PRESSURE-TIME HISTORIES FOR EXAMPLE 4A-7 (AFTER (TM 5-1300, 1969)).	112
FIGURE 4.26 PRESSURE-TIME HISTORIES FOR EXAMPLE 4A-7 FROM <i>VECTOR-BLAST</i> .	112
FIGURE 4.27 PRESSURE-TIME HISTORY COMPARISONS FOR EXAMPLE 4A-7.	113
FIGURE 4.28 LOADING AND STRUCTURE DIMENSIONS OF EXAMPLE 2A-10 (AFTER (TM 5-1300, 1990)).	114
FIGURE 4.29 PRESSURE-TIME HISTORIES FOR EXAMPLE 2A-10 (AFTER (TM 5-1300, 1990)).	115
FIGURE 4.30 PRESSURE-TIME HISTORIES FOR EXAMPLE 2A-10 FROM <i>VECTOR-BLAST</i> .	116
FIGURE 4.31 PRESSURE-TIME HISTORY COMPARISONS FOR EXAMPLE 2A-10.	116

LIST OF FIGURES

FIGURE 5.1 FINITE ELEMENT MODEL OF A BEAM.	119
FIGURE 5.2 BLAST FORCES ON A BEAM.	119
FIGURE 5.3 LATERAL BLAST FORCES ON A BEAM.	120
FIGURE A.1 <i>VECTOR-BLAST</i> INTERFACE.	133
FIGURE A.2 BLAST LOAD PARAMETERS DIALOG BOX.	136
FIGURE A.3 BUILDING DETAILS DIALOG BOX.	138
FIGURE A.4 BLAST LOCATION DIALOG BOX.	139
FIGURE A.5 DIFFRACTION FACTOR DIALOG BOX.	141
FIGURE A.6 GRAPH PRESSURE DIALOG BOX.	142
FIGURE A.7 AXES BUTTONS.	144
FIGURE A.8 GRAPH SCALE DIALOG BOX.	144
FIGURE A.9 EXAMPLE BLAST LOAD PARAMETERS DIALOG BOX.	147
FIGURE A.10 EXAMPLE VIEW WINDOW WITH BLAST LOAD PARAMETERS.	148
FIGURE A.11 EXAMPLE BUILDING DETAILS DIALOG BOX.	149
FIGURE A.12 EXAMPLE VIEW WINDOW WITH THE STRUCTURE.	149
FIGURE A.13 EXAMPLE BLAST LOCATION DIALOG BOX.	150
FIGURE A.14 EXAMPLE VIEW WINDOW WITH THE BLAST LOCATION.	150
FIGURE A.15 EXAMPLE GRAPH PRESSURE DIALOG BOX.	151
FIGURE A.16 EXAMPLE VIEW WITH GRAPH.	152
FIGURE A.17 EXAMPLE GRAPH SCALE DIALOG BOX.	152
FIGURE A.18 EXAMPLE VIEW WITH MODIFIED GRAPH.	153
FIGURE A.19 EXAMPLE DATA FILE.	154
FIGURE C.1 FLOW CHART OF <i>VECTOR-BLAST</i>	189
FIGURE C.2 FLOW CHART OF <i>VECTOR-BLAST</i>	190
FIGURE D.1 STRUCTURE LOADED BY A SURFACE BURST.	220
FIGURE D.2 EXAMPLE 1.1 X-COMPONENT PRESSURE-TIME HISTORY AT POINT A.	226
FIGURE D.3 EXAMPLE 1.1 Y-COMPONENT PRESSURE-TIME HISTORY AT POINT A.	226
FIGURE D.4 EXAMPLE 1.1 Z-COMPONENT PRESSURE-TIME HISTORY AT POINT A.	227
FIGURE D.5 EXAMPLE 1.1 PRESSURE-TIME HISTORY AT POINT B.	230
FIGURE D.6 EXAMPLE 1.1 PRESSURE TIME HISTORY FROM R_S	241
FIGURE D.7 EXAMPLE 1.1 PRESSURE TIME HISTORY FROM R_R	242
FIGURE D.8 EXAMPLE 1.1 PRESSURE TIME HISTORY FROM R_N	242
FIGURE D.9 EXAMPLE 1.1 PRESSURE-TIME HISTORY AT POINT C.	243
FIGURE D.10 STRUCTURE LOADED BY AN AIR BURST.	243
FIGURE D.11 EXAMPLE 1.2 X-COMPONENT PRESSURE-TIME HISTORY AT POINT A (INCIDENT WAVE).	257
FIGURE D.12 EXAMPLE 1.2 Y-COMPONENT PRESSURE-TIME HISTORY AT POINT A (INCIDENT WAVE).	258
FIGURE D.13 EXAMPLE 1.2 X-COMPONENT PRESSURE-TIME HISTORY AT POINT A (REFLECTED WAVE).	258
FIGURE D.14 EXAMPLE 1.2 Y-COMPONENT PRESSURE-TIME HISTORY AT POINT A (REFLECTED WAVE).	259
FIGURE D.15 EXAMPLE 1.2 COMBINED X-COMPONENT PRESSURE-TIME HISTORY AT POINT A.	259
FIGURE D.16 EXAMPLE 1.2 COMBINED Y-COMPONENT PRESSURE-TIME HISTORY AT POINT A.	260

LIST OF TABLES

TABLE 2.1 TNT EQUIVALENCY COMPARISON BY DIFFERENT METHODS (AFTER (MOHANTY, 1998)).....	12
TABLE 2.2 DESCRIPTION OF BLAST WAVE PARAMETERS	17
TABLE 2.3 DRAG COEFFICIENTS (AFTER (KINNEY, 1985)).....	27
TABLE 2.4 DATA FROM HOFFMAN AND MILLS	40
TABLE 2.5 SMALL SCALE URBAN SCENARIOS (AFTER (RIPLEY ET AL., 2004))	55
TABLE 2.6 FAILURE CRITERIA (AFTER (KRAUTHAMMER ET AL., 1994)).....	61
TABLE 2.7 RESULTS OF DISTANCE EFFECT STUDIES ON CYLINDRICAL TOWERS (AFTER (DHARANEEPATHY ET AL, 1995))	63
TABLE 3.1 AVAILABLE EXPLOSIVES.....	69
TABLE 3.2 LIMITATIONS OF SCALED DISTANCE	70
TABLE 3.3 DATA LIMITATIONS FOR MACH STEM FORMATION CURVES	80
TABLE 3.4 DRAG COEFFICIENTS	90
TABLE 4.1 DATA COMPARISON FOR PRESSURE: <i>VECTOR-BLAST</i> AND HOFFMAN AND MILLS	95
TABLE 4.2 DATA COMPARISON FOR IMPULSE: <i>VECTOR-BLAST</i> AND HOFFMAN AND MILLS	95
*DATA COULDN'T BE MEASURED	95
TABLE 4.2 DATA COMPARISON FOR DURATION: <i>VECTOR-BLAST</i> AND HOFFMAN AND MILLS	96
TABLE 4.3 RESULTS FROM 4A-7 (1)	111
TABLE 4.4 RESULTS FROM 4A-7 (2)	111
TABLE 4.5 DIFFERENCE IN SCALED NORMALLY REFLECTED IMPULSE	111
TABLE 4.6 RESULTS FROM 2A-10 (1).....	114
TABLE 4.7 RESULTS FROM 2A-10 (2).....	115
TABLE 4.8 RESULTS FROM 2A-10 (3).....	115

NOTATION

p	absolute pressure
α	angle of deflection
β	angle of incidence
β_1	angle of incidence made with the base of the structure
β_2	angle the reflected shock makes in Region II
Φ	angle through which flow is deflected
P_a	ambient atmospheric pressure
t_a	arrival time of the blast wave
t_c	clearing time
k_j	coefficient relating actual energy released in a blast wave from a nuclear explosion to the total energy released
ρ	density of shocked air mass
D_f	diffraction factor
R	distance from the explosion
D	distance from the nearest edge to the analysis point
C_d	drag coefficient
t_o^-	duration of the negative phase of the blast wave
t_o^+	duration of the positive phase of the blast wave
q	dynamic pressure
ρ_f	fluid density
E	entropy of fluid element
C_E	equivalency factor
λ	explosive yield factor
t_{of}^+	fictitious positive duration
t_{fneg}	fictitious negative duration
G	greater of height or half width
R_g	ground distance from the explosion
H	heat of combustion

NOTATION

H_C	height of charge
H_T	height of triple point
i_s^+	incident (side-on) positive impulse
i_s^-	incident (side-on) negative impulse
e	internal energy
J	jacobian
W	mass of explosive
M_x	mach number of normal component
M_1	mach number of incoming blast wave
M_2	mach number behind the shock front
β_{\max}	maximum possible angle in the deflection angle iteration procedure (either α_{crit} or β_1)
α_{crit}	minimum angle necessary for mach stem formation
i_s^{W-}	negative scaled impulse
i_m^-	normally reflected negative impulse
i_m^{W-}	normally reflected negative scaled impulse
P_m	normally reflected overpressure
i_m^W	normally reflected positive scaled impulse
P_m^-	normally reflected underpressure
P_{mach}	peak incident (side-on) mach overpressure
P_s^+	peak incident (side-on) overpressure
P_s^-	peak incident (side-on) underpressure
P_r^+	peak reflected overpressure
P_r^-	peak reflected underpressure
i_{mach}^W	positive incident (side-on) scaled mach impulse
t_o^W	positive scaled duration of the blast wave
i_s^W	positive scaled incident (side-on) impulse
i_r^W	positive scaled reflected impulse
$P(t)$	pressure at any time t
R_c	ratio of S/G

NOTATION

γ	ratio of specific heat at constant volume and specific heat at constant temperature
P_r^-	reflected negative pressure
t_r	reflected positive duration
i_r^+	reflected positive impulse
$C_{r\beta}$	reflection coefficient
t_{rise}	rise time
S_d	Sach's distance multiplier
S_i	Sach's impulse multiplier
S_p	Sach's overpressure multiplier
S_t	Sach's time multiplier
t_a^w	scaled arrival time
Z	scaled distance
H_C^w	scaled height of charge
H_T^w	scaled height of triple point
U	shock front velocity
ε	shock strength
S	smaller of height or half breadth of the face
C_r	speed of sound in the reflected medium
U_x	speed of the incident shock
P_0	standard sea level atmospheric pressure
N_i	TNT equivalency based on impulse
N_p	TNT equivalency based on pressure
P_r	total reflected wave pressure
u	velocity
a	wave decay constant
b	wave decay constant
c	wave decay constant
u_w	wind velocity
X_{AP}	x-coordinate of the analysis point

NOTATION

X_b	x-coordinate of the blast location
X_s	x dimension of the structure
Y_{AP}	y-coordinate of the analysis point
Y_b	y-coordinate of the blast location
Y_s	y dimension of the structure
Z_{AP}	z-coordinate of the analysis point
Z_b	z-coordinate of the blast location
Z_s	z dimension of the structure

CHAPTER 1 INTRODUCTION

1.1 Background

Research on blast loading and the effects of explosives on structures was not systematically studied until World War I. Very little was published until World War II. As two Japanese cities were devastated by single nuclear bombs, the criteria on which simple shelter structures could be designed underwent major changes (Beshara, 1994).

Since 1945, the number of reported experimental and analytical studies on blast loading has been increasing with major advances in rocketry and nuclear weapons. However, many of the techniques available for analysis of blast events have been developed for use in the military. Much of the information is restricted and research and development in the civil sector has tended to be limited and problem specific (Williams, 1991).

This may slowly be changing as a result of the bombing of the Murrah Building in Oklahoma City (1999). Further interest and research in explosives and their interaction with structures have intensified with recent terrorist activities (e.g. the collapse of the World Trade Centre Towers in New York in 2001). Consequently, blast loads are becoming an important design load for not only military but also for civil structures.

Research on blast waves and their interaction with structures is multidisciplinary encompassing dynamic structural analysis, material behaviour, shock wave physics and ballistics, in addition to the physics and thermochemistry of explosives.

In order to understand a structure's resistance to explosives, its structural response must be evaluated. To predict the realistic response of structures to blast

loads, an accurate prediction of the pressure-time history at various points on the structure is required.

1.2 Objectives

The objectives of this research can be broken down into four major components:

- A thorough review of the issues related to explosions and their interaction with structures.
- The development of a blast load prediction tool in the form of a computer program, *VecTor-Blast*, with graphical user interface capabilities.
- Verification of the tool and determination of its limitations.
- Identifying the areas requiring further research and development.

1.3 Organization

This thesis is organized into six chapters with the subsequent five chapters summarized below:

2. Literature review - includes a review of the theory of shock load physics and blast-structure interaction in addition to relevant analytical and experimental work.
 3. Theoretical basis - outlines the process by *VecTor-Blast* for calculating blast loads on a structure.
 4. Verification - contains the comparisons of experimental data with the results from *VecTor-Blast*.
 5. Discussion and Recommendations - describes how the results from *VecTor-Blast* can be implemented into finite element analysis; an evaluation of the comparisons in Chapter 4, and an examination of the limitations of *VecTor-Blast*.
 6. Conclusions
- References

Appendices - contains a manual for *VecTor-Blast*, equations for all fitted lines, a description of the major subroutines and operations in *VecTor-Blast*, sample calculations, and sample data file outputs from the verifications in Chapter 5.

CHAPTER 2 LITERATURE REVIEW

2.1 Theoretical Background

2.1.1 External Blast Wave Characteristics

2.1.1.1 Ideal Blast Waves

An external blast wave is created when the atmosphere surrounding the explosion is pushed back due to a compressive pulse travelling outward from the center of the explosion (Kinney, 1985). The front of the wave, known as the shock front, has a pressure (overpressure) much greater than the region behind it and thus immediately begins to decay as the shock propagates outward (Beshara, 1994). The pressure may drop to below ambient atmospheric pressure causing suction. An explosion of ideal form has an overpressure phase called the positive phase and an underpressure phase known as the negative phase with an assumed exponential form as shown in Figure 2.1

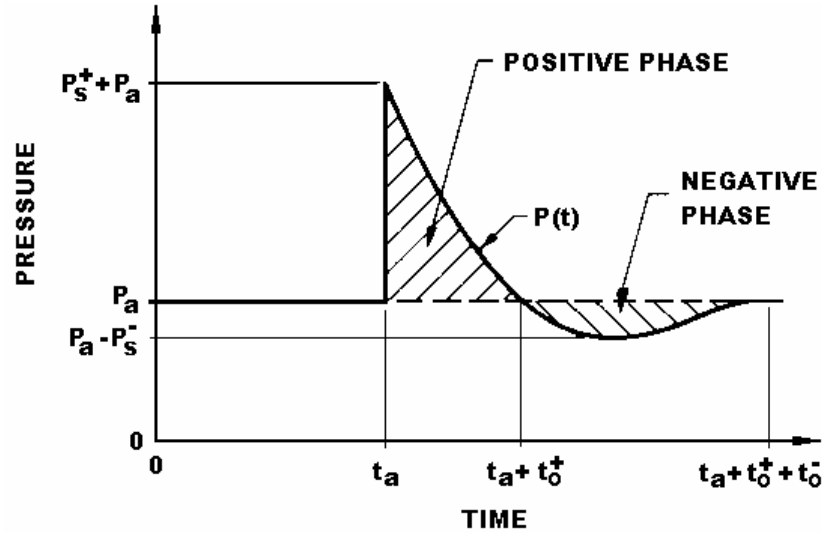


Figure 2.1 Ideal Blast Wave (after Baker (1973)).

with the following parameters:

t_a is the wave arrival time,

t_0^+ is the duration of the positive phase,

t_0^- is the total duration of the negative phase,

P_s^+ is the peak overpressure,

P_a is the ambient atmospheric pressure,

P_s^- is the peak underpressure.

The positive and negative impulses are defined by (Baker, 1973):

$$i_s^+ = \int_{t_a}^{t_a+t_0^+} [P(t) - P_a] dt \quad (2.01)$$

$$i_s^- = \int_{t_a+t_0^+}^{t_a+t_0^++t_0^-} [P_a - P(t)] dt \quad (2.02)$$

Several authors have recommended the use of various functions to represent the pressure-time history $P(t)$ of the ideal blast wave, generally emphasizing only the positive phase. The simplest form assumes a linear decay given by (Baker, 1973):

$$P(t) = P_a + P_s^+ \left(1 - \frac{t}{t_0^+}\right), \quad 0 < t \leq t_0^+ \quad (2.03)$$

Further attempts were made to allow for an exponential decay parameter and more freedom in selecting blast wave characteristics, such as in the modified Frielander equation (Baker, 1973),

$$P(t) = P_a + P_s^+ \left(1 - \frac{t}{t_0^+}\right) e^{-b \frac{t}{t_0^+}} \quad (2.04)$$

where b is the blast wave decay rate. Perhaps the most complex is the five parameter model (Baker, 1973)

$$P(t) = P_a + P_s^+ \left(1 - \frac{t}{t_0^+}\right) \left[a e^{-b \frac{t}{t_0^+}} + (1-a) e^{-c \frac{t}{t_0^+}} \right] \quad (2.05)$$

where the additional constants a, b, and c can be used to provide better matches with experimental data.

The characteristics of the negative phase, with its relatively low amplitude, have often been ignored either because most investigators considered them relatively unimportant compared to the characteristics of the positive phase, or because of the considerable difficulty in measuring or computing the characteristics of the negative phase (Baker, 1973). A function for the negative phase, given by Baker (1973), is:

$$P(t) = P_a - P_s^- \left(\frac{t}{t_0^-}\right) \left(1 - \frac{t}{t_0^-}\right) e^{-4 \frac{t}{t_0^-}} \quad (2.06)$$

where time, t, begins at the start of the negative pressure phase. A complete function representing the entire positive and negative phase is described by Dharaneepathy et al. (1995) by the following:

$$P(t) = P_s^+ \left[1 - \frac{(t - t_a)}{t_0^+} \right] e^{\left[-b \frac{(t - t_a)}{t_0^+} \right]}, \quad t \geq t_a \quad (2.07)$$

2.1.1.2 Non-Ideal Blast Waves

Non-ideal blast waves can differ significantly from ideal blast waves discussed in the previous section. If the blast source is of low specific energy content, the finite pressure pulse may progress some time before “shocking up”. For example, the pressure-time history will exhibit a rise-time to maximum pressure that is of the same order of magnitude as the time for decay back to atmospheric pressure (Baker, 1973).

Blast sources from cased explosives can produce pressure time histories containing many small pressure disturbances superimposed on the primary pressure wave. This can be attributed to ballistic shocks generated by fragments of the casing moving at supersonic speeds. These moving fragments can also produce disturbances prior to the blast wave arrival, as they may initially outrun the blast wave as shown in Figure 2.2.

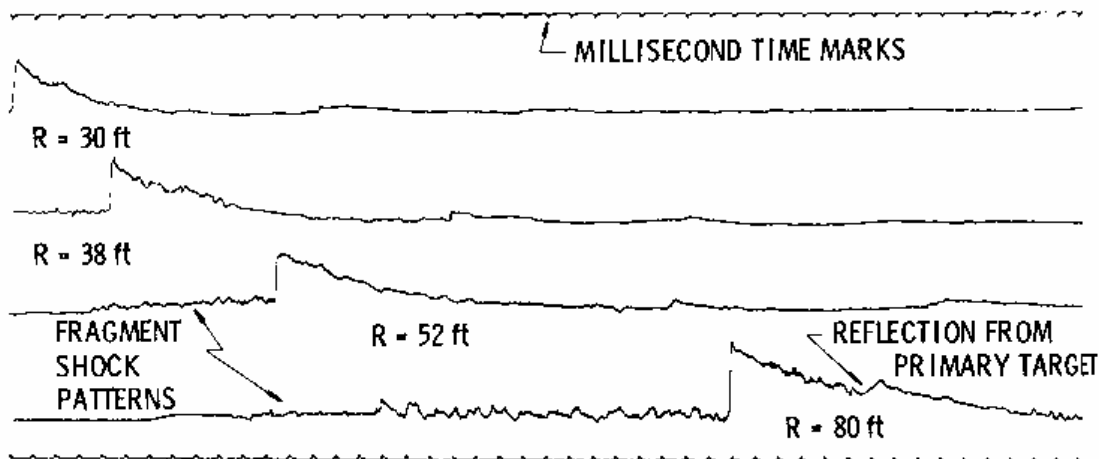


Figure 2.2 Pressure time curve produced by a cased charge (after Baker (1973)).

Thermal effects from nuclear radiation can also preheat air near the ground causing atmospheric inhomogeneity affecting the passage of a blast wave shown in Figure 2.3.

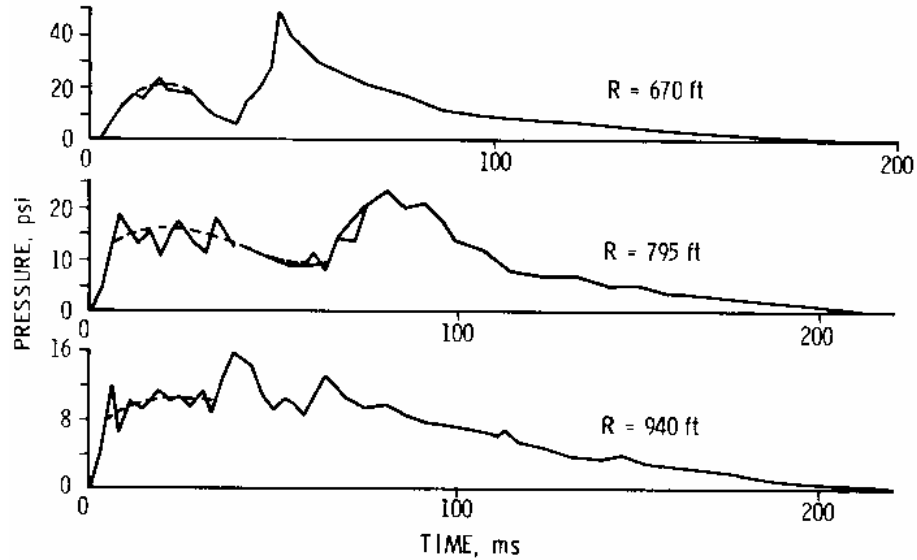


Figure 2.3 Non-ideal pressure-time curve (after Baker (1973)).

Many other deviations from ideal blast wave characteristics exist. However, small differences from ideal conditions will smooth out as the blast wave passes through the air. This results in relatively ideal blast waves as the distance from the source increases (Baker, 1973).

2.1.2 Blast Scaling Laws

The most commonly used blast wave scaling is the cube root scaling law, otherwise known as Hopkinson's Law (Baker, 1973). This law states that any pressure generated at a distance R_1 from a reference explosion with weight W_1 will generate the same pressure at a distance R_2 from the same explosive with weight W_2 provided the charges are of similar geometry and in the same atmosphere.

$$\frac{R_2}{R_1} = \left(\frac{W_2}{W_1} \right)^{\frac{1}{3}} = \lambda \quad (2.08)$$

The parameter λ is referred to as the explosive yield factor. It is customary to use the scaled distance, Z ($\text{m}/\text{kg}^{1/3}$), rather than charge distance when dealing with blast waves:

$$Z = \frac{R}{\sqrt[3]{W}} \quad (2.09)$$

Therefore, similar blast waves are produced at the same scaled distance when:

$$\frac{R_1}{\sqrt[3]{W_1}} = \frac{R_2}{\sqrt[3]{W_2}} = Z \quad (2.10)$$

Similar relationships exist for time (t) and impulse (i),

$$\frac{t_2}{t_1} = \frac{R_2}{R_1} = \left(\frac{W_2}{W_1} \right)^{\frac{1}{3}} \quad (2.11)$$

$$\frac{i_2}{i_1} = \frac{R_2}{R_1} = \left(\frac{W_2}{W_1} \right)^{\frac{1}{3}} \quad (2.12)$$

The exponential decay parameter, b, and the overpressure are not scaled. A similar blast wave with overpressure P, duration λt and impulse λi would be observed at a distance λR from the centre of an explosive charge with dimension λd as a reference explosion with overpressure P, duration t, and dimension d as shown in Figure 2.4.

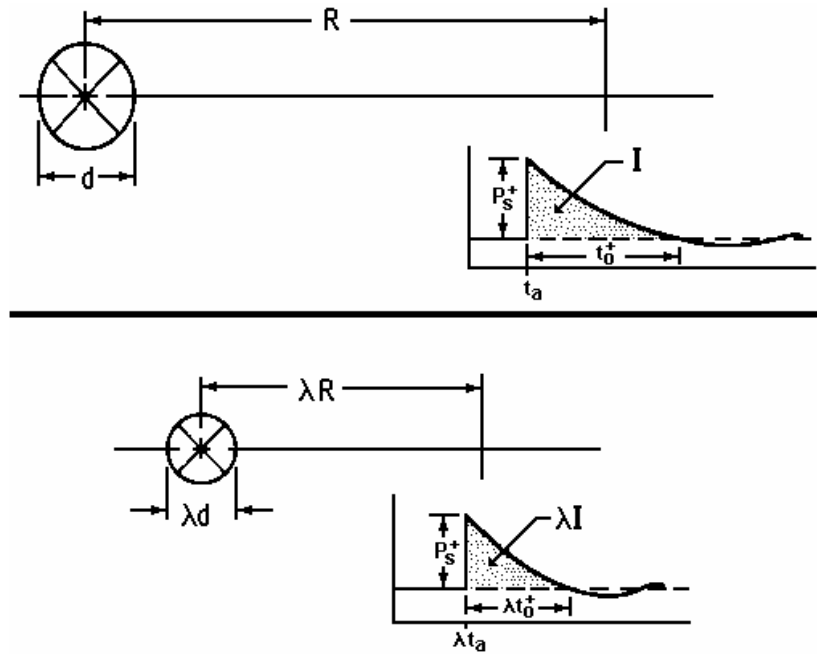


Figure 2.4 Hopkinson scaling (after Baker (1973)).

Another scaling law known as Sach's scaling attempts to correct for changes in atmospheric pressure and temperature. The multipliers for overpressure, distance, time, and impulse (S_p , S_d , S_t , and S_i) are given below (Mohanty, 1998)

$$S_p = \left(\frac{P_a}{P_0} \right) \quad (2.13)$$

$$S_d = \left(\frac{\sqrt[3]{W_2}}{\sqrt[3]{S_p}} \right) \quad (2.14)$$

$$S_t = \left(\frac{\sqrt[3]{W_2}}{\sqrt[3]{S_p}} \right) \times \sqrt{\frac{288}{T_a} + 273} \quad (2.15)$$

$$S_i = \left(\frac{\sqrt[3]{W_2}}{S_p^{2/3}} \right) \times \sqrt{\frac{288}{T_a} + 273} \quad (2.16)$$

where P_a is the ambient pressure, P_0 is the standard sea level atmospheric pressure and T_a is the ambient temperature in °C. Both scaling laws only apply to similar types of explosives with spherical or nearly spherical charges and assume that gravity and

viscosity effects are negligible. Sach's Law includes Hopkinson's Law as a special case when no changes in atmospheric ambient conditions exist between the reference explosion and the actual explosion.

2.1.3 TNT Equivalence

As pointed out in by many researchers (Beshara, 1994; Bulson, 1997; Henrych, 1979), most of the data pertaining to explosions deals with TNT explosives. Thus, it is necessary to be able to relate any explosive with a TNT equivalent. This is achieved through either calculation or experiment. The mass of an explosive can be related to an equivalent TNT amount using its heat of combustion (Henrych, 1979):

$$w_{TNT} = \frac{H_{EXP}}{H_{TNT}} w_{EXP} \quad (\text{Chemical Explosion}) \quad (2.17)$$

$$w_{TNT} = k_j W_j \quad k_j = \frac{0.5}{0.7} \quad (\text{Nuclear Explosion}) \quad (2.18)$$

where w_{TNT} is the equivalent TNT weight, H_{TNT} is the heat of combustion for TNT, H_{EXP} is the heat of combustion for the explosive, w_{EXP} is the weight of the explosive, W_j is the energy equivalent to a nuclear explosion (i.e. a charge of TNT which on explosion releases the same amount of energy as a nuclear explosion), and k_j is a coefficient relating the amount of energy actually released as a blast wave (a nuclear explosion shock wave consumes about 70% of the total energy of the explosion, the remainder is diffused as light and radiation) (Henrych, 1979). The heat of combustion of various explosives can be found in Baker et al. (1983) or in Kinney (1985). The above formulations assume that the detonation reaction is ideal and that all energy calculated is actually released.

The alternative and more accurate approach is to measure the pressure and impulse from an explosive and compare them to standard charts of equivalent TNT weight which would yield the same pressure or impulse at the same distance (Mohanty, 1998). The equivalency can be expressed as

$$N_p = \left(\frac{W_{TNT}}{W} \right) = \left(\frac{Z}{Z_{TNT}} \right)^3 P_s \quad (2.19)$$

$$N_i = \left(\frac{W_{TNT}}{W} \right) = \left(\frac{Z}{Z_{TNT}} \right)^3 i_s \quad (2.20)$$

where W is the weight of the explosive, Z is the scaled distance, and N_p and N_i represent equivalency based on incident pressure and impulse.

The calculation method and the experimental method do not always yield the same TNT equivalency (Mohanty, 1998) as shown in Table 2.1.

Table 2.1 TNT equivalency comparison by different methods (after (Mohanty, 1998))

Explosive	TNT Equivalency		
	Pressure	Impulse	Calculated Energy
TNT	1.0	1.0	1.00
Composition B	1.2	1.3	1.09
Pentolite	1.5	1.0	1.09
PBX-9404	1.7	2.0	1.11

It is difficult to arrive at a TNT equivalency for explosives with non-ideal detonation behaviour (e.g. commercial explosives in small diameters). Such explosives may have long run-up distances before reaching steady detonation. Dust or vapour cloud explosions for example can have much higher calculated energies than actually occur because of an assumed optimum dispersion of fuel and oxidizer elements within the cloud (Mohanty, 1998).

2.1.4 Atmospheric and Ground Affects

Variations in ambient atmospheric pressure and temperature will modify blast waves. Some of the changes to blast waves can be accounted for if Sach's scaling is used. Variations in humidity, heavy fog, or rain have been found to have negligible effects on the properties of blast waves (Baker et al., 1983; Kinney, 1985).

However, significant atmospheric effects such as low level temperature inversions or severe wind shear can induce non-ideal behaviour. These can cause, for example, a hemispherical blast front to refract and focus on the ground in an annular

direction as in the first case, or cause focusing of the blast wave in the downwind direction as in the second (Baker et al., 1983).

Irregular ground surfaces can also affect blast wave properties. Gentle up-slopes can cause enhancement while a steep upward slopes will cause Mach waves to form indirectly causing enhancement. Downward slopes cause expansion and weakening of the shock. The effects are usually localized only (Baker et al., 1983).

2.1.5 Types of Blast Loads

An external blast wave can be categorized as an air blast or an underground blast depending on whether the point of detonation of the explosive is above or below the ground surface (Dharaneepathy et al., 1995). Air blasts can be further subdivided into air bursts or surface bursts, depending on the height above ground of the detonation. Free-air bursts are a special case of air bursts where the detonation occurs directly above the structure such that no interference takes place with the blast wave before reaching the structure (TM 5-1300, 1990).

2.1.5.1 Air Bursts

2.1.5.1.1 Quantifying Air Bursts

Explosions can generally be classified as physical, chemical, or nuclear. Physical explosions often come about from sudden pressure or temperature changes without any chemical reaction happening such as in the eruption of a volcano. Physical explosions will not be discussed in this paper. Chemical explosions involve the rapid oxidation of fuel elements. Nuclear explosions, on the other hand, arise from the formation of different atomic nuclei by the redistribution of protons and neutrons within the interacting nuclei. Due to the forces existing between the components of the nucleus being orders of magnitude higher than those existing between atoms, the energy released by a nuclear explosion will be much higher than that released from the same mass in a chemical explosion (Kinney, 1985; Smith and Hetherington, 1994). This phenomenon is depicted in Figure 2.5.

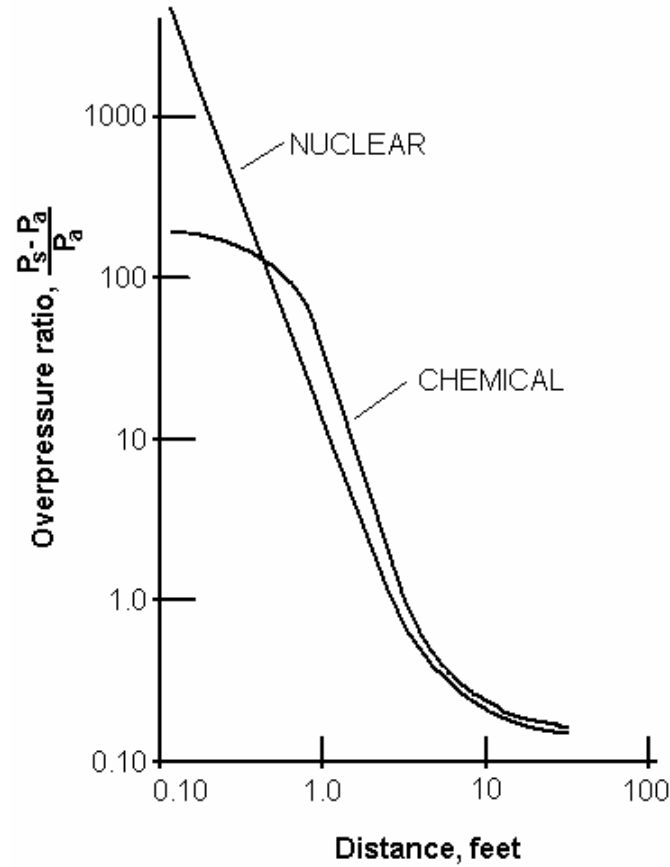


Figure 2.5 Overpressure from chemical and nuclear weapons (after Kinney (1985)).

Thus, formulations for chemical and nuclear explosions will be considered separately.

2.1.5.1.2 Nuclear Burst

Newmark and Haltiwanger (1962) and Newmark (1963) provided many analytical approximations to nuclear burst overpressures as a function of time and distance. Detailed explanations of nuclear airbursts are available in Baker (1973). The following provides an approximation for the variation of peak overpressure, P_s^+ , with distance and explosion yield for a surface nuclear burst (Beshara, 1994)

$$P_s^+ = 15 \left[\frac{1000}{10^{15}} \right] \left[\frac{1000}{R} \right]^3 + 11 \left[\frac{W}{10^{15}} \right]^{\frac{1}{2}} \left[\frac{1000}{R} \right]^{\frac{3}{2}} \quad (N/cm^2) \quad (2.21)$$

where W is the weapon yield in joules (weapon yield is often presented in units of one megatonne; $1\text{Mt}=4.184\times 10^{15}$ J) and R is the range from the explosion to the point of interest in metres. The overpressure can be scaled to other yields, W , by multiplying R by the yield factor, λ . Surface bursts are assumed to be twice as effective as air bursts for blast effects and thus, one half of the actual burst yield, W , can be used to calculate the peak overpressure of a nuclear airburst (Beshara, 1994).

2.1.5.1.3 Chemical Burst

Many formulations for peak overpressure from conventional (chemical) explosives exist (Beshara, 1994; Bulson, 1997; Dharaneepathy, 1993; Henrych, 1979; Kinney, 1985; Newmark, 1963; Newmark and Haltiwanger, 1962; Smith and Hetherington, 1994) which vary slightly based on specific explosive types and researcher. A formulation (Beshara, 1994) for a conventional chemical air burst is given below:

$$\frac{P_s^+}{P_0} = \frac{808 \left[1 + \left(\frac{Z}{4.5} \right)^2 \right]}{\left\{ \left[1 + \left(\frac{Z}{0.048} \right)^2 \right] \left[1 + \left(\frac{Z}{0.32} \right)^2 \right] \left[1 + \left(\frac{Z}{1.35} \right)^2 \right] \right\}^{\frac{1}{2}}} \quad (2.22)$$

where Z is scaled distance ($\text{m}/\text{kg}^{1/3}$).

Peak overpressure curves (as well as other blast wave parameter curves) as a function of scaled distance exist in the TM 5-1300 document of the Dept. of the Army (1969,1990) and can also be used to determine peak overpressure (see Figure 2.6). The curves result from experimental data pertaining to TNT explosions and can be related to other explosions using TNT equivalency methods outlined previously.

The parameters in Figure 2.6 are described Table 2.2.

Table 2.2 Description of Blast Wave Parameters

P_{so}	Peak Positive Incident Pressure, psi	$t_o/w^{1/3}$	Scaled Duration of Positive Phase, ms/lb ^{1/3}
P_{so}^-	Peak Negative Pressure, psi	$t_o^-/w^{1/3}$	Scaled Duration of Negative Phase, ms/lb ^{1/3}
P_r	Peak Positive Normal Reflected Pressure, psi	$L_w/w^{1/3}$	Scaled Wave Length of Positive Phase, ft/lb ^{1/3}
P_r^-	Peak Negative Normal Reflected Pressure, psi	$L_w^-/w^{1/3}$	Scaled Wave Length of Negative Phase, ft/lb ^{1/3}
$i_s/w^{1/3}$	Scaled Unit Positive Incident Impulse, psi-ms/lb ^{1/3}	U	Shock Front Velocity, ft/ms
$i_s^-/w^{1/3}$	Scaled Unit Negative Incident Impulse, psi-ms/lb ^{1/3}	u	Particle Velocity, ft/ms
$i_r/w^{1/3}$	Scaled Unit Positive Reflected Impulse, psi-ms/lb ^{1/3}	W	Charge Weight, lb
$i_r^-/w^{1/3}$	Scaled Unit Negative Reflected Impulse, psi-ms/lb ^{1/3}	R	Radial Distance from Charge, ft
$t_A/w^{1/3}$	Scaled Time of Arrival of Blast Wave, ms/lb ^{1/3}	Z	Scaled Distance, ft/lb ^{1/3}

2.1.5.2 Surface Bursts

When an explosive charge detonates on or very near the ground, the shock wave in perfect conditions has a hemispherical wave front unlike the spherical wave front produced in an air burst (Bulson, 1997; Smith and Hetherington, 1994). Thus the energy released is concentrated over a smaller area and modifications must be made to airburst equations in order to quantify overpressures from surface bursts. Newmark (1963) suggests using the following for peak overpressure resulting from a chemical explosion at the ground surface

$$P_s = 6784 \frac{W}{R^3} + 93 \left(\frac{W}{R} \right)^{\frac{1}{2}} \quad (bars) \quad (2.23)$$

where P_s is the peak incident overpressure, W is the weight of equivalent TNT (in metric tons) and R is distance from the centre of detonation on the ground to the point of interest (m).

However, an alternative has been suggested (Beshara, 1994; Bulson, 1997; Smith and Hetherington, 1994). Instead of developing new functions, airburst relationships will still be valid if twice the charge weight ($2W$) is substituted for W in the equations provided the earth is perfectly unyielding. Since the earth is capable of absorbing part of the released energy through the production of craters, the factor of 2 should be reduced to between 1.7-1.8 to correlate better with experimental results (Bulson, 1997; Smith and Hetherington, 1994).

It has also been suggested that the “ $2W$ ” method is only valid for pressure ranges under about 70 kPa (TM 5-1300 1969). To obtain incident pressures for all scaled distances, blast wave parameter curves have been created for surface bursts shown in Figure 2.7. The parameters in Figure 2.7 are described Table 2.2.

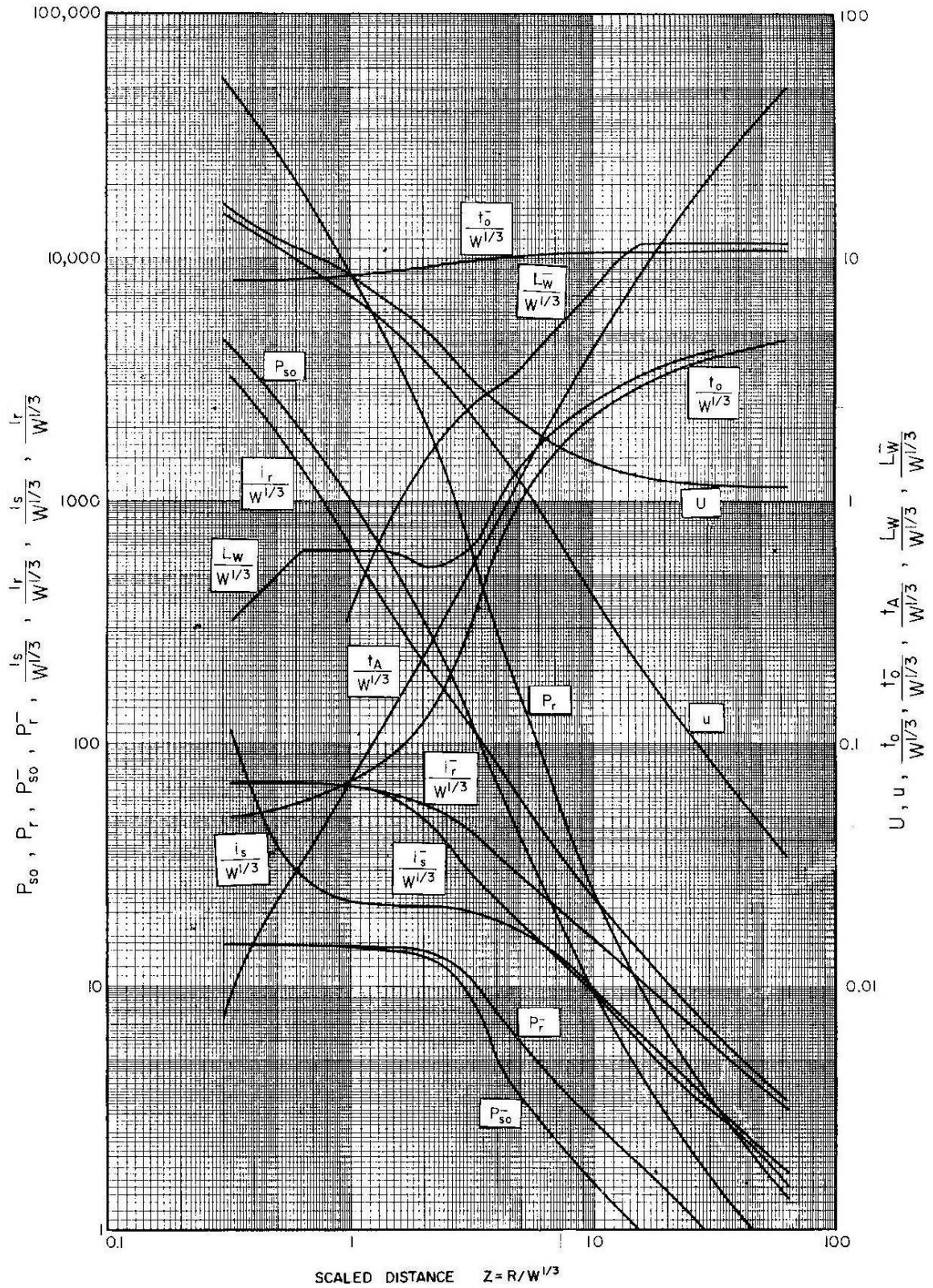


Figure 2.7 Shock wave parameters for hemispherical TNT explosion in free air at sea level (after TM 5-1300 (1969)).

2.1.6 Dynamic Pressure

The high velocity wind associated with a blast wave results in another pressure known as the dynamic pressure (Mohanty, 1998). The dynamic pressure, q , is proportional to the square of the wind velocity, u_w , and density of the shocked air mass, ρ , as follows

$$q = \frac{1}{2}(\rho u_w^2) \quad (2.24)$$

or in terms of incident pressure P_s , ambient pressure P_o , and specific heat ratio γ .

$$q = \frac{P_s^2}{[2\gamma P_o + (\gamma - 1)P_s]} \quad (2.25)$$

The relevance of the dynamic pressure in calculation of blast loads is shown in the following section.

2.1.7 Wave Reflection and Reflected Overpressure

As the blast wave travels outward, it is reflected when it hits an object denser than the atmosphere such as the ground surface or a structure. The reflected wave travels back through the atmosphere at a higher velocity and pressure. This occurs because the reflected wave travels back through air which has been pressurized and heated. Three reflection phenomena exist: (1) normal reflection occurring when the wave hits a surface at 90° , (2) oblique reflection (or regular reflection) where the wave impinges on some angle between the plane of the wave front and the plane of the reflecting surface, (3) Mach stem formation, a special case of condition 2 where the wave front impinges on a surface at near grazing incidence (Kinney, 1985).

Any point above the ground surface receives two shocks from an airburst: one from the incident wave and one from the reflected wave (Mohanty, 1998). Both incident and reflected waves have different arrival times due to varying wave velocities. As the waves hit the structure, they are reflected again and it is these final reflected pressures which load the structure.

The literature contains much data on normally reflected blast waves from high explosive sources, usually bare spheres of Pentolite and TNT (Baker et al, 1983). From these sources, it is possible to construct scaled curves for reflected pressure and reflected impulse over large scaled distances many of which are presented in TM 5-1300 (1969, 1990). For explosive sources other than bare spheres of solid high explosives, little data for normally reflected overpressure and specific impulses exist (Baker, 1983).

For shock waves weak enough to behave like an ideal gas ($\gamma = 1.4$), the normal reflected pressure, P_m , is given by Baker (1983):

$$P_m = 2P_s + (\gamma + 1)q \quad (2.26)$$

The normally reflected pressure will vary from 2 times the incident pressure (the acoustic limit) at low incident pressure ($P_s \rightarrow 0$) to 8 times the incident pressure for strong shocks. In reality, the reflected pressure can be much higher as air behaves less and less in an ideal manner at elevated incident pressures.

The maximum ratio, P_r/P_s , for normal reflection of shocks in sea level air assuming air dissociation and ionisation for a spherical charge has also been calculated. The maximum P_r/P_s ratio is calculated to be 13.92 (Baker, 1983).

In the case of oblique reflection, calculating the deflection angle and the reflected pressure can be quite complicated if non-ideal gas behaviour is taken into account. A review of theory and experiment on regular reflection and the limit of regular reflection is presented in Harlow and Amsden (1970). Two of their curves are shown in Figure 2.8 and Figure 2.9 depicting the angle of incidence versus angle of reflection for varying shock strengths as well as the limit of oblique reflection for varying shock strengths assuming ideal gas behaviour.

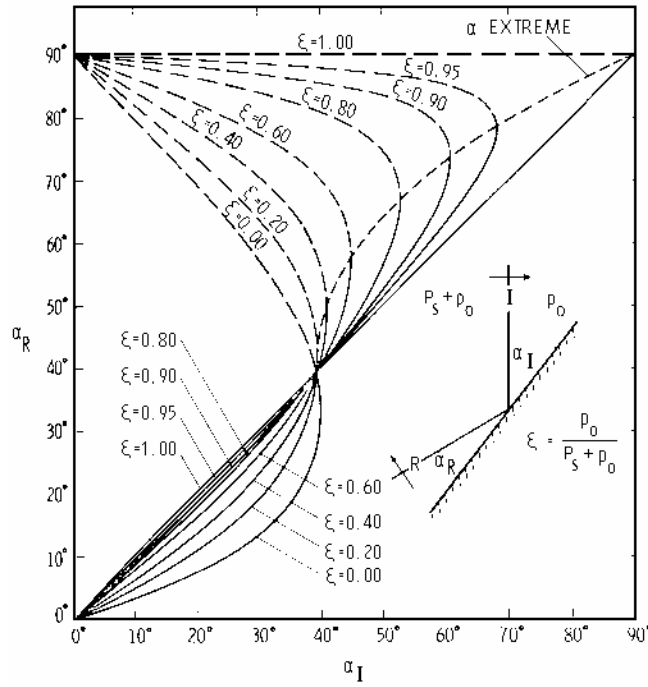


Figure 2.8 Incidence angle vs. reflection angle for shocks undergoing regular reflection (after Baker (1983)).

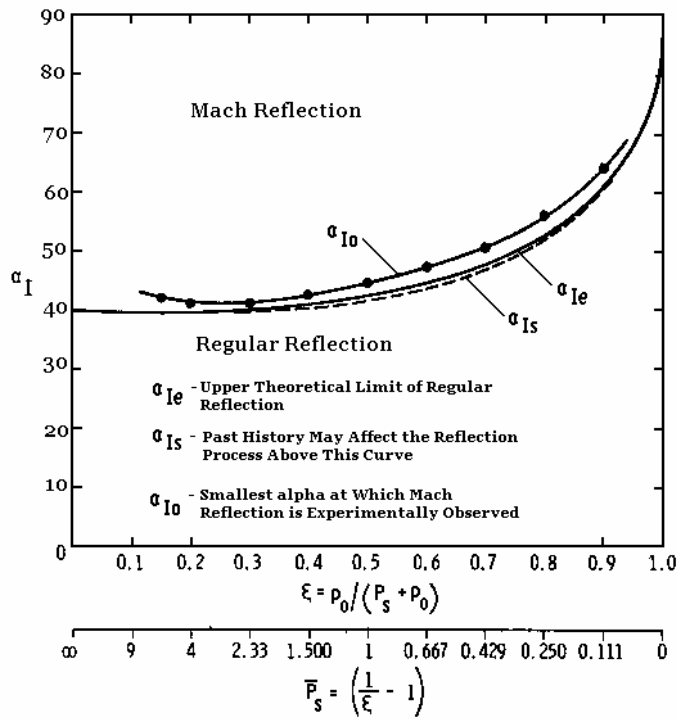


Figure 2.9 Limit of Mach stem formation under ideal gas conditions (after Baker (1983)).

Research summarized in Baker (1983) and Dharaneepathy et al. (1995) describes the calculation of reflected peak pressure for oblique shocks. Curves give reflected pressure as a function of incident pressure and angle of incidence for incident shock strengths up to 34.5 MPa (5000 psi). Similar curves are presented in the TM 5-1300 document of the Dept. of the Army (1969, 1990) shown in Figure 2.10. For angles greater than 90°, the reflection coefficient, $C_{r\beta}$, is determined as (Dharaneepathy et al., 1995):

$$C_{r\beta} = 1.5 - \frac{\beta}{180} \quad (2.27)$$

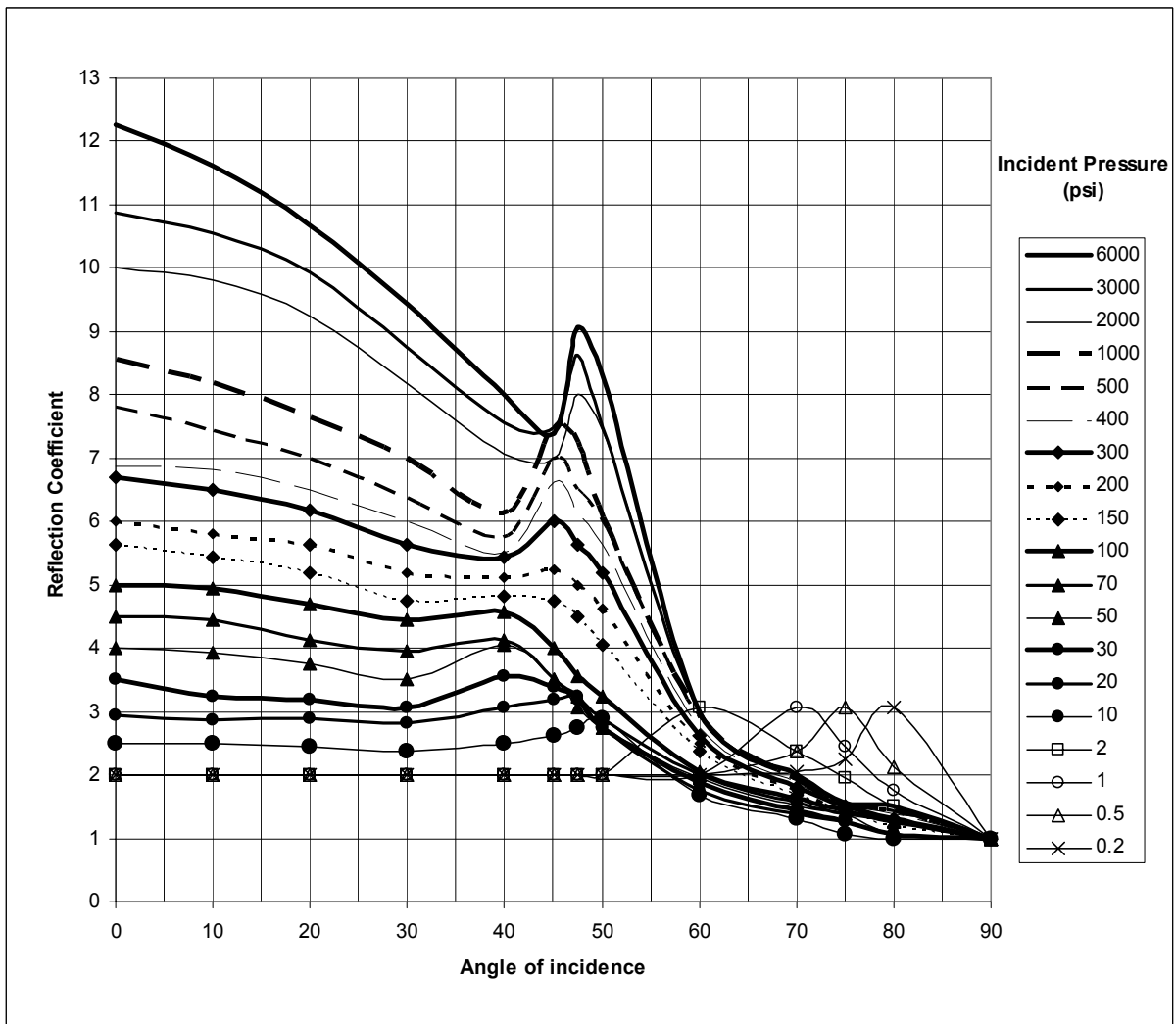


Figure 2.10 Variation in reflection coefficient with incidence angle (after TM 5-1300 (1990)).

A further complication that can arise is the formation of a Mach stem. This occurs when the interaction of the reflected wave and the incident wave produces an enhanced shock front known as the Mach front or Mach stem (Beshara, 1994; Bulson, 1997; Dharaneepathy et al., 1995; Kinney, 1985; Henrych, 1979) and the point of intersection of incident, reflected, and Mach waves is known as the triple point as shown in Figure 2.11.

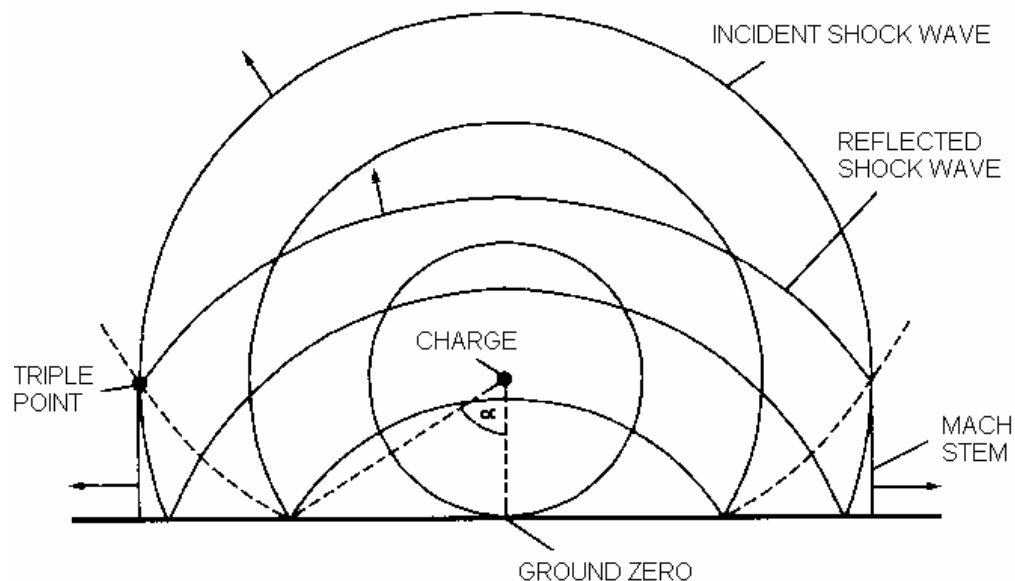


Figure 2.11 Mach formation and regular reflection from (after Bulson (1997)).

Although some variation in pressure over the height of the Mach front occurs, it can be considered as a plane wave over the full height of the front. The presence of a limiting ground zero distance (horizontal distance from the point directly below explosion to the structure) for a Mach stem to form has been shown to exist (TM 5-1300, 1969, 1990; Dharaneepathy et al., 1995; Kinney, 1985). A Mach front can only form provided the angle of incidence with the ground is between approximately 40° and 50° (Beshara, 1994; Bulson, 1997; Dharaneepathy et al., 1995; Henrych, 1979; Kinney, 1985) for most shock strengths.

Theoretical formulations for wave reflection off plane surfaces (for regular and Mach reflection) based on fluid dynamics can be found in Kinney (1985). It is possible

to calculate the angles of reflection, reflected wave pressure, dynamic pressure, as well as other wave parameters which are given in the form of experimentally derived curves as a function of scaled distance in TM 5-1300 (1969, 1990). The calculations however depend on a constant ratio of specific heats as well as air behaving as an ideal gas. For low pressure ranges and temperatures, this assumption is valid; however, with increasing pressure and temperature, this assumption becomes more and more erroneous.

2.1.8 Structural Loading

The dynamic load generated by a blast wave is characterized by a rapidly reached peak pressure followed by decay towards a peak negative pressure followed again by subsequent decay towards ambient conditions. However, only in very rare cases do these properties represent the true loads applied to the structure. The actual net load on the structure is a function of the magnitude of the explosion, the location of the explosion relative to the structure, as well as the structural geometry and orientation (Baker, 1983; TM 5-1300, 1990; Kinney, 1985). In view of many uncertainties involved in evaluating blast loads and their interaction with structures, it is recommended that the pressure-time profiles be approximated by equivalent triangular pulses (Baker, 1983; TM 5-1300, 1969, 1990; Newmark, 1963; Newmark and Halthiwanger, 1962).

It is assumed that the shock loads can be decoupled from the structural response and that the structure remains relatively rigid throughout the loading period. The large density differences between air and most solids, and the great mismatches in acoustic impedance render these assumptions acceptable for most air blast loading problems (Baker, 1983).

It will be further assumed that the structure contains few openings. The presence of many windows or the collapse of vital structural members can lead to lower exterior pressures as rapid pressure equalization occurs between pressure inside and outside the structure changing the pressure-time history (Mohanty, 1998).

The propagation of a plane wave over a structure can be seen in Figure 2.12 and Figure 2.13.

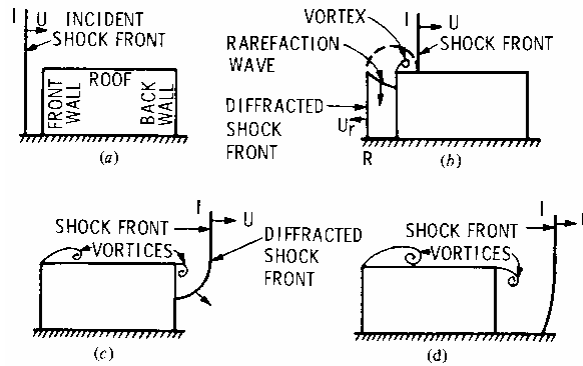


Figure 2.12 Plane-wave propagation over a rectangular structure (side view) (after Baker (1973)).

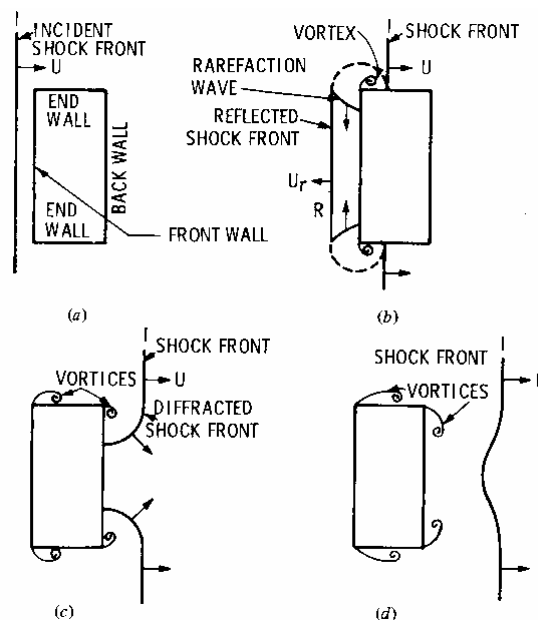


Figure 2.13 Plane-wave propagation over a rectangular structure (top view) (after Baker (1973)).

2.1.8.1 Blast Face

The blast face (or faces) is described as the area or face on a structure which is directly loaded by the incoming blast wave either from an incident wave or from a wave hitting the structure after undergoing reflection off the ground surface.

A point on the blast face loaded by the incoming blast wave will experience a sudden rise in pressure to the reflected overpressure followed by decay. The time required to relieve the reflected pressure, known as the clearing time can be calculated as follows (Kinney, 1985):

$$t_c = \left(\frac{2S + D}{U_x} \right) \leq t_o^+ \quad (2.28)$$

where t_c is the clearing time, S is the height or the half breadth of the face, whichever is smaller, D is the distance from the point in question to the structure's edge, U_x is the speed of the incident shock, and t_o^+ is the positive duration of the blast wave. This formulation is valid under plane wave conditions and for rectangular faces.

The pressure relief (i.e. the rarefaction wave (see Fig. 2.12 and 2.13)) is provided by the flow of air around the edges of the face. In reality, the rarefaction wave is moving with the speed of sound in the reflected medium. The speed also varies with time as the blast wave decays. In view of the uncertainties in the interaction of the blast wave with the structure, it not necessary to establish the wave speed with a high degree of precision. Hence for many practical purposes, the speed of sound of the original shock front, U_x , may be taken as representing the speed of sound in the medium over the blast face.












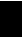


A formulation (TM 5-1300, 1990) to include effects of the rarefaction wave moving with the speed of sound in the reflected medium is expressed as:

$$t_c = \frac{4S}{(1 + R_c)C_r} \leq t_o^+ \quad (2.29)$$

where R_c is ratio of S/G where G is the greater of the height or half width and C_r is the sound velocity in the reflected medium. Equation 2.29 is valid for incident pressures up to 517 kPa (75 psi) and under plane wave conditions.

If the duration of the positive phase exceeds the clearing time, the point on the blast face will experience an additional load due to the dynamic pressure known as drag loading. Drag loading is a combination of the overpressure and a drag coefficient, C_d , times dynamic pressure. The drag coefficient is a function of the shock intensity and the shape of the blast face. Estimates for drag coefficients are given in Baker (1983), Kinney (1985), and TM 5-1300 (1990). Typical values are shown in Table 2.3.

Table 2.3 Drag Coefficients (after (Kinney, 1985))

Flow Directions from Left to Right. For High Reynolds Numbers			
Bodies of Revolutions		C_d	
Sphere		0.10	
Half sphere		0.42	
Half sphere		1.42	
Circular Plate		1.17	
Structural Shapes (long members, without end effects)			
	C_d		C_d
	2.0		1.45
	2.0		1.8
	1.65		1.55
	2.05		2.0
	2.0		1.55

Once the blast wave decays to zero in the positive phase, the point on the structure will experience increasing suction, during a period known as the negative rise time, t_{rise} , towards a peak suction or negative pressure, P_r^- . This pressure will then again decay towards ambient conditions. The peak suction is assumed to occur at 27% of the negative duration and is defined as (TM 5-1300, 1990):

$$t_{rise} = 0.27t_0^- \quad (2.30)$$

where t_0^- is the negative duration. The effects of dynamic pressure in the negative phase region can usually be neglected.

Triangular equivalent loads are defined such that the impulse and peak pressure from the exponentially decaying blast wave are maintained but the duration is adjusted to create a triangular load. The fictitious positive duration, t_{of} , and the fictitious reflected positive duration, t_r , are defined as (TM 5-1300, 1990):

$$t_{of} = \frac{2i_s^+}{P_s^+} \quad (2.31)$$

$$t_r = \frac{2i_r^+}{P_r^+} \quad (2.32)$$

where i_r is the reflected positive impulse and P_r^+ is the peak reflected overpressure.

The triangular pressure-time curve must be checked to determine its accuracy. The actual pressure-time curve used to load the structure is the one with the smallest impulse (area under the curve) due to reflected pressure or cleared reflected pressure plus incident pressure. This check must be performed because the procedure outlined, where the dynamic pressure is used, is only valid at lower pressure ranges. At higher pressure ranges, the above procedure may yield fictitious results because of the extremely short pressure pulse durations involved (TM 5-1300, 1969). The P_r - t_r impulse curve corresponds to an infinite surface. At high pressure ranges, the positive duration is extremely short and clearing will not have time to occur causing infinite surface behaviour. In the lower pressure ranges, clearing has time to occur. The check is necessary to determine which behaviour governs. An idealized triangular loading is shown in Figure 2.14.

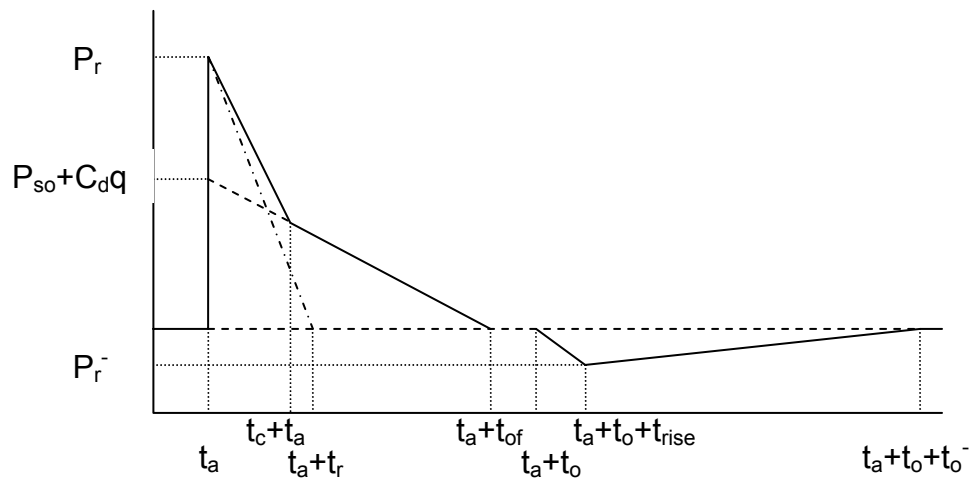


Figure 2.14 Idealized Triangular Front Face Loading.

Since the fictitious duration of the positive phase will be smaller in magnitude than the actual duration, a time gap will occur between the fictitious duration and the onset of the negative phase. This time gap should be maintained in an analysis for consistency of the onset of various load phasings (TM 5-1300, 1990).

For a point loaded by a Mach wave, the procedure for calculating the pressure-time history is the same as aforementioned however adjustments must be made to the peak incident and reflected pressure in addition to the peak incident and reflected

impulse to account for the enhancements created by a Mach wave. Those procedures are outlined in the TM 5-1300 document of the Dept. of the Army (1990).

A point above the triple point will be loaded by two waves, the incident wave and the ground reflected wave as shown in Figure 2.15. Two pressure histories can be created for each wave and then superimposed to obtain the combined effect of the loading from both waves.

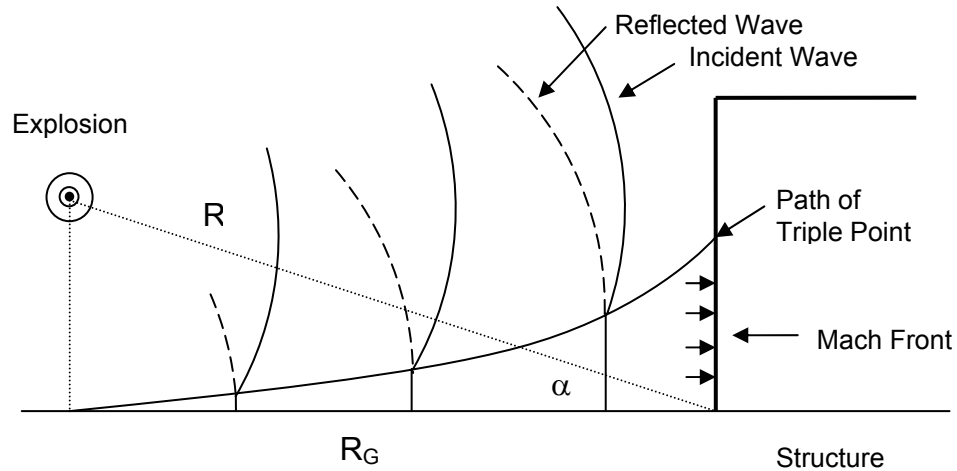


Figure 2.15 Air blast loading on the front face of a structure.

2.1.8.2 Roof and Side Faces

The loading experienced by a point on the top or side of a structure is a function of the incident overpressure, the drag pressure, and the effects of diffraction. The time at which the load is first felt is a function of the distance that the point is away from the detonation point. Points near the edge of the structure close to the blast face will also be influenced by the flow of air causing pressure relief off the front face and that which gives a pressure build-up in the rear. Thus a vortex forms near the front edges and gives local pressures somewhat less than had the vortex effects been neglected. However for many purposes, this complicating effect can be ignored (Kinney, 1985).

As the shock wave hits an edge it will diffract around the structure as shown in Figure 2.16 causing the loading on the roof or sides of the structure.

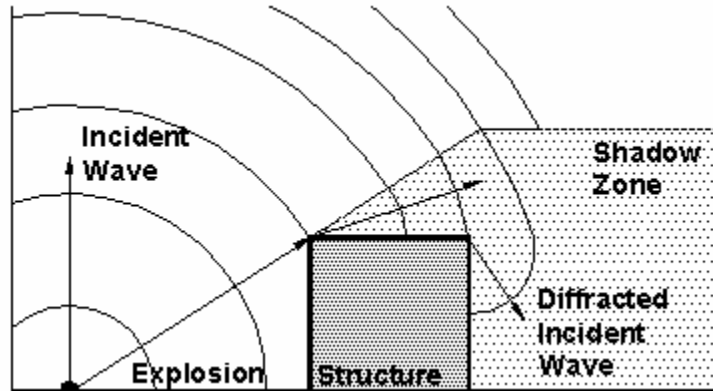


Figure 2.16 Diffraction of a shock wave.

Diffraction reduces both the side-on over and underpressure on the structure in the “shadow zone” as the wave diffracts in all directions but only a portion continues to load the structure. The overpressure is continuously reduced with each edge the wave encounters. The reduction in overpressure also has the effect of increasing the duration.

A formulation to calculate roof and side pressure-time histories proposed in TM 5-1300 (1990) suggests using an equivalency factor, C_E , based on wavelength to reduce the free-field side-on overpressure to obtain the correct side-on overpressure for the roof or side. The C_E factor takes into account the positive and negative pressure reduction due to diffraction and also averages the pressure over an entire span length. Positive and negative durations for the roof or sides are also found as a function of wavelength. Since the pressures are found to be averages over the entire span length, a rise time to maximum pressure exists and is also found as a function of wavelength. This formulation is only valid for plane waves and assumes that the reinforcement is continuous across the span length on both faces of the roof or side wall.

2.1.8.3 Rear Face

As a shock front passes over the rear edges of the roof and side walls, the shock front will undergo diffraction forming secondary waves which combine on the rear wall. In addition, the waves will be reinforced by their reflection off the ground

surface at the base of the wall. Little information is available on the overall effects on the rear wall loading by the reflections of secondary waves (TM 5-1300, 1990).

Like roof and sidewalls, the blast loading acting on the rear of the structure is a function of the incident pressure reduced by the drag and dynamic pressure. The same formulation proposed for calculating pressure-time histories in TM 5-1300 (1990) for the roof and sides of a structure is used to calculate the loads on the rear wall.

2.2 Previous Experimental Work

Research in the area of blast loading has generally been performed in two broad areas: (1) research studying the behaviour of blast waves and their parameters through airblast experimentation (2) simulating blast loads on structures to determine the response of individual members, the overall structural response, and the dynamic properties of the structural materials.

Very few experiments seem to exist where both areas were studied at the same time. While much work in the area of blast analysis has been done, a majority of this information is still restricted due to its military significance (Olatidoye et al., 1998).

2.2.1 Airblast Experimentation

2.2.1.1 Air Bursts

Many experiments have been conducted to measure free air (or free field) blast parameters some of which will be discussed in further detail. Few large-scale free air experiments exist due to the practical limits of the height above ground at which these experiments must be conducted to avoid ground reflection effects (Baker, 1973).

The earliest experiments date to World War II. Since World War II, the majority of free field experiments by various investigators in the United States were conducted at the U.S. Army Ballistic Research Laboratories (BRL) and the U.S. Naval Ordnance Laboratory (NOL). Two main reports will be cited which compile and condense free-field blast data.

A report summarized in Baker (1973) compiles measurements from 1945 to 1960 of peak overpressure, positive impulse, positive duration, and reflected overpressure from bare spherical Pentolite explosions. Empirical fits to the data are given as well as the spread in each data set. Some of curves are reproduced here in Figure 2.17 and Figure 2.18.

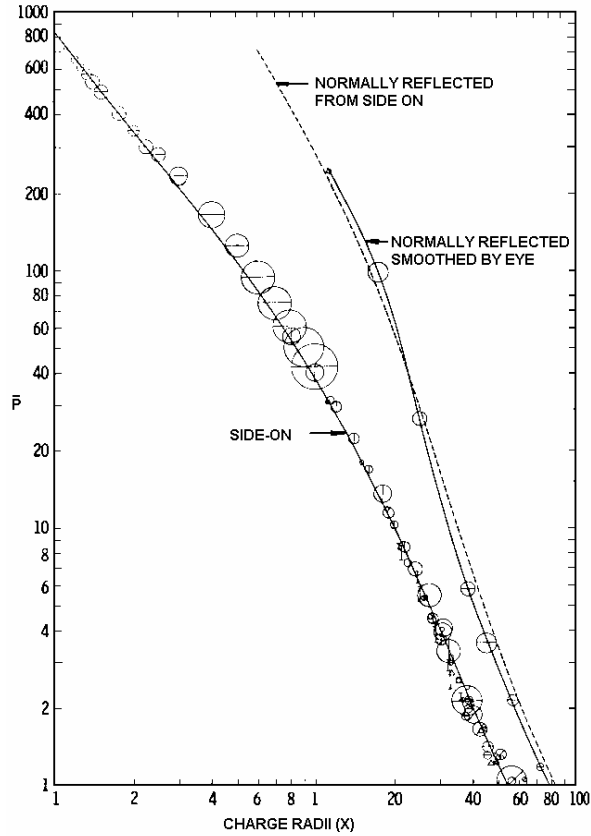


Figure 2.17 Side-on and normally reflected pressure vs. scaled distance (after Baker (1973)).

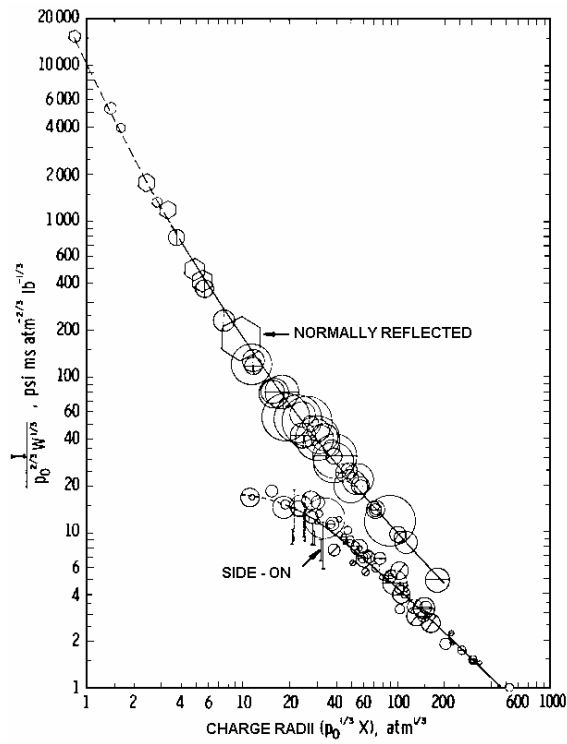


Figure 2.18 Side-on and normally reflected impulse vs. scaled distance (after Baker (1973)).

Another report from the Naval Ordnance Laboratory (Baker, 1973) primarily compares theory with experiment but also provides seldom reported free air blast parameters, such as first and second shock arrival times and the time history of motion of the contact surface (the boundary between the hot explosion products and surrounding air).

Research by Henrych (1979) gives approximate relations for negative pressures, negative impulses, negative duration, and wavelength based on experimental results.

2.2.1.2 Surface Bursts

More surface burst experiments are available as the height restriction imposed by air burst experimentation is removed. Data exists for explosions from conventional weapons and nuclear weapons as well as from large and small-scale experiments. Surface burst experiments also date to World War II. (Baker, 1973) reports data (Fig 2.19 and 2.20) from ground bursts of hemispherical TNT charges ranging in weight from 5 tons to 500 tons and of nuclear devices ranging in yield from 20 tons to 1.8 kilotons. The blast yield from nuclear explosions was assumed to be only half of the blast yield of TNT.

Many experimental tests using TNT hemispheres have also been conducted at the Suffield Experiment Station in Canada. In addition to the usual blast parameters, rarely measured parameters such as time history of particle velocity and density are noted in Baker (1973) (see Fig 2.21).

A final important set of ground burst tests noted in Baker (1973) were conducted at Nevada Proving Ground with 20 ton spherical TNT charges half buried underground. The objective of these tests was to extend the range of available data into the high overpressure range up to 69000 kPa and compare with previous Canadian tests. Three tests were conducted collecting data on arrival times, overpressures, impulses, and dynamic pressure. A typical plot from some of these experiments is shown in Fig 2.22.

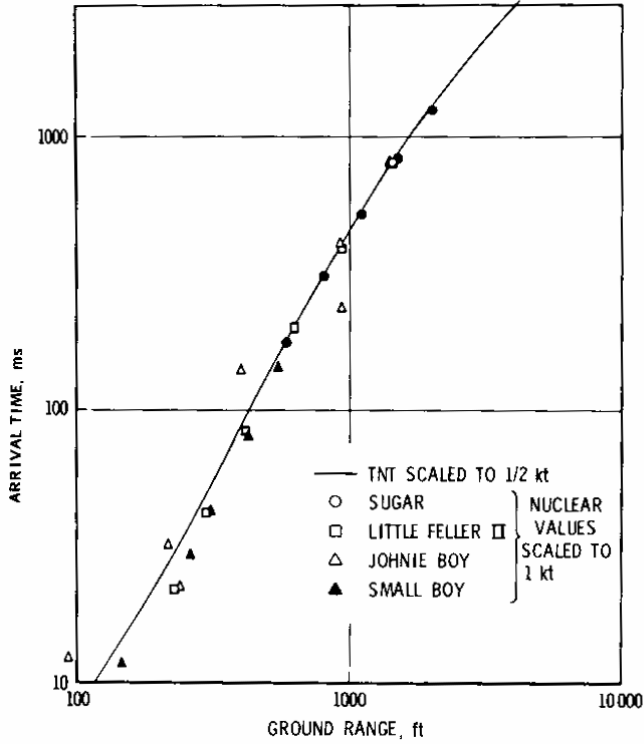


Figure 2.19 Scaled arrival time vs. ground range (after Baker (1973)).

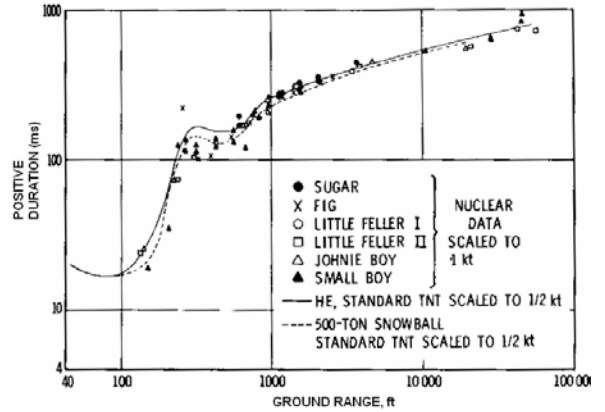


Figure 2.20 Scaled positive duration vs. ground range (after Baker (1973)).

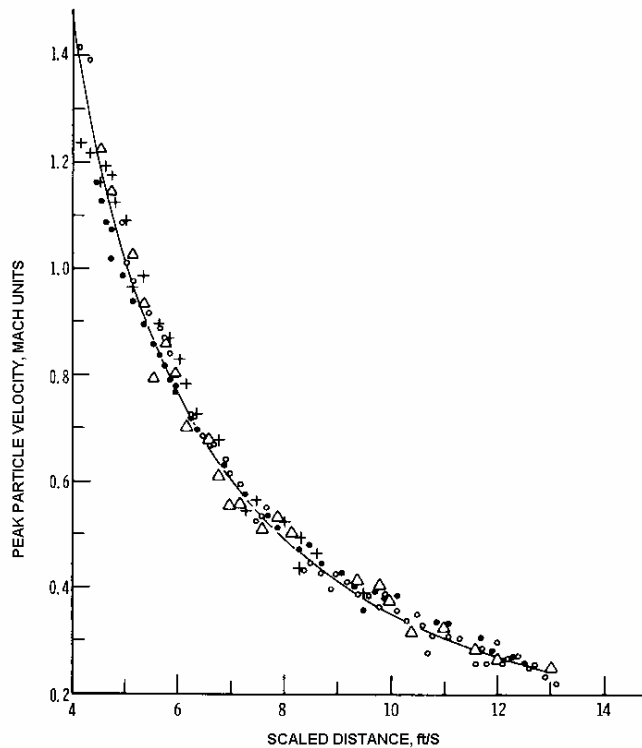


Figure 2.21 Comparisons of peak particle velocities for surface burst TNT (after Baker (1973)).

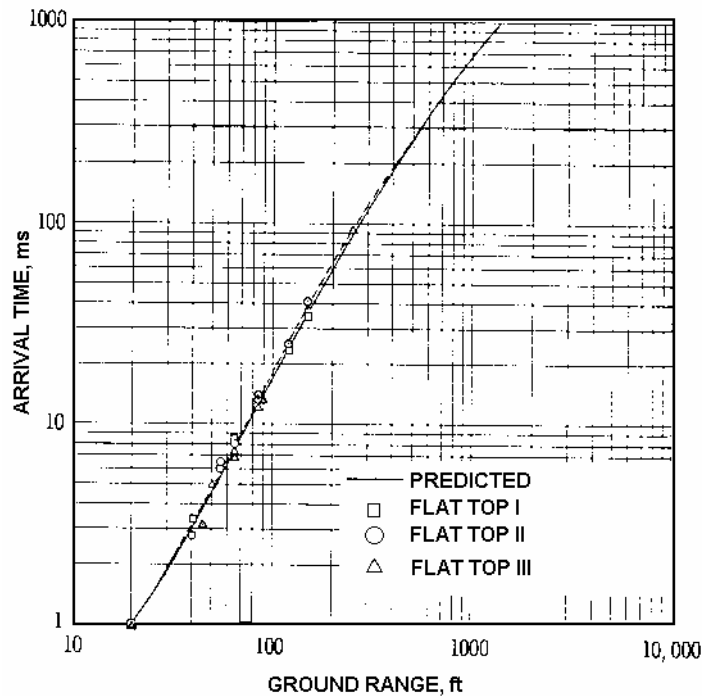


Figure 2.22 Measured arrival times for surface burst TNT compared to prediction (after Baker (1973)).

2.2.1.3 Mach and Reflected Waves

Initial experiments showed that the peak overpressure and impulse increased as the charges were elevated off the ground up to some optimum height. Further testing in this area was initially conducted to find the optimum height of detonation and was used by weapon designers. Figure 2.23 shows curves for choosing the height of burst at which the area on the ground subjected to a given impulse is maximized (Baker, 1973).

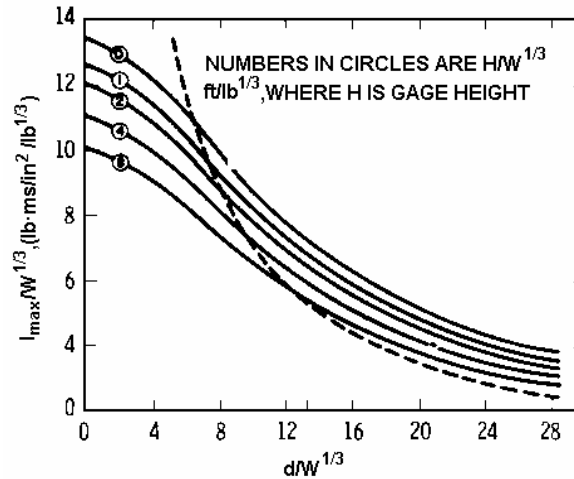


Figure 2.23 Optimum height for maximum impulse (after Baker (1973)).

Experiments by Schleuter, Hippensteel, and Armendt (1965) determined time histories of blast waves in the region of regular reflection at various scaled heights over a plane rigid surface using Pentolite spheres. Data on normally reflected pressure can be seen in Hoffman and Mills (1956) from tests on a reinforced concrete wall for incident overpressures up to 10000 kPa. Olson and Wenig (1961) and Dewey (1963) extended data on normally reflected pressure up to 207000 kPa with the development of improved gages for short duration tests (Baker, 1973).

2.2.2 Blast Experiments on Concrete Structures

Initial blast testing on concrete structures examined high strain rate effects and dynamic properties of concrete and steel. Elevated strain rates were used to try to simulate blast conditions.

Early tests began with Abrams (1917) and Jones and Richart (1942) where they used levers to obtain strain rates above static conditions. Various hydraulic methods later arose increasing the maximum strain rate. The Split-Hopkinson Pressure Bar (SHPB) experiments began in the late 1970s with Bhargaave and Rhenström (1977) (Bischoff and Perry, 1991). The SHPB is still often used and current use of the SHPB experiments can be seen in such investigators as Ross et al. (1995). These tests created strain rates simulating blast conditions.

Most of these early tests developed the understanding of dynamic behaviour of concrete at elevated strain rates. A summary of these and other previous experiments and results up to 1989 is available from Bischoff and Perry (1991).

In examining the structural response and dynamic properties of structures, researchers often simulated blast loads by applying uniformly distributed loads or more commonly applying point load impulses to create blast conditions such as in Feldman et al. (1962). Some experiments from various investigators will be summarized as follows.

2.2.2.1 Hoffman and Mills (1956)

These investigators took measurements of peak pressures, positive impulses, and positive durations for both side-on and normal incidence from bare 50/50 spherical Pentolite charges. Measurements were taken using charges ranging in weight from about 0.2 kg to 3.6 kg (0.5-8 lbs) with scaled distances ranging from about $0.6 \text{ m/kg}^{1/3}$ to $5.9 \text{ m/kg}^{1/3}$ ($1.5\text{-}14.8 \text{ ft/lb}^{1/3}$). The purpose of these experiments was to increase the range of data available for stronger shocks primarily side-on and face-on impulse. Data was previously primarily limited to detonations at scaled distances greater than $1.6 \text{ m/kg}^{1/3}$ ($5 \text{ ft/lb}^{1/3}$).

The test apparatus included creating a large enough surface to prevent the occurrence of pressure relief from clearing before the completion of the positive loading phase. Two surfaces were used: one a 600 mm (2 ft) thick reinforced concrete wall of a chamber, and the other a 3 m x 3 m x 0.3 m (10 ft x 10 ft x 1 ft) concrete slab poured on the ground surface. Mounting pipes 38 mm (1.5 in) in length were inserted in each of the surfaces to hold face-on transducers flush with the surface. The test setup can be seen in Figure 2.24.

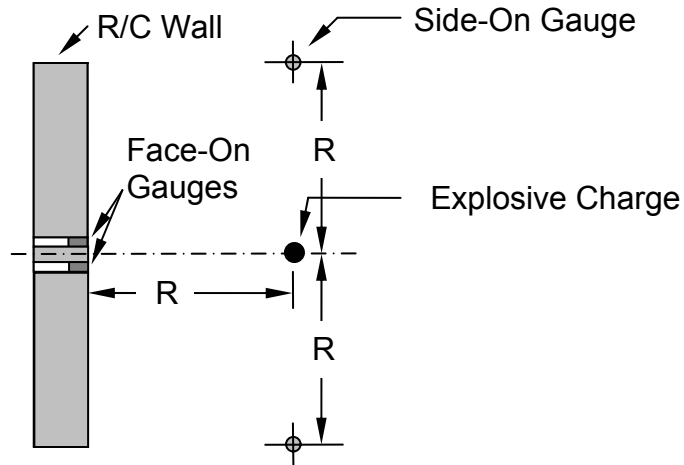


Figure 2.24 Hoffman and Mills Experiment (after Hoffman and Mills (1956)).

The data collected represented 269 test firings, some of which are reported in Table 2.4.

Table 2.4 Data from Hoffman and Mills

Charge Wt (lb)	Scaled Distance (ft/lb ^{1/3})	Avg. Peak Pressure (psi)		Standard Deviation of Pressure		Avg. Scaled Impulse (psi-ms/lb ^{1/3})		Standard Deviation of Scaled Impulse		Avg. Scaled Duration (ms/lb ^{1/3})		Standard Deviation of Scaled Duration	
		Side-On	Face-On	Side-On	Face-On	Side-On	Face-On	Side-On	Face-On	Side-On	Face-On	Side-On	Face-On
1.98	1.51	465.4	3229.9	-	-	16.9	119.3	-	-	0.17	0.19	-	-
7.88	2.01	265.1	1673.4	6.77	66.55	17.4	79.3	1.21	6.05	0.29	0.28	0.05	0.05
8.17	2.48	176.2	1019.3	4.92	31.53	-	-	-	-	-	-	-	-
7.94	3.01	108.6	552.2	5.78	38.76	14.3	53.6	1.76	7.77	0.42	0.43	-	-
1.05	3.44	79.2	384.2	8.96	10.49	18.2	51.9	0.40	3.16	-	-	-	-
1.98	3.62	80.5	371.7	-	-	-	47.9	-	-	-	0.45	-	-
1.05	4.03	59.0	246.2	-	4.96	15.7	44.8	1.34	2.70	0.74	0.74	-	-
1.05	4.42	46.5	179.8	1.27	7.13	12.3	40.5	4.74	2.72	0.87	0.84	0.07	0.04
0.53	5.00	35.7	126.2	1.12	5.90	11.6	34.9	1.25	-	1.09	1.02	0.13	0.04
1.05	5.65	24.6	76.4	0.56	1.67	9.7	24.2	0.37	4.77	1.74	1.20	0.08	0.11
1.05	6.50	18.2	52.6	0.42	1.56	8.4	20.2	0.49	-	1.30	1.45	0.10	0.15
0.53	7.45	15.6	43.7	0.54	1.20	7.8	22.2	0.37	2.04	1.43	1.49	0.06	0.10
0.53	9.49	8.7	21.4	0.03	1.07	6.1	14.9	0.39	0.29	1.74	1.76	0.14	0.11
1.98	9.71	9.2	22.7	0.13	0.58	6.6	14.0	2.40	0.65	1.78	1.53	0.08	0.15
0.53	11.84	7.0	16.6	0.16	0.42	5.2	11.7	0.41	2.09	2.01	2.02	0.12	0.10
1.05	13.46	4.7	10.5	0.27	0.68	5.0	9.3	0.35	0.21	1.89	1.73	0.09	0.06
0.53	14.81	5.9	8.7	0.14	0.35	4.3	8.6	0.16	0.32	2.43	2.37	0.11	0.13

The experimental side-on impulse data were compared against side-on impulse as predicted by Kirkwood and Brinkley (Hoffman and Mills, 1956). Furthermore,

experimentally determined peak side-on pressures were compared against Rankin-Hugoniot predictions. Experimentally determined peak face-on pressures were also compared against Rankin-Hugoniot predictions in low pressure regions (less than 20 atm). In higher pressure regions, comparisons were made against predictions using analyses from Doering and Burkhardt (Hoffman and Mills, 1956).

Experimental peak side-on and face-on pressures compared quite well numerical predictions however a significant variation was found in the comparisons against side-on impulse.

Suggested future work included investigating the effect of altitude to assess the accuracy of Sach's scaling law.

2.2.2.2 Feldman, Kennan, and Seiss (1962)

An investigation by Feldman et al. (1962) was undertaken examining the behaviour of reinforced concrete beams under severe dynamic load. The objective was to determine the resistance behaviour of single span reinforced concrete beams subjected to impulsive loading in addition to checking the existing methods of computing dynamic resistance and strain rate effects. The dynamic tests consisted of two series of beams (Figure 2.25)

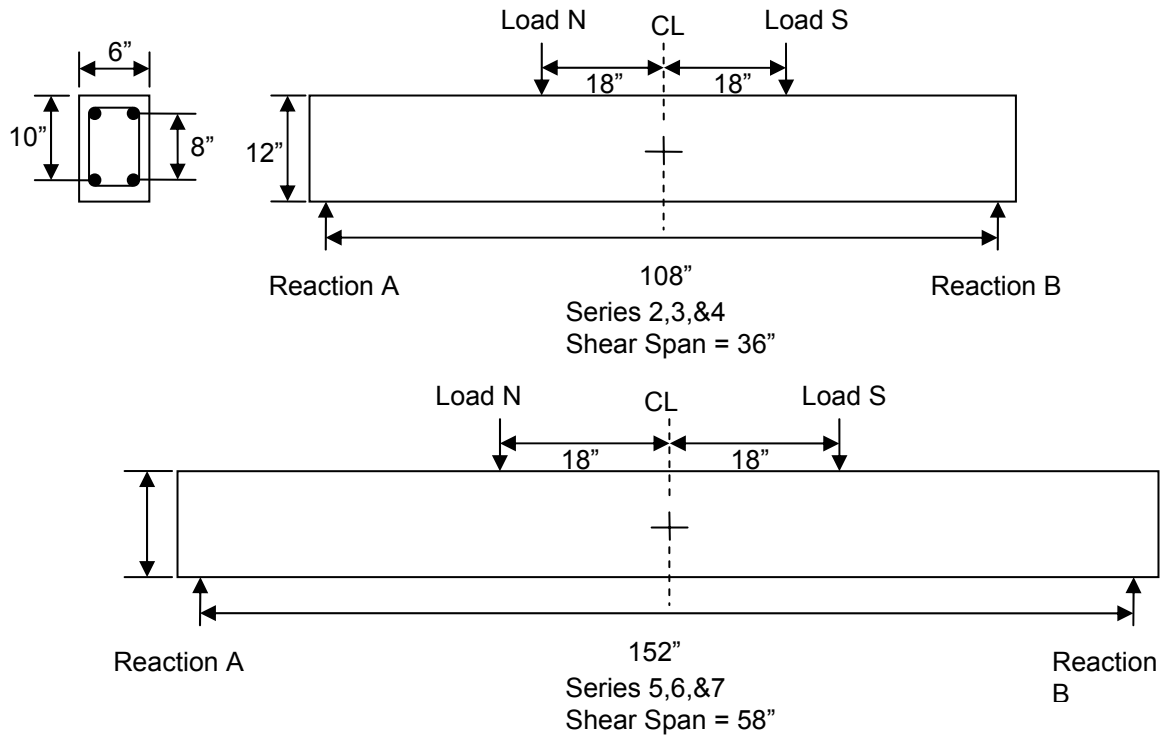


Figure 2.25 Beam series (after Feldman et al. (1962)).

which were tested under two-point loads. In series 2, 3, and 4, the amount of compression steel and the configuration of ties holding the compression were varied. Series 5, 6, and 7 were essentially duplicates of 2, 3, and 4 but with a longer span to vary the moment to shear ratio as well as the load rise time to natural period ratio. The concrete strength, steel yield strength, beam width, beam height, and beam depth were all kept constant.

The beams were loaded using a 60 kip capacity pneumatic loading machine as seen in Figure 2.26 (a) and Figure 2.26 (b). The load is applied when the piston hits the transfer beam loading the experimental beam at 2 points (Figure 2.26 c). The impulse load simulating blast conditions is created by the sudden release of compressed gas into the atmosphere from the loading machine. The pressure differential created on the main piston loads the beam.

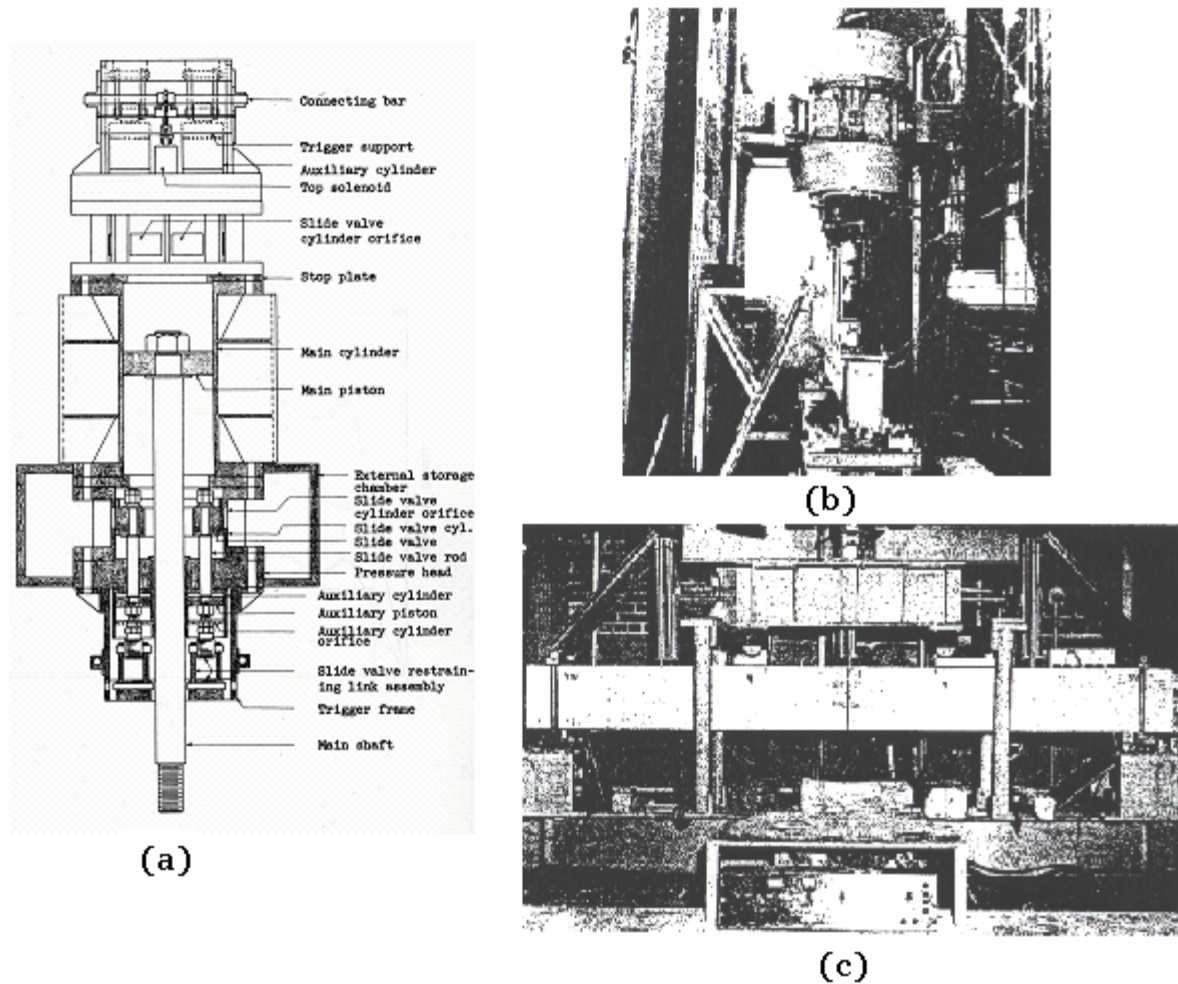


Figure 2.26 Loading apparatus (after Feldman et al. (1962)).

Some of their conclusions are summarized as follows:

- The level of dynamic yield resistance was increased over the static level in direct proportion to the increase in strength of the tensile reinforcement. In most cases, yield deflection and elastic stiffness also increased with respect to beams loaded statically.
- A small but consistent increase in collapse deflection under dynamic loading was noted. The collapse deflection increased with the use of compression reinforcement in dynamic loading as in static loading.
- In general, the computations for dynamic resistance level based on the procedures and formulas from U.S. Army (1957) provided adequate results.

Failure mode prediction was also quite accurate. Computations for yield deflection resulted in values that were too small with respect to measured values and maximum deflection values that were too large.

2.2.2.3 Slawson (1984)

Slawson (1984) tested 11 underground reinforced concrete box structures subjected to simulated nuclear blast loads. Two main parameters were studied in the tests: the span to effective depth ratio and the reinforcement ratio. Two series of tests were conducted; the first designated DS1 to DS5 and the second designated DS2-1 to DS2-6. The main difference between the two series of tests was the span to depth ratio, L/d . The first test series (DS1-DS5) had an effective depth of 122 mm (4.8 in) and a clear span of 1219 mm (48 in) with L/d being 10 as shown in Figure 2.27.

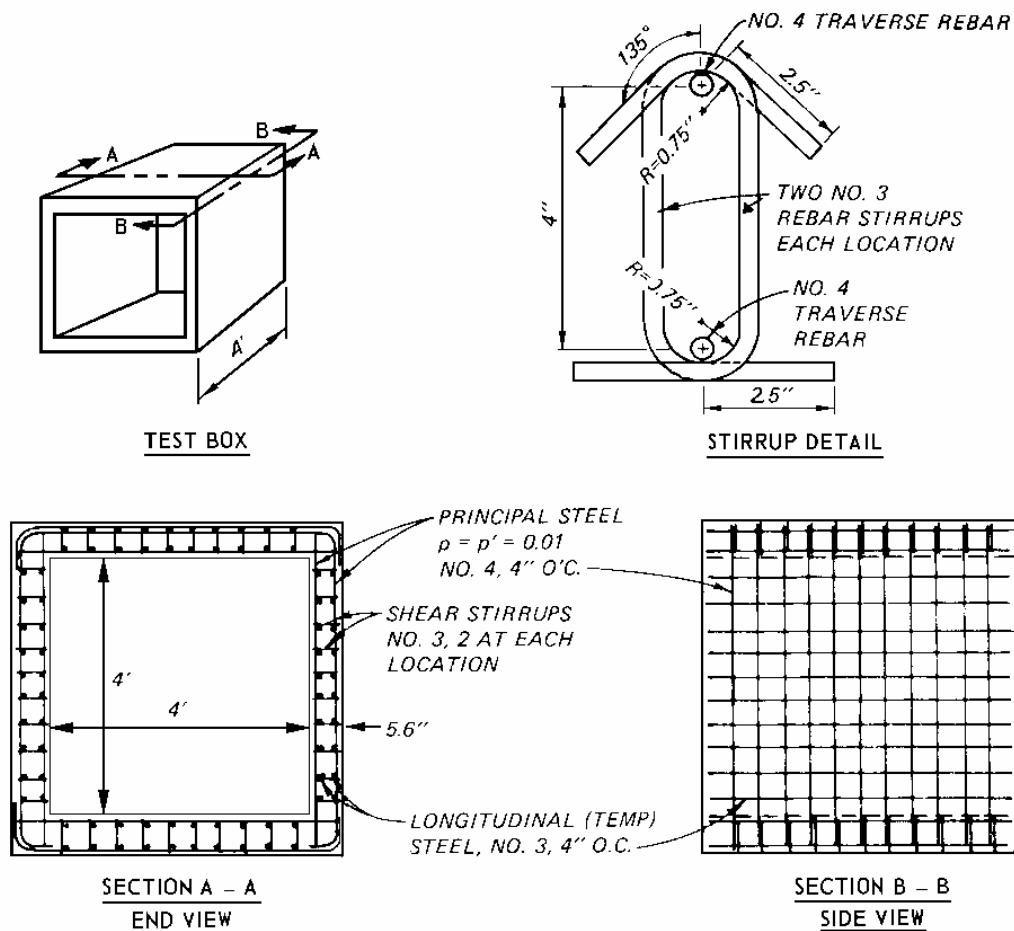
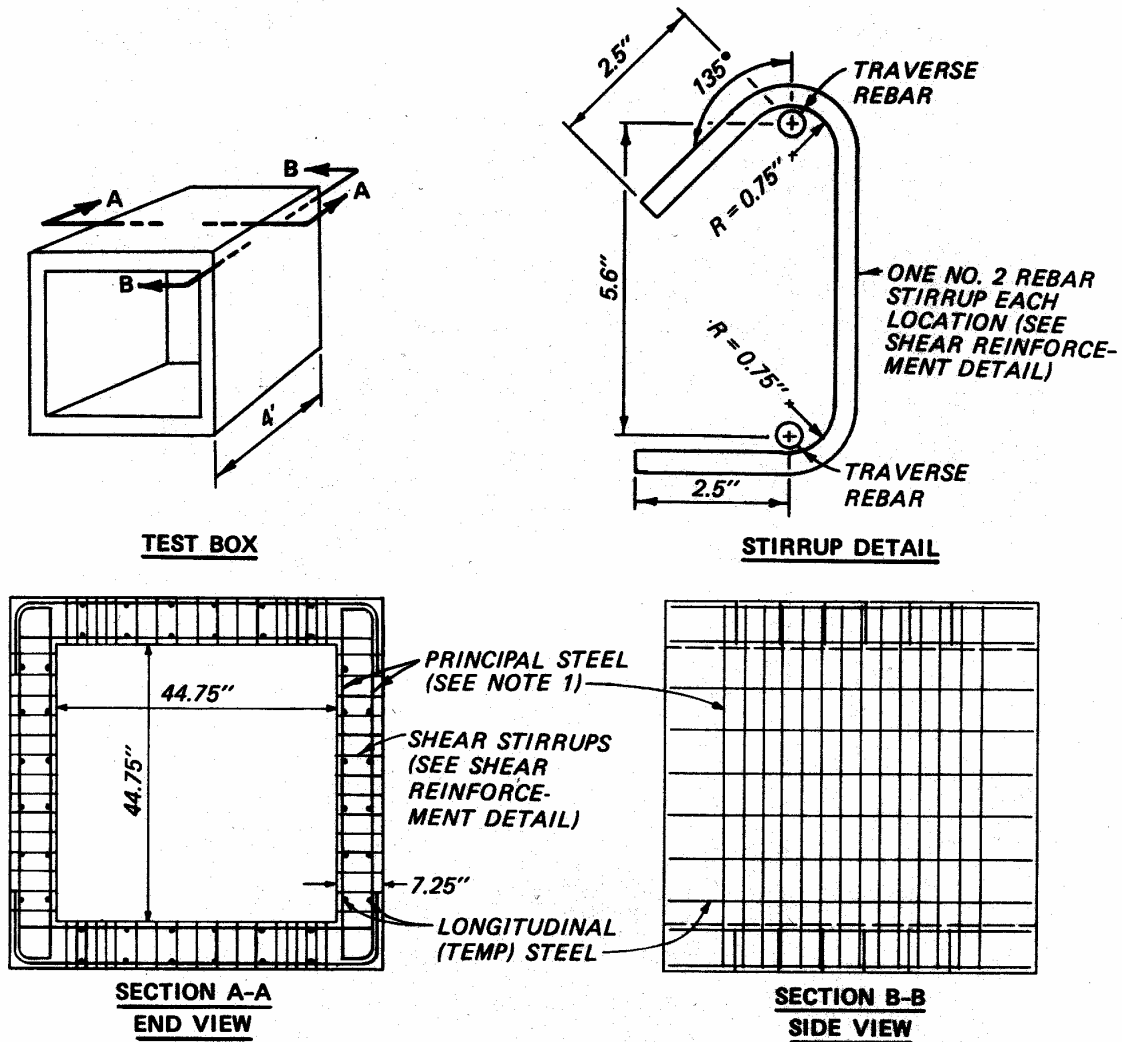


Figure 2.27 (FY81) DS1-DS5 construction details (after Slawson (1984)).

In the second series, the effective depth was 163 mm (6.44 in) with a clear span of 1137mm (44.75 in); thus L/d was 7 as shown in Figures 2.28 and 2.29. The box structures in the first series had 1% main reinforcement while the in the second series, three tests had 0.75% reinforcement and the other three had 1.2%.



- NOTES: 1 - FOR $\rho = 0.012$, #5 ~ 4" O.C. (INSIDE AND OUTSIDE FACE)
 FOR $\rho = 0.075$, #4 ~ 4" O.C. (INSIDE AND OUTSIDE FACE)
 2 - LONGITUDINAL STEEL ~ #2 ~ 7.5" O.C. (INSIDE AND OUTSIDE FACE)

Figure 2.28 (FY82) DS2-1 to DS2-6 construction detail (after Slawson (1984)).

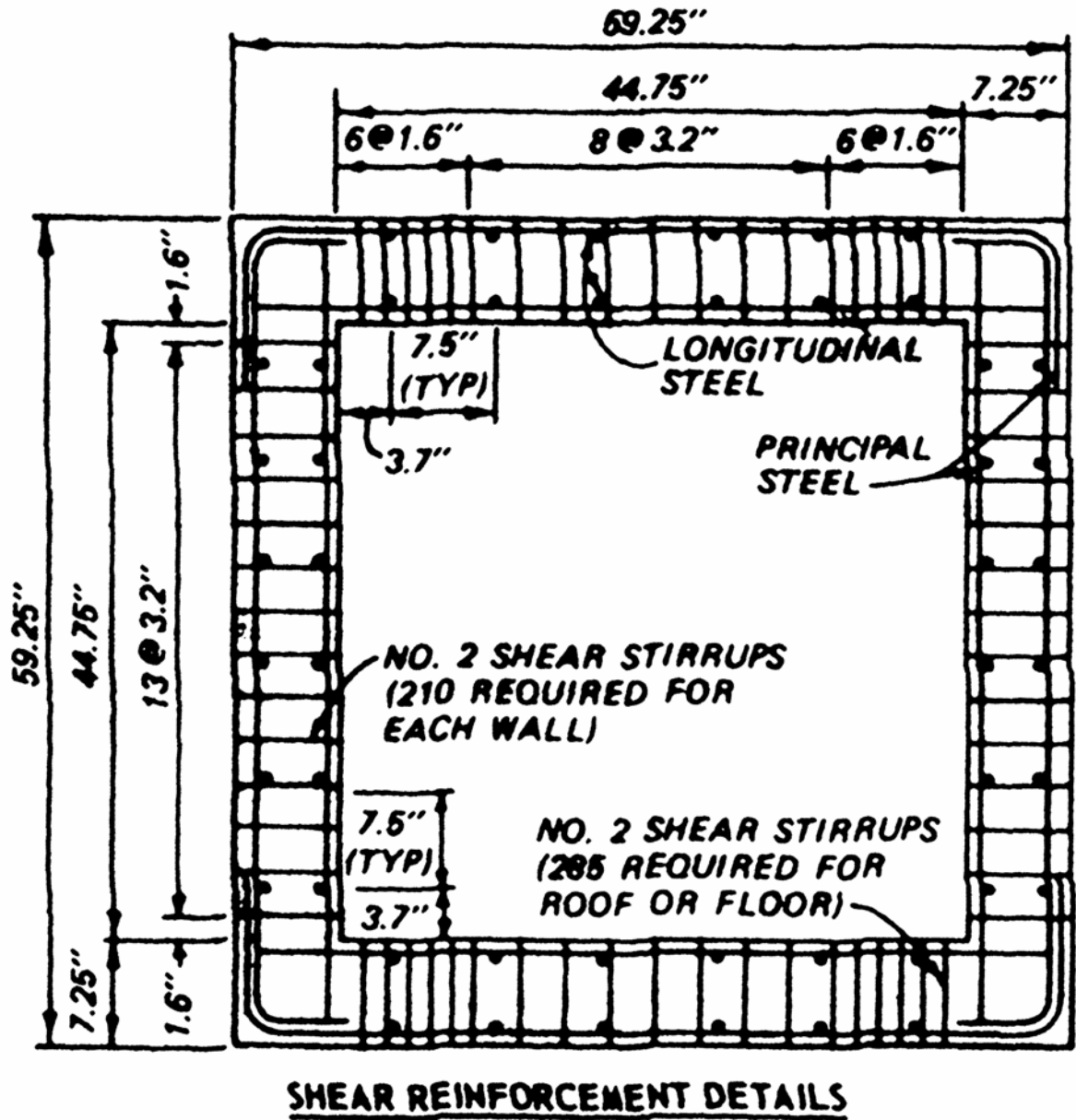


Figure 2.29 (FY82) Shear reinforcement for DS2-1 to DS2-6 (after Slawson (1984)).

The test configuration for the five element tests is shown in Figure 2.30. The test element was placed on a sand pit which was cast into the reaction structure. The elements were tested using a HEST (High Explosive Simulation Technique) (Wampler, 1978) that simulated the peak overpressure, rate of decay, and overpressure duration associated with a nuclear detonation. Sand overburden was placed over the charge

cavity to contain the blast and simulate the overpressure duration of a low yield nuclear weapon. The explosive used was Pentaerthritol tetranitrate (PETN).

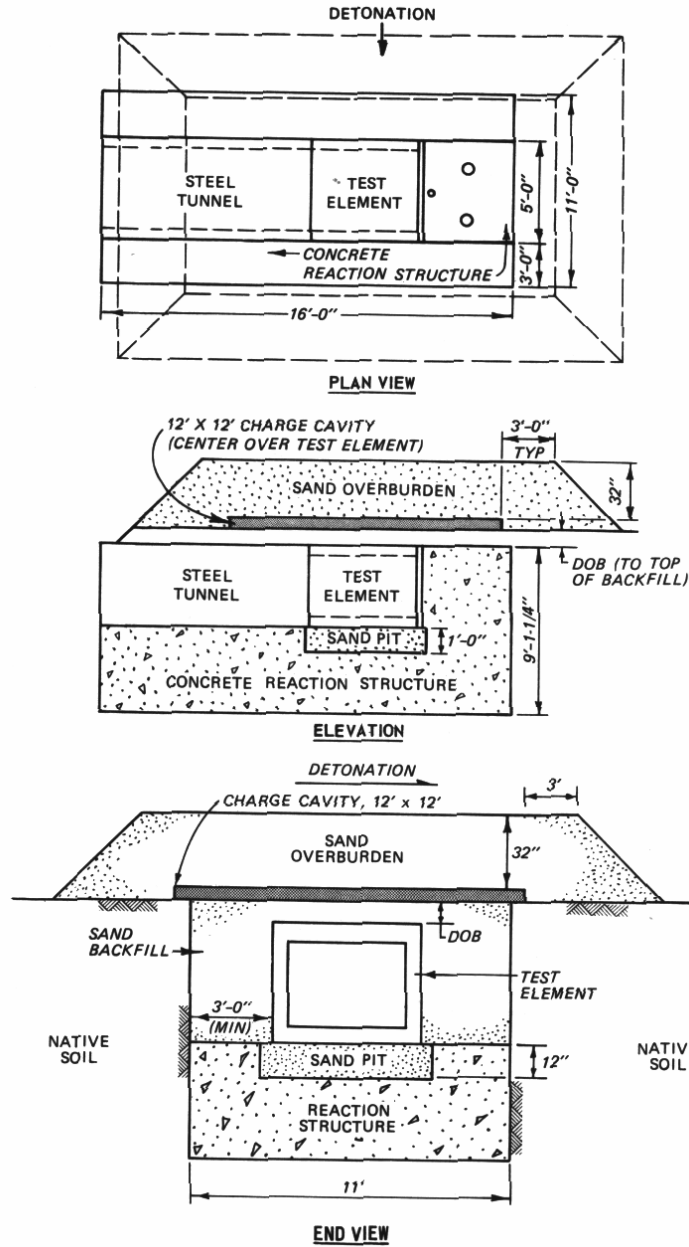


Figure 2.30 Experiment setup (after Slawson (1984)).

Slawson made the following conclusions:

- high frequency dynamic shear failure in shallow-buried structures with L/d ratios of 7 and 10 may be induced and the threshold overpressure level that will generate shear failure is greater than the flexural failure overpressure;
- failure mode depended on concrete strength in that lower strength concrete (4000psi (27.5MPa)) was crushed at supports allowing premature failure of roof slab by reinforcement pullout;
- the measurement of rebar strains gives an indication of the amount of dowel action occurring at the support during roof slab failure. The length of reinforcement effective in dowel action ranges from 4 to 8 inches (100-200mm). Permanent strains of 10 to 15 percent are noted for the Dynamic shear tests.

2.2.2.4 Smith et al. (1999)

Smith et al. (1999) illustrated the effect of clearing on a target of finite size. PE4 charges were detonated over rigid 300mm and 400mm diameter steel plates at standoff distances ranging from 0.3m to 0.5m. The charge masses varied from 17.4g to 43.5g resulting in equivalent TNT scaled distances of $0.814 \text{ m/kg}^{1/3}$ to $1.474 \text{ m/kg}^{1/3}$. Piezoelectric pressure transducers were mounted flush with the top surface of each plate. The experimental set-up can be seen in Figure 2.31.

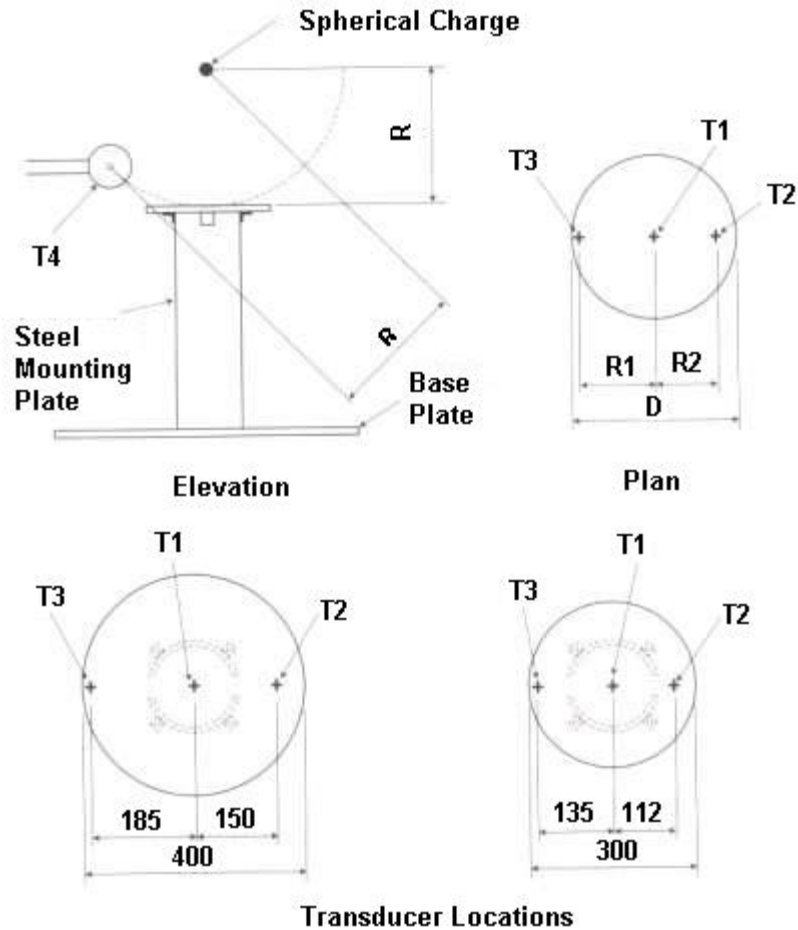


Figure 2.31 Experimental set-up (dimensions in mm) (after Smith et al. (1999)).

For each plate, 16 firings were carried out at 8 different scaled distances and then repeated to obtain average values. Whenever possible, comparisons were made between experimental results and the CONWEP (Hyde, 1992) program for infinite reflecting surfaces (i.e. CONWEP is unable to take clearing into account in its predictions). Some of the results are presented in Figures 2.32 to 2.34. A significant amount of scatter in the data was reported in the reflected overpressures from transducer 1. The scatter was attributed to instantaneous loading of the transducer diaphragm causing some “ringing” leading to some slight overshoot in the initial peak. The effects of ringing appear to cancel out when the pressure time history is integrated to obtain impulse.

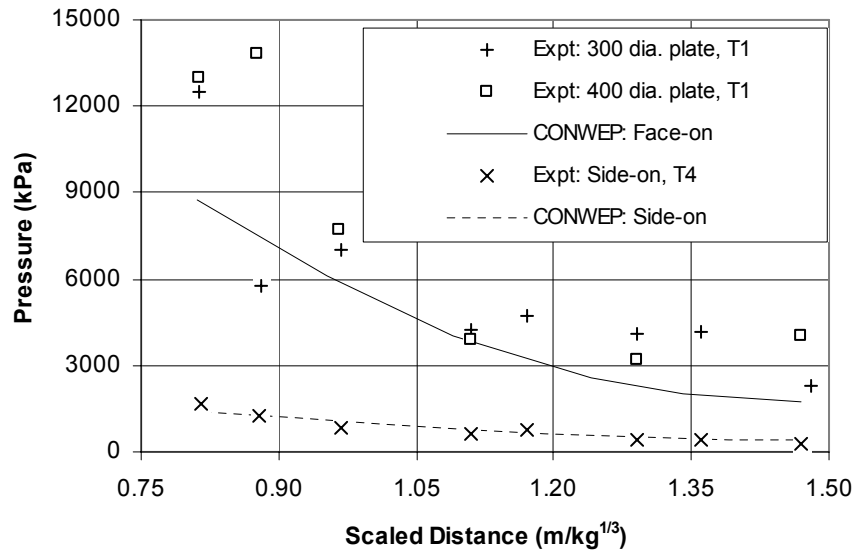


Figure 2.32 Normal pressure vs. scaled distance (after Smith et al. (1999)).

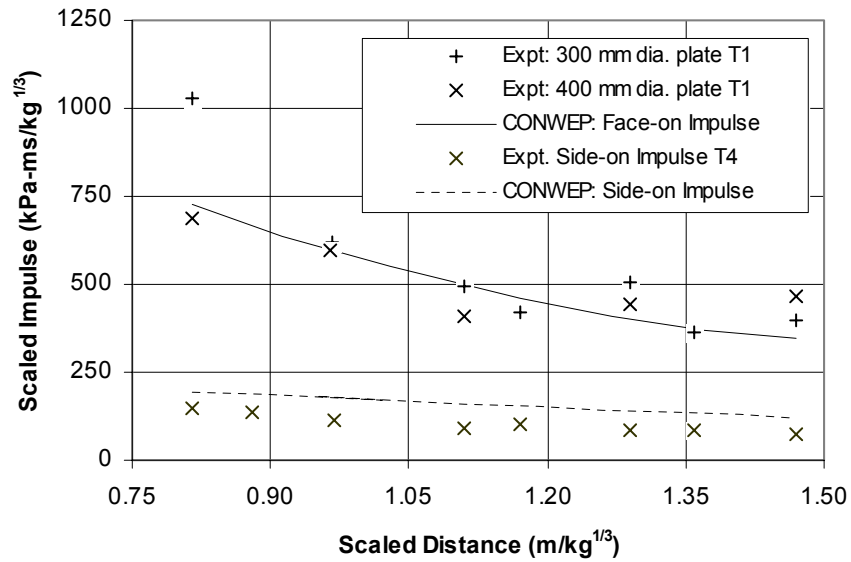


Figure 2.33 Normal impulse vs. scaled distance (after Smith et al. (1999)).

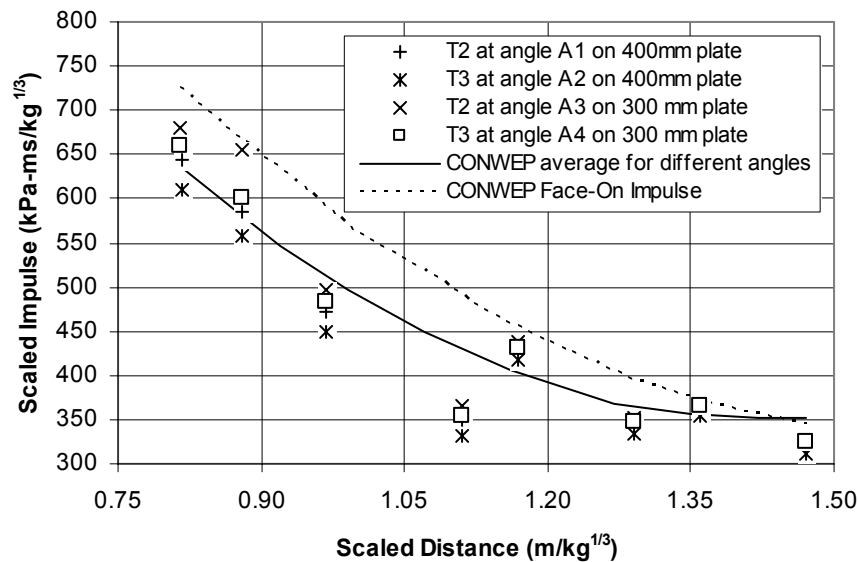


Figure 2.34 Impulse vs. scaled distance for varying angles incidence (after Smith et al. (1999)).

The angles A1 and A2 correspond to transducers T2 and T3 for the 400mm plate while angles A3 and A4 are the corresponding angles on the 300mm plate.

The effect of clearing on impulse is apparent in Figure 2.34. The broken line is the CONWEP prediction for face-on scaled impulse and, as expected, is seen to lie above all data points. The solid line is the CONWEP prediction for angles of incidence on an infinite reflecting surface. The experimental data mostly lie below this average line. This demonstrates that the process of clearing results in impulses on a finite surface that are less than those on an infinite surface. The process of clearing does not reduce the peak reflected overpressure.

2.2.2.5 Dennis, Baylot, and Woodson (2002)

Dennis et al. (2002) conducted five blast experiments on ¼-scale concrete masonry unit (CMU) walls. The purpose was to provide data to validate the U.S. Army Corps of Engineers' "High Performance Computing for Force Protection against Terrorist Threats (HPC)" method of response prediction of CMU walls to blast loads. The CMUs were ¼-scale versions of a standard nominal 20 cm (8 in) concrete block (20x20x40 cm). Finite element models using the computer code DYNAD3D (Whirley and Engelmann, 1993) were created to predict the results of the experiment.

The test wall was 15 blocks tall and 15.5 blocks wide. A large reaction structure was built behind the wall such that there would be no pressure relief on the CMU wall provided by the airblast pressures travelling around the edges of the wall. A preliminary numerical blast analysis was performed to predict the failure standoff distance for the explosive charge.

In tests, the explosive charge was placed opposite the center of the length of the CMU wall. Three different standoff distances were used in the 5 tests. The first was based on the pre-test analysis predicting failure of the wall. In Test 2, the charge was moved to 75% of the range in Test 1. Test 3 was a repeat of Test 2, and Test 4 a repeat of Test 1. Test 5 was conducted at 1.25 times the standoff distance of Test 1. Five pressure gauges were attached to wall as shown in Figure 2.35.

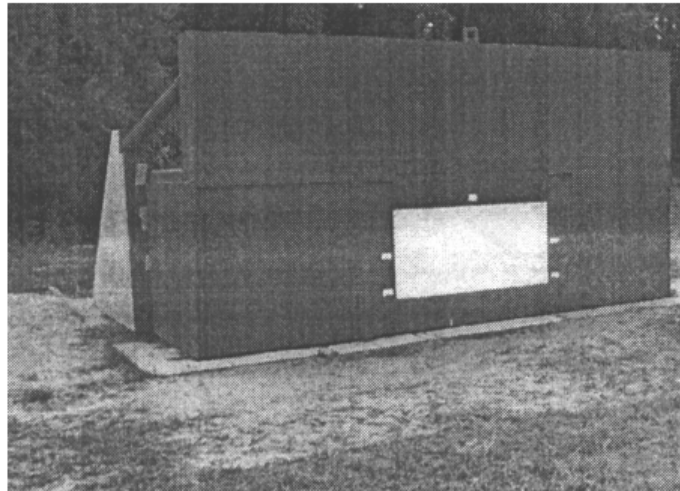


Figure 2.35 Experimental setup (after Dennis et al. (2002)).

Data from gauges was very consistent indicating a uniform pressure on the wall. Thus, the pressure-time histories were averaged for the five pressure gauges. The finite element model was not able to allow the wall to fail and fall in place. It is believed this was due to not modelling the removal of the mortar material when the mortar joint fails. This could lead to increased compression in the wall increasing the friction between the blocks and keeping the wall together when it should fall apart. In three of the experiments, the wall failed when the analysis predicted it would not.

2.2.2.6 Rickman and Murrell (2004)

Rickman and Murrell (2004) investigated the effects of airblast shielding of structures by blast walls. A series of 40 experiments were conducted at a scale of 1/20 to 1/50. The experiments were designed to quantify the effects of: (a) barrier wall height, (b) charge-to-surface wall distance, and (c) structure distance behind the barrier wall. The apparatus was a 5 m by 6 m steel table representing an ideal plane ground surface upon which a 5 m long by 16 mm thick steel barrier was placed as well as 12.7 mm thick aluminum plated structure as shown in Figure 2.39.

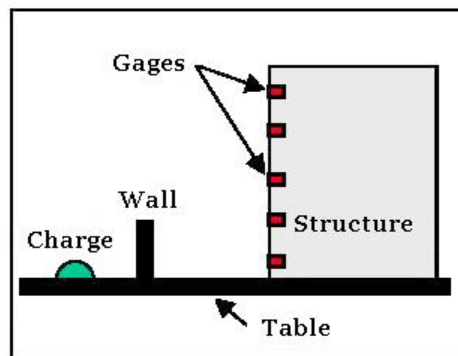


Figure 2.39 Experimental setup (after Rickman and Murrell (2004)).

The experiment involved idealizing the charge shape as a surface hemispherical burst and the structure, barrier walls, and ground surface were assumed to be perfectly rigid. The explosive charge used consisted of precision cast PBX-9407 with masses of 18.2 g and 72.6 g. To check experimental results, the program CONWEP was used. Rickman and Murrell found that CONWEP could only accurately model the blast wave form until the arrival of pressure relief around the structure's edge as depicted in Figure 2.40.

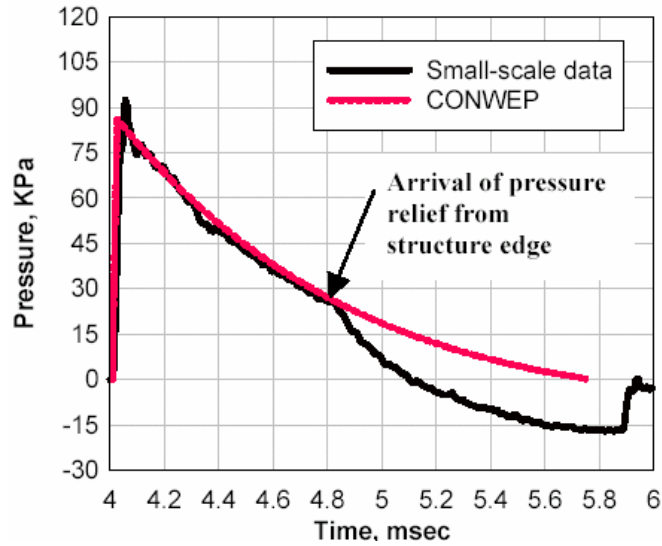


Figure 2.40 Comparison of a blast wave form (after Rickman and Murrell (2004)).

Some of the results of the effect of charge-to-wall standoff distance on the peak reflected pressure at a point on the structure’s center-line are shown in Figure 2.41.

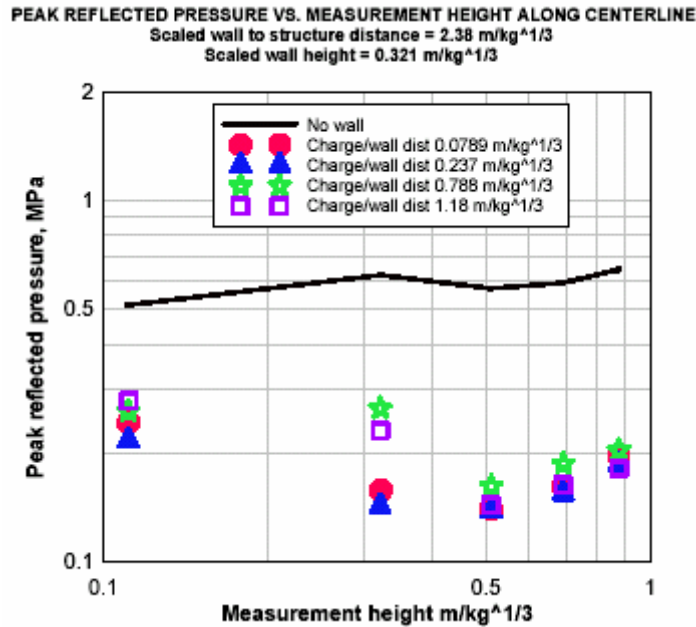


Figure 2.41 Effect of charge-to-wall standoff on peak reflected pressure (after Rickman and Murrell (2004)).

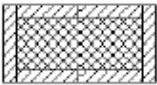
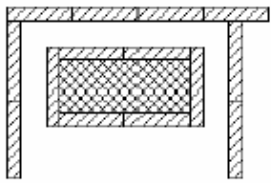

Barrier walls may reduce both reflected pressure and reflected impulse to a greater degree than previously thought. The experimental data indicated that the

barrier wall provided substantial shielding of the structure at heights extending well above the top of the barrier wall. Further numerical analysis is necessary to confirm these findings.

2.2.2.7 Ripley et al. (2004)

Research by Ripley et al. (2004) examined the effects of wave reflection and diffraction on a structure in a simulated urban environment. A layout of the testing scenarios is shown in Table 2.5 and Figure 2.36(b).

Table 2.5 Small Scale Urban Scenarios (after (Ripley et al., 2004))

Series	Schematic	Description
1		The first scenario involves a single building target that is 91.4 cm by 38.1 cm and 38.7 cm tall (including a 0.6 cm thick plate covering the walls to enclose the building).
2		The second scenario adds 38.1 cm tall walls adjacent to three sides of the rectangular block to simulate streets between buildings. The width of the side and rear passages is 15.2 cm. This configuration highlights the shock channeling effects and complex shock interactions behind the building and in the passages.
3		The third scenario removes the primary building, leaving the surrounding walls to form an empty courtyard. This setup demonstrates shock focusing in a re-entrant corner scenario, and identifies the effect of removing the building.

The charge mass for all trials consisted of a 50 g C4 rectangular cube (2.5 x 2.5 x 5.0 cm) with its longitudinal axis oriented upwards. Three separate stand-off distances were tested but only the results of 1.37 m are presented. The pressure gauge and charge locations are shown in Figure 2.36. All gauges were mounted on the table surface.

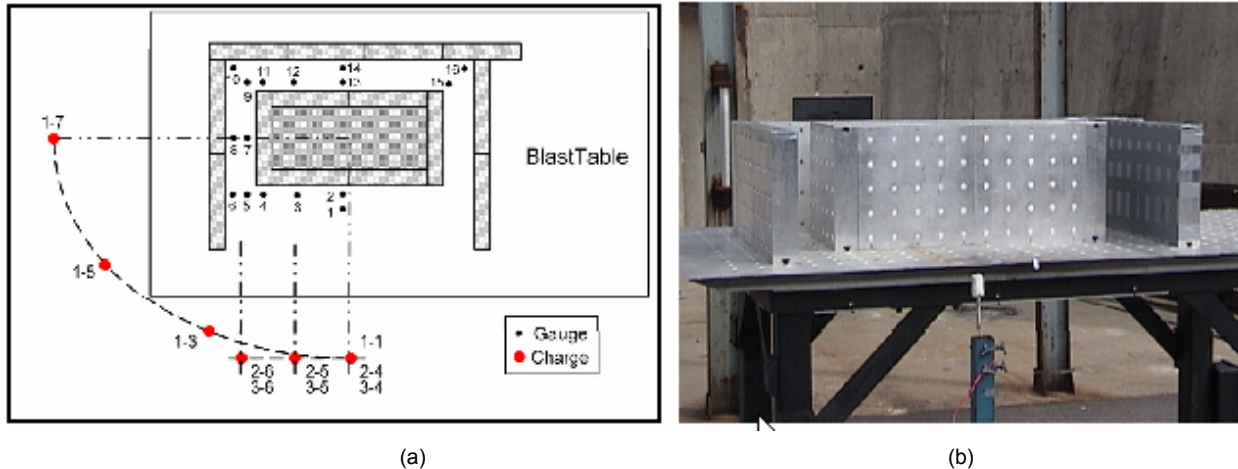


Figure 2.36 (a) Pressure and charge locations (b) Blast table (after Ripley et al. (2004)).

The experimental work was also used to validate the capability of the Chinook CFD computer hydrocode using coarse meshes.

The effect of diffraction angle was investigated using series 1 where charges were positioned in a radial array through 90° (see Figure 2.37(a)). Gauge 10 was selected for comparison. Overall, good agreement of the pressure-time histories was achieved, as seen in Figure 2.37(a). Peak pressures typically differed by 19% and impulse by 15%. This was considered excellent agreement considering a very coarse mesh was used.

The effect of charge location on the reflected pressure at gauge 16 for series 3 is shown in Figure 2.37 (b). For all charge locations, numerical results were found to be less than experimental values but captured the reflected blast decay. Impulses predicted by the numerical results are about 20% greater than experimental. The numerical results were considered acceptable again considering a coarse mesh was used in the model. The effect of the different scenario configurations is evident in Figure 2.38. The results behind the building indicate that the building alone (series 1) had the lowest pressure while the building with surrounding walls (series 2) had the highest pressure. This is mainly caused by the superposition and enhancement of the waves that are channelled through the passages and ultimately colliding behind the structure. Most importantly, the removal of the building (series 3) resulted in lower peak pressures than with the building present although this is often considered the

worst case because the incident waves in series 3 are unobstructed. Furthermore, the Chinook code was accurately able to capture the effects of diffraction, blast channelling and complex wave reflection.

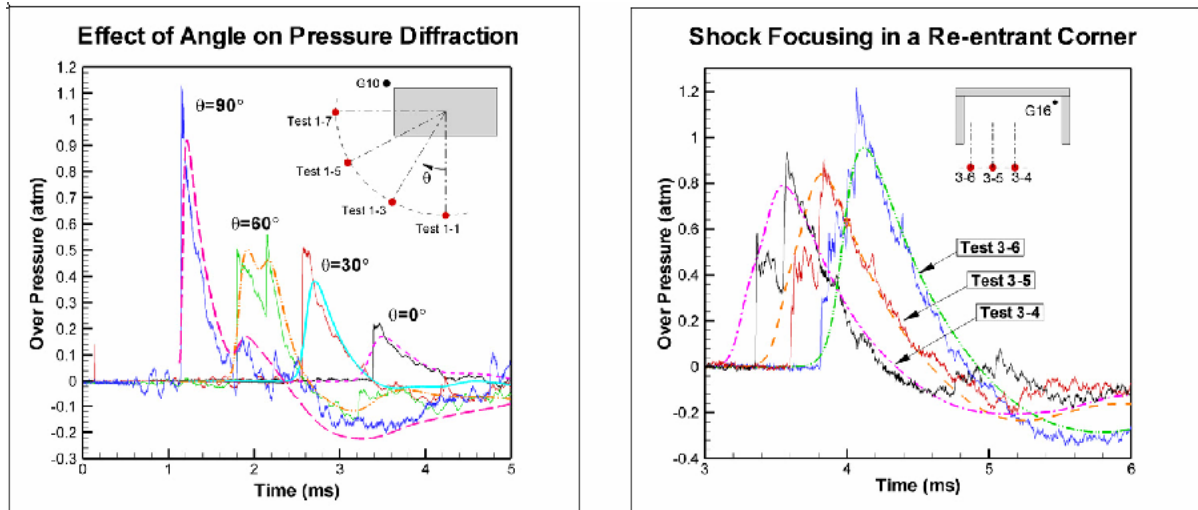


Figure 2.37 (a) Diffraction Angle (b) Shock Focusing (solid lines – experimental; broken lines – numerical) (after Ripley et al. (2004)).

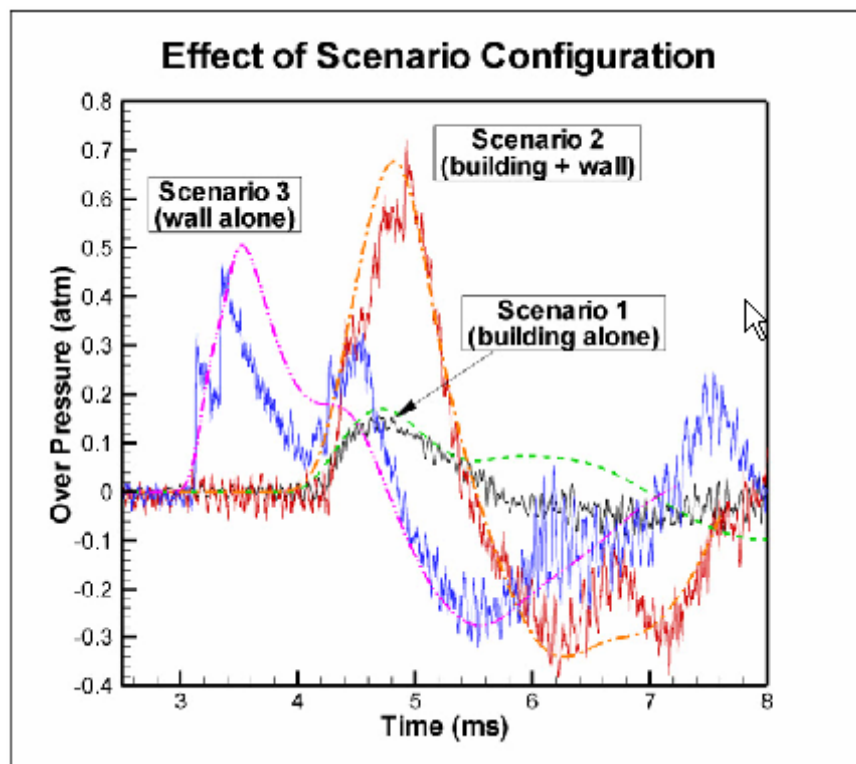


Figure 2.38 Effect of scenario configuration (Gauge 14) (solid lines – experimental; broken lines – numerical) (after Ripley et al. (2004)).

2.3 Analytical Work

2.3.1 Numerical Formulations

The general fluid dynamics equations involved in airblast problems are summarized below from Baker (1973). In mixed Eulerian-Lagrangian form, consideration of the conservation of momentum of moving fluid elements leads to the set of equations

$$\rho \frac{\partial^2 x_i}{\partial t^2} + \frac{\partial p}{\partial x_i} = 0 \quad (2.33)$$

where ρ is fluid density and p is absolute pressure while gravity and body forces are assumed negligible. From conservation of mass, one obtains the equation

$$J = \frac{\rho_l}{\rho} = \frac{\partial(x_1, x_2, x_3)}{\partial(a_1, a_2, a_3)} \quad (2.34)$$

where J is the Jacobian.

In shock theory, viscosity and heat-conduction effects are usually assumed negligible everywhere but in the shock fronts expressed as

$$\dot{S} = 0 \quad (2.35)$$

where S is the entropy of the fluid element. A final equation of state is required to complete the set of equations in the form

$$p = f(\rho, S) \quad (2.36)$$

In the steep gradients within a shock front, not all of the above equations are valid because viscosity and heat-conduction effects become important. In blast theory, the even more complex equations that take these effects into account are seldom used but are replaced by a set of “jump” conditions first formulated by Hugoniot (1887) called

Rankine-Hugoniot conditions. These equations for a coordinate system moving with a discontinuity are given by

$$u_1 \rho_1 = u_2 \rho_2 \quad (2.37)$$

$$p_1 + \rho_1 u_1^2 = p_2 + \rho_2 u_2^2 \quad (2.38)$$

$$e_1 + \frac{p_1}{\rho_1} + \frac{1}{2} u_1^2 = e_2 + \frac{p_2}{\rho_2} + \frac{1}{2} u_2^2 \quad (2.39)$$

where e is the internal energy and subscripts 1 and 2 denote one side or the other of the discontinuity. The equations will apply for all shock fronts of any curvature. The general equations for air blast transmission given previously are very difficult to solve for arbitrary three-dimensional cases. Computer formulations have been developed to solve these highly non-linear equations.

Computational methods can be divided into two classes: (1) methods with discontinuous shock fronts (Kirkwood and Brinkley (1945, 1947)), and (2) methods that smear properties over shock fronts of finite thickness (Brode, 1955; Harlow, 1957, 1959; Daly et al., 1964; Gentry, Martin and Daly, 1966) so that no discontinuities are permitted (method of fictitious viscosity). A good summary of the various methods can be found in Baker (1973).

2.3.2 Computer Codes

Various computer codes exist to calculate blast pressures and the interaction of blast waves with structures three of which are described as follows.

2.3.2.1 CONWEP

Conventional Weapons Effects Program (CONWEP) (Hyde, 1992) is capable of producing free field pressures from hemispherical surface bursts and spherical airbursts. CONWEP is often used in conjunction with other finite element programs and provides the loads and pressure-time histories used in finite element analysis.

2.3.2.2 LS-DYNA

LS-DYNA (Halquist, 1991) is a general finite element code for analysing the large deformation dynamic response of three dimensional structures including structures coupled to fluids. Pre- and post-processor tools, LS-INGRID and LS-POST, provide a graphical user interface and are interfaced with leading CAD, FEA, and FEM systems. Some of LS-DYNA's capabilities include fluid-structure interaction, underwater shock, multi-physics coupling (structural, thermal, fluid, acoustics, etc.), crack propagation, and crashworthiness simulations.

2.3.2.3 SHAMRC

Second-Order Hydrodynamic Automatic Mesh Refinement Code or SHAMRC (Crepeau, 1988) is a Eulerian finite difference code for calculating airblast propagation. SHAMRC can be used to solve a variety of airblast related problems which include high explosive detonations, nuclear detonations, structural loading, and thermal effects on airblast, among others.

2.3.3 Analytical Analysis

2.3.3.1 Krauthammer et al. (1994)

Krauthammer et al. (1994) studied the behaviour and response of structural concrete elements under severe short duration dynamic loading. Timoshenko beam theory models were used for the analysis of concrete beams and one-way slabs. Detailed failure criteria were established for predicting the collapse of structural members shown in Table 2.6.

Table 2.6 Failure criteria (after (Krauthammer et al., 1994))

Flag ID	Failure Flag	Description
1	Direct Shear (at support)	The slip reached the maximum slip on the Hawkins' direct shear relationship
2	Diagonal shear hinge initiated (at a support)	The shear strain reached the ultimate shear strain of shear force-strain relationship as computed from the Modified Compression Field Theory
3	Diagonal shear hinge formed (at a support)	The average shear strain over the hinge length reached the ultimate shear strain of the shear force-strain relationship as computed from the Modified Compression Field Theory
4	Flexural hinge initiated (at a support)	The curvature (at support) reached the ultimate curvature on moment-curvature relationship
5	Flexural hinge formed (at a support)	The average curvature (at support) over the hinge length reached the ultimate curvature of the moment-curvature relationship
6	Flexural hinge initiated (at center)	The curvature (at center) reached the ultimate curvature on moment-curvature relationship
7	Flexural hinge formed (at center)	The average curvature (at center) over the hinge length reached the ultimate curvature of the moment-curvature relationship

The results were compared to beams under localized impact loads (Feldman et al., 1962) and roof slabs subjected to distributed explosive loads (Slawson, 1984). The beams were modelled using 54 nodes resulting in a nodal spacing of 2 inches. Stability was ensured by calculating the critical time step based on dilatational wave speed and thus a time step of 10×10^{-6} s was used.

The slabs were modelled assuming a fixed support rotation condition. Experimental results indicated that only very small support rotations and very little cracking occurred at the supports at failure. A time step of 1×10^{-6} s was used although a larger critical time step was calculated. The larger time step did not produce enough time increments for the short duration explosive load and thus a smaller time step was chosen.

The numerical approach was successfully able to predict the response of one-way structural elements under various impulsive loads. Some of the results are shown in Figure 2.42.

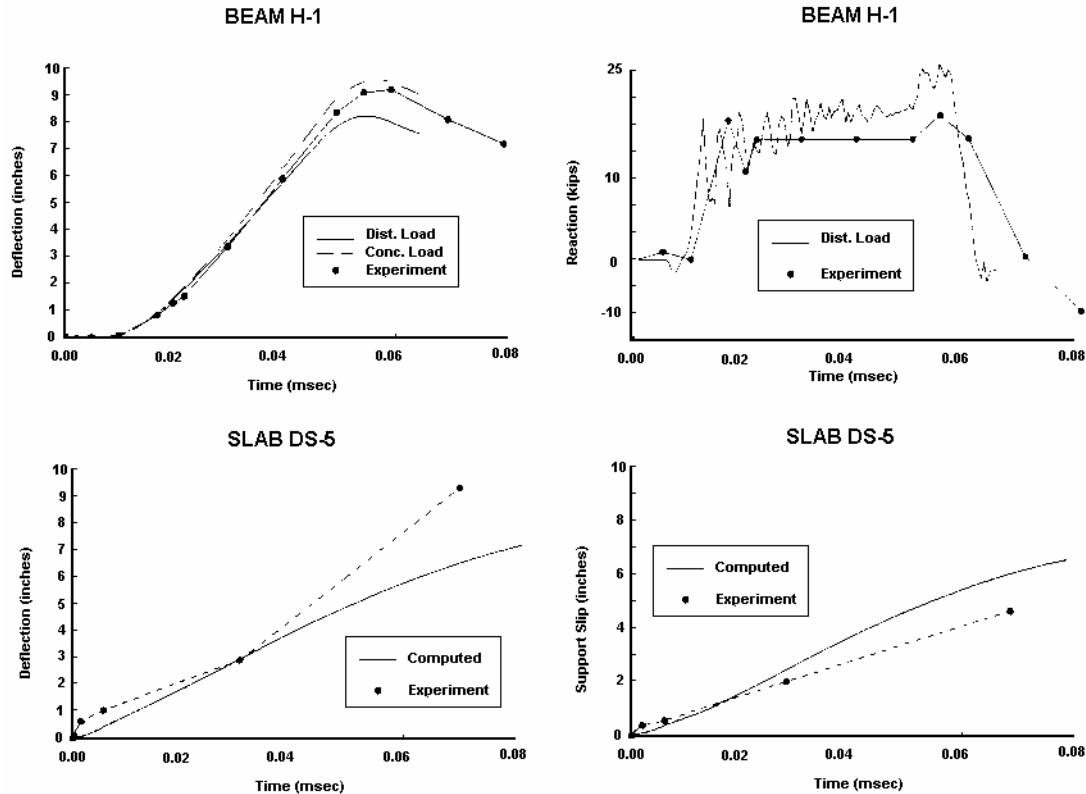


Figure 2.42 Comparison of experimental with numerical results (after Krauthammer et al. (1994)).

2.3.3.2 Dharaneepathy et al. (1995)

Dharaneepathy et al. (1995) examined the design practice of blast resistance for structures. The distance of the explosion from the structure is an important datum governing the magnitude and duration of blast loads. The current design practice is to choose some arbitrary distance for design purposes. Such a notion is shown to be erroneous particularly for tall and slender structures. The growth of the Mach stem and the Triple Point is examined and related back to a critical detonation distance. It is at this distance that the blast pressure and transient dynamic response rise to a maximum for a given charge weight.

Numerical simulations were conducted on 100, 200, and 300 m high cylindrical structures with 5 m diameters. A charge weight of 125 kg of TNT was used at distances varying from 30 to 110 m. The results are shown in Table 2.7 with the numbers in bold representing maximum stresses and displacements.

Table 2.7 Results of distance effect studies on cylindrical towers (after (Dharaneepathy et al, 1995))

H (m)	Diameter (m)	Distance (m)	Displacement Top (mm)	Meridional Stresses at	
				Bottom (t/m ²)	Mid-height (t/m ²)
100	5	30	35	373	481
100	5	40	116	1282	1230
100	5	55.5	98	1754	1252
100	5	70	85	1507	1012
200	5	50	29	202	257
200	5	60	92	319	360
200	5	70.6	146	508	492
200	5	90	113	459	287
300	5	70	32	131	167
300	5	80	52	205	256
300	5	94.6	157	303	194
300	5	110	155	296	176

The results indicated that there exists a critical ground zero distance at which the blast response rises to a maximum and this distance should be used as the design distance.

2.3.3.3 Krauthammer and Ottani (1997)

Finite element simulations were performed on a reinforced concrete blast containment structure designed based on the procedures in TM 5-1300 (1990). The mesh size was varied as well as gravity and loading conditions to determine their influence on the results. The effect of lumping shear reinforcement was also examined (lumping steel into larger diameter bars with increased spacing but maintaining reinforcement ratio). The design load simulated a 300 lb TNT contained explosion. The structure is shown in Figure 2.43 and the mesh in Figure 2.44.

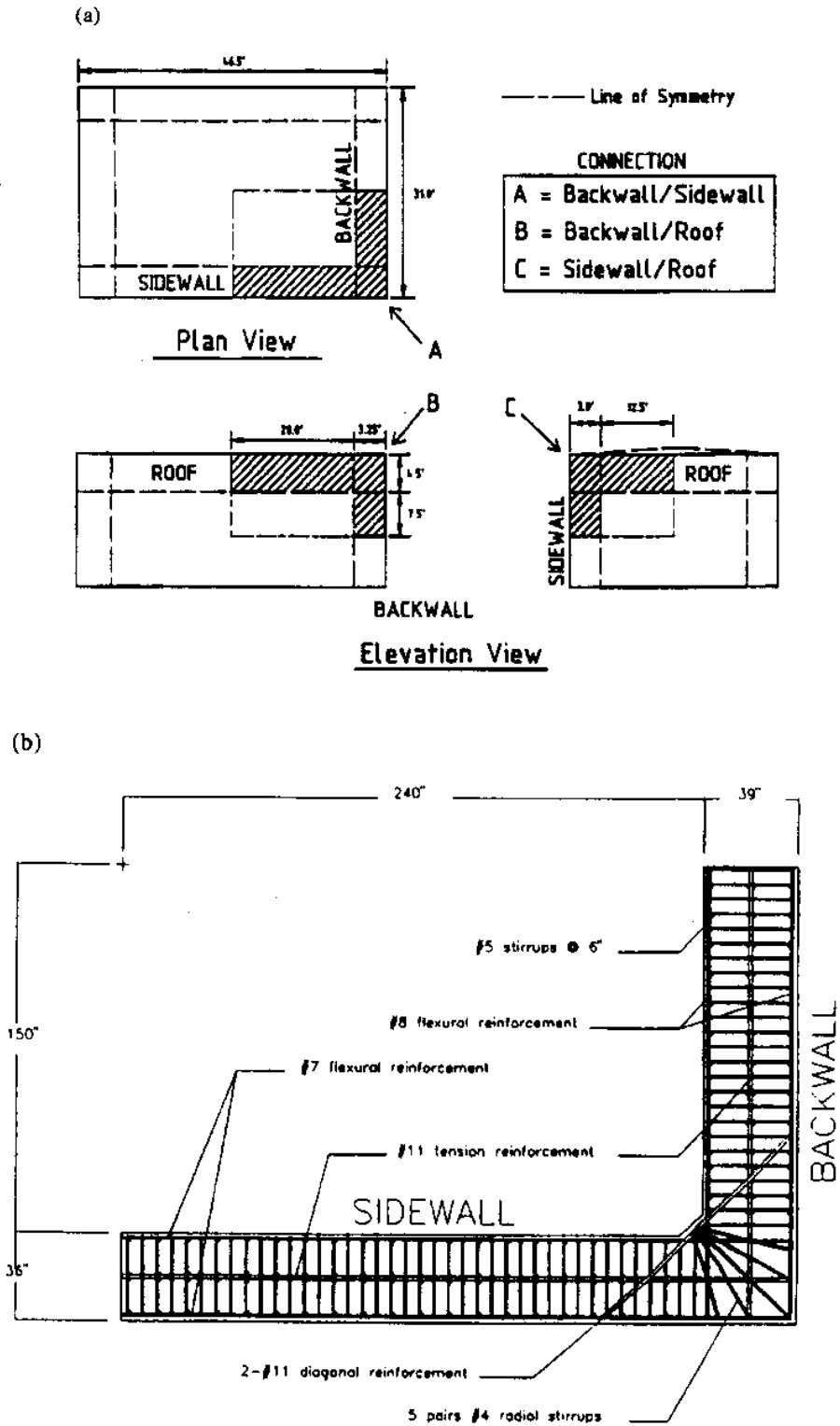


Figure 2.43 Blast containment structure (after Krauthammer and Ottani (1997)).

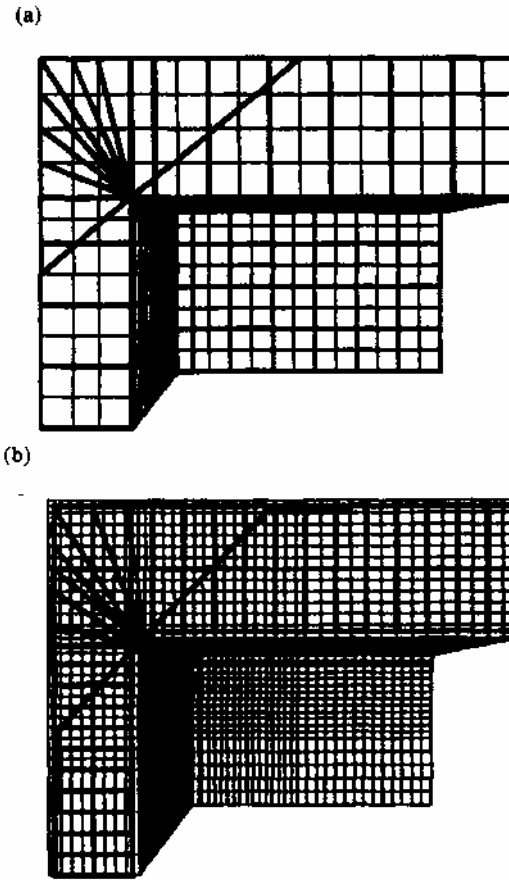


Figure 2.44 Fine and coarse mesh (after Krauthammer and Ottani (1997)).

The effect of varying mesh size indicated that a fine mesh was very important to simulate realistic deformations. Lumping shear reinforcement in the simulation did not capture the correct stresses. Thus, shear reinforcement must be accurately spaced to properly model its role. In addition, it is important to perform gravity initialization prior to the application of blast loads especially if blast loads are applied to heavy structural elements that can cause significant forces on lighter components.

2.3.3.4 Armstrong et al. (2002)

Four experiments conducted at the U.S. Army Engineer Research and Development Centre (ERDC) were simulated using SHAMRC in order to evaluate the accuracy of the code. The experiments included a free-field experiment, a barrier wall experiment, a single structure experiment, and an experiment with a barrier wall and a

structure previously conducted by Joachim et al. (2002). The explosive PBX-9407 was used in the experiments. However, SHAMRC did not have the equation of state constants for PBX-9407 and thus C4 was used. Previous studies have shown that using the C4 equation of state constants would provide similar predictions had PBX-9407 been used. SHAMRC results were also compared with CONWEP's capabilities. Results from the free field experiments can be seen in Figure 2.45 (a) and (b) while some of the results from the other experiments can be seen in Figure 2.46 (a)-(c).

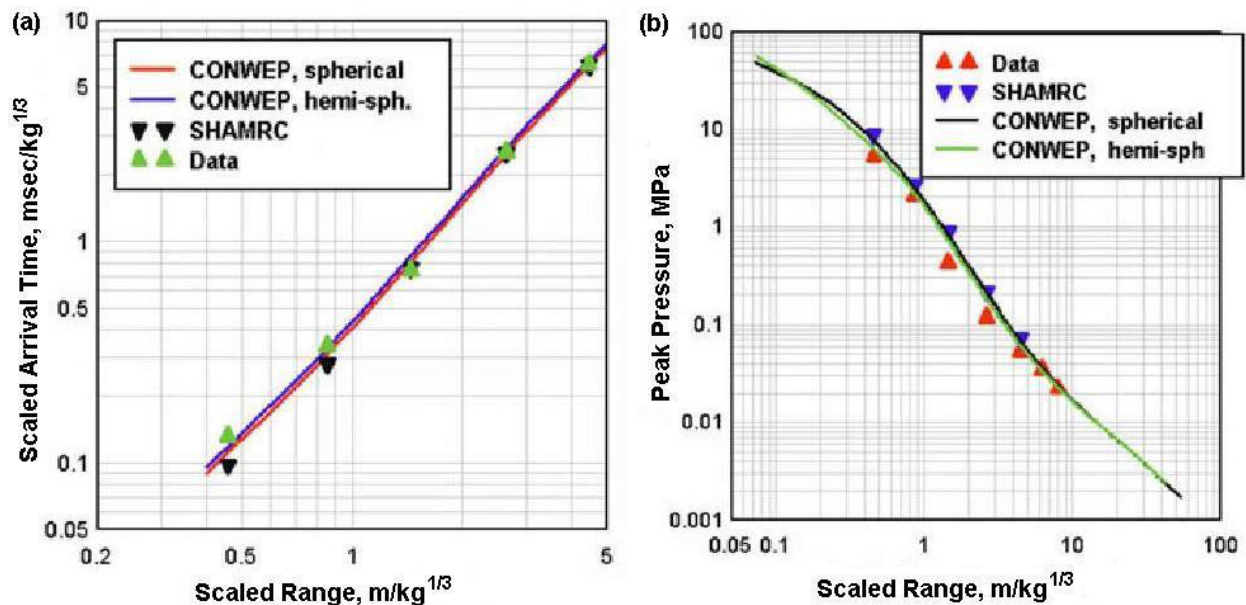


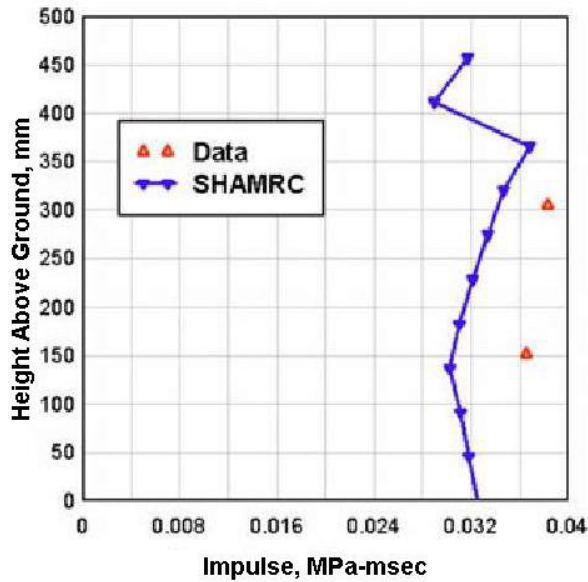
Figure 2.45 Free-field results comparing SHAMRC, CONWEP, and data (after Armstrong et al. (2002)).

Generally, free field results from SHAMRC are quite good. However, at close standoffs (small scaled range) the arrival time is under-predicted, the peak pressure is over-predicted, and maximum impulse is under-predicted.

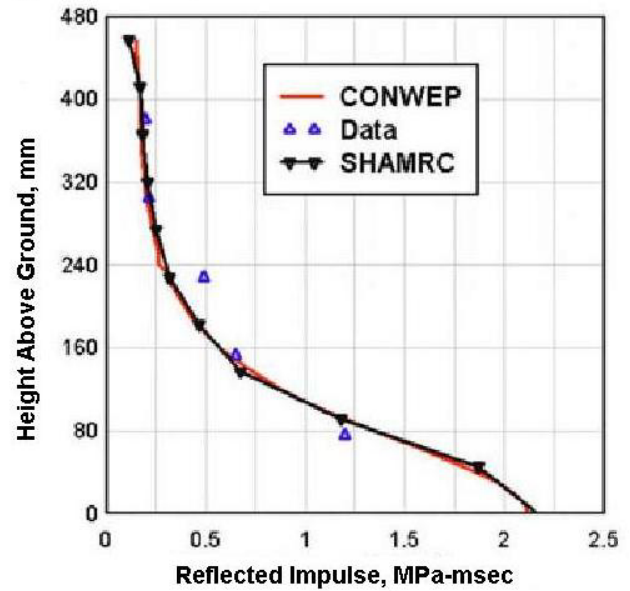
Results from the single building experiment showed that peak pressure comparisons as well as reflected impulse comparisons between SHAMRC and experiment were very good. SHAMRC was found to model wave propagation around the structure in a very accurate manner as well as the pressures on the roof, rear wall, and side wall. Experimental data for comparison with the blast barrier and the structure were not yet authorized for release.

Validation of SHAMRC against free-field and structure experiments have indicated that SHAMRC does a good job of predicting air blast pressures and the propagation of those pressures around corners.

(a) Impulse at center of Rear Wall



(b) Reflected Impulse on center of Front Face



(c) Wrapping of Blast Wave Around the Structure

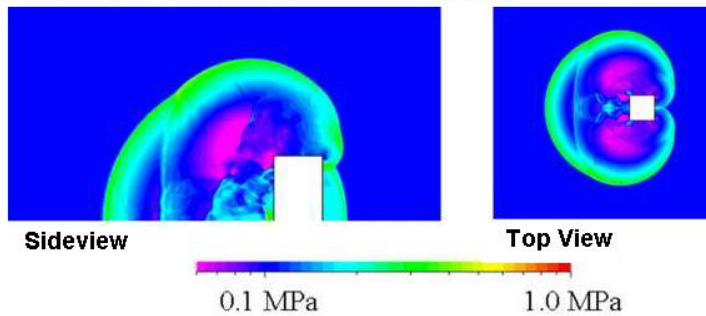


Figure 2.46 SHAMRC Results with a Structure (after Armstrong et al. (2002)).

CHAPTER 3 THEORETICAL BASIS FOR PROGRAM *VECTOR-BLAST*

3.1 Introduction

The theoretical approach behind the computer program *VecTor-Blast* is examined in this chapter. Full numerical formulations and the limitations are described.

3.2 Explosives

The formulations derived will apply only to conventional high explosives with ideal behaviour as described in Chapter 2.

A high explosive is characterized by the extreme rapidity with which its decomposition into a gaseous state occurs (Technical Service of the Explosives Division, 1946).

Since a significant amount of data exists for TNT explosions, the predicted behaviour of other explosives is based on TNT data. Much of the data pertaining to TNT is limited to certain charge shapes such as bare spheres or bare hemispheres (TM 5-1300, 1990).

The equivalency between TNT and other high explosives is achieved through energy output (heat of combustion) given in Eq. 2.17. The alternative method of using equivalency based on experiment (Eqs. 2.19 and 2.20) has the disadvantage that the impulse and pressure curves for the explosive must be known beforehand and this is not always the case. The TNT equivalency method using heat of combustion is only valid if the other explosive is also a high explosive exhibiting ideal behaviour.

Terrorists often use non-ideal explosives such as ANFO (a mix ammonium nitrate and fuel oil). Calculation of TNT equivalency is not straight forward and requires

experimental investigation as the equivalency can vary anywhere from 0.3 to 0.8 depending on the amount of explosive (diameter of explosive).

The explosives included as options in *VecTor-Blast* are shown in Table 3.1.

Table 3.1 Available Explosives

Explosive	Heat of Combustion (kJ/mol)
60% Nitroglycerin Dynamite	2710
Amatol 80/20	2650
Compound B (60%RDX, 40%TNT)	5190
HMX	5680
Lead Azide	1540
Mercury Fulminate	1790
Nitroglycerin (liquid)	6700
PBX - 9407	5740
PE4	5111
Pentolite 50/50	5110
PETN	5800
RDX	5360
SEMTEX	5660
Tetryl	4520
TNT	4520

In addition to the built-in explosives, the user has the option of specifying a custom explosive instead of using the explosives from Table 3.1. The user must enter the heat of combustion of the custom explosive.

Different charge shapes, casings, or containers can also affect the behaviour of the explosive but these effects are not taken into account in *VecTor-Blast*. Explosives with casings can be analyzed provided the ratio of casing weight to explosive weight is small such that the energy lost by breaking the casing is negligible. Furthermore, the effects of fragments, released from cased explosives, impacting the target are not modelled in *VecTor-Blast*.

3.3 Structures

In order to keep this research manageable and within the boundaries of available data, the analyses will be limited to cuboid structures with few or no openings.

3.4 Free Field Blast Parameter Data

All TNT blast parameter data was extracted from a series of curves from TM 5-1300 (1969, 1990). These curves are generated from an extensive amount of data collected from bare spherical TNT explosions in free air at sea level and data from bare hemispherical TNT surface explosions at sea level.

Whenever possible, data was extracted from TM 5-1300 (1990) as it is the most recent source. However, this was not always possible. Thus some data from TM 5-1300 (1969) had to be used. This is particularly true for free-field blast parameters.

Since the equations from the curves were not easily obtainable, the curves were scanned to create graphic files. The graphic files were then imported into a computer program which was used to extract the data for the existing curves. Equations, formulated from the extracted data using a statistics program, were then implemented into *VecTor-Blast*. The comparison between the results of the equations for the curves and actual data can be seen in Appendix B. To remain within the boundaries of available data, the scaled distance must remain within the values shown in Table 3.2.

Table 3.2 Limitations of Scaled Distance

	Scaled Distance (m/kg ^{1/3})	Scaled Distance (ft/lb ^{1/3})
Spherical Air Burst	0.06<Z<11.9	0.15<Z<30
Hemispherical Surface Burst	0.12<Z<19.8	0.3<Z<50

3.5 The Origin

All distances are measured from the same origin point, O. The origin in *VecTor-Blast* and the sign convention for directions are shown in Figure 3.1.

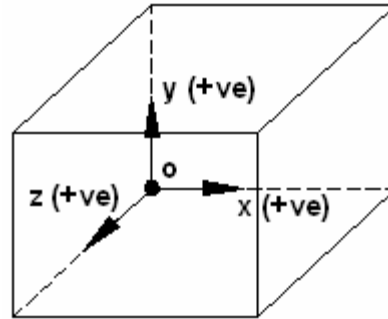


Figure 3.1 Origin.

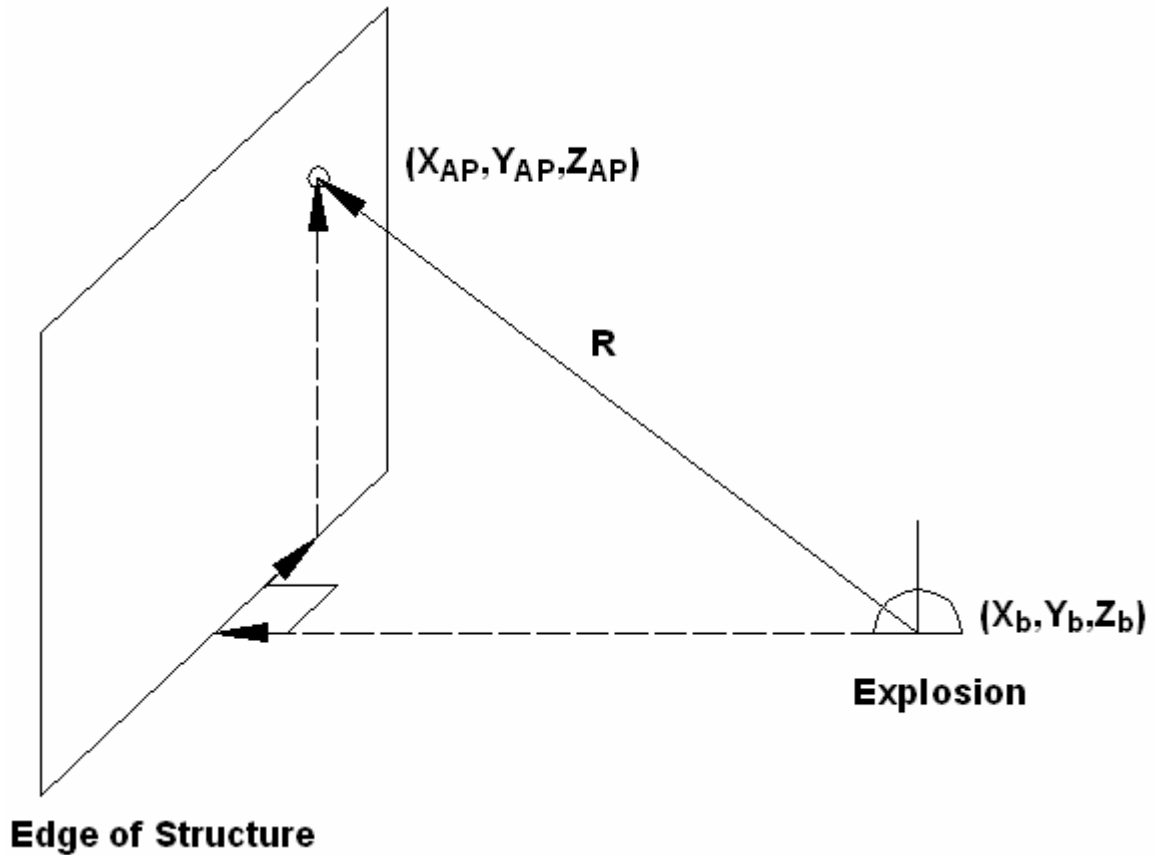
3.6 Ray Paths

The ray path of the blast wave is the path of one point on the shock front. The point on the structure for which the loading history is being calculated will be known as the analysis point (AP). The shortest ray path will correspond to the shortest distance the wave must travel to reach the AP and therefore the path of the blast wave to that point. The scaled distance, calculated from the ray path distance by Eq. 2.09, is used to calculate the blast parameter data for the AP.

3.6.1 Ray Paths on the Blast Face

3.6.1.1 Ground Burst or Free Air Bursts

For an explosion on the ground or one directly above the structure, calculating the distance of the ray path, R , is achieved through geometry shown in Figure 3.2.

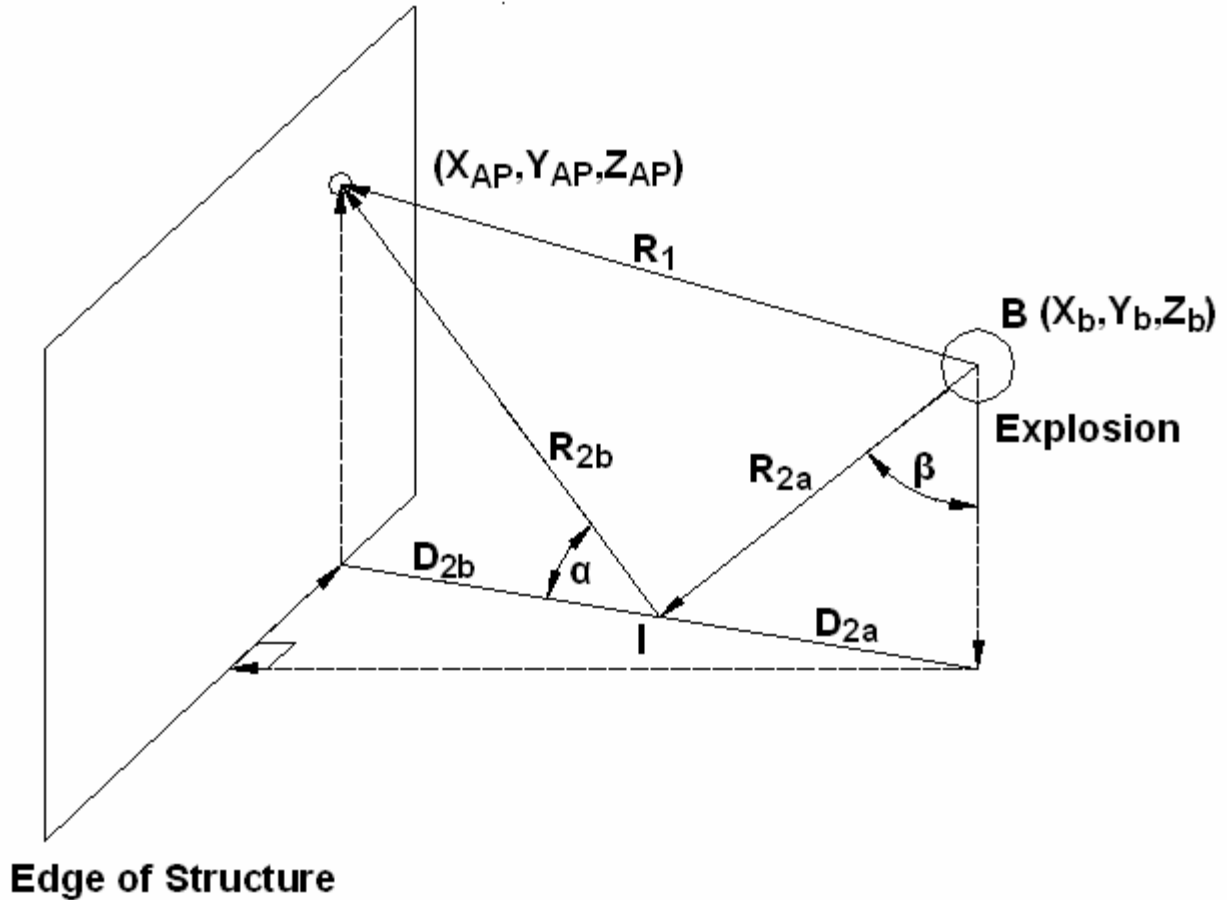


$$R = \sqrt{\left((X_b - X_{AP})^2 + (Y_b - Y_{AP})^2 + (Z_b - Z_{AP})^2\right)}$$

Figure 3.2 Simple ray path calculation.

3.6.1.2 Air Bursts

For the case where the explosion is located such that blast waves can be modified by the ground before reaching the structure, two potential ray paths, R_1 and R_2 , are calculated. Ray path R_1 is the distance with the wave arriving directly from the explosion. Ray path R_2 is the distance including the ground reflection and is the sum of R_{2a} and R_{2b} as shown in Figure 3.3.



$$R_1 = \sqrt{((X_b - X_{AP})^2 + (Y_b - Y_{AP})^2 + (Z_b - Z_{AP})^2)}$$

$$R_2 = R_{2a} + R_{2b}$$

Figure 3.3 Ground reflected ray path calculations.

This will result in two pressure-time histories combining at the AP. The ray path, R_1 , for the incident wave is calculated as aforementioned in Section 3.6.1.1.

The formulation for calculating the ground reflected ray path, R_2 , is obtained from Kinney (1985) for waves of constant pressure and ideal gas conditions but modifications are introduced to account for the deterioration of blast wave parameters with distance.

For a mathematical analysis of oblique wave reflection, an important preliminary step is to transform the problem into its counterparts in steady flow as shown in Figure 3.4.

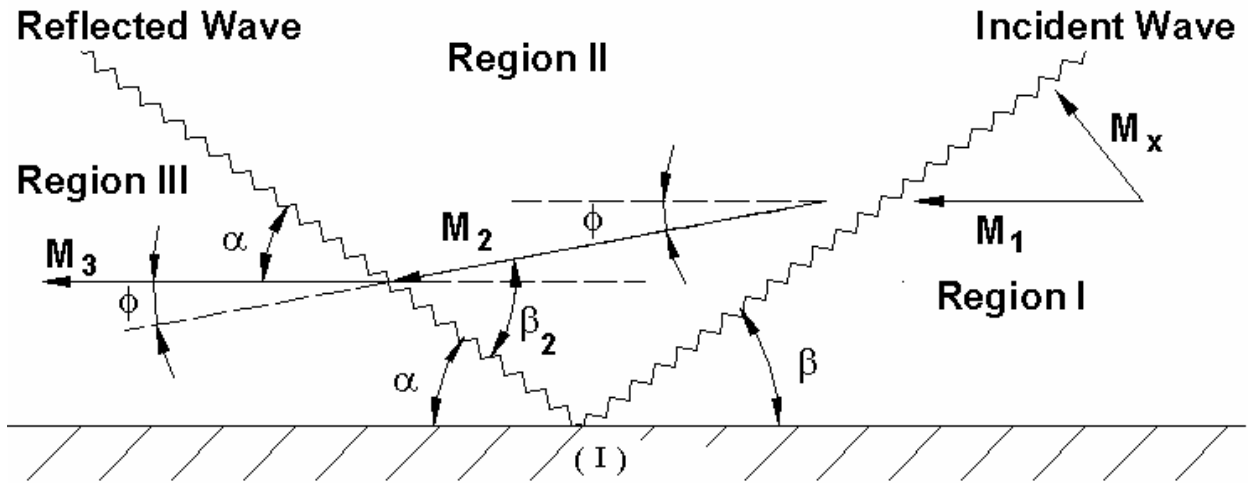


Figure 3.4 Steady flow counterpart of oblique reflection (after Kinney (1985)).

The steady flow stream is divided into three regions which are separated by two stationary shocks. Region I is the undisturbed atmosphere. Region II is the new existing atmospheric conditions produced by the passage of the incident shock front. Upon striking the ground surface, reflection occurs and the wave travels back through Region II causing shock enhancement. Region III represents new atmospheric conditions produced behind the reflected shock front.

Steady flow conditions are accomplished by subtracting from all the various velocities the velocity of the incoming blast wave at intersection point I and by considering a medium moving from left to right through the stationary shocks. The medium to the right of the incident shock is then considered to be streaming in steady flow, into an oblique shock plane oriented at angle β with the surface. On passing through an oblique shock (incident shock) into Region II, the flow is deflected toward the surface. The shock is re-deflected to a position parallel with the ground as it passes through the second oblique shock (reflected shock) into Region III (Kinney, 1985).

The mach number of the incoming flow is calculated as follows:

$$M_1 = \frac{M_x}{\sin \beta} = \frac{\left(\sqrt{1 + \frac{6P_s^+}{7P_a}} \right)}{\sin \beta} \quad (3.01)$$

where M_x is the Mach number for the component normal to the shock wave, P_s^+ is the incident overpressure at point I (Figure 3.4), P_a is ambient atmospheric pressure (101.3 kPa in *VecTor-Blast*), and β is the angle of incidence.

The angle, θ , through which the flow is deflected, is calculated as follows:

$$\frac{\tan(\beta - \phi)}{\tan \beta} = \frac{5 + (M_1 \sin \beta)^2}{6(M_1 \sin \beta)^2} \quad (3.02)$$

The Mach number, M_2 , behind the shock front is found from:

$$[M_2 \sin(\beta - \phi)]^2 = \frac{5 + (M_1 \sin \beta)^2}{6(M_1 \sin \beta)^2} \quad (3.03)$$

The angle, β_2 , which the reflected shock makes with the stream in Region II is given by:

$$\frac{\tan(\beta_2 - \phi)}{\tan \beta_2} = \frac{5 + (M_2 \sin \beta_2)^2}{6(M_2 \sin \beta_2)^2} \quad (3.04)$$

Finally, the angle of deflection, α , is calculated by:

$$\alpha = \beta_2 - \phi \quad (3.05)$$

Initially, the angle of incidence, β , is unknown and an iteration procedure is developed to cycle through angles of incidence, β , to calculate corresponding angles of deflection, α . The angle of incidence will range from almost 0 to β_{\max} . The angle β_{\max} is the smallest of the angle necessary for Mach Stem formation or the angle of incidence, β_1 , made with the structure (see Section 3.6.1.3).

From the angles, β and α , the height to which the ground reflected wave will travel upon reaching the structure can be found. If this height equals the height of the

AP, the correct angles have been found. The iteration procedure is summarized in Figure 3.5.

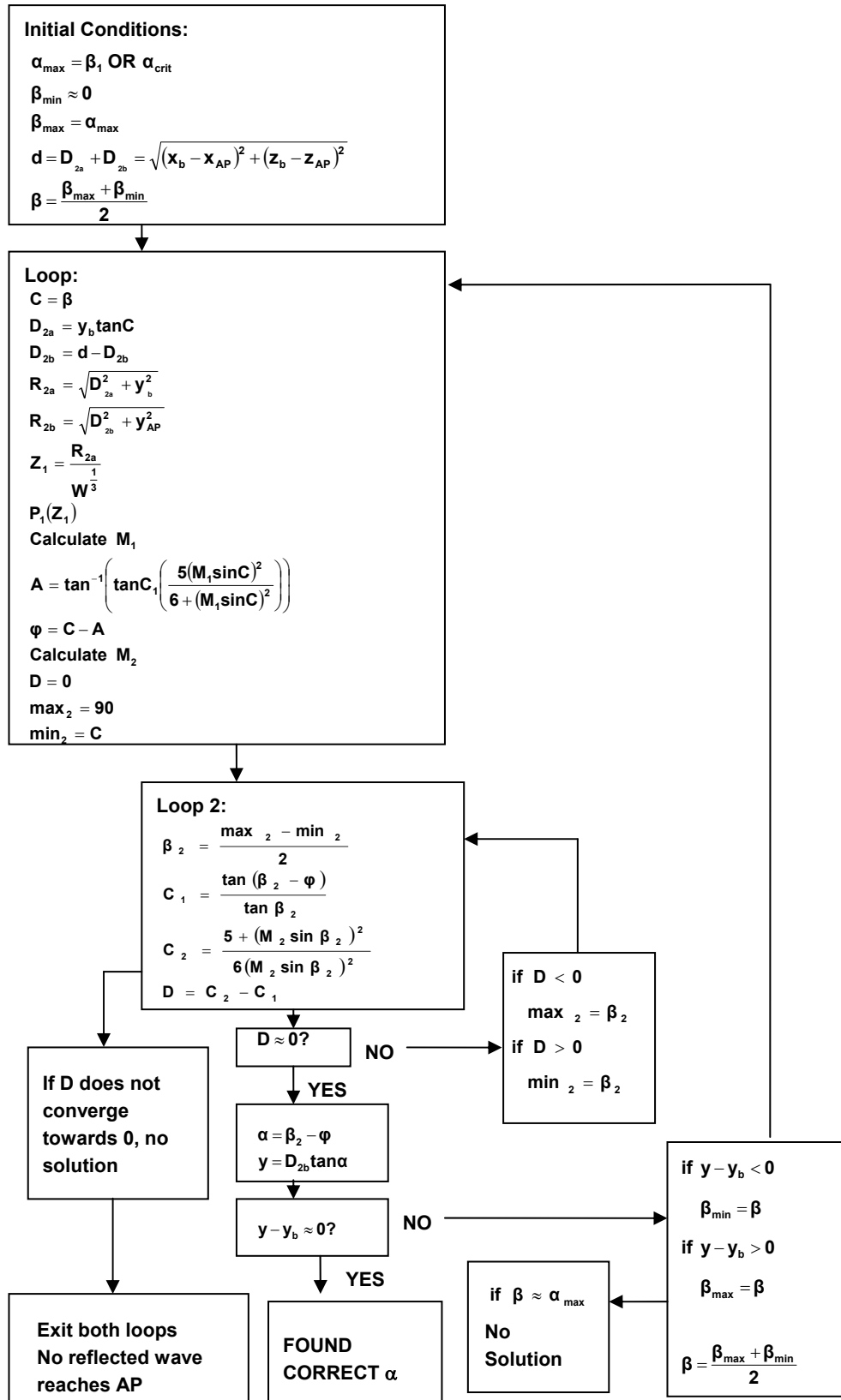


Figure 3.5 Flow chart of the iteration procedure.

Once the angles have been determined, the distances R_{2a} and R_{2b} can be calculated from geometry. Blast parameters cannot be found directly by simply calculating the scaled distance using R_2 because ground enhancement effects have not been included. Since only free-field parameter curves exist, modifications must be made to account for the blast parameter enhancement (see Section 3.6.1). The recommendation, after consultation with experts (Mohanty, 2003), is to create an equivalent scaled distance.

The pressure, from a detonation with equivalent TNT mass, w_0 , just before the wave hits the ground is found first (see Figure 3.3):

$$z_1 = \frac{R_{2a}}{w_0^3} \quad (3.06)$$

$$P_s^+(z_1) \quad (3.07)$$

where P_s^+ is the total incident pressure.

The effects of ground reflection when the wave hits the ground (see Section 3.6.1) are taken into account through the following:

$$P_m(P_s^+, \beta) \quad (3.08)$$

where P_m is the normal reflected component of the pressure.

The total reflected wave is found from:

$$P_r = \sqrt{P_m^2 + (P_s^+ \sin \beta)^2} \quad (3.09)$$

The equivalent weight, w_1 , which would produce the same pressure in free-field, is then found by:

$$z_2(P_r) \quad (3.10)$$

$$w_1 = \left(\frac{R_{2a}}{z_2} \right)^3 \quad (3.11)$$

The modified scaled distance becomes:

$$z_3 = \frac{(R_{2a} + R_{2b})}{w_1^{\frac{1}{3}}} \quad (3.12)$$

The pressure just before the wave hits the structure can be found by using the modified scaled distance, z_3 . The same procedure is used to maintain impulse.

It is possible for only one ray path to the AP to exist from a detonation above ground if the following conditions occur:

1. A Mach stem forms, forming one wave which is plane along the height.
2. The geometry is not compatible.

It is possible for the geometry to be incompatible with wave reflection theory as the maximum angle of deflection is about 45° for incident shock waves approaching an infinite mach number.

3.6.1.3 Mach Stem

It is possible for a mach front to form from an airburst. The formulation describing if a mach front will form, and what its characteristics will be, are discussed as follows.

3.6.1.3.1 Mach Stem Formation

A mach front can only form provided the angle of incidence is at least greater than a minimum angle, α_{crit} . This minimum angle, α_{crit} , is obtained from Baker et al. (1983), (see Figure 2.9 or Appendix B). This angle is compared against the angle of incidence, β_1 , which is calculated from the geometry in Figure 3.6. Provided β_1 is larger than the minimum angle for mach stem formation, a mach front will form.

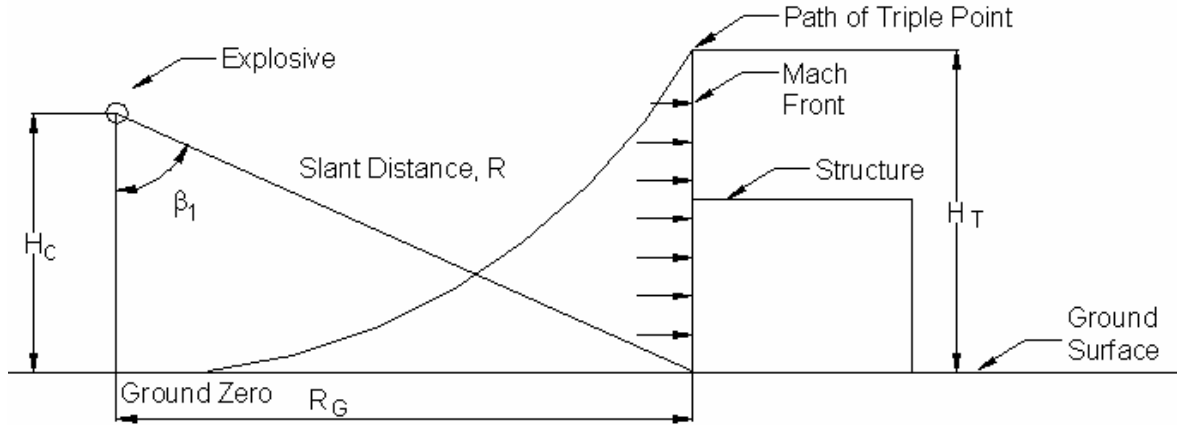


Figure 3.6 Geometry of mach stem formation.

To conclude whether the AP is loaded by the mach front, the height of the triple point at the face of the structure must be determined. The scaled triple point height, H_T^w , can be calculated from curves found in TM 5-1300 (1990) (see Appendix B). If the triple point height is higher than the AP, the AP is loaded by a mach front. Conversely, if a mach front does not form or the triple point height does not reach the AP, the scenario described in Section 3.6.1.2 occurs.

Data for the scaled triple point height is limited to the values shown in Table 3.3.

Table 3.3 Data limitations for mach stem formation curves

Scaled Charge Height, H_c^w	(m/kg^{1/3})	0.39	0.59	0.79	1.19	2.78
	(ft/lb^{1/3})	1	1.5	2	3	7
Scaled Distance, z	(m/kg^{1/3})	$Z \leq 3.58$	$Z \leq 4.36$	$Z \leq 5.55$	$Z \leq 5.95$	$Z \leq 7.14$
	(ft/lb^{1/3})	$Z \leq 9.04$	$Z \leq 11$	$Z \leq 14$	$Z \leq 15$	$Z \leq 18$

3.6.1.3.2 Mach Stem Parameters

Once it has been concluded that a mach front will load the AP, the parameters of the mach front are calculated to determine the load history on the AP as indicated in TM 5-1300 (1990).

The peak incident pressures and impulse are computed not from the free-field curves but from separate curves for mach stem formation (Appendix B). These curves

take into account the pressure and impulse enhancement in a mach stem from the combining of incident and ground reflected waves. The pressures and impulses are then used to find corresponding values of scaled distance from the free-field blast parameter curves (Figure 2.6, Appendix B). Two scaled distances will be found; one corresponding to incident impulse, the other to pressure. The scaled distance corresponding to pressure is used to calculate arrival time and wave velocities while the scaled distance corresponding to impulse is used to calculate negative incident impulses and positive and negative durations as suggested in TM 5-1300 (1990).

3.6.1.4 Flow Chart for Blast Face

A flow chart is shown in Figure 3.7 depicting the process outlined in Section 3.6.1 in *VecTor-Blast*.

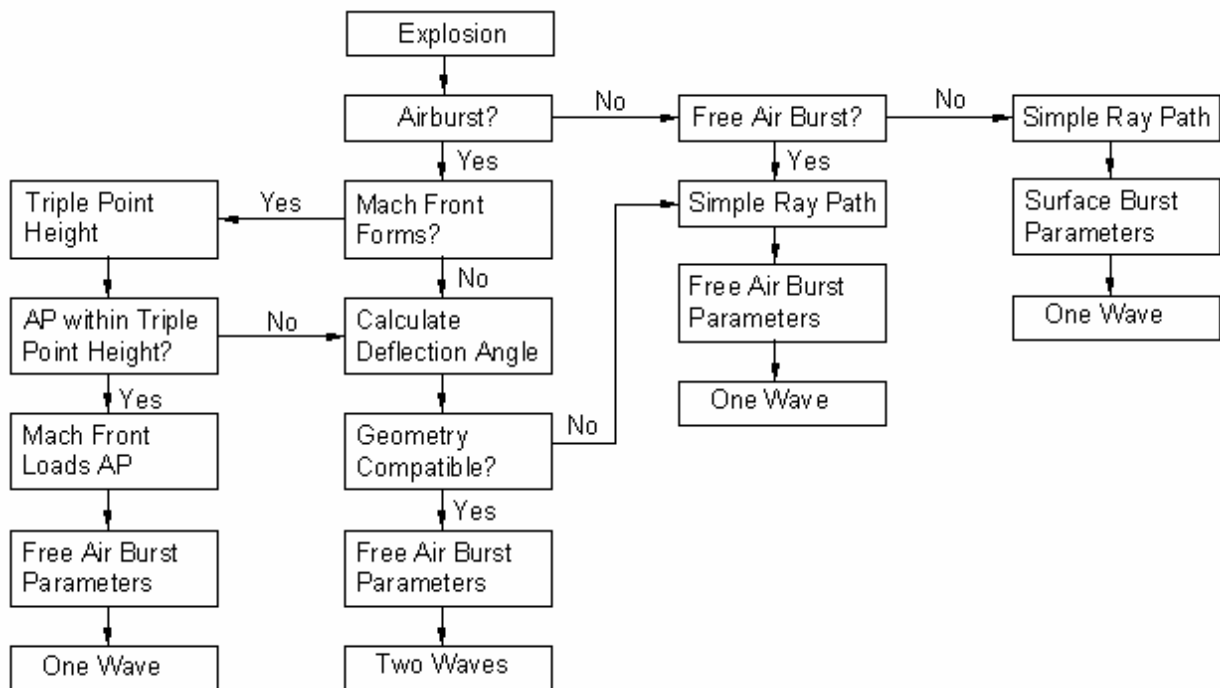


Figure 3.7 Flow chart depicting the process for determining the loading on the blast face.

3.6.2 Ray paths on Sides, Roof, and Rear

3.6.2.1 Diffraction

When a point on the wave front hits a corner, it diffracts around it. The process of diffraction causes energy to be sent into all directions as shown in Figure 3.8.

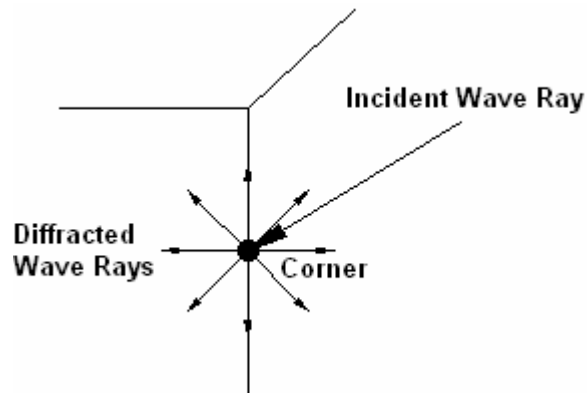


Figure 3.8 Diffraction at a corner.

The pressure and impulse loading the structure are greatly reduced as only part of the energy from the incident wave ray is transferred to the structure. The loss of energy also slows down the diffracted wave. Realistically, a point on the side of the structure would be loaded by many diffracted wave rays as the entire wave front diffracts around the corner as shown in Figure 3.9.

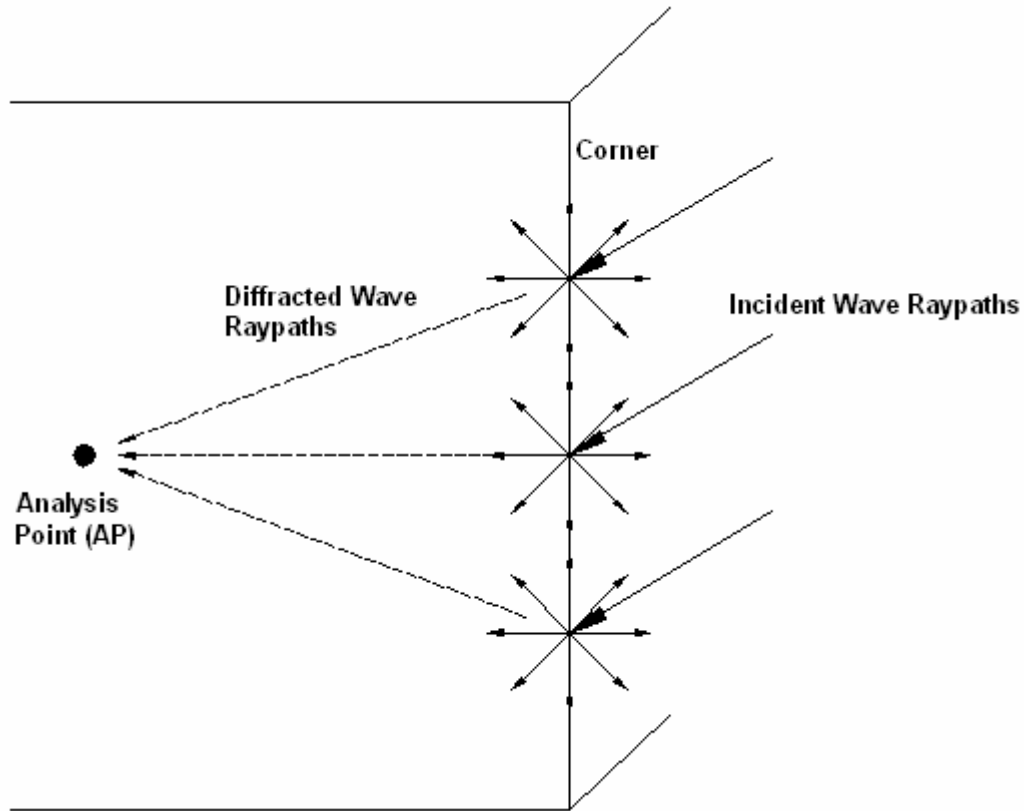


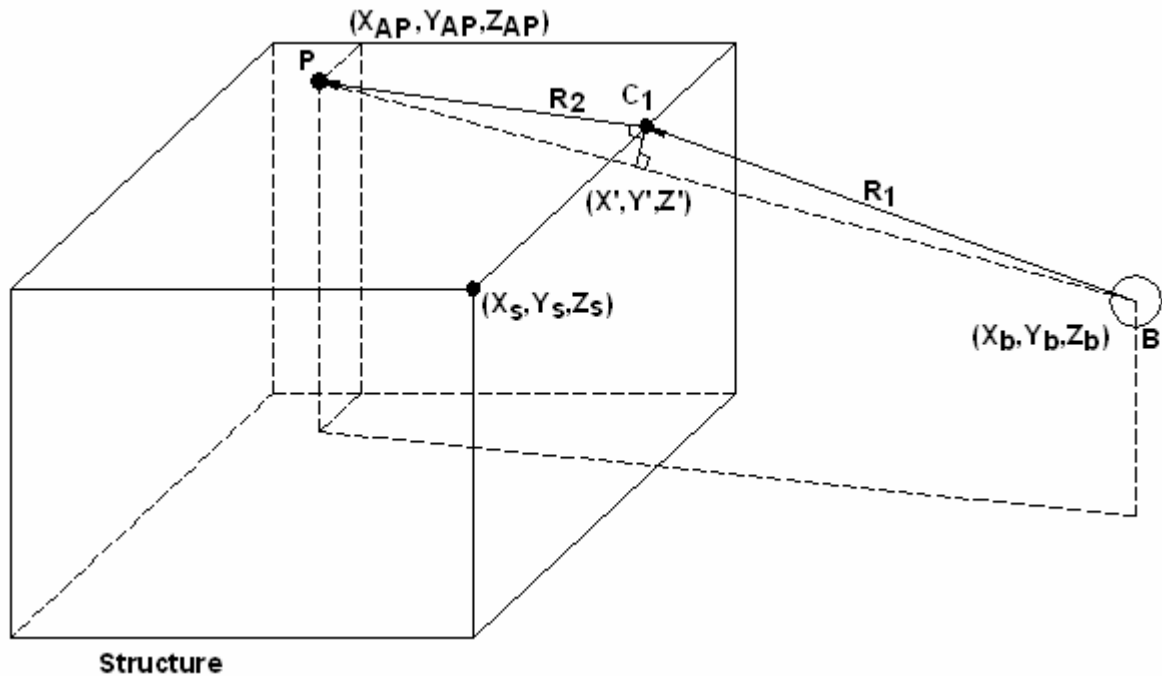
Figure 3.9 Diffraction loading on the Analysis Point (AP).

Each diffracted wave ray will arrive at different times. The rays travelling the shortest distance will thus be the strongest. The diffraction phenomenon is quite complex and determining the contribution from all diffracted rays is difficult in addition to determining the energy loss, arrival times, and durations. The most exact manner would be to divide the corner into a mesh of nodes and add in time the contribution at the AP of every diffracted ray coming from each node.

Consultation with experts suggested an approximate method (Mohanty, 2004). The ray travelling the shortest distance would be the most damaging and have the highest pressure and impulse. The pressures coming about from other rays would affect the AP later in time relative to the ray travelling on the shortest ray path and have smaller peak pressures. This approximate method assumes the shortest ray path will capture the peak pressure from all combining diffracted waves at the AP.

3.6.2.2 Calculating Ray Paths

Ray paths are calculated based on a straight line from the explosion to the AP. Few guidelines exist for determining the shortest distance from a point in space to a point on the surface of a cube. Two methods were adopted. The first involves connecting the point where the explosion occurs to the AP and projecting the line on to the surface of the cuboid. The line BP is the direct distance from the explosion to the AP in Figure 3.10.



$$X' = X_s$$

$$Y' = Y_s$$

$$\frac{X_b - X_{AP}}{X' - X_{AP}} = \frac{Z_b - Z'}{Z_b - Z_{AP}}$$

$$Z' = Z_b - \frac{(X_b - X')(Z_b - Z_{AP})}{(X_b - X_{AP})}$$

$$R_1 = \sqrt{((X_b - X')^2 + (Y_b - Y')^2 + (Z_b - Z')^2)}$$

$$R_2 = \sqrt{((X' - X_{AP})^2 + (Y' - Y_{AP})^2 + (Z' - Z_{AP})^2)}$$

Figure 3.10 Ray path calculations.

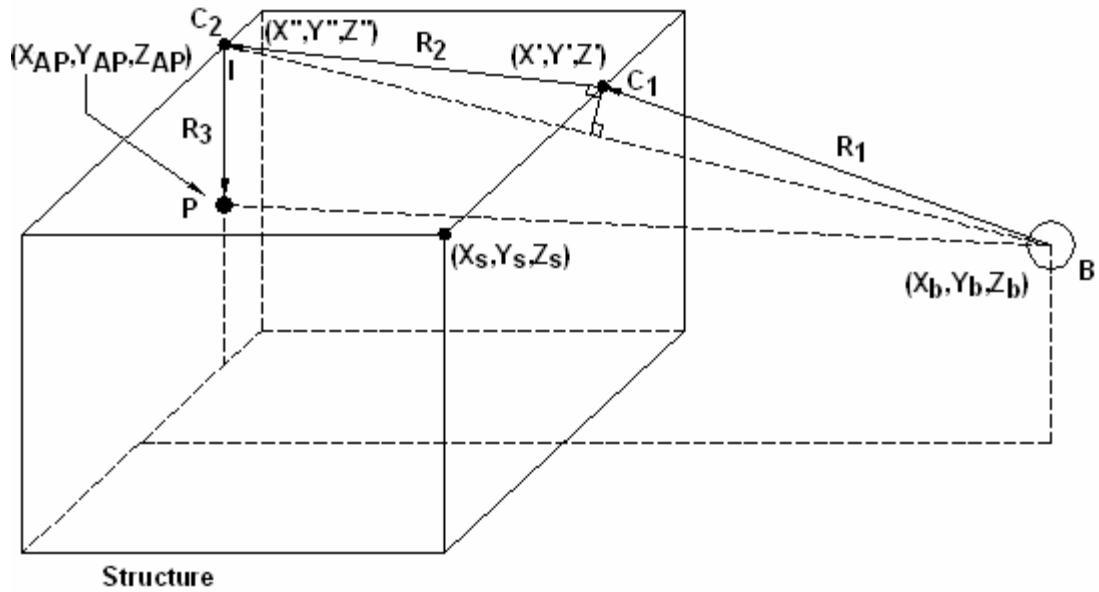
The coordinates X' , Y' , and Z' of the intersection point I at the corner are found from ratios of the other distances for a structure with dimensions X_s , Y_s , and Z_s . The same calculation methods are valid for analysis points on the sides provided the y and z variables are interchanged.

The second method for calculating the ray path involves simply projecting the AP to the intersection point with a horizontal line such that the coordinates of point C_1 become:

$$\begin{aligned}X' &= X_s \\Y' &= Y_{AP} \\Z' &= Z_{AP}\end{aligned}$$

It was noticed that under certain extreme geometric conditions, this method provided a shorter distance so both methods were implemented into *VecTor-Blast* and the method giving the shortest distance was used to calculate the ray path distance.

The outlined calculations can be extended to an AP on the rear of the structure with the following modifications shown in Figure 3.11.



Note: Only one ray path is depicted here. The effects of diffraction around the sides and on to the analysis point would also have to be considered.

$$X' = X_s$$

$$Y' = Y_s$$

$$Z' = Z_b - \frac{(X_b - X')(Z_b - Z_{AP})}{(X_b - X_{AP})}$$

$$X'' = X_{AP}$$

$$Y'' = Y_{AP}$$

$$Z'' = Z_{AP}$$

$$R_1 = \sqrt{((X_b - X')^2 + (Y_b - Y')^2 + (Z_b - Z')^2)}$$

$$R_2 = \sqrt{((X' - X'')^2 + (Y' - Y'')^2 + (Z' - Z'')^2)}$$

$$R_3 = \sqrt{((X'' - X_{AP})^2 + (Y'' - Y_{AP})^2 + (Z'' - Z_{AP})^2)}$$

Figure 3.11 Ray path calculations for an AP on the rear face.

Modifications for the second method where vertical and horizontal lines are projected from the AP through corner intersection points C_1 and C_2 give coordinates as follows:

$$\begin{aligned}
 X' &= X_s \\
 Y' &= Y_{AP} \\
 Z' &= Z_{AP} \\
 X'' &= X_{AP} \\
 Y'' &= Y' \\
 Z'' &= Z'
 \end{aligned}$$

In the case where ground deflected waves become involved, the same method is used however the ray path distance is initially calculated from point I (see Figure 3.3 and 3.4). The calculated coordinates of the intersection point, C_1 , are used directly in the iteration process (see Section 3.6.1.2) where they are simply substituted for X_{AP} , Y_{AP} , and Z_{AP} . The coordinates of point C_1 change as iteration proceeds because point I slowly moves due to the iteration through the various angles of incidence. The distance from the explosion to the ground, BI , is then added to the ground reflected ray path distance, R_2 , to obtain the final distance.

For the case where a mach stem forms, the formation of a plane wave along the height causes the Y term in the aforementioned calculations to be set to zero and the ray path distance is calculated as mentioned at the beginning of this section.

3.7 Wave-Structure Interaction

3.7.1 Wave Reflection

3.7.1.1 Positive Pressure and Impulse

As the blast wave hits the front face of the structure, it will undergo enhancement in a similar fashion as when the wave hit the ground surface. The actual peak pressure, P_r^+ , on the AP is obtained by multiplying the incident pressure, P_s^+ , by a reflection coefficient, $C_{r\beta}$.

$$P_r^+ = C_{r\beta} P_s^+ \quad (3.13)$$

In 3.13, P_r^+ , is the normal component of the wave while P_s^+ is the total incident peak wave pressure. The other components could also be multiplied by reflection

coefficients but since they are travelling at 90° to the structure's surface (for cuboid structures), the reflection coefficient is 1 and the component peak pressures are not enhanced.

The reflection coefficients, as a function of angle of incidence and incident pressure, are shown in Figure 2.10 (see Appendix B) for incident pressures up to 6000 psi (41300kPa).

As the pressure is enhanced with reflection, impulse is also enhanced. Curves in TM 5-1300 (1990), depicting scaled reflected impulse as function of angle of incidence and incident pressure, are used to calculate reflected impulse. The computed scaled reflected impulse is associated with the normal components. Non-normal components do not undergo impulse enhancements for the same reason that they do not undergo pressure enhancement.

3.7.1.2 Negative Pressure and Impulse

Since the normal positive pressure is enhanced by wave reflection, the negative pressure is also enhanced. Peak negative pressures for normal components are calculated from peak positive reflected pressures as described in TM 5-1300 (1990). The negative pressures can be found directly from either Figure 2.6 or Figure 2.7 depending on the location of detonation provided the scaled distance is modified to account for the enhancement. The scaled distance corresponding to the normally reflected positive pressure is found and this scaled distance is used to find the normally reflected negative pressure (Appendix B).

For non-normal components, the negative pressure corresponds to the incident negative pressure. The incident negative pressure is found using the scaled distance employed to find the positive incident pressure.

The same formulation is used to find reflected negative impulses and incident negative impulses.

3.7.2 Wave Diffraction

The shortest ray path method described in Section 3.6.2 provides a distance with which a scaled distance can be calculated. The scaled distance is used to

determine incident (side-on) blast parameters. Since the wave does not directly strike the surfaces when diffracting, no wave reflection enhancement occurs. Furthermore, pressures act essentially only normal to the surface. By using the scaled distance however, the actual energy lost through the diffraction process has not been taken into account. As previously mentioned, a wave diffracting around a corner slows down, peak impulses and pressures are reduced, and the duration tends to increase.

Little information is available on direct methods to calculate the change in blast parameters due to diffraction. The most detailed method described in TM-1300 (1990) does not take into account the reduction in wave speed but does take into account peak pressure reductions and duration increases. The method uses wavelengths over a surface length to come up with average durations and an equivalency factor C_E for pressure reductions. The factor C_E takes into account the losses from diffraction in addition to creating an average uniform pressure over an area. The average durations are only valid over the specified surface length. This method does not work well for determining individual pressures at specific points.

Ripley et al. (2004) used a factor of 0.35 to reduce side-on overpressures to correlate with experimental data (Mohanty, 2004). In essence, for every number of diffractions, n , a ray path encounters, the side-on overpressure and underpressure corresponding to the ray path distance is multiplied by 0.35^n . Side-on impulses would approximately be reduced by the same amount.

The diffraction factor was implemented in *Vector-Blast* with arrival times and durations remaining unchanged for lack of more available information. Dynamic pressure is calculated based on the modified overpressure.

3.8 Pressure-Time Histories

Once the appropriate modifications have been made to peak pressures, and all necessary blast parameters obtained using the appropriate scaled distances, the final pressure-time histories can be calculated.

3.8.1 Blast-Face Time Histories

For the normal component of the blast wave hitting the front face of the structure, a drag coefficient of 1 is used. For other components, a dynamic pressure varying drag coefficient is used as shown in Table 3.4. The drag coefficients are consistent with suggested values in TM 5-1300 (1990).

Table 3.4 Drag Coefficients

	Drag Coefficient, C_d	
Normal Component	1	
Others Components	$0 \leq q \leq 25$ (<i>psi</i>)	-0.4
	$0 \leq q \leq 172$ (<i>kPa</i>)	
	$25 < q \leq 50$ (<i>psi</i>)	-0.3
	$172 < q \leq 345$ (<i>kPa</i>)	
	$50 < q \leq 130$ (<i>psi</i>)	-0.2
$345 < q \leq 896$ (<i>kPa</i>)		

The clearing time is calculated according to Eq. 2.29 for incident pressures up to 517 kPa (75 psi). For higher pressures, Eq. 2.28 is used. Although the relations are only valid for plane waves, unless the explosion is very near to the structure, the shock front can be approximated as close to plane and the formulation will still give a reasonable approximation for the clearing time.

All components are affected by the clearing time. The pressure reduction after clearing has occurred for normal components is well described in Kinney (1985) and in TM 5-1300 (1969, 1990). The pressure after clearing has occurred drops to the stagnation overpressure which is a function of the dynamic pressure times the drag coefficient and the incident pressure as described in Section 2.1.8.1.

The pressure reduction for the non-normal components is very difficult to predict. Thus a conservative approach is adopted where the pressure reduction from clearing is ignored.

Fictitious durations, t_{of} , t_r , t_{rise} , and t_{neg} are calculated according to Equations 2.30, 2.31, and 2.32. Furthermore, an impulse check is performed for the normal

component to determine which final curve is used as explained in Section 2.1.8.1. The pressure-time histories for x, y, and z components would resemble those in Figure 3.12.

3.8.2 Other Faces

The pressure-time history is constructed in a similar manner as described in Section 3.8.1 for faces on the structures not directly loaded by the blast wave. The drag coefficient is obtained from Table 3.4 but since the blast wave is travelling parallel to the structure's surface, the drag coefficient is obtained from the so called "other components". The fictitious durations are calculated as described in Section 3.8.1 using the modified pressure and impulse. The final pressure time history would resemble Figure 3.12 (b) or (c). Only the component normal to the surface will have a pressure time history since the wave is diffracting and travelling parallel to the surface.

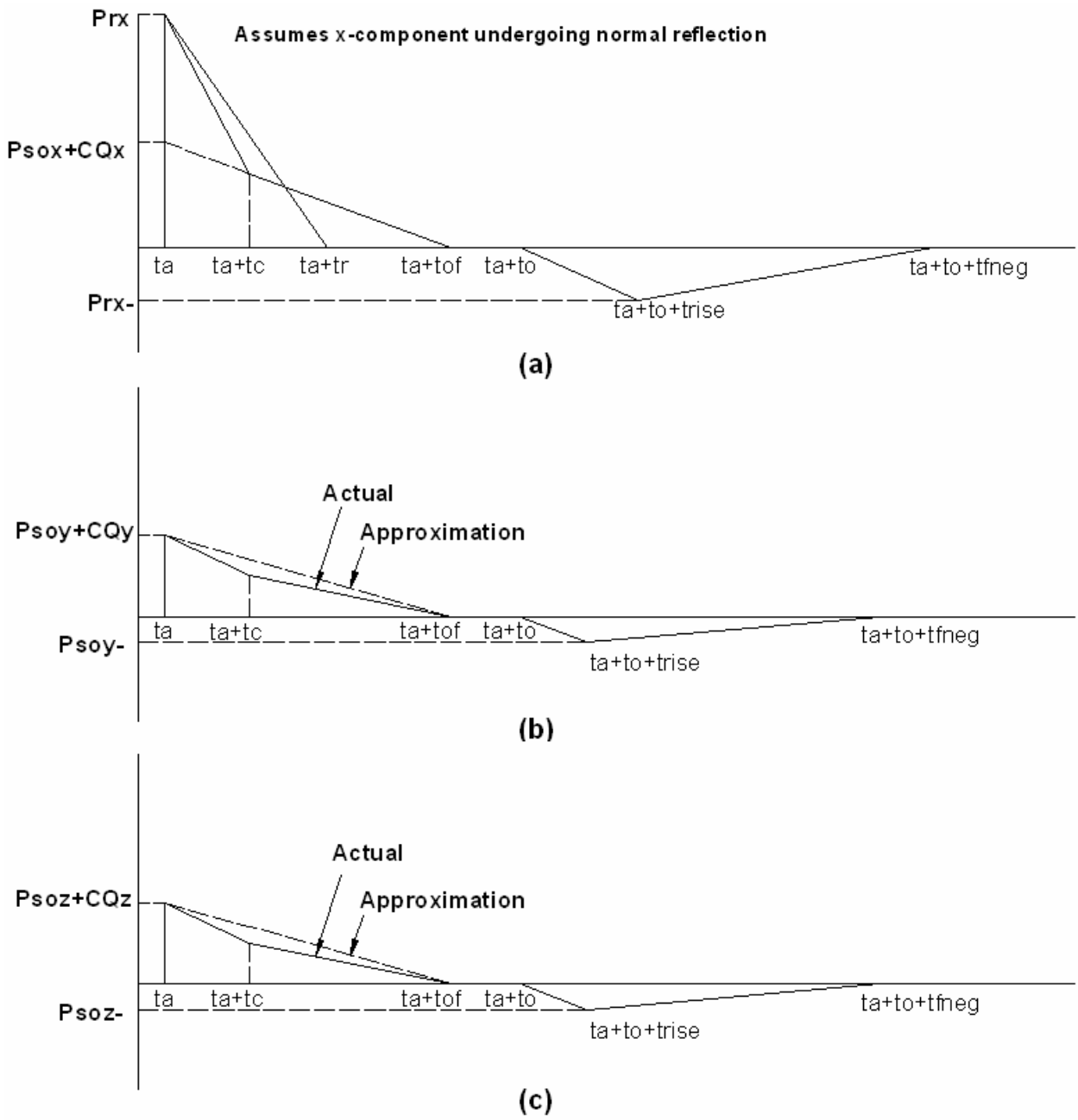


Figure 3.12 Component pressure-time history for the blast face.

CHAPTER 4 VERIFICATION

To assess the accuracy of *VecTor-Blast* presented in Chapter 3, a series of experimental and numerical corroborations were performed and the results are discussed in this chapter.

4.1 Hoffman and Mills (1956)

4.1.1 Modelling

The experiment conducted by Hoffman and Mills (1956) (see 2.2.2.1) was modelled by creating a 100 m x 1 m x 100 m structure. The size was selected to model an infinite concrete wall such that clearing effects would not affect the blast wave. The charge was placed at $1+R$ m above the structure (R is the standoff distance) and at 50 m from either edge of the structure as shown in Figure 4.1.

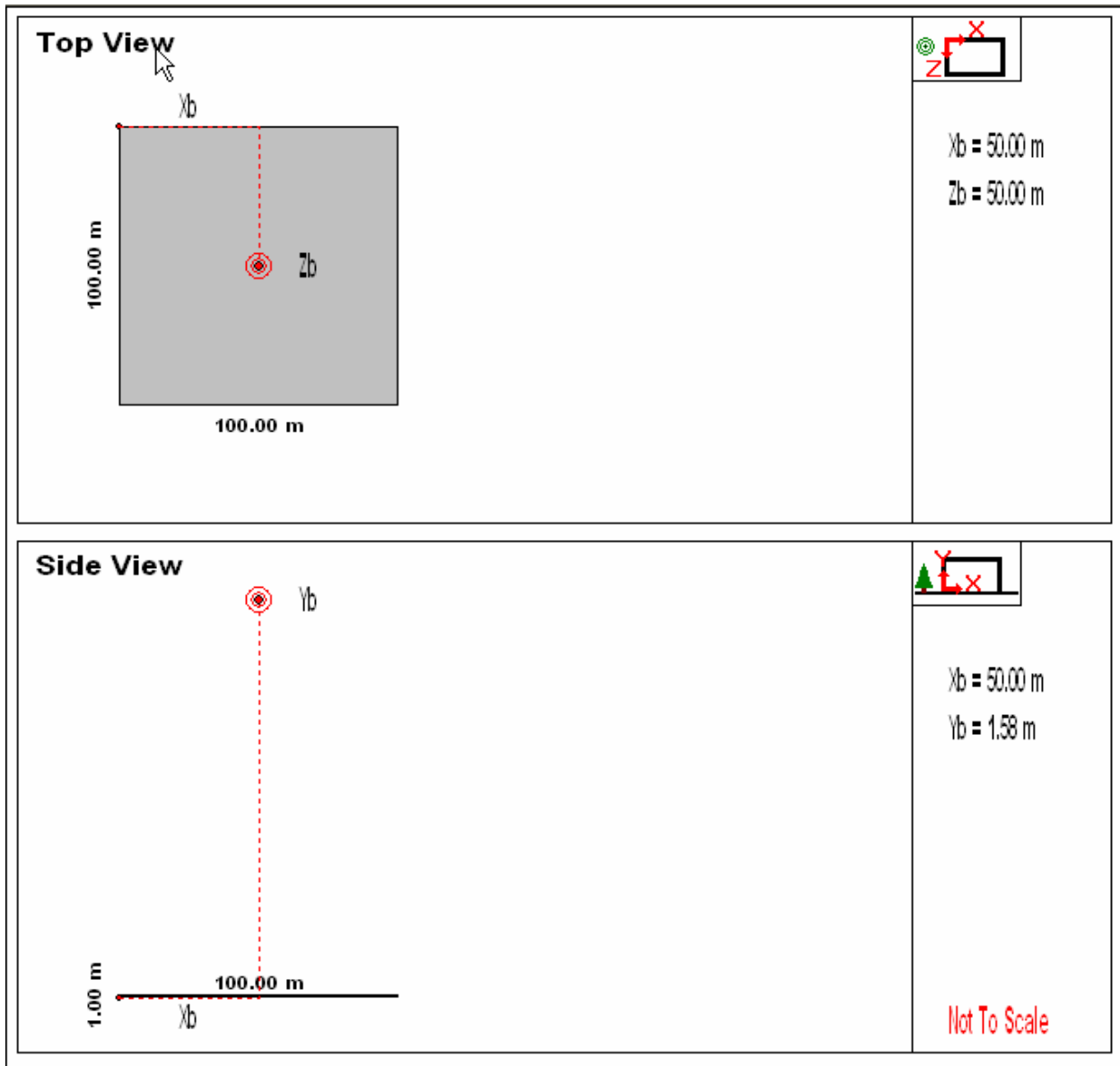


Figure 4.1 *VecTor-Blast* model of a concrete slab.

4.1.2 Results and Conclusions

VecTor-Blast's results are shown in Table 4.1 and Table 4.2 for a series of experiments from Hoffman and Mills, as well as in graphical form in Figures 4.2 to 4.4

Table 4.1 Data Comparison for Pressure: *VecTor-Blast* and Hoffman and Mills

Charge Wt (kg)	Standoff Distance (m)	Scaled Distance (m/kg ^{1/3})	Avg. Peak Pressure, P (kPa)		VecTor-Blast Peak Pressure, P (kPa)		P _{VECTOR-BLAST} /P _{EXP}	
			Incident	Reflected	Incident	Reflected	Incident	Reflected
0.8981	0.5779	0.60	3208.54	22269.38	3026.7	21920.5	0.94	0.98
3.5720	1.2189	0.80	1828.01	11537.69	1842.5	11909.8	1.01	1.03
3.7054	1.5224	0.98	1214.72	7027.69	1192.6	6916.9	0.98	0.98
3.6015	1.8303	1.19	748.63	3806.94	755	3865.2	1.01	1.02
0.4758	1.0654	1.36	546.13	2648.62	551.8	2498.4	1.01	0.94
0.8981	1.3855	1.44	554.82	2562.51	472.6	2109.7	0.85	0.82
0.4776	1.2497	1.60	407.07	1697.76	358.1	1449.9	0.88	0.85
0.4781	1.3710	1.75	320.74	1239.75	282.9	1068.2	0.88	0.86
0.2422	1.2364	1.98	246.35	870.39	208.5	731.2	0.85	0.84
0.4772	1.7515	2.24	169.27	526.90	156.5	483.4	0.92	0.92
0.4758	2.0130	2.58	125.35	362.87	114.6	319.6	0.91	0.88
0.2400	1.8365	2.96	107.63	300.96	85.4	222.4	0.79	0.74
0.2413	2.3438	3.76	59.92	147.41	50.5	119.5	0.84	0.81
0.8981	3.7164	3.85	63.16	156.72	47.9	112.3	0.76	0.72
0.2404	2.9205	4.70	47.99	114.11	32.6	72.5	0.68	0.64
0.4776	4.1738	5.34	32.06	72.39	26.8	57.9	0.84	0.80
0.2409	3.6554	5.88	40.75	59.78	23.5	49.9	0.58	0.83

Table 4.2 Data Comparison for Impulse: *VecTor-Blast* and Hoffman and Mills

Charge Wt (kg)	Standoff Distance (m)	Scaled Distance (m/kg ^{1/3})	Avg. Positive Impulse, I (kPa-ms)		VecTor-Blast Positive Impulse, I (kPa-ms)		I _{VECTOR-BLAST} /I _{EXP}	
			Incident	Reflected	Incident	Incident	Reflected	Incident
0.8981	0.5779	0.60	146.58	1033.52	157.90	146.58	1033.52	157.90
3.5720	1.2189	0.80	238.97	1087.58	249.00	238.97	1087.58	249.00
3.7054	1.5224	0.98	*	*	241.00	*	*	241.00
3.6015	1.8303	1.19	196.22	742.50	221.00	196.22	742.50	221.00
0.4758	1.0654	1.36	127.21	384.59	105.80	127.21	384.59	105.80
0.8981	1.3855	1.44	*	414.72	127.50	*	414.72	127.50
0.4776	1.2497	1.60	110.18	313.64	97.50	110.18	313.64	97.50
0.4781	1.3710	1.75	86.18	284.06	92.40	86.18	284.06	92.40
0.2422	1.2364	1.98	66.19	194.78	68.10	66.19	194.78	68.10
0.4772	1.7515	2.24	62.67	170.02	78.40	62.67	170.02	78.40
0.4758	2.0130	2.58	58.81	140.79	70.30	58.81	140.79	70.30
0.2400	1.8365	2.96	43.78	123.83	49.80	43.78	123.83	49.80
0.2413	2.3438	3.76	33.92	83.43	39.80	33.92	83.43	39.80
0.8981	3.7164	3.85	57.02	121.42	60.30	57.02	121.42	60.30
0.2404	2.9205	4.70	29.03	65.50	31.70	29.03	65.50	31.70
0.4776	4.1738	5.34	30.68	65.16	34.90	30.68	65.16	34.90
0.2409	3.6554	5.88	24.13	48.26	25.20	24.13	48.26	25.20

*data couldn't be measured

Table 4.2 Data Comparison for Duration: *VecTor-Blast* and Hoffman and Mills

Charge Wt (kg)	Standoff Distance (m)	Scaled Distance (m/kg ^{1/3})	Positive Duration, T (ms)		VecTor-Blast Positive Duration, T (ms)		T _{VECTOR-BLAST} /T _{EXP}	
			Incident	Reflected	Incident	Reflected	Incident	Reflected
0.8981	0.5779	0.60	0.23	0.24	0.12	0.12	0.52	0.50
3.5720	1.2189	0.80	0.59	0.56	0.31	0.31	0.53	0.56
3.7054	1.5224	0.98	*	*	0.56	0.56	*	*
3.6015	1.8303	1.19	0.91	0.86	0.93	0.93	1.02	1.09
0.4758	1.0654	1.36	0.67	0.59	0.63	0.63	0.94	1.06
0.8981	1.3855	1.44	*	0.56	0.86	0.86	*	1.54
0.4776	1.2497	1.60	0.77	0.75	0.84	0.84	1.10	1.13
0.4781	1.3710	1.75	0.89	0.85	0.97	0.97	1.09	1.14
0.2422	1.2364	1.98	0.88	0.83	0.94	0.94	1.07	1.14
0.4772	1.7515	2.24	1.19	1.24	1.35	1.35	1.13	1.09
0.4758	2.0130	2.58	1.32	1.44	1.55	1.55	1.18	1.08
0.2400	1.8365	2.96	1.16	1.21	1.41	1.41	1.22	1.17
0.2413	2.3438	3.76	1.74	1.78	1.72	1.72	0.99	0.97
0.8981	3.7164	3.85	2.24	2.42	2.72	2.72	1.22	1.12
0.2404	2.9205	4.70	1.62	1.54	2.00	2.00	1.24	1.30
0.4776	4.1738	5.34	1.89	1.74	2.71	2.71	1.44	1.56
0.2409	3.6554	5.88	1.97	1.92	2.26	2.26	1.15	1.18

* Data couldn't be measured

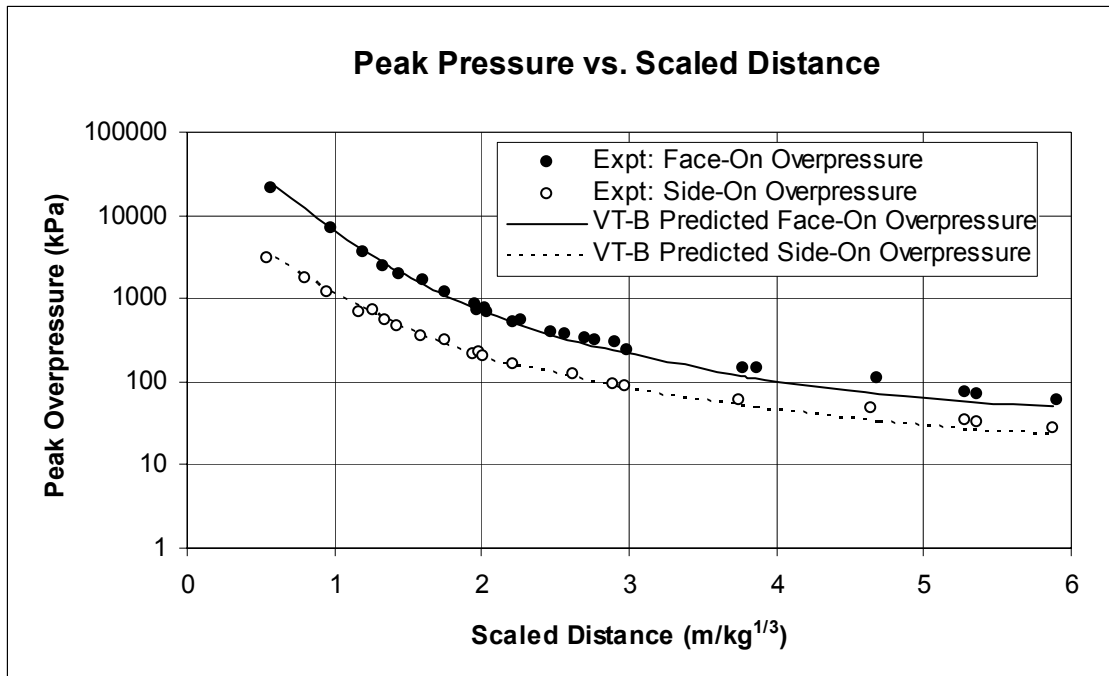


Figure 4.2 Overpressure comparisons: *VecTor-Blast* and Hoffman and Mills.

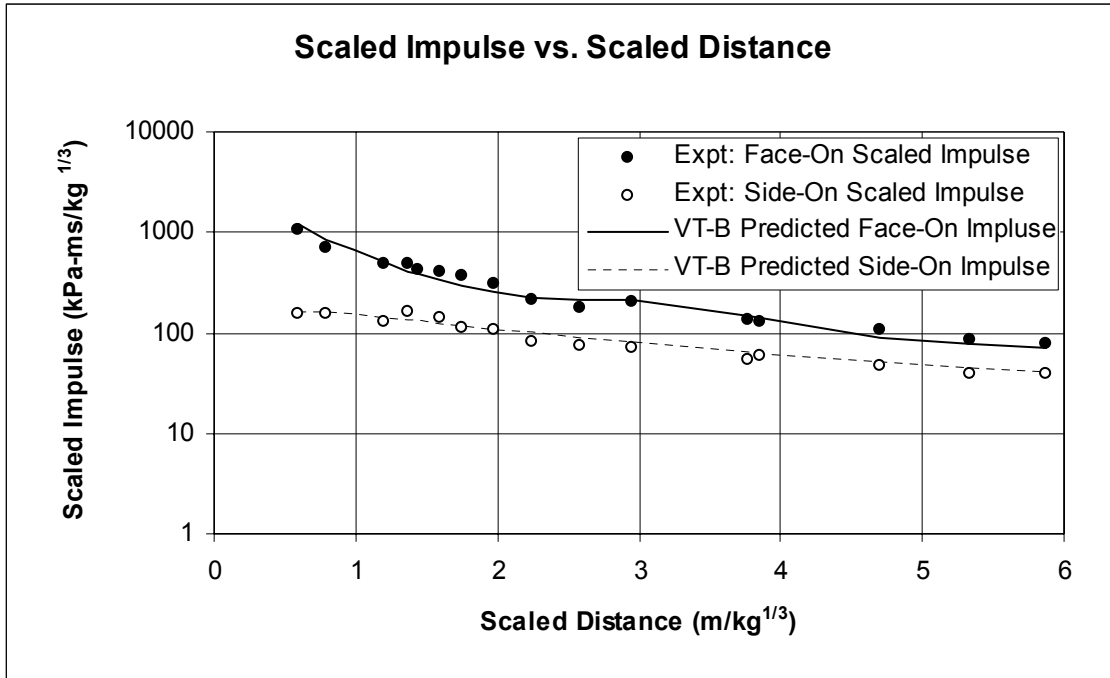


Figure 4.3 Impulse comparisons: *VecTor-Blast* and Hoffman and Mills.

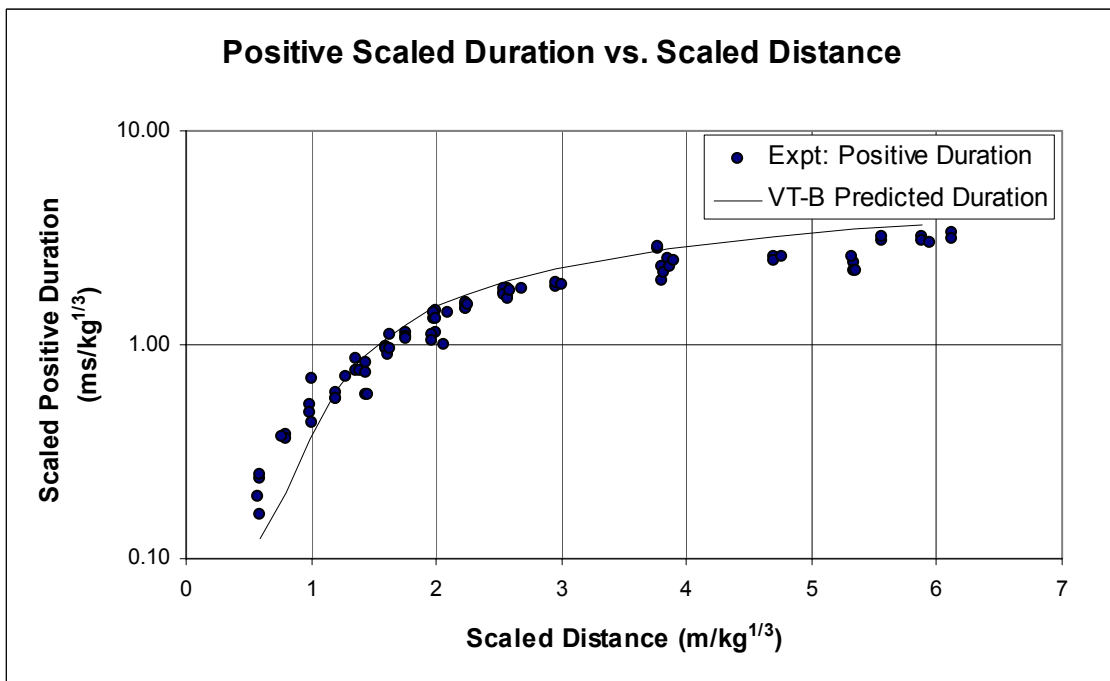


Figure 4.4 Positive duration comparisons: *VecTor-Blast* and Hoffman and Mills.

Face-on and side-on overpressure are quite well predicted with *VecTor-Blast*, as is face-on impulse, side-on impulse, and positive duration. Positive durations are less well predicted at lower scaled distances. Hoffman and Mills noted that the quality of

the records deteriorated as the explosive was placed closer and closer to the gauges. Values at scaled distances of less than $0.6\text{m/kg}^{1/3}$ ($1.5\text{ft/lb}^{1/3}$) were therefore deemed questionable. These observations may have contributed to the scatter seen in Figure 4.4 at small scaled distances and an appearance of an under-prediction of scaled positive duration by *VecTor-Blast*.

4.2 Smith et al. (1999)

4.2.1 Modelling

An experiment to study the effect of clearing of blast waves (Smith et al., 1999) involved blast loading two plates of 400 mm and 300 mm diameters (see 2.2.2.4). Measurements were taken along the centerline of the plates as shown in Figure 2.31. *VecTor-Blast* is currently only able to model rectangular structures so the plates were modeled as 400 mm x 400 mm or 300 mm x 300 mm rectangles. The clearing phenomenon is most affected by the distance from the AP to the nearest edge and the distance to the centre of the plate. Since the APs lie on the centerline, the clearing distances will all be similar and it was determined that square plates would provide a reasonable approximation. Thus, the experiment was modeled in a similar fashion as in Section 4.1.1 for experiments by Hoffman and Mills (1956).

4.2.2 Results and Conclusions

A series of plots from Smith et al. showing experimental impulse and pressure are given in Figures 4.14 to 4.23, along with calculations from *VecTor-Blast*.

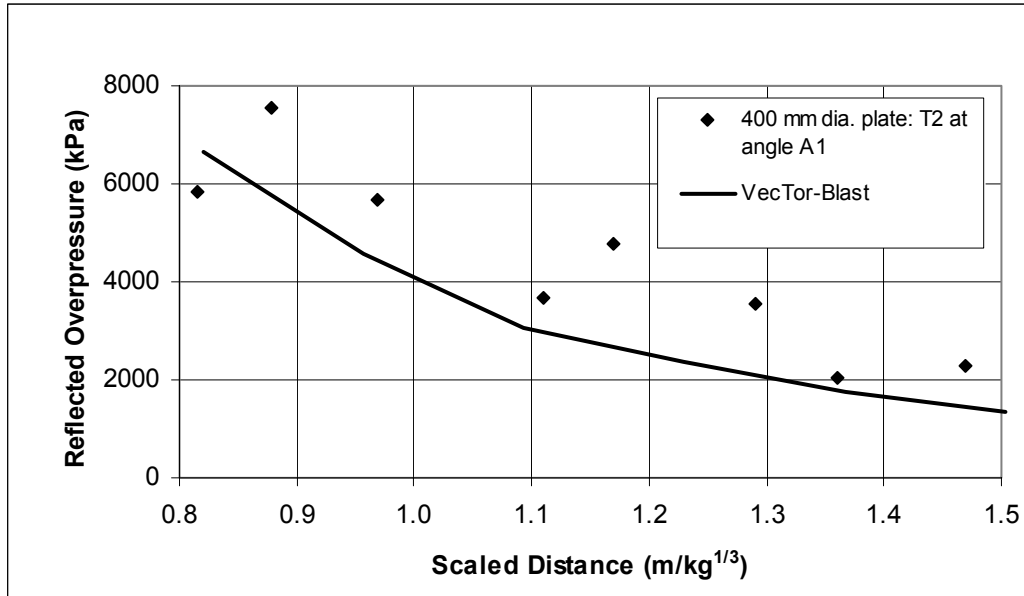


Figure 4.14 Reflected overpressure T2-A1.

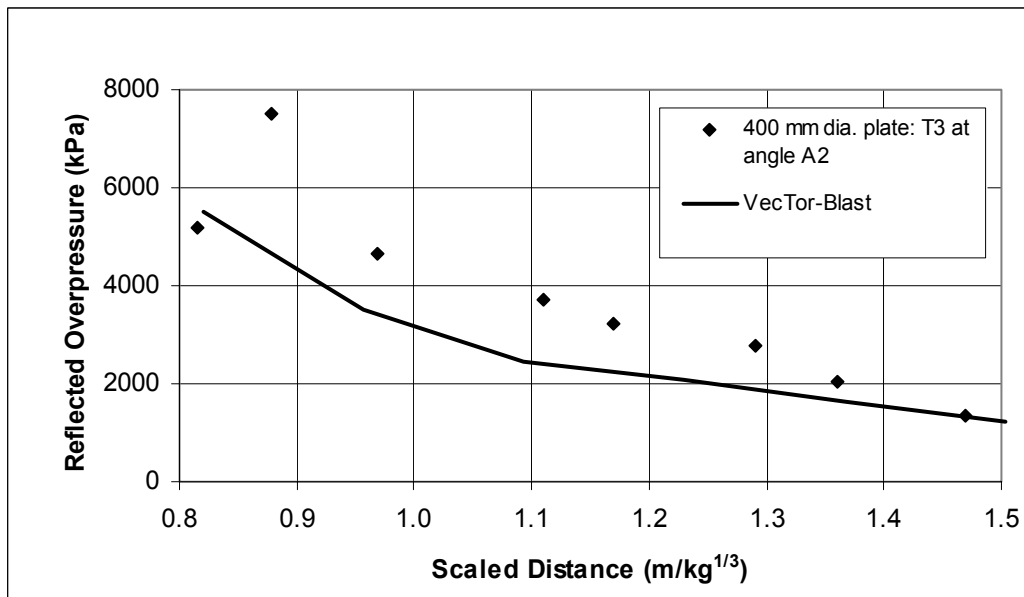


Figure 4.15 Reflected overpressure T3-A2.

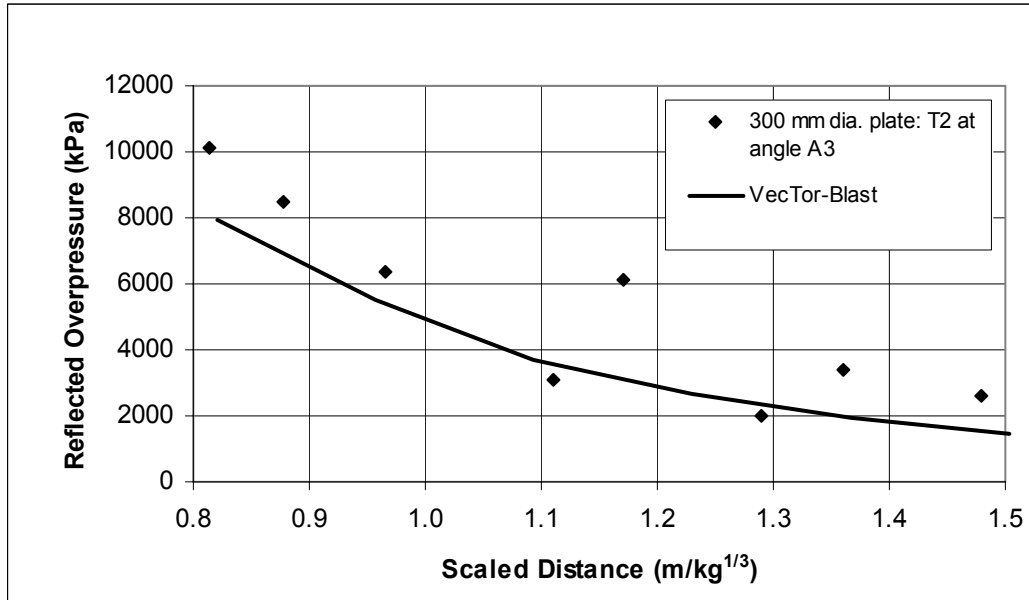


Figure 4.16 Reflected overpressure T2-A3.

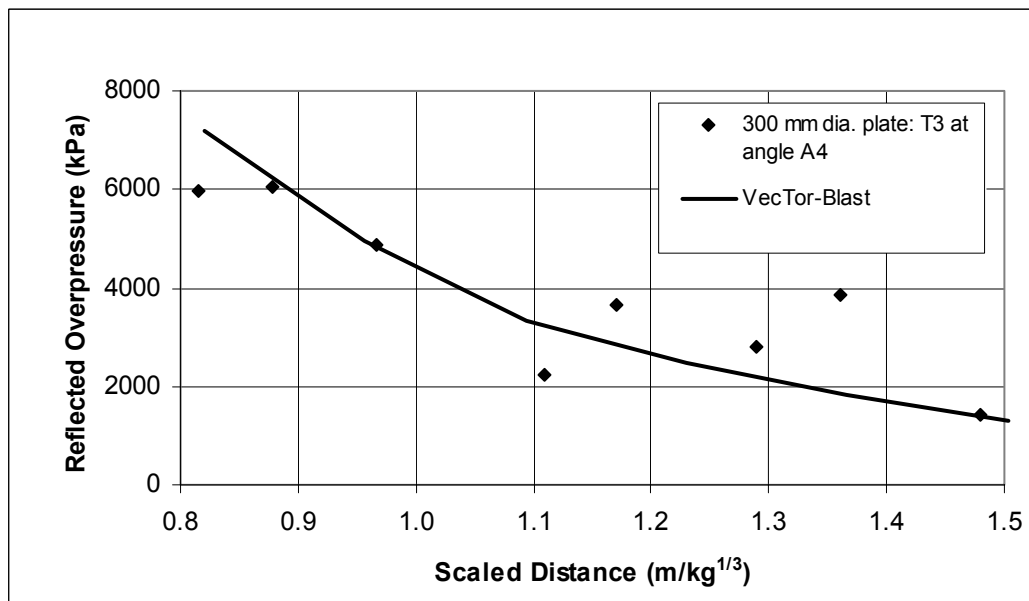


Figure 4.17 Reflected overpressure T3-A4.

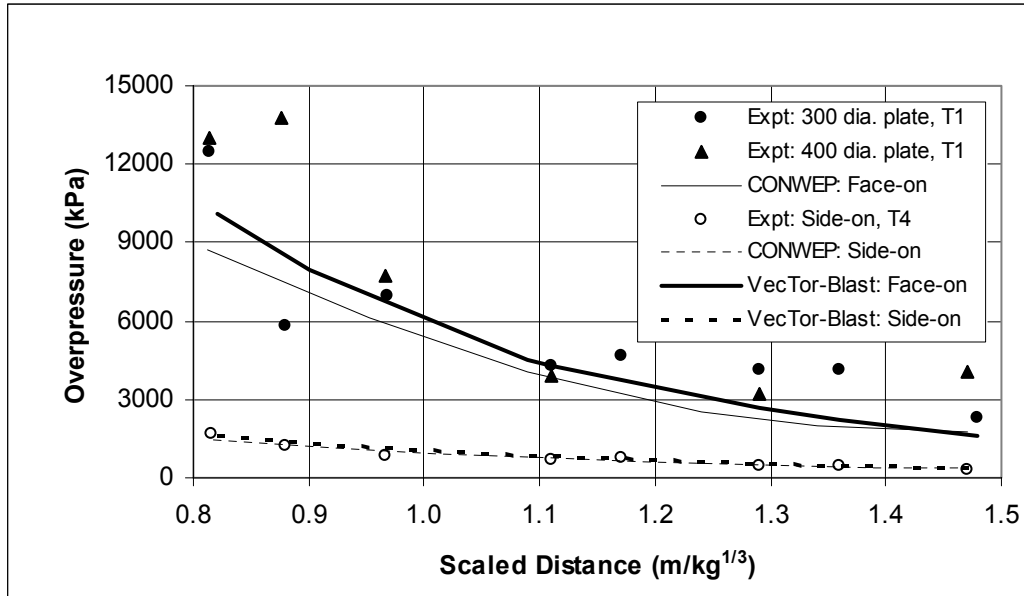


Figure 4.18 Normal overpressure.

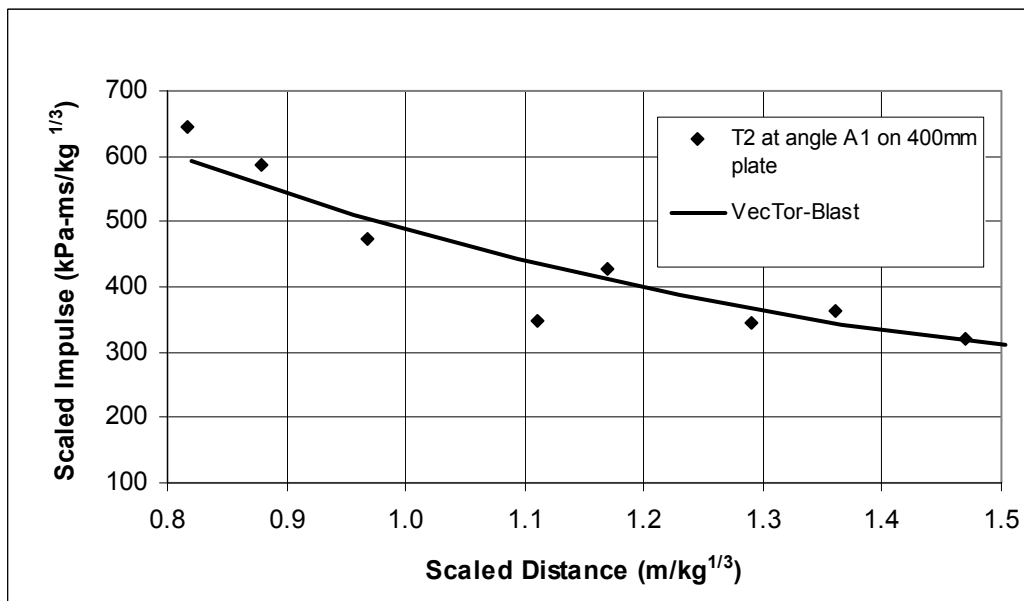


Figure 4.19 Reflected scaled impulse T2-A1.

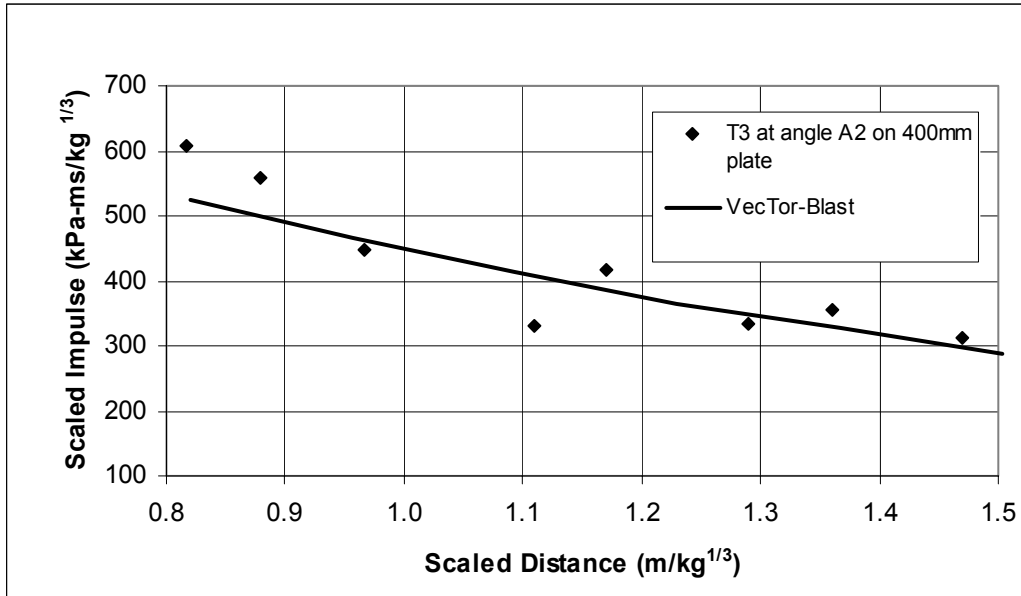


Figure 4.20 Reflected scaled impulse T3-A2.

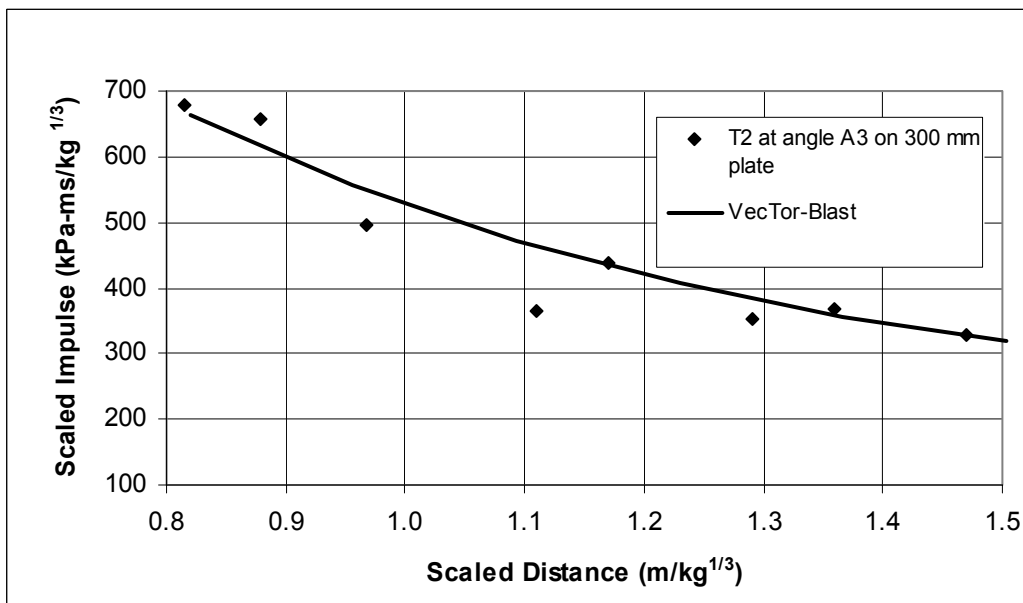


Figure 4.21 Reflected scaled impulse T2-A3.

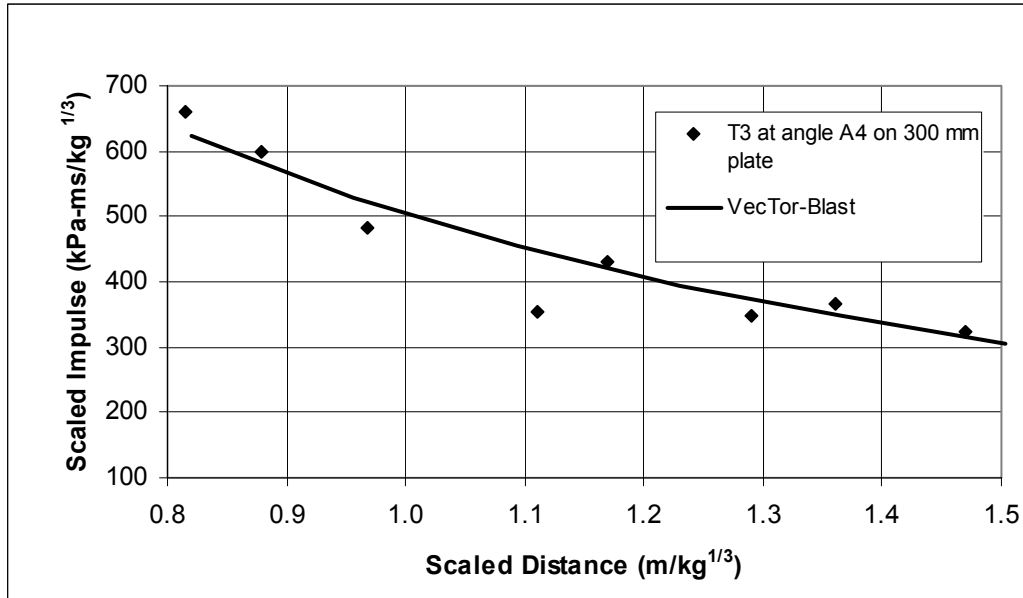


Figure 4.22 Reflected scaled impulse T3-A4.

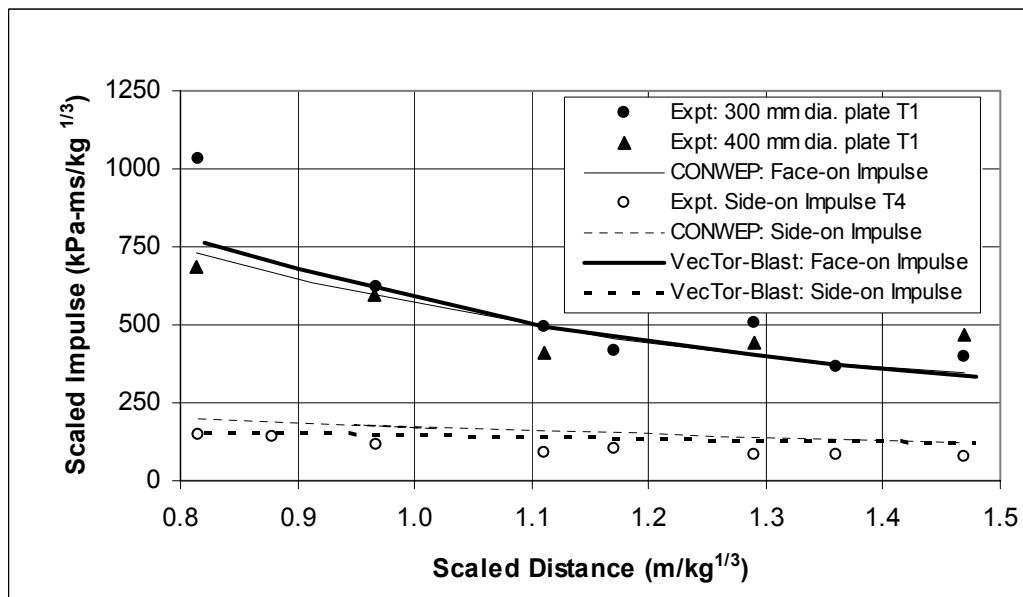


Figure 4.23 Normal scaled impulse.

Figures 4.14 to 4.23 indicate there is agreement between calculations from *VecTor-Blast* and experimentally determined reflected overpressure. *VecTor-Blast* appears to under-predict reflected overpressure in some cases, however there is scatter in the experimental data. In the case of normal face-on (reflected) and side-on overpressure, there is much better agreement between *VecTor-Blast* and experimental values as seen in Figure 4.18 particularly when comparing against side-on

overpressure. There is again much scatter in the normally reflected values making it difficult to evaluate the accuracy of *VecTor-Blast* against experimental data. *VecTor-Blast* does however make similar predictions as the well known and tested CONWEP program.

Reflected impulse values from *VecTor-Blast* compare well with experimental data as seen in Figures 4.19 to 4.22. Normal face-on and side-on values from *VecTor-Blast* also compare well with experimental data and CONWEP as seen in Figure 4.23.

4.3 Armstrong et al. (2002)

4.3.1 Experimental Characterization

The experimental data is supplied from Armstrong et al. (2002) (see Section 2.3.3.4) who performed numerical simulations to compare against results of an experiment in Joachim et al. (2002) (due to the difficulty in obtaining the data directly from Joachim et al., the data was extracted from Armstrong). One of the main objectives by Armstrong was to test the accuracy of the program SHAMRC (Crepeau, 1988).

The experiment consisted of a rectangular structure subjected to a 72.6 g hemispherical charge of PBX-9407. A layout of the experiment is shown in Figure 4.5.

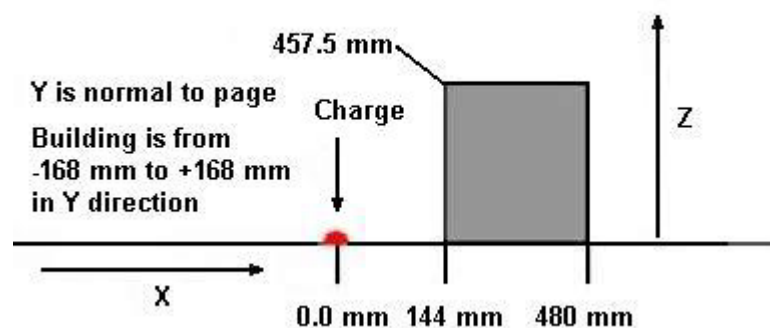


Figure 4.5 Experiment set up (after (Armstrong, 2002)).

The results from *VecTor-Blast* are compared against the results from two computer programs, CONWEP and SHAMRC, in addition to the experimental data. This provides an indication of *VecTor-Blast's* prediction abilities against other software.

4.3.2 Results and Conclusions

4.3.2.1 Free Field Results

The first series of corroborations examines free-field arrival time, free-field pressure, and free-field impulse. *VecTor-Blast* does not directly measure the change in free-field parameters with distance however they can be measured indirectly. *VecTor-Blast* calculates the incident (side-on) blast parameters at any point on the structure. Free-field parameters were computed by subjecting the same AP on the front face of the structure to explosions of equal mass at varying distances. Thus, blast parameters over a range of scaled distances are obtained. A comparison of the free-field results from *VecTor-Blast* can be seen in Figures 4.6 through 4.8.

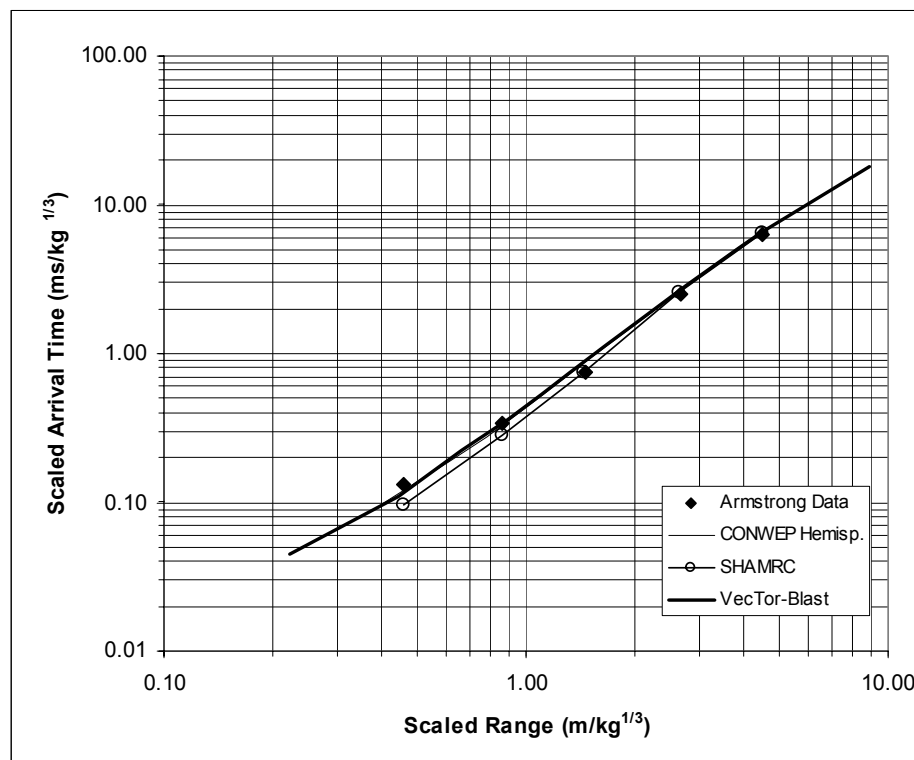


Figure 4.6 Free-field scale arrival time comparisons.

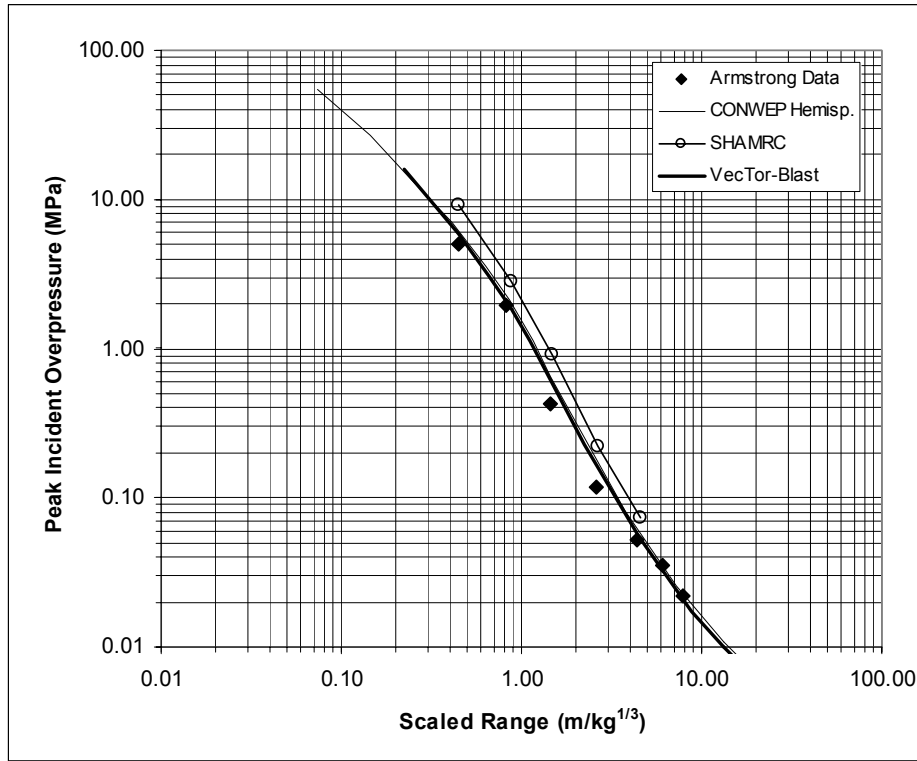


Figure 4.7 Free-field pressure comparisons.

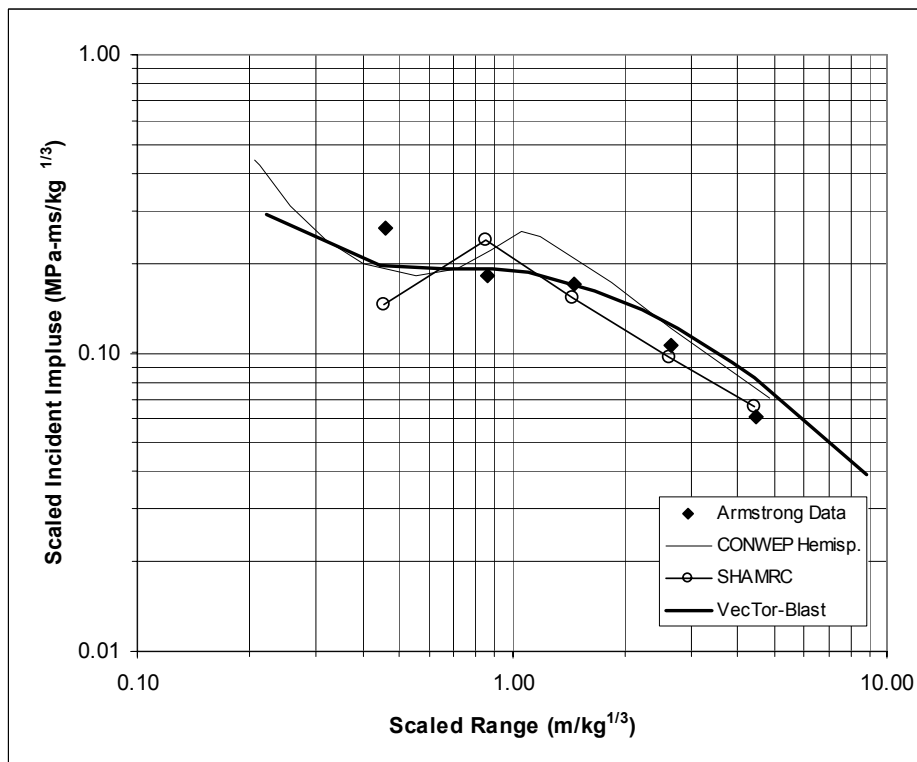


Figure 4.8 Free-field impulse comparisons.

There is good agreement between *VecTor-Blast* and the experimental data as well as between *VecTor-Blast* and the other programs for scaled arrival time and overpressure. *VecTor-Blast* does a fairly good job at predicting impulse with maximum deviations of up to 30%. This appears to be consistent with the results of CONWEP and SHAMRC.

4.3.2.2 Results from the Structure

The second series of corroborations examines the blast wave interaction with the structure. Peak impulse and peak pressure predictions are compared on the various walls along the height. For cases where diffraction is occurring (side wall and rear wall), the results from *VecTor-Blast* using the suggested diffraction factor ($DF=0.35^n$) are also compared to the side-on results from *VecTor-Blast* ($DF=1$). The results are shown in Figures 4.9 to 4.13.

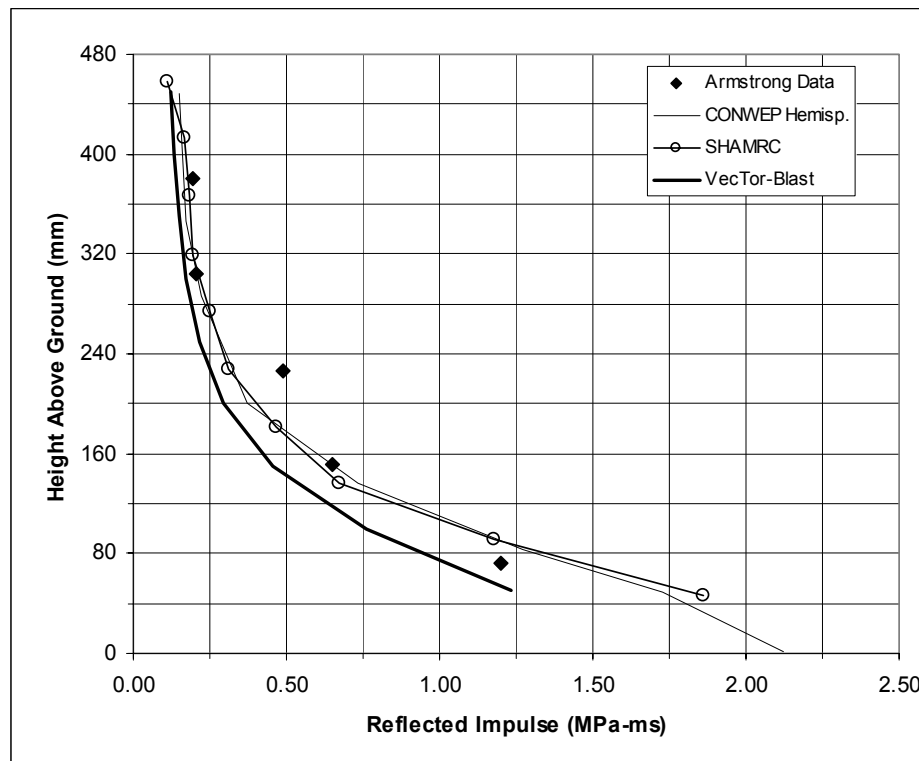


Figure 4.9 Peak reflected impulse at center of front wall.

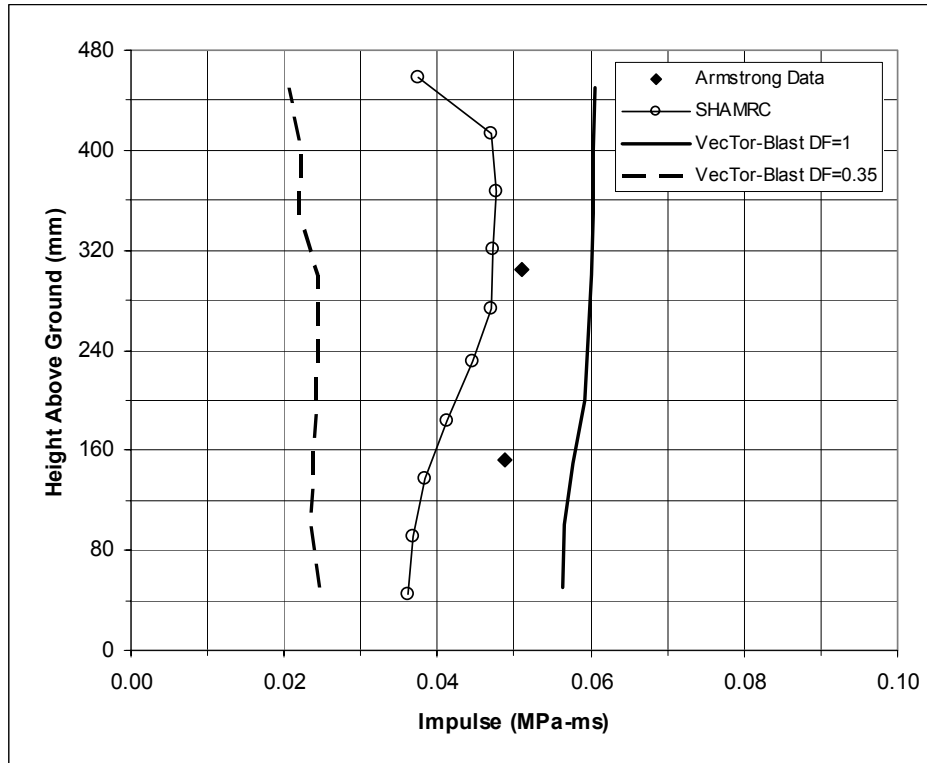


Figure 4.10 Peak impulse at center of side wall.

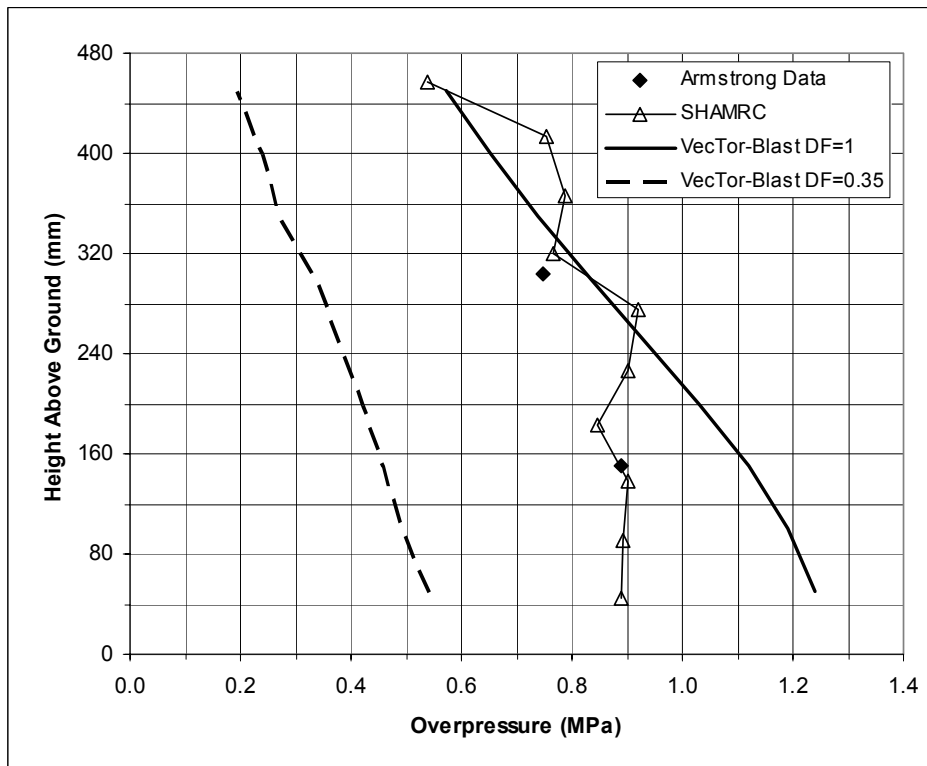


Figure 4.11 Peak overpressure at center of side wall.

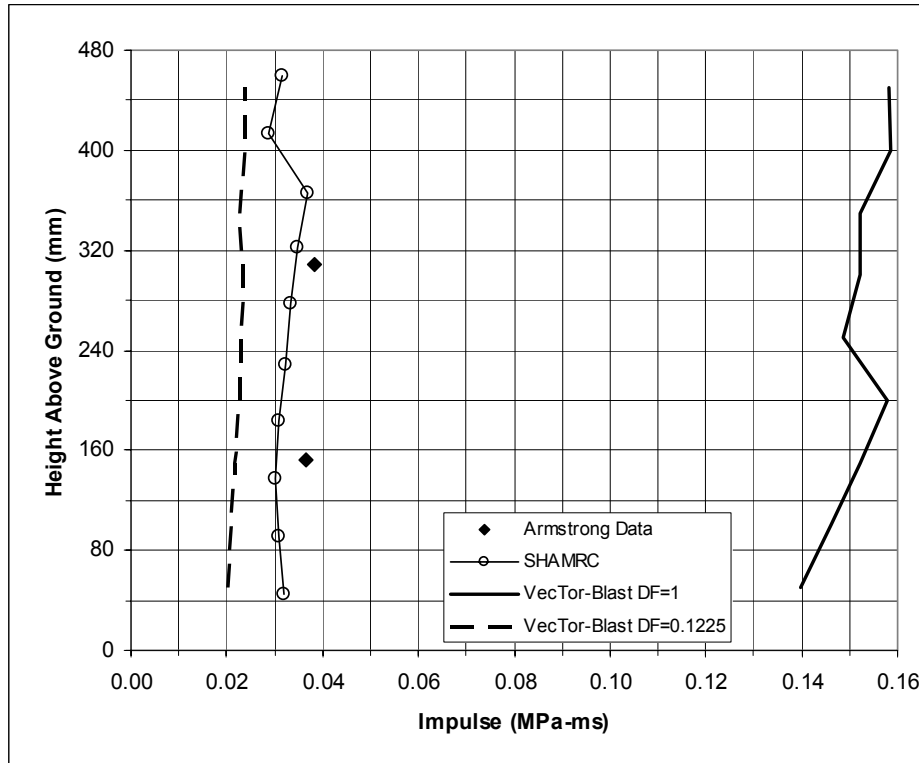


Figure 4.12 Peak impulse at center of rear wall.

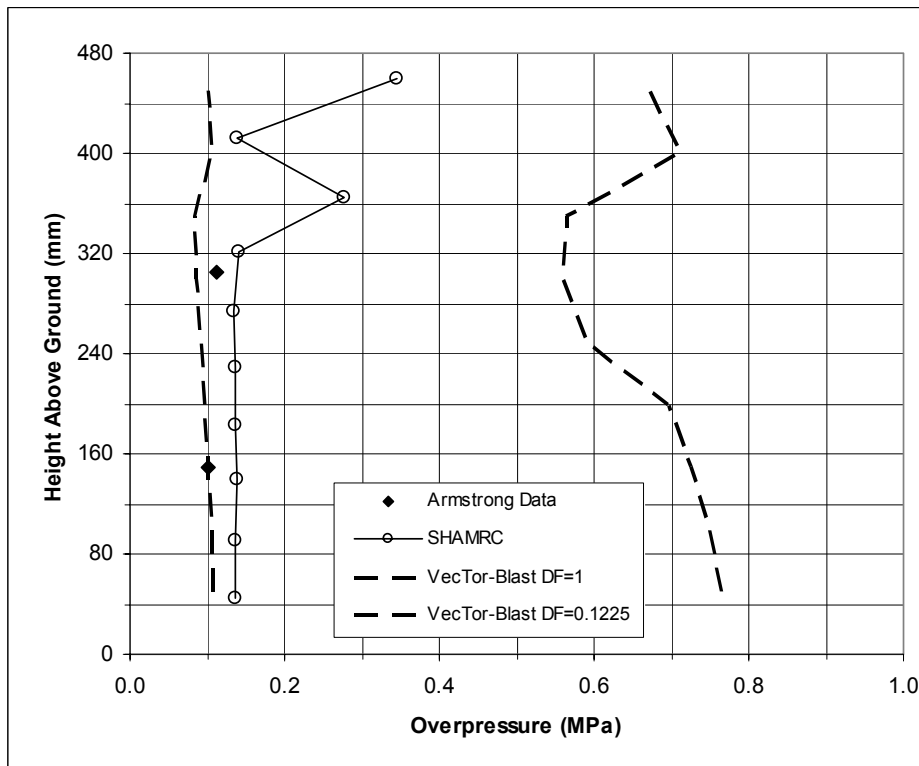


Figure 4.13 Peak overpressure at center of rear wall.

Results from the front face match well with experimental data although there appears to be a slight under-prediction of reflected impulse. For side walls, using a diffraction factor of 0.35 appears to heavily under-estimate the experimental results. On the rear wall however, using the diffraction factor of 0.1225 adequately estimates experimental results.

4.4 TM 5-1300 (1969) Example 4A-7

4.4.1 Problem Definition

A numerical problem is taken from TM 5-1300 (1969). This example involves a rectangular structure loaded by a surface burst, as shown in Figure 4.24, and assumes the wave front is plane when reaching the structure.

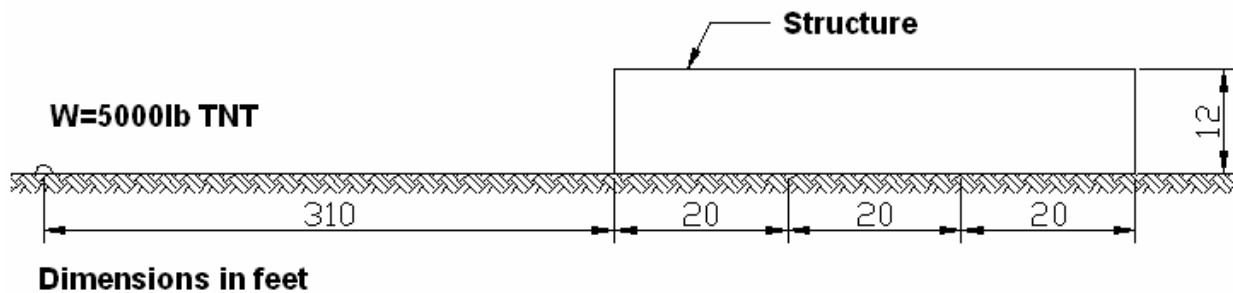


Figure 4.24 Loading and structure dimensions of example 4A-7 (after (TM 5-1300, 1969)).

Blast parameters are measured on the front face in TM 5-1300 (1969) and since a plane shock front is assumed, the blast parameters would be the same across the height and width of the face. Results from the negative phase were not calculated in this example.

Since *VecTor-Blast* takes into account the curvature of the shock front, results were taken at the middle point of the base of the front face as plane wave conditions would be occurring there.

4.4.2 Results and Conclusion

The results from TM 5-1300 (1969) and *VecTor-Blast* are shown below in Table 4.3 to Table 4.4

Table 4.3 Results from 4A-7 (1)

	R (m)	Z (m/kg ^{1/3})	β (deg)	P_s^+ (kPa)	q (kPa)	U (m/ms)	i_s^+ (kPa-ms)
TM 5-1300, 1969	94.49	7.18	0.00	24.13	1.90	0.38	654.31
VecTor-Blast	94.49	7.19	0.00	23.80	1.91	0.37	647.79
VecTor-Blast/ TM 5-1300, 1990	1.00	1.00	1.00	0.99	1.01	0.98	0.99

Table 4.4 Results from 4A-7 (2)

	t_o (ms)	t_A (ms)	t_c (ms)	$C_{r\beta}$	P_r^+ (kPa)	i_r^+ (kPa-ms)
TM 5-1300, 1969	55.60	181.00	29.00	2.23	53.78	1392.74
VecTor-Blast	54.54	176.97	27.60	2.12	50.47	904.10
VecTor-Blast/ TM 5-1300, 1969	0.98	0.98	0.95	0.95	0.94	0.65

Agreement with numerical results is quite good with maximum deviations of up to 6%. There appears to be a large difference with the predicted reflected positive impulse, i_r^+ , with a difference of 35%. This difference can be attributed to the fact that whenever possible in *VecTor-Blast*, the most current curves and calculation methods from TM 5-1300 (1990) are used. In the most recent version of the army manual (TM 5-1300, 1990), the normally reflected impulse curve has been modified at higher scaled distances. The difference is shown in tabular form in Table 4.5.

Table 4.5 Difference in scaled normally reflected impulse

	Z (ft/lb ^{1/3})	Z (m/kg ^{1/3})	i_r^w (psi-ms/lb ^{1/3})	i_r^w (kPa-ms/kg ^{1/3})	i_r^+ (psi-ms)	i_r^+ (kPa-ms)
TM 5-1300, 1969	18.1	7.2	11.8	106.0	202.0	1392.7
TM 5-1300, 1990	18.1	7.2	7.9	70.9	135.1	931.4
VecTor-Blast	18.1	7.2	7.6	68.2	131.1	904.1

The results in Table 4.5 from TM 5-1300 (1990) closely match the results from *VecTor-Blast* and thus the large difference in normally reflected impulse can be attributed to the example being from an older version of the manual.

The same applies for the reflection coefficients (i.e. reflected pressure) and clearing time. In TM 5-1300 (1990), an updated curve of reflection coefficients is also used which is implemented in *VecTor-Blast* and therefore accounts for the deviation in reflection coefficients and reflected pressure. The more recent clearing time equation (Equation 2.29) is used in *VecTor-Blast* whereas the example uses Equation 2.28.

The pressure-time histories created from the results can be seen in Figures 4.25 to 4.27.

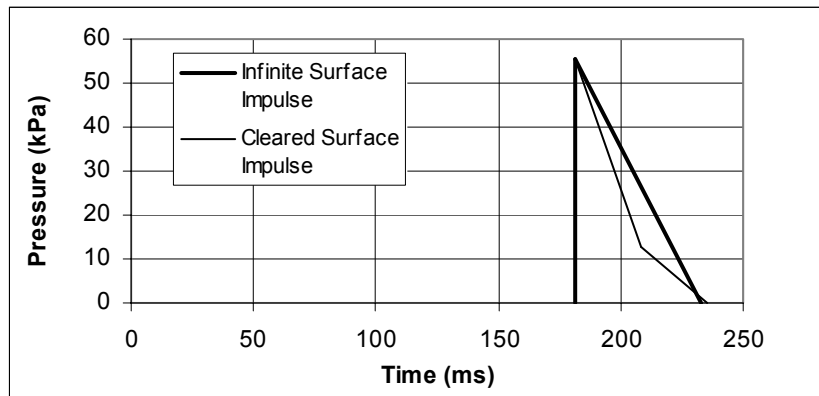


Figure 4.25 Pressure-time histories for example 4A-7 (after (TM 5-1300, 1969)).

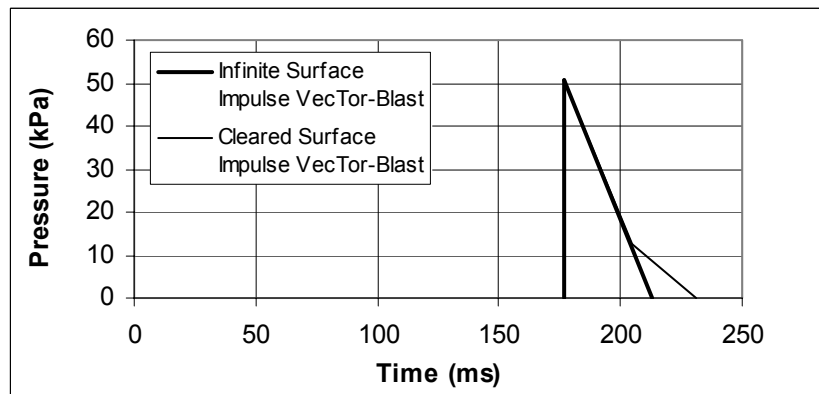


Figure 4.26 Pressure-time histories for example 4A-7 from *VecTor-Blast*.

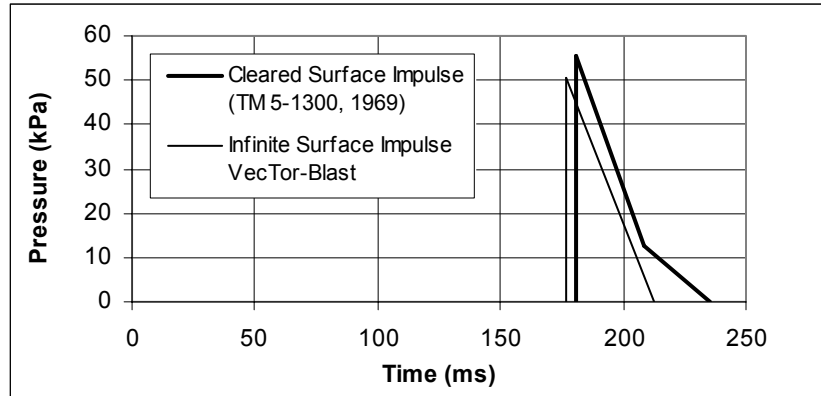


Figure 4.27 Pressure-time history comparisons for example 4A-7.

Figure 4.25 shows the two pressure-time histories from TM 5-1300 (1969). The cleared surface impulse pressure-time curve governs. The governing curve is shown as the actual pressure-time curve in Figure 4.27. The two pressure-time histories from *VecTor-Blast* are shown in Figure 4.26.

Since the value of reflected impulse computed by *VecTor-Blast* is significantly different than that in TM 5-1300 (1969) (see Table 4.4(2)), a different curve governs according to *VecTor-Blast* as seen in Figure 4.27. The difference in the governing curve is attributed primarily to the difference in the calculation of the normally reflected impulse.

4.5 TM 5-1300 (1990) Example 2A-10

4.5.1 Problem Definition

A similar problem to example 4A-7 (TM 5-1300, 1969), example 2A-10 (TM 5-1300, 1990) is modelled in *VecTor-Blast*. The main purpose of this example was to compare the results from the negative phase which were previously not considered in TM 5-1300 (1969).

The structure and loading dimensions are shown in Figure 4.28.

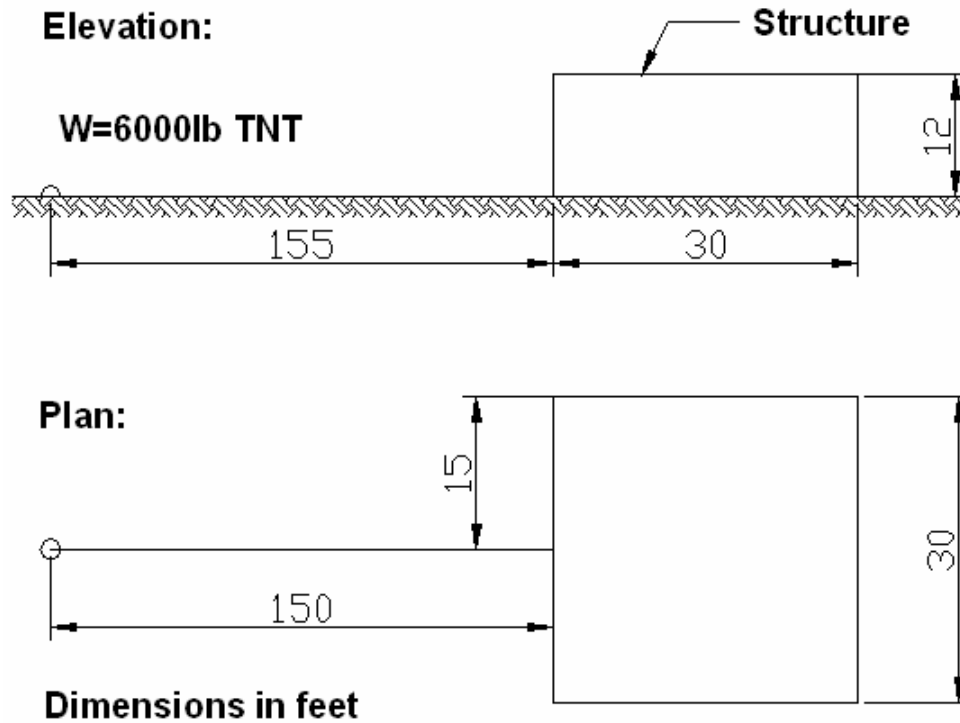


Figure 4.28 Loading and structure dimensions of example 2A-10 (after (TM 5-1300, 1990)).

Blast parameters are measured at the middle point of the base of the front face to obtain comparable wave parameters because of the assumption of plane shock in the example.

4.5.2 Results and Conclusion

The results from TM 5-1300 (1990) and *VecTor-Blast* are shown below in Table 4.6 to Table 4.8.

Table 4.6 Results from 2A-10 (1)

	R (m)	Z (m/kg ^{1/3})	β (deg)	P_s^+ (kPa)	q (kPa)	i_s^+ (kPa-ms)
TM 5-1300, 1990	47.24	3.38	0.00	88.25	24.13	1127.29
VecTor-Blast	47.24	3.38	0.00	92.53	24.53	1456.64
VecTor-Blast/ TM 5-1300, 1990	1.00	1.00	1.00	1.05	1.02	1.29

Table 4.7 Results from 2A-10 (2)

	t_o (ms)	t_A (ms)	t_C (ms)	$C_{r\beta}$	P_r^+ (kPa)	i_r^+ (kPa-ms)
TM 5-1300, 1990	42.70	60.90	20.10	2.70	238.56	2129.79
VecTor-Blast	33.82	57.47	19.94	2.65	245.04	2230.90
VecTor-Blast/ TM 5-1300, 1990	0.79	0.94	0.99	0.98	1.03	1.05

Table 4.8 Results from 2A-10 (3)

	P_r^- (kPa)	i_r^- (kPa-ms)	t_{neg} (ms)	t_{rise} (ms)
TM 5-1300, 1990	22.41	1829.18	163.30	44.09
VecTor-Blast	22.60	1866.35	165.29	44.63
VecTor-Blast/ TM 5-1300, 1990	1.01	1.02	1.01	1.01

The results from *VecTor-Blast* compare well with those in TM 5-1300 (1990) especially with respect to the negative phase parameters. There are some discrepancies in some of the results relating directly to free-field parameters (i_s^+ , t_o , and t_A) and this is expected. As mentioned in Section 3.4, free-field parameters were taken from TM 5-1300 (1969) due to a lack of available recent data.

The pressure-time histories created from the results can be seen in Figures 4.29 to 4.31.

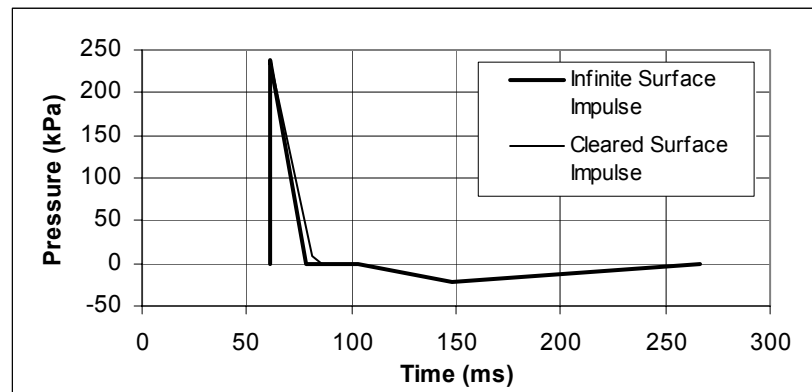


Figure 4.29 Pressure-time histories for example 2A-10 (after (TM 5-1300, 1990)).

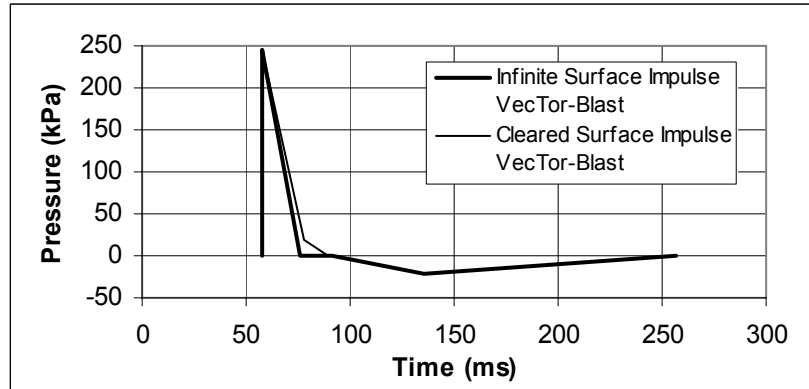


Figure 4.30 Pressure-time histories for example 2A-10 from *VecTor-Blast*.

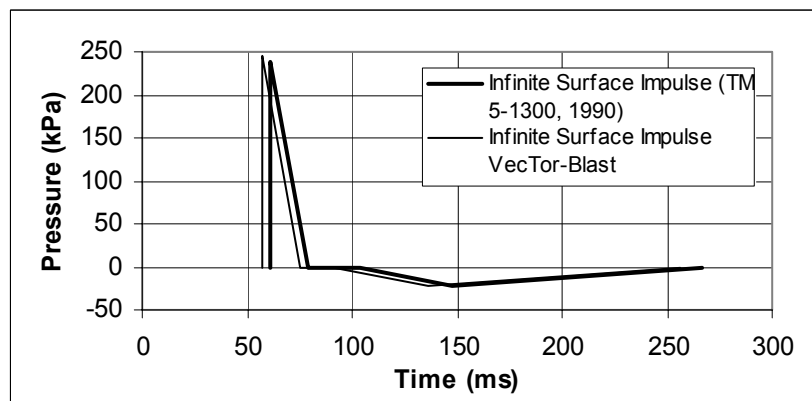


Figure 4.31 Pressure-time history comparisons for example 2A-10.

VecTor-Blast is able to closely predict the pressure-time profiles despite the discrepancies in the free-field results. In Figure 4.31, the effect of less accurate free-field parameter predictions by *VecTor-Blast* is evident as the infinite surface curve is slightly shifted to the left due to an under-estimation of arrival time compared to the curve suggested by TM 5-1300 (1990).

4.6 General Conclusions

Generally, *VecTor-Blast* does an acceptable job at predicting peak pressures, impulses, and durations for a surface directly loaded by an explosion. Diffraction events are less well predicted, particularly with regard to pressures and impulses on side walls. Difficulty arises in determining the degree of error as only one test case is used. More testing is required.

It should be noted that due to lack of available experimental data, not all aspects of *VecTor-Blast* have been adequately tested. The corroborations are only valid for explosions on the ground or directly above the structure. In the cases where a mach stem could form or ground reflected waves strike the structure, a lack of available data prevented adequate testing. Therefore the results from *VecTor-Blast* when used to model those conditions should be used with caution.

CHAPTER 5 DISCUSSION AND RECOMMENDATIONS

5.1 Application to Finite Element Analysis of Concrete Structures

VecTor-Blast is designed primarily for use with finite element analysis (FEA) programs which do not have blast load prediction capabilities. Specifically, *VecTor-Blast* is intended for use with the FEA suite of programs, *VecTor*, developed at the University of Toronto. This section will examine how blast loads can be incorporated into *VecTor2*.

5.1.1 *VecTor-Blast* and *VecTor2*

VecTor2 is a nonlinear finite element analysis (NLFEA) program for the analysis of two-dimensional reinforced concrete membrane structures. *VecTor2* uses a smeared, rotating-crack formulation for reinforced concrete based on the Modified Compression Field Theory (Vecchio and Collins, 1986) and the Disturbed Stress Field Model (Vecchio, 2000). The program's solution algorithm is based on a secant stiffness formulation using a total-load iterative procedure.

The results in the *VecTor-Blast* data file provide the user with pressure-time histories over a variety of points on the structure. *VecTor2* has the option of entering force-time loads in the form of impulse loads at every node on a structure. The force variation between two entered force-time points is calculated using a straight line approximation. This corresponds well with *VecTor-Blast* whose pressure-time points are also connected via straight lines.

In order to input blast loads in *VecTor2*, the user must convert the pressures from *VecTor-Blast* into nodal forces. This is accomplished by multiplying the pressures

by the tributary area of the elements surrounding the nodes to obtain a nodal force. A beam example is used to demonstrate these ideas.

The user may not necessarily want to load every node. If the distance from the explosion to the beam is much greater than its length, or the elements are very small, the blast pressures will not vary significantly between adjacent elements. Thus, fewer nodal forces are necessary and blast forces can be taken over larger areas.

The process of converting blast pressures to forces is described by examining the beam shown in Figure 5.1 with length, L , height, H , breadth, B , and element length, E .

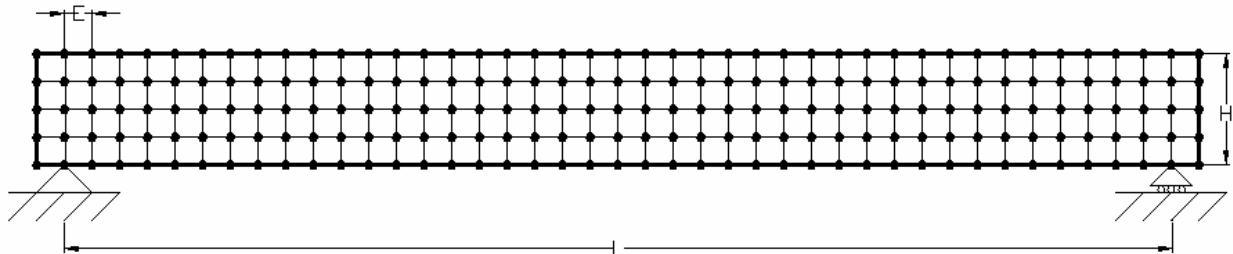


Figure 5.1 Finite element model of a beam.

It will be assumed that the user chooses to load every $L/10$ points. The pressure-time history at each location can be found from *VecTor-Blast*. The pressure-time profiles are converted into force-time profiles by multiplying the pressures by the area between the nodes as shown in Figure 5.2.

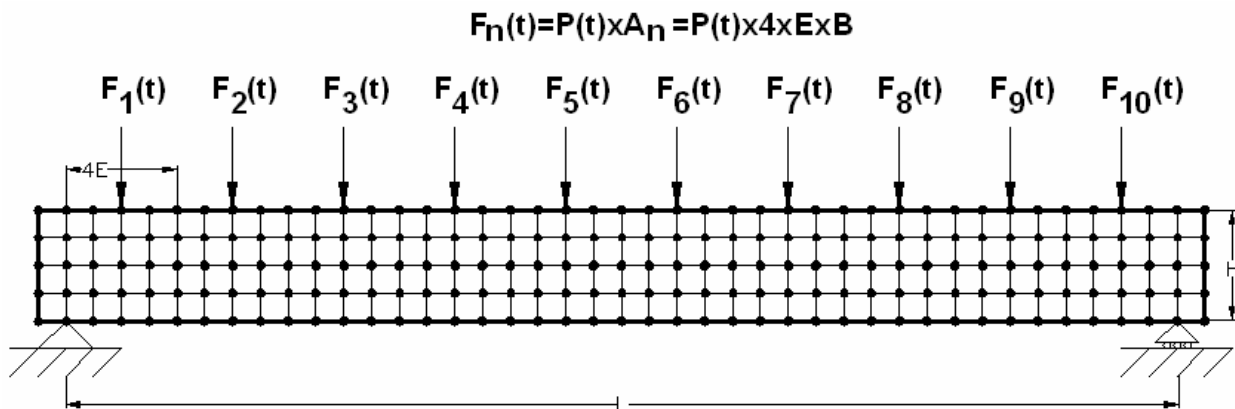


Figure 5.2 Blast forces on a beam.

The applied axial and lateral forces produced by the explosion are ignored in Figure 5.2. However, depending on their magnitude or the desired model requirements, they may have to be included. These forces can be found in much the same manner. The pressure-time profile is found at the centre of the area shown in Figure 5.3 and the force-time profile is found by multiplying the pressure by the area. The forces acting on the sides could play a particularly interesting role in this example as they could add a confining effect to the beam assuming the beam was loaded symmetrically in all planes.

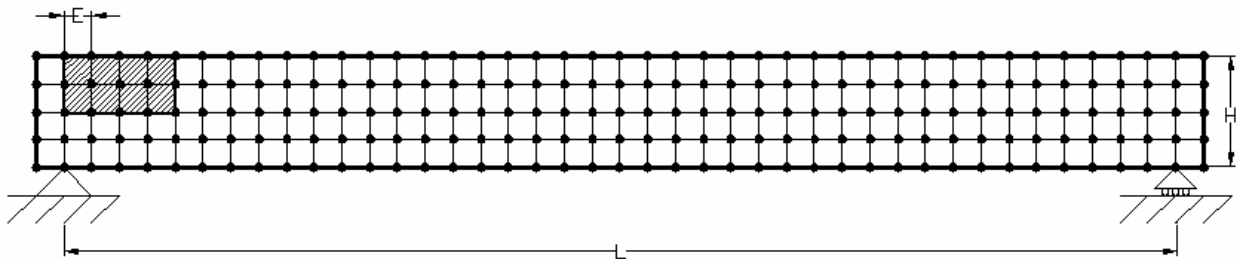


Figure 5.3 Lateral blast forces on a beam.

The application of blast forces in *VecTor2* is accomplished by applying “impulse loads” (time varying nodal forces) to the nodes. The main restriction is that *VecTor2*’s pre-processor allows only four entries corresponding to four points on a force-time curve. This may be adequate for simple cases where only the effect of the positive phase of the blast wave is examined. However, where the blast load may have more points (i.e. if the negative phase is included or the particular point is loaded by multiple waves), four points are insufficient. This limitation would have to be expanded.

Of important note, the direction of the blast pressures is stated in the *VecTor-Blast* data file. The directions are relative to those in Figure 3.1. Since blast pressures can act in two directions, (positive phase and negative phase), it is important to note that in *VecTor-Blast*, the direction given in the data file refers to the direction of the pressure acting at the arrival time of the first pressure. This pressure is considered positive. As the sign of the pressure changes so does the direction of the pressure.

5.1.2 *VecTor-Blast* and the remaining *VecTor* suite of programs

To be able to adequately model a structure's response to blast loads, a three-dimensional model is recommended. *VecTor-Blast* is unfortunately only compatible with *VecTor2* as other programs within the *VecTor* suite do not currently have dynamic loading and dynamic material response capabilities.

5.2 Trends in the Analytical Work

5.2.1 Direct Loading

From the results of the series of verification scenarios performed in Chapter 4, *VecTor-Blast* is able to calculate peak pressures, impulses, and durations matching those seen in experimental tests for elements directly loaded by an explosion.

There appears to be a little more disagreement between calculated and experimentally observed impulse values than with corresponding peak pressures and durations. This trend has been observed by other researchers (Armstrong et al., 2002). Armstrong reports that the variation in side-on impulse values varied much more than the variation in side-on peak pressure at the same scaled distance. However, calculated impulse values still match reasonably well with experimental results.

Accurate calculation of direct loads resulting from an explosion is paramount as these loads will often govern in a design. However, with complex loading scenarios involved in urban settings where blast waves are enhanced by multiple reflections off neighbouring structures, the direct load may not always govern.

5.2.2 Diffraction Events

Numerical corroborations showed that *VecTor-Blast* does not accurately calculate peak pressures and impulses when diffraction events are occurring. Comparison between calculated and experimental values demonstrates that *VecTor-Blast's* results are only adequate for multiple diffraction events occurring when a blast wave loads the rear of a structure. *VecTor-Blast's* calculated impulses and pressures

on the sides of the structure (one diffraction event) do not compare well with experimental results.

It was assumed that using one wave ray could capture the dominant effect of diffraction on the sides of the structure. This method has been found to be overly simplistic in this case and produces highly unconservative results as shown in Fig. 4.10 and 4.11. Therefore, a conservative approach is adopted in *VecTor-Blast* where the reduction in blast wave characteristics caused by diffraction is ignored and attenuation of the characteristics occurs only due to distance (on the sides and roof only, $DF=1$). However, ignoring the reduction of wave characteristics due to diffraction has led to overly conservative results in some cases.

Thus, there is a need to further develop diffraction calculations in *VecTor-Blast*. Instead of using only one wave ray, multiple rays should be used in an attempt to capture the full effects of diffraction.

This influence can be seen on the rear of the structure. Although only one wave ray is used per side, the blast wave is diffracting around three separate corners to reach the rear. The result is three wave rays combining at the rear. The dominant effects of diffraction are captured in this case as results on the rear of the structure match experimental results as shown in Figure 4.12 and Figure 4.13. Calculated impulse values are not as close to experimental values as are the calculated peak pressures. This is expected as only three combining wave rays are used to calculate impulse. Other diffracting wave rays, although arriving at later times, would also contribute to the overall impulse but because they are arriving later and travelling longer distances, their peak pressures will be lower and they will contribute less to the overall peak pressure.

Few experimental data points are reported in Armstrong et al. (2002) for the cases where diffraction events are occurring. Comparisons between experimental and calculated results are therefore difficult to evaluate precisely.

In addition, only one test case was used to verify *VecTor-Blast's* results during diffraction events. There was considerable difficulty in obtaining experimental data due to the nature and military sensitivity of blast research. This highlights the need for more

testing of *VecTor-Blast* and the need to develop an experimental program to produce the needed data.

5.3 Limitations of Analytical Work

- The structures appearing in this research are assumed to be in open areas where the interaction of the blast waves with other structures before reaching the target structure does not occur. This is not representative of a heavily built-up urban setting where the effects of the other structures would have to be taken into account.
- *VecTor-Blast* uses triangular equivalent loads instead of using exponentially decaying loads.
- Only rectangular structures with few openings can currently be analysed accurately.
- Explosives are restricted to conventional high explosives exhibiting ideal behaviour.
- Blast pressure calculations are limited by the data provided in TM 5-1300 (1969, 1990). Loading scenarios can exist that are outside of the data range but the pressure-time histories cannot be calculated for those scenarios.
- Thermal effects are neglected. Although the heat generated by an explosion can be extreme, thermal effects act for such a short period of time that they cannot produce significant effects on the concrete or steel. Usually, only local effects such as surface charring or spalling occur as a result.
- Ideal gas conditions are assumed to be valid.
- Vortex effects occurring at the corners of a structure created by the diffraction of the blast wave are neglected.
- Only blast wave interactions created by surface and free air bursts were adequately tested due to a lack of available data. More testing is required for air bursts generating mach waves or ground reflected waves.

5.4 Recommendations for Future Analytical Work

The following recommendations are suggested to improve the function of *Vector-Blast* and its integration with the *VecTor* suite of programs.

5.4.1 Recommendations for *VecTor*

- Increase the number of available force-time entries in *VecTor2*'s pre-processor to allow for better modelling of complex force-time histories.
- Include dynamic effects in the other *VecTor* suite of programs such that *VecTor-Blast*'s capabilities can be incorporated enabling full three-dimensional analyses of structures subjected to blast loads.
- Implement a Eulerian mesh in *VecTor* as the current Lagrangian mesh is not suited for high deformation situations created by blast loading. Many commercial programs used to predict blast loads employ hydrocodes which integrate Eulerian and Lagrangian methods as well as Smooth Particle Hydrodynamics where solid or fluid media are modeled as a collection of particles which move under the influence of hydrodynamic and gravitational forces.
- Implement spalling and scabbing capabilities in *VecTor* to account for local damage from blast loading.

5.4.2 Recommendations for *VecTor-Blast*

- Continue the testing of *VecTor-Blast*'s capabilities to verify the results produced by complex wave interactions such as mach stem formations. The need for more available data is particularly necessary. Experimental programs could be developed where data is difficult to obtain.
- Improve the method used to predict diffraction events. Multiple wave rays could be used to calculate pressure-time histories.
- Increase the integration with *VecTor* to facilitate the use of both programs. It is suggested that the loads calculated by *VecTor-Blast* could be directly inserted in the load files of *VecTor*.

- Expand *VecTor-Blast* to allow for more variance in structure shapes.
- Develop the ability to account for frangible portions in a structure which are blown out by an explosion leading to changes in blast pressures at other locations on the structure.
- Enlarge the explosive library of *VecTor-Blast* to enable the effects of non-ideal explosives to be analysed.
- Extend the TNT data in *VecTor-Blast* to allow for fewer restrictions in the loading scenarios particularly in the area of mach stem formations.

CHAPTER 6 CONCLUSIONS

Blast loads are becoming an increasingly important design consideration for civilian structures. As such, an in-depth understanding of explosives and their interaction with structures is necessary. Numerical tools can aid greatly in determining the design pressures and impulses as well as their respective influence with time.

The successful creation of *VecTor-Blast*, an analytical tool designed to calculate pressure-time histories on a structure is demonstrated in this research. *VecTor-Blast* can accurately calculate blast load characteristics and their dissipation with time at locations on an element directly loaded by the blast wave.

For locations on the element where diffraction occurs, more testing and further development is necessary. *VecTor-Blast* can calculate reasonable values on the rear of structures where the blast wave diffracts twice. However, *VecTor-Blast* currently over-predicts the pressure-time history on the sides of the structure because of a conservative approach adopted in the program. To obtain more accurate values, multiple ray paths should be used to create the pressure-time history. Despite some of the shortcomings in the diffraction modelling, results are generally satisfactory. The need for more data and more testing is also emphasized as data limitations hindered the testing of certain components of *VecTor-Blast*.

Further development is necessary such that the numerical tool can apply to urban settings where highly complex wave interactions occur and the threat of loss of life from explosions is extremely high.

Dynamic capabilities need to be expanded in most of the *VecTor* suite of programs. Furthermore, a Eulerian approach may need to be integrated into *VecTor* to allow for high deformation analysis.

REFERENCES

1. TM 5-1300, Department of the Army, (1969). "Structures to resist the effects of Accidental Explosions". TM 5-1300.
2. TM 5-1300, Department of the Army, (1990). "Structures to Resist the Effects of Accidental Explosions".
3. Armstrong et al. (2002). "Code Validation Studies for Blast in Urban Terrain" Proceedings of HPC Users Group Conference. June 10-14, Austin TX.
4. Baker, W.E. (1973). "Explosions in Air". University of Texas Press, Austin, Texas.
5. Baker, W.E., Cox, P.A., Westine, P.S., Kulesz J.J., Strehlow, R.A., (1983). "Explosion Hazards and Evaluation". Elsevier, Amsterdam.
6. Beshara, F.B.A. (1994). "Modelling of Blast Loading on Aboveground Structures-I. General Phenomology and External Blast", Computers and Structures, Vo. 51. No. 5, pp. 585-596.
7. Bischoff, P.H. and Perry, S.H. (1991). "Compressive Behaviour of Concrete at High Strain Rates", Materials and Structures, Vo. 24, pp. 425-450.
8. Bulson, P.S., (1997). "Explosive Loading of Engineering Structures". Chapman and Hall.
9. Dennis et al. (2002). "Response of 1/4-Scale Concrete Masonry Unit (CMU) Wall to Blast", Journal of Engineering Mechanics, Vo. 128, No. 2, pp. 134-142.
10. Crepeau, J. (1988). "SHAMRC Second-Order Hydrodynamic Automatic Mesh Refinement Code, Vol. 2 User's Manual". Applied Research Associates, Inc., Albuquerque, NM.

11. Dharaneepathy, M.V. (1993). "Air-Blast Effects on Shell Structures". Ph.D. thesis, Anna University, Madras.
12. Dharaneepathy, M.V., Keshava Rao, M. N., Santhakumar, A.R. (1995). "Critical Distance for Blast Resistant Design", Computers and Structures, Vo. 54. No. 4, pp. 587-595.
13. Feldman et al. (1962) "Investigation of Resistance and Behaviour of Reinforced Concrete Members Subjected to Dynamic Loading Part III", Technical Report to the Office of the Chief of Engineers Department of the Army, Contract DA 49-129-Eng-344.
14. Halquist, J. (1991). "LS-DYNA Theoretical Manual", Livermore Software Technology Corporation.
15. Harlow, F.H. and Amsden, A.A. (1970). "The SMAC Method: A Numerical Technique for Calculating Incompressible Fluid Flows," Los Alamos Scientific Laboratory Report, LA-4370.
16. Henrych, Josef, (1979). The Dynamics of Explosion and Its Use." Academia.
17. Hoffman, A.J. and Mills, (1956) S.N. Jr. "Air Blast Measurements About Explosive Charges At Side-On and Normal Incidence". BRL Report No. 988. Aberdeen Proving Ground, Maryland.
18. Hyde, D.W., (1992). "CONWEP, Conventional Weapons Effects Program", U.S. Army Engineer Waterways Experiment Station, Vicksburg, M.S.
19. Joachim, C.E., Armstrong, B.J., and Rickman, D.D. (2002). "Free-Field Airblast on Structures: Computational Model, "Proceedings of Symposium on Military Applications of Blast Simulations, June 10-14, 2002, Las Vegas, NV.
20. Kinney, Gilbert F. and Graham, Kenneth J., (1985). "Explosive Shocks in Air, 2nd Edition". Springer-Verlag, New York Inc.
21. Krauthammer, T et al. (1994). "Response of Structural Concrete Elements To Severe Impulsive Loads", Computers and Structures. Vo. 53, No. 1, pp. 119-130.

22. Krauthammer, T. and Ottani, R.K. (1997). "Mesh, Gravity and Load Effects on Finite Element Simulations of Blast Loaded Reinforced Concrete Structures," *Computers and Structures*, Vo 63, pp. 1113-1120.
23. Mohanty, B. (1998). "Physics of Explosion Hazards". In *Forensic Investigation of Explosions* edited by Alexander Beveridge, pp.15-44. Taylor and Francis Ltd., London.
24. Mohanty, B. (2003) University of Toronto, Engineering Geosciences. Meeting, Toronto, ON, 29 October, 2003.
25. Mohanty, B. (2004) University of Toronto, Engineering Geosciences. Meeting, Toronto, ON, 22 April, 2004.
26. Newmark, N.M. (1963). "Design of Structures for Dynamic Loads Including the Effects of Vibration and Ground Shock". In *Symposium on Scientific Problems of Protective Construction*, pp. 148-248. Swiss Federal Institute of Technology, Zurich.
27. Newmark, N.M. and Haltiwanger, J.D. (1962). *Air Force Design Manual: Principles and Practice of Hardened Structures*. SWL TDR-62-138, Air Force Special Weapons Centre, Kirkland, Air Force Base, NM.
28. Olatidoye et al. (1998). "A Representative Survey of Blast Loading Models and Damage Assessment Methods for Buildings Subjected to Explosive Blasts". Atlanta University, Atlanta GA 30314. A report funded by U.S. Department of Defence High Performance Computing Modernization Program. CEWES MSRC/PET TR/98-36.
29. Rickman, Denis and Murrell, Donald. (2004) "Small Scale Studies of Airblast Shielding of Structures: Preliminary Results", *Proceedings of the 24th Army Science Conference*, Orlando, Florida.
30. Ross, Tedesco, and Kuennan. (1995). "Effects of Strain Rate on Concrete Strength," *ACI Materials Journal*. Vo. 92, pp. 37-47.
31. Ripley et al. (2004). "Small-Scale Modelling of Explosive Blasts in Urban Scenarios", Prepared for the 21st International Symposium on Ballistics,

- Jan. 2004, Adelaide Australia, CERL (Canadian Explosives Research Laboratory) Report #2004-02(OP)
32. Schleuter, S.D., Hippensteel, R.G., and Armendt, B.F. (1965). "Measurements of Air Blast Parameters Above a Reflecting Surface". BRL Memo Report No. 1645, Aberdeen Proving Ground, Md.
33. Slawson, T.R. (1984). Dynamic Shear Failure of Shallow-Buried Flat Roofed Reinforced Concrete Structures Subjected to Blast Loading. Technical Report SL-84-7, Structures Laboratory, U.S. Army Engineer Waterways Experiment Station, Vicksburg, Miss.
34. Smith, P.D. and Hetherington, J.G., (1994). "Blast and Ballistic Loading of Structures". Butterworth-Heinemann Ltd., Oxford, © 1994.
35. Smith, P.D., Rose, T.A., Saotonglang, E. (1999). "Clearing of Blast Waves from Building Facades", Proc. Instn. Civ. Engrs. Structs & Bldgs, Vo. 134, pp. 193-199.
36. Technical Service of the Explosives Division. (1946). "Blaster's Handbook". Canadian Industries Ltd. Explosive Division, Montreal, Que.
37. U.S. Army. (1957) "Design of Structures to Resist the Effects of Atomic Weapons". Manuals – Corps of Engineers, EM 1110-345-414, 415, 416, Washington, D.C.
38. Vecchio, F.J. and Collins, M.P. (1986). "The Modified Compression Field Theory for Reinforced Concrete Elements Subjected to Shear", ACI Journal, Vo. 183, No. 2, pp. 219-231.
39. Vecchio, F.J. (2000). "Disturbed Stress Field Model For Reinforced Concrete: Formulation", Journal of Structural Engineering-ASCE, Vo. 126, No. 9, pp. 1070-1077.
40. Wampler, H.W., Leigh, G.G., and Furbee, M.E. (1978). "A Status and Capability Report on Nuclear Airblast Simulations Using HEST," Proceedings of the Nuclear Airblast and Shock Simulation Symposium, 28-30 November 1978, Vol. 1, General Electric-TEMPO, Santa Barbara, Calif.

41. Williams et al. (1991). "Method for the Assessment of the Blast Response of Structures". In Earthquake, blast, and impact: measurement and effects of vibration edited by SECED (Society for earthquake and civil engineering dynamics), pp.176-185. Elsevier Applied Science, London.
42. Whirley, R.G., and Engelmann, B. E. (1993). "DYNAD3D – A Nonlinear, Explicit, Three-Dimensional Finite Element Code for Solid and Structural Mechanics – User Manual." *Rep. UCRL-MA-107254, Rev. 1*, Lawrence Livermore National Laboratory, Livermore, Calif.

APPENDIX A VECTOR-BLAST USER'S MANUAL

A.1 Introduction

VecTor-Blast is a pre-processor that generates blast loads for use in finite element analysis of concrete structures. The role of *VecTor-Blast* is to provide a graphical user interface through which blast pressure calculations can be made. This manual provides assistance for using *VecTor-Blast*. *VecTor-Blast* was created in Visual C++ and works most efficiently in Windows XP. *VecTor-Blast* may not run well in older versions of Microsoft Windows because the operating system has been changed by Microsoft. Updating the comctl32.dll file, that can be downloaded from the following site,

<http://support.microsoft.com/default.aspx?scid=kb;en-us;167121>

will fix many of the problems. Furthermore, updating the version of Microsoft Internet Explorer should accomplish the same result.

A.2 *VecTor-Blast* Basics

A.2.1 *VecTor-Blast* Interface

Upon starting *VecTor-Blast*, an introduction window appears over the view window. The introduction window disappears if you click the mouse, hit a key, or wait a few seconds and the view window remains as shown in Figure A.1. *VecTor-Blast* is a single document interface. The exact appearance will vary slightly depending on the operating system.

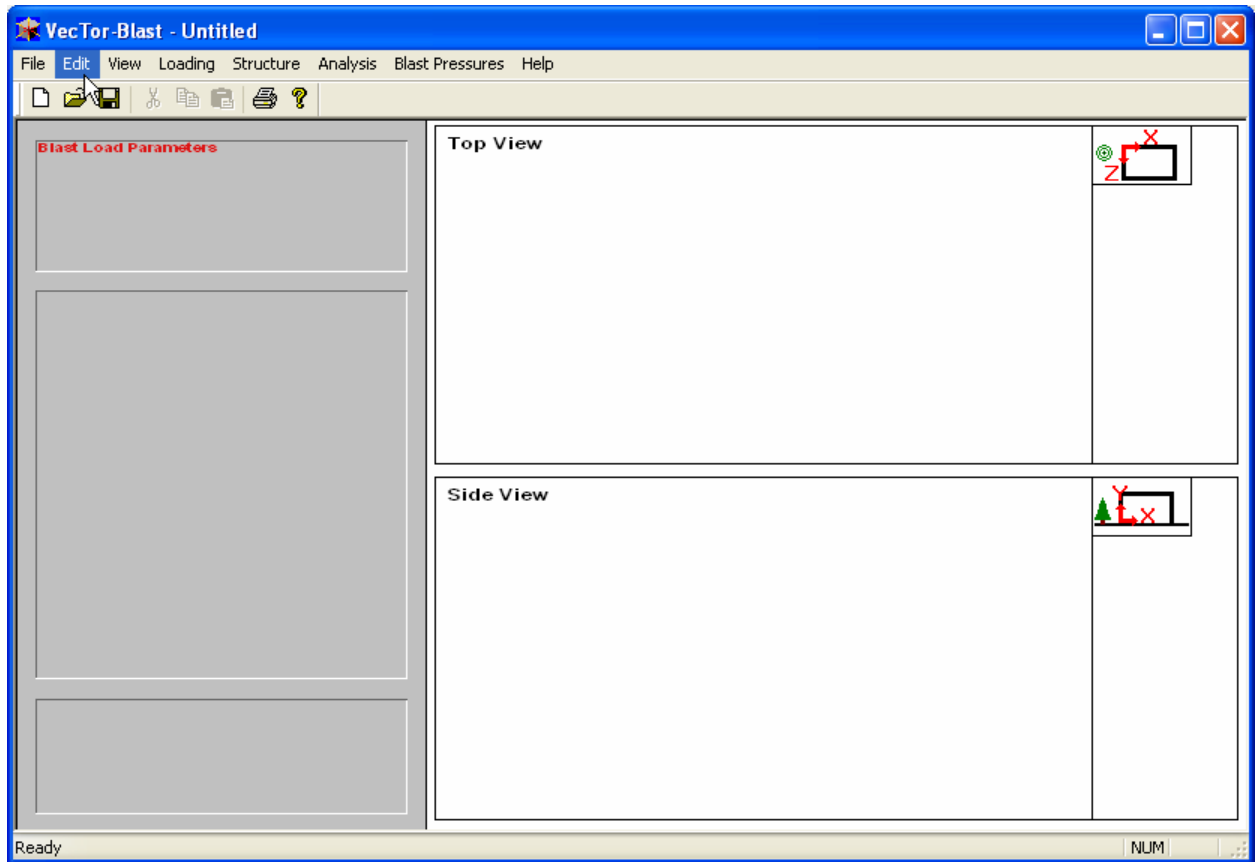


Figure A.1 *VecTor-Blast* Interface.

The menu bar contains the following visible menus: **File**, **Edit**, **View**, **Loading**, **Structure**, **Analysis**, **Blast Pressures**, and **Help**. Not all of the submenus are immediately available but become available as the modelling proceeds.

The window is divided into five major boxes.

- **Blast Load Parameters**

This box displays the details of the explosive used in the model.

- **The Middle Grey Box**

This box graphically displays the predicted blast load at a location on the structure.

- **The Bottom Grey Box**

This box contains the axes modification buttons. These buttons enable the user to change the scales of the axes on the graph.

- **Top View**

This box displays the plan view of the structure. The smaller box with the x-z coordinate system displays the x and z distances to the explosion from the origin. The origin in the x-z coordinate system occurs at the top left corner of the structure.

- **Side View**

This box displays the elevation view of the structure. The smaller box with the x-y coordinate system displays the x and y distances to the explosion from the origin. The origin in the x-y coordinate system is the bottom left corner of the structure.

A.2.1.1 Creating and Saving the File

To create a new file:

1. Select the **File/New** menu item. You will be asked if you want to save the current file. Click Yes or No. Everything on the screen will be erased and a blank screen will be shown.
2. To save the file:
3. Select the **File/Save** menu item.
4. Select the directory in which to save the file.
5. Enter a name for the file.

6. Click **Save**.

To save another version of the same file, select **File/Save As** menu item and follow steps 1 to 4 while changing the name of the file.

A.2.1.2 Opening a Saved File

To open a saved file:

1. Select the **File/Open** menu item. The **Open** dialog box appears.
2. Browse for and selected the desired *VecTor-Blast* file.
3. Click **Open**.

A.2.2 Menus

Control in *VecTor-Blast* is achieved through menu options allowing the user to make inputs and selections. This section will provide a description of the various menus and their individual options.

A.2.2.1 Blast Load Parameters Menu

To open the Blast Load Parameters dialog box:

1. Select the **Loading/Blast Parameters** menu item. The Blast Load Parameters dialog box appears as shown in Figure A.2.

Blast Load Parameters

General Information

Title:

Job File:

Analysis By:

OK

Cancel

Loading

Explosion

Conventional High Explosive

Amount of Explosive

Mass (kg):

Explosive Type

Built In

Custom

Explosive Name:

Heat of Combustion (kJ/mol):

Example (TNT): 4520 kJ/mol

Figure A.2 Blast Load Parameters dialog box.

2. Input the required data.
3. Click **OK**.
4. A summary of the entered information will appear in the grey Blast Load Parameters Box in the left hand corner of the main window (see Figure A.1).

A.2.2.1.1 Menu Options

A.2.2.1.1.1 General Information

- **Title**
Enter an alpha-numeric title up to 30 characters long. The title appears in the data file generated at the end of the analysis.
- **Job File**
Enter the name of the job file using up to 6 alpha-numeric characters. This will set the name of the data file.
- **Analysis By**
Enter the name of the user doing the analysis up to 30 characters long. The name appears in the data file.

A.2.2.1.1.2 Loading

- **Explosion**
Currently *VecTor-Blast* is restricted to conventional high explosives and this option cannot be changed.
- **Amount of Explosive**
Enter the mass of explosive in kg to which the structure will be subjected.
- **Explosive Type**
Select either Built-In or Custom explosive. The default built-in explosive is TNT. Others can be selected from the pull down list.
If Custom is chosen, it is recommended that a name be entered for the explosive using up to 20 characters. The heat of combustion in kJ/mol must be entered. Only one explosive type can be selected at once. The other will be inactive.

A.2.2.2 Building Details Menu

Once the blast parameters have been entered, the **Structure/Building** menu will become active.

To open the Building Details dialog box:

1. Select the **Structure/Building** menu item. The Building Details dialog box appears as shown in Figure A.3.

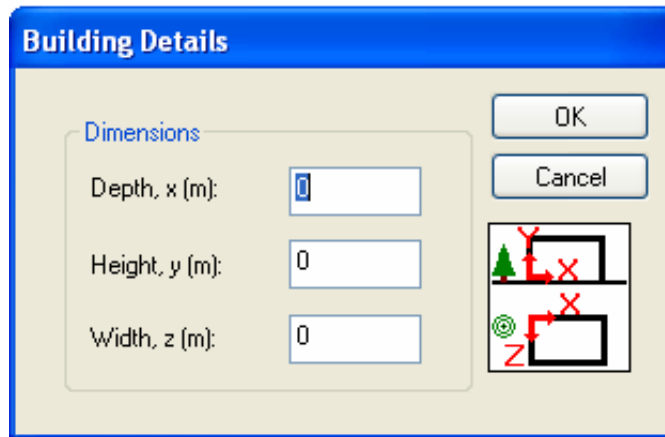


Figure A.3 Building Details dialog box.

2. Input the required data.
3. Click **OK**.
4. The plan and elevation view of the structure will appear in the Top View and Side View boxes along with the dimensions of the structure (see Figure A.1).

A.2.2.2.1 Menu Options

A.2.2.2.1.1 Dimensions

- **Depth, x (m):**
Enter the depth or x-dimension of the structure in m.
- **Height, y (m):**
Enter the height or y-dimension of the structure in m.
- **Width, z (m):**
Enter the width or z-dimension of the structure in m.

A.2.2.3 Blast Location Menu

The **Analysis/Blast Location** menu is now active.

To open the Blast Location dialog box:

1. Select the **Analysis/Blast Location** menu item. The Blast Location dialog box appears as shown in Figure A.4.

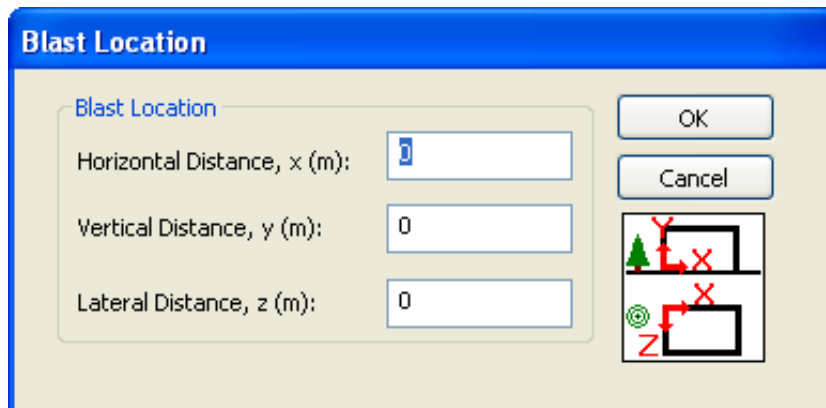


Figure A.4 Blast Location dialog box.

2. Input the required data.
3. Click **OK**.
4. The location of the explosion and the explosion itself will appear in the Top View and Side View boxes (see Figure A.1).

A.2.2.3.1 Menu Options

A.2.2.3.1.1 Blast Location

- **Horizontal Distance, x (m):**
Enter the horizontal distance from the origin to the explosion in m.
- **Vertical Distance, y (m):**
Enter the vertical distance from the origin to the explosion in m.
- **Lateral Distance, z (m):**
Enter the lateral distance from the origin to the explosion in m.

The entered distances must always place the explosive outside the structure and within the boundaries of the width (z-dimension) of the structure.

A.2.2.4 Diffraction Factor Menu

The Analysis/Diffraction Factor menu is now active.

To open the Diffraction Factor dialog box:

1. Select the **Analysis/Diffraction Factor** menu item. The Diffraction Factor dialog box appears as shown in Figure A.5.
2. The default base factors are displayed.
3. Click **Ok** to close the dialog box.

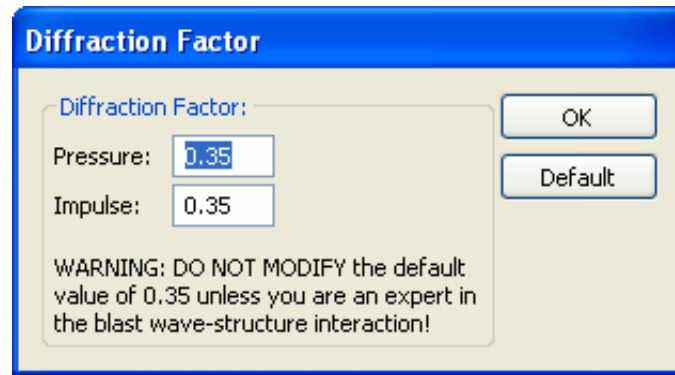


Figure A.5 Diffraction Factor dialog box.

A.2.2.4.1 Menu Options

A.2.2.4.1.1 Diffraction Factors

- **Pressure:**

This base factor is used to create a diffraction coefficient to account for the pressure reduction due to diffraction.

- **Impulse:**

This base factor is used to create a diffraction coefficient to account for the impulse reduction due to diffraction.

The diffraction coefficient, DC, is calculated by Eq. A.1

$$DC = DF^n \quad (A.1)$$

DF is the base factor for pressure or impulse and n represents the number of corners the blast wave must travel around to reach the point on the structure for which the analysis is being performed.

A.2.2.5 Graph Pressures Menu

The Blast Pressures/Pressure-Time Profile menu is now active.

To open the Graph Pressure dialog box:

1. Select the **Blast Pressures/Pressure-Time Profile** menu item. The Graph Pressure dialog box appears as shown in Figure A.6.

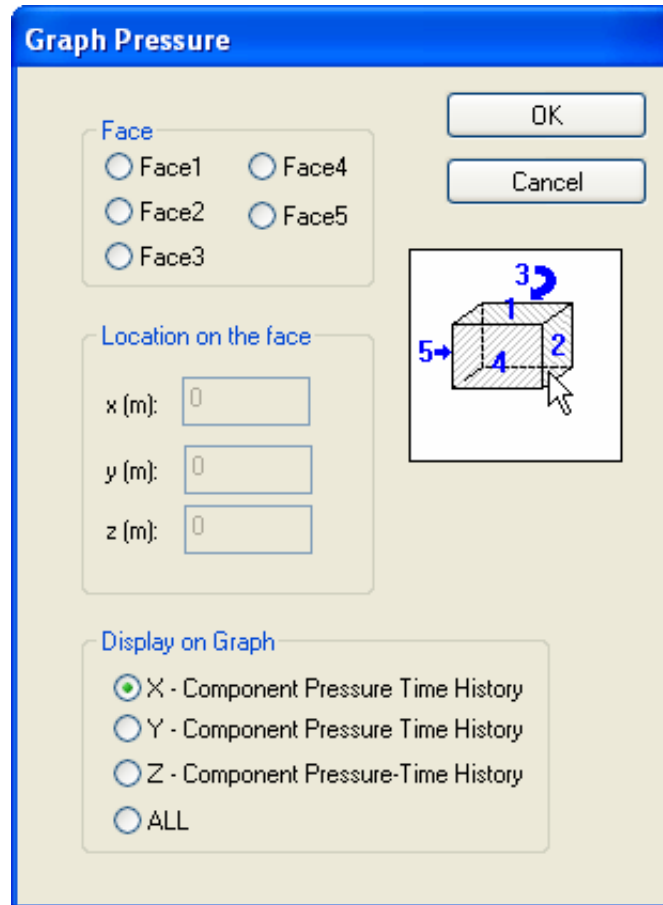


Figure A.6 Graph Pressure dialog box.

2. Click on the face for which the analysis is required. The x, y, and z coordinate boxes will now be active.
3. Input the required data.
4. Select which pressure-time components are to be displayed on the graph.
5. Click **OK**.

A graph of the pressure-time history on the entered analysis point is displayed in the middle grey box (see Figure A.1).

A.2.2.5.1 Menu Options

A.2.2.5.1.1 Face

Click on the face where the analysis is required. This will activate the coordinates on the face. Depending on which face is selected, some of the input locations will be disabled. This is to ensure that the entered coordinates are on the surface of the face selected.

A.2.2.5.1.2 Location on the Face

- **x (m):**

Enter the horizontal or x-coordinate of the analysis point in m.

- **y (m):**

Enter the vertical or y-coordinate of the analysis point in m.

- **z (m):**

Enter the lateral or z-coordinate of the analysis point in m.

A.2.2.5.1.3 Display on Graph

Select the pressure-time components that you wish to have displayed on the graph. If you are unsure which ones will appear, click **All**. There can be situations where some of the components are zero and nothing will be displayed on the graph if you select that particular component to be displayed.

A.2.3 Axes Buttons

The user is able to scale the graph using the axes buttons, shown in Figure A.7, only after the graph appears.

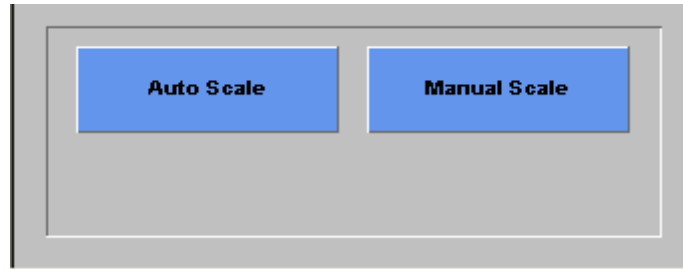


Figure A.7 Axes buttons.

A.2.3.1 Auto Scale

Clicking this button will scale the graph to the default setting such that the entire graph is displayed.

A.2.3.2 Manual Scale

Clicking the Manual Scale button will launch a menu shown in Figure A.8. The user is able to insert custom maximum and minimum values for the x and y axes on the graph.

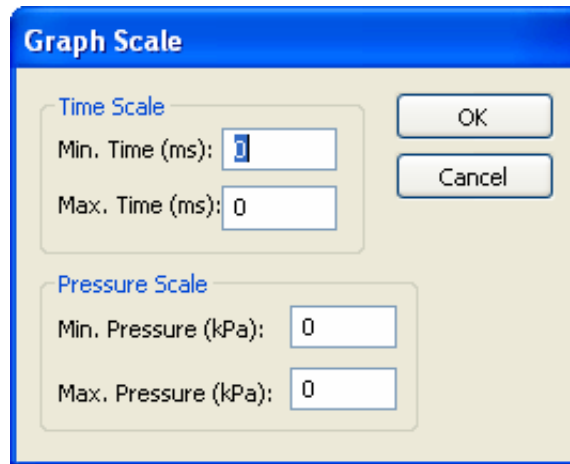


Figure A.8 Graph Scale dialog box.

A.2.3.2.1 Time Scale

- **Min Time (ms):**
Enter the minimum value of the time axis in milliseconds (ms).
- **Max Time (ms):**
Enter the maximum value of the time axis in milliseconds (ms).

A.2.3.2.2 Pressure Scale

- **Min Pressure (kPa):**
Enter the minimum value of the pressure axis in kPa.
- **Max Pressure (kPa):**
Enter the maximum value of the pressure axis in kPa.

A.2.4 The Data File

A data file, "Job.txt", is created after the analysis. The data file contains greater detail than the graph can provide. Information for the data file is generated after each analysis. If the same analysis point is chosen two or more times in a row, the data will only be written once to the data file. As a new point is chosen, the corresponding generated information is added to the data file. The data file can be broken down into three sections: blast parameters, structural parameters, and wave parameters.

- **Blast Parameters**
This section contains the details entered in the Blast Load Parameters dialog box.
- **Structural Parameters**
This section contains the following details:
 - the size of the structure

- the location of the explosive
 - the face on which the analysis point is located
 - the coordinates of the analysis point
 - the distance and scaled distance from the analysis point to the explosive
 - the angles of incidence
- **Wave Parameters**
- This section contains the details of each x, y, and z component of every wave hitting the analysis point. The parameters included are all the basic side-on and face-on values. The pressure-time histories are obtained by combining certain parameters together. The final pressure-time histories of each component of every wave are also included in addition to final combined pressure-time histories if there are multiple waves striking the analysis point.

A.3 General Modelling Considerations

The following are few general tips and modelling suggestions.

- *VecTor-Blast* was not designed for extremely near explosions (i.e. explosion almost on the surface of the structure); therefore the results may not be accurate in such cases.
- Model near ground explosions as explosions on the ground. Blast wave parameters are calculated based on scaled height of the blast (height of the explosion/mass of explosive^{1/3}). Data in *VecTor-Blast* for scaled heights of blast does not cover a large range and is generally limited to significant heights, thus a small blast height may be out of range.
- If a custom explosive is used, ensure that the custom explosive is a high explosive exhibiting ideal behaviour, otherwise it cannot accurately be compared to TNT using heat of detonation and the results will not be accurate.

A.4 Example

An example is provided with a step by step procedure to help a new user become more familiar with *VecTor-Blast*.

The pressure-time history is found at the centre point of the roof of a 20 m long by 30 m wide by 10 m high structure from 100 kg of Compound B detonating at the following location: x=15 m, y=30 m, and z=15 m.

1. Double click the **VecTor-Blast.exe** file
2. Select the **Loading/Blast Parameters** menu to bring up the Blast Load Parameters dialog box and enter the information as shown in Figure A.9.

Blast Load Parameters

General Information

Title: Example

Job File: Job

Analysis By: User's Name

OK

Cancel

Loading

Explosion

Conventional High Explosive

Amount of Explosive

Mass (kg): 100

Explosive Type

Built In

Compound B (60%RDx, 40%TNT)

Custom

Explosive Name: Custom Explosive

Heat of Combustion (kJ/mol): 0

Example (TNT): 4520 kJ/mol

Figure A.9 Example Blast Load Parameters dialog box.

3. Click **OK**.
4. Note that a summary of the entered input parameters as well as the equivalent TNT mass, appear in the top left grey rectangle as shown in Figure A.10.

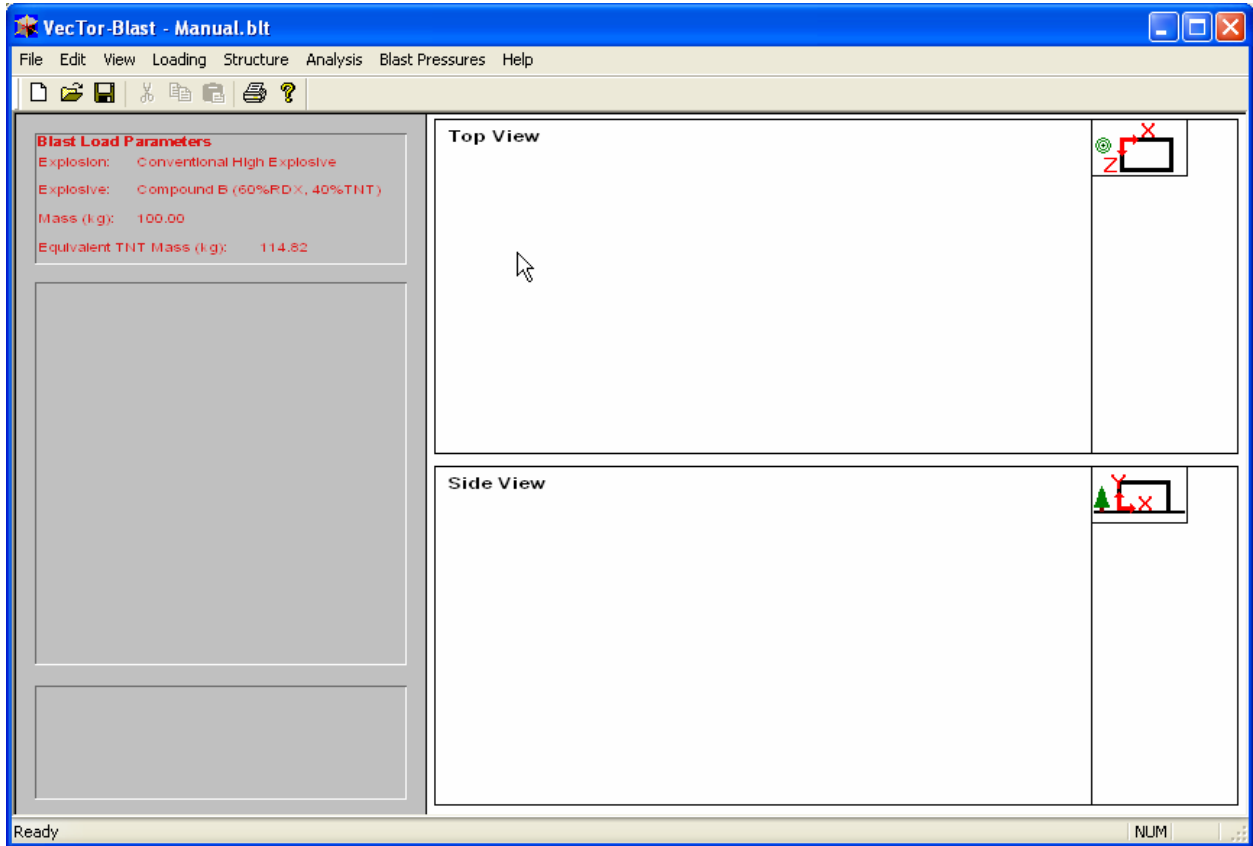


Figure A.10 Example view window with blast load parameters.

5. Select the **Structure/Building** menu to bring up the Building Details dialog and enter the building dimensions as shown in Figure A.11.

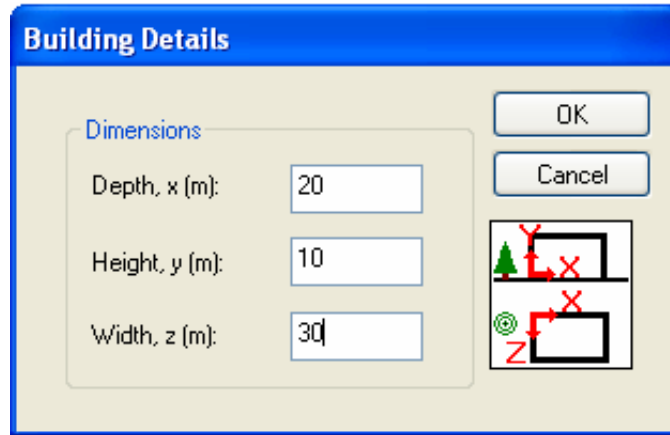


Figure A.11 Example Building Details dialog box.

6. Click **Ok**. The structure appears with dimensions as shown in Figure A.12.



Figure A.12 Example view window with the structure.

7. Select the **Analysis/Blast Location** menu to bring up the Blast Location dialog box and enter the blast location dimensions as shown in Figure A.13.

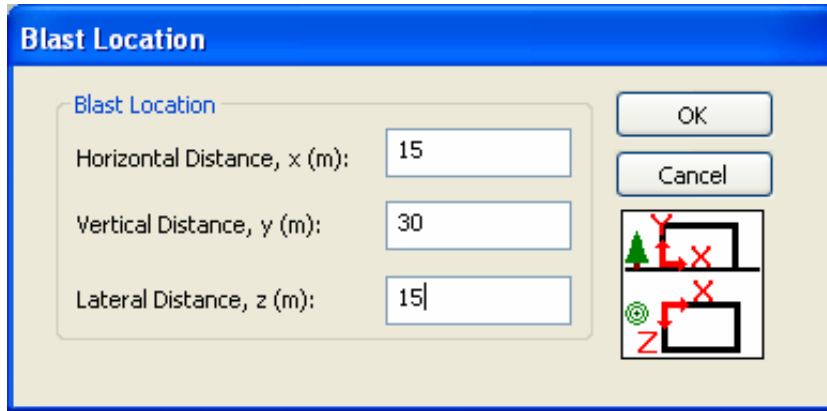


Figure A.13 Example Blast Location dialog box.

8. Click **OK**. The blast location is displayed as shown in Figure A.14.

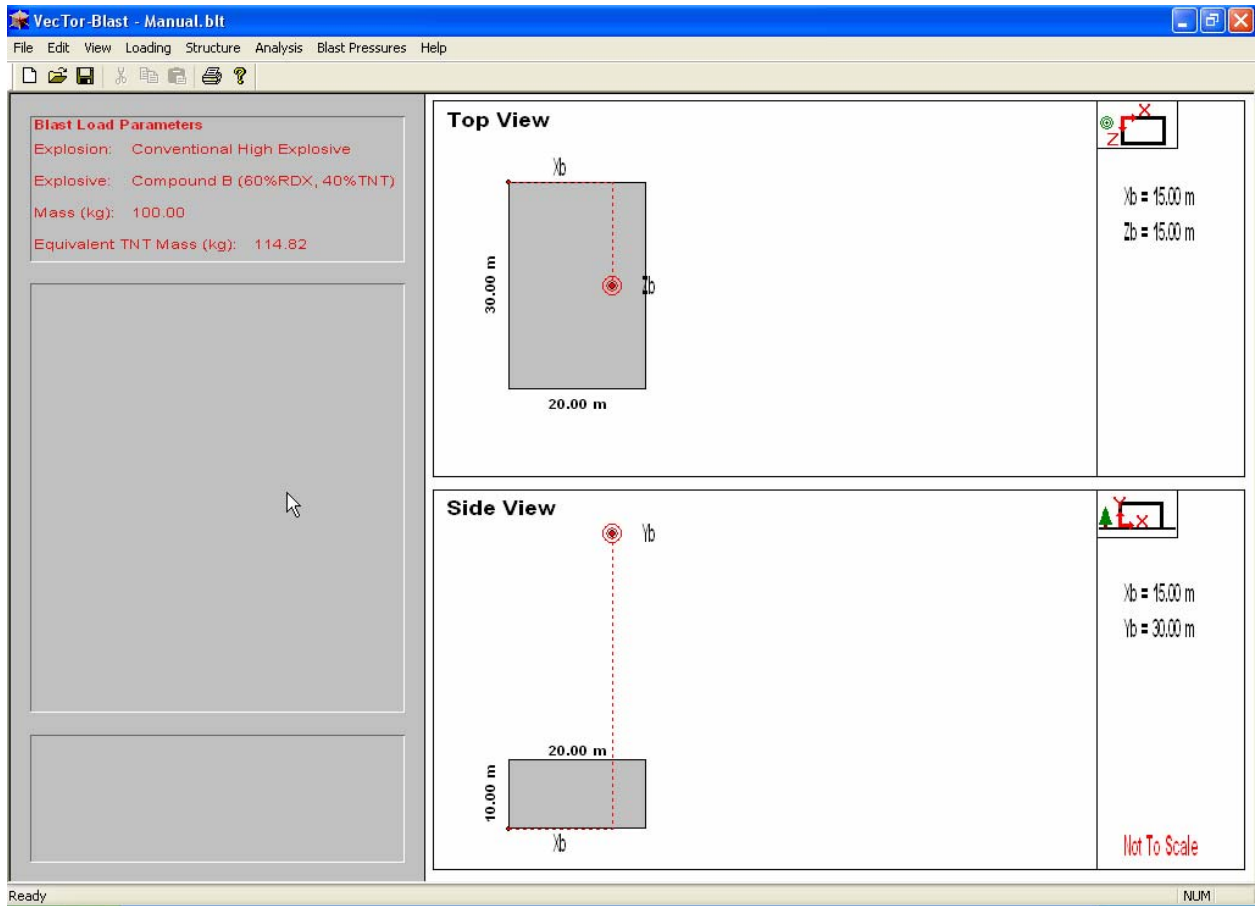


Figure A.14 Example view window with the blast location.

9. Select the **Blast Pressures/Pressure-Time Profile** menu to bring up the Graph Pressure dialog box and enter the location of the centre of the roof as shown in Figure A.15. Select **ALL** so all component pressure-time histories can be seen on the graph.

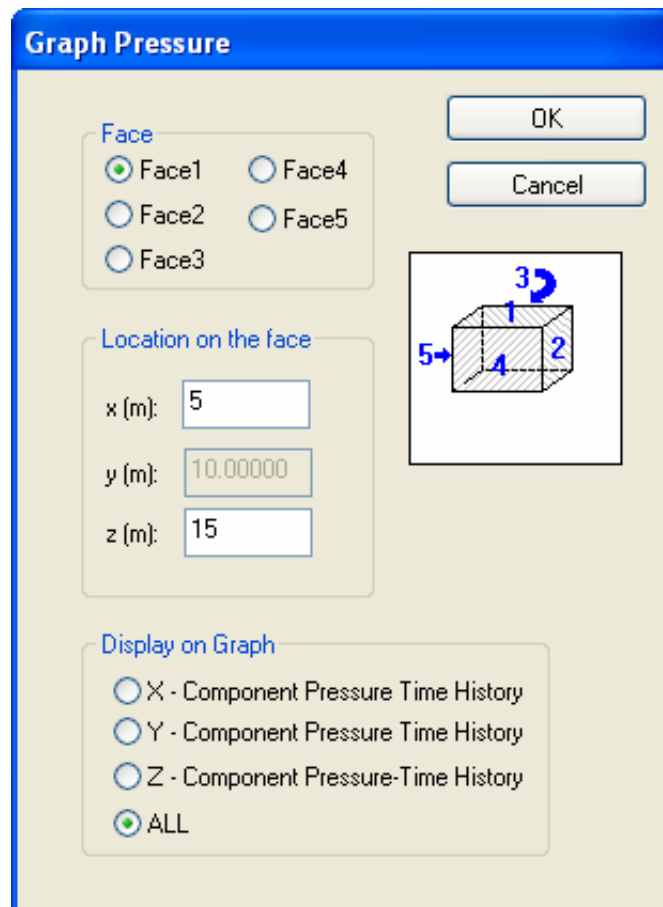


Figure A.15 Example Graph Pressure dialog box.

10. Click **OK**. The graph is displayed as shown in Figure A.16.

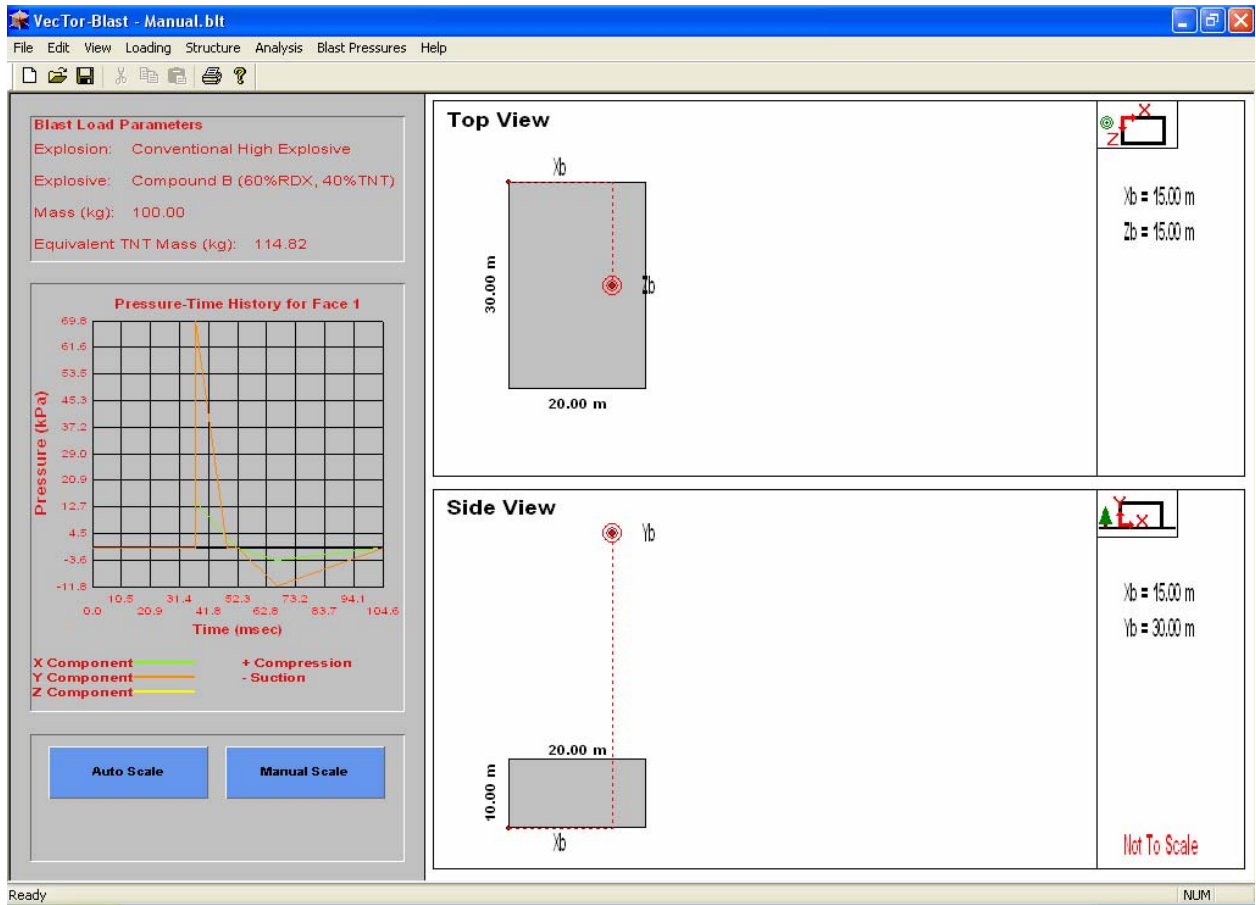


Figure A.16 Example view with graph.

- To examine only the positive phase, click the manual scale button to display the Graph Scale dialog box and enter the values shown in Fig. A.17.

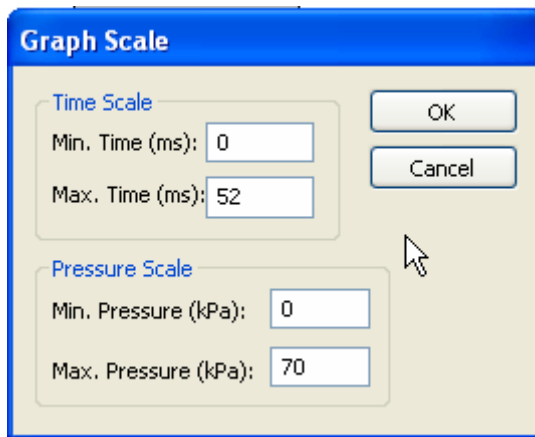


Figure A.17 Example Graph Scale dialog box.

12. Click **OK**. The new graph is displayed as shown in Figure A.18.

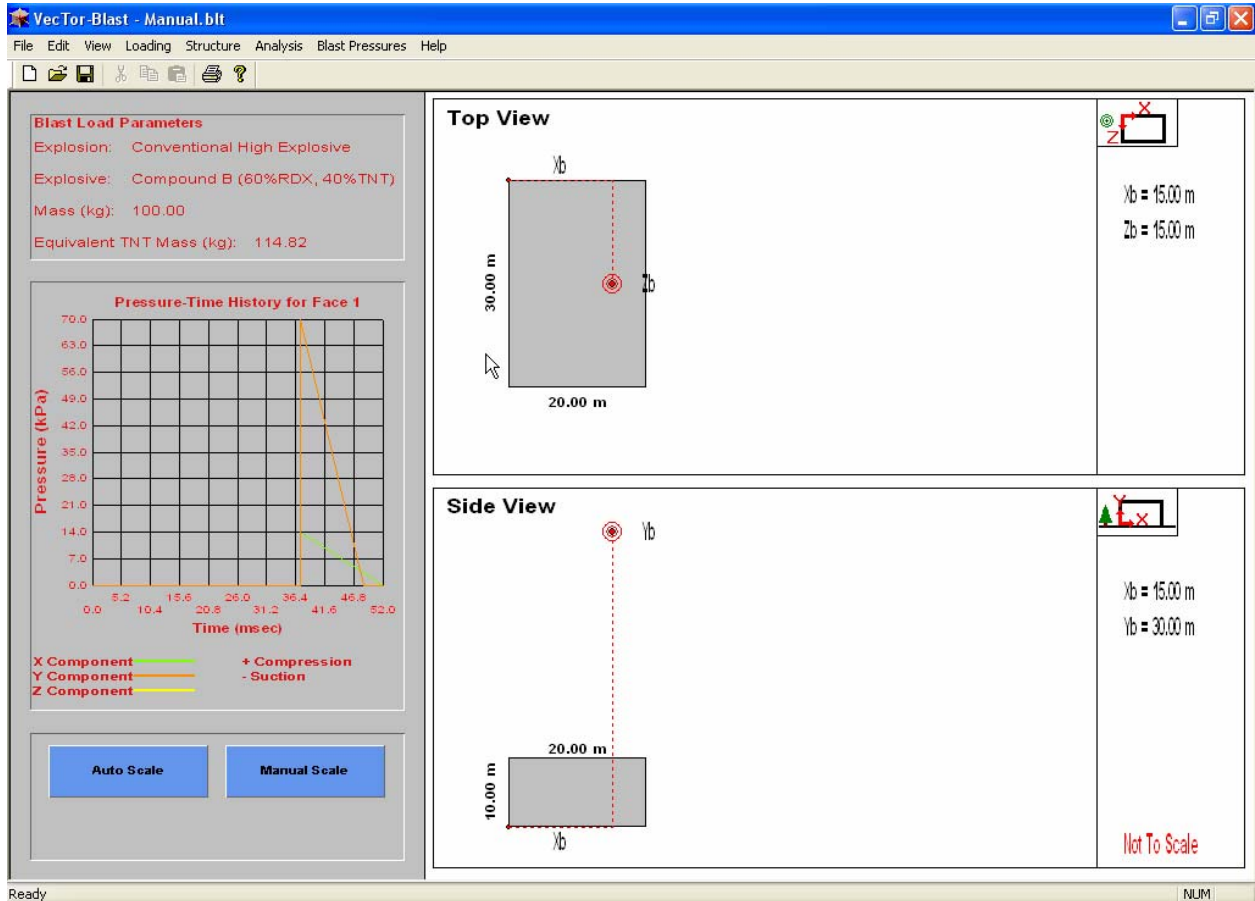


Figure A.18 Example view with modified graph.

13. The user may want to examine the data file for a more detailed look at the information. Locate the folder in which the VecTor-Blast.exe file is residing and double click on Job.txt.
14. The data file will open and look similar to Figure A.19. Only a portion of the data file is displayed here due to its size.
15. To view the pressure-time history at other locations, repeat steps 9 to 12 changing the face and the coordinates of the location.

```

Job - Notepad
File Edit Format View Help
Title: Example
Analysis By: User's Name
Job File: Job

BLAST PARAMETERS
Explosive: Compound B (60%RDX, 40%TNT)
Mass(kg): 100.000
Equivalent
TNT Mass(kg): 114.823
Explosion Type: FREE AIR BURST

STRUCTURAL PARAMETERS
Structure x(m) y(m) z(m)
Blast Location 20.00 10.00 30.00
Face: 15.00 30.00 15.00
Face: 1
Analysis Point 5.00 10.00 15.00
Distance(m): 22.361
Scaled
Distance(m/kg^(1/3)): 4.601
alphazxy(deg): 26.57
alphazx(deg): 90.00

WAVE PARAMETERS
Arrival Ps+ Dynamic Drag Impulse+
Time(ms) (kPa) Pres.(kPa) Coeff. (kPa-msec)
X-Compt 37.35 14.1 0.0 0.0 104.2
Y-Compt 37.35 28.2 2.7 1.0 208.3
Z-Compt 0.00 0.0 0.0 0.0 0.0

Ref. Imp.+ Pr+ Clearing Fict. Pos. Ref. Pos.
(kPa-msec) (kPa) Time(ms) Dur.(ms) Dur.(ms)
X-Compt 104.2 14.1 0.00 14.78 14.78
Y-Compt 390.1 69.8 15.20 14.78 11.18
Z-Compt 0.0 0.0 0.00 0.00 0.00

Positive Ps- Pr- Neg. Rise Negative
Dur.(ms) (kPa) (kPa) Time(ms) Dur.(ms)
X-Compt 15.20 4.0 4.0 13.68 50.67
Y-Compt 15.20 9.4 11.8 14.05 52.04
Z-Compt 0.00 0.0 0.0 0.00 0.00

****Pressure-Time Results****

```

Figure A.19 Example data file.

A.5 List of Data File Symbols

Mach Stem Forms: 1 means yes, 0 means no

Point in Mach Stem: 1 means yes, 0 means no

Z from Pressure

Scaled distance corresponding to incident (side-on) overpressure

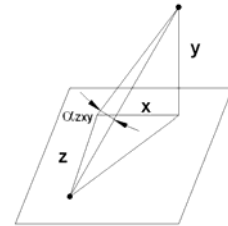
Z from Impulse

Scaled distance corresponding to incident (side-on) impulse

alphazxy

angle between the incident wave and the analysis point on the structure.

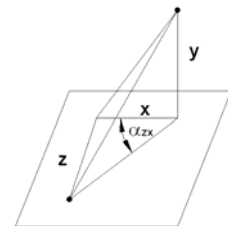
$$\alpha_{zxy} = \tan^{-1} \left(\frac{z}{\sqrt{x^2 + y^2}} \right)$$



alphazx

angle between the incident wave and the analysis point on the structure (z-x plane only).

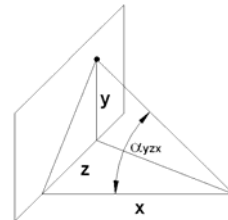
$$\alpha_{zx} = \tan^{-1} \left(\frac{z}{x} \right)$$



alphazyx

angle between the incident wave and the analysis point on the structure.

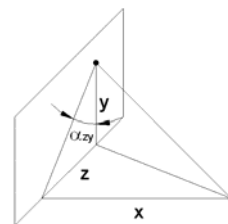
$$\alpha_{zxy} = \tan^{-1} \left(\frac{\sqrt{y^2 + z^2}}{x} \right)$$



alphazy

angle between the incident wave and the analysis point on the structure (z-y plane only).

$$\alpha_{zy} = \tan^{-1} \left(\frac{z}{y} \right)$$



Ps+	Incident (side-on) overpressure*
Impulse+	Incident (side-on) impulse*
Ref. Imp.+	Reflected positive impulse
Pr+	Reflected positive overpressure
Fict. Pos. Dur.	Fictitious positive duration
Ref. Pos. Dur.	Reflected positive duration
Positive Dur.	Positive duration
Ps-	Incident (side-on) underpressure*
Pr-	Negative reflected underpressure
Neg. Rise Time	Negative rise time
Negative Dur.	Negative duration
dir	The direction of the overpressure relative the positive sign convention

*where a diffraction coefficient is used, the pressures and impulses have already been multiplied by the diffraction coefficient

A.6 Error Messages

All available error messages are shown here with an explanation of what they mean. These error messages appear if the user has entered invalid information or the calculations cannot proceed because the combined inputs places certain values out of range.

Message:	<i>Reflected Impulse too high. Out of range of computable scaled distances.</i>
Description:	The calculated reflected impulse is out of range of available surface burst data. The scaled distance corresponding to the reflected impulse cannot be calculated. $26.6 < I_r < 30780 \text{ kPa}\cdot\text{ms}/\text{kg}^{1/3} \text{ (} 4.25 < I_r < 3430 \text{ psi}\cdot\text{ms}/\text{lb}^{1/3}\text{)}$
<hr/>	
Message:	<i>Reflected Pressure out-of-range of computable scaled distances. 12.7 < P_r < 373000 kPa</i>
Description:	The calculated reflected pressure is out-of-range of available surface burst data. The scaled distance corresponding to the reflected pressure cannot be calculated. $12.7 < P_r < 373000 \text{ kPa (} 1.85 < P_r < 54100 \text{ psi)}$
<hr/>	
Message	<i>No Face Selected</i>
Description	The user has not chosen a surface on the structure where the pressure-time history will be calculated.
<hr/>	
Message	<i>The point selected is not on the structure. Please make another selection.</i>
Description	The entered x, y, and z coordinates does not place the analysis point on the structure's surface.
<hr/>	
Message:	<i>Positive Reflected Scaled Impulse out-of-range of computable scaled distances. 23.63 < I_r < 24200 (kPa-ms)/kg^(1/3) Negative Pressure-Time history cannot be calculated for this wave component.</i>
Description:	The calculated reflected impulse is out of range with the available free air burst data. The scaled distance corresponding to the reflected impulse cannot be calculated. $23.6 < I_r < 24200 \text{ kPa}\cdot\text{ms}/\text{kg}^{1/3} \text{ (} 4.46 < I_r < 4570 \text{ psi}\cdot\text{ms}/\text{lb}^{1/3}\text{)}$
<hr/>	
Message:	<i>Positive Reflected Pressure out-of-range of computable scaled distances. 19.31 < P_r < 572000 kPa Negative Pressure-Time history cannot be calculated for this wave component.</i>

Description:	The calculated reflected pressure is out-of-range of available surface burst data. The scaled distance corresponding to the reflected pressure cannot be calculated. $19.31 < P_r < 572000 \text{ kPa}$ ($2.8 < P_r < 83000 \text{ psi}$)
Message:	<i>Incident Pressure out-of-range.</i> <i>Pressure must be less than 44800 kPa (6500 psi)</i>
Description:	The dynamic pressure can only be calculated for incident (side-on) overpressures up to 44800 kPa to correspond with available data. $P_{so} < 44800 \text{ kPa}$ ($P_{so} < 6500 \text{ psi}$)
Message:	<i>Z Outside Range for Surface Burst.</i> $0.12 \leq Z \leq 19.8 \text{ m/kg}^{1/3}$
Description:	The available blast parameters for surface burst only exist for a range of scaled distances. $0.12 < Z < 19.8 \text{ m/kg}^{1/3}$ ($0.3 < Z < 50 \text{ ft/lb}^{1/3}$)
Message:	<i>Scaled Height of Charge Outside Range of Available Data.</i> $2.53 \leq H_c \leq 17.6 \text{ m/kg}^{1/3}$ <i>Change Vertical Charge Height or Charge Weight</i>
Description:	To calculate mach pressures and impulses, the scaled height of charge must remain within limits of available data. $2.53 < H_c < 17.6 \text{ m/kg}^{1/3}$ ($1 < H_c < 7 \text{ ft/lb}^{1/3}$)
Message:	<i>Mach Pressure out-of-range to calculate scaled distance.</i>
Description:	The calculated mach pressure must be at least 10 kPa in order to calculate the corresponding scaled distance. $P > 10 \text{ kPa}$ ($P > 1.45 \text{ psi}$)
Message:	<i>Mach Impulse out-of-range to calculate scaled distance</i>
Description:	The calculated scaled mach impulse must lie in an appropriate range to calculate corresponding scaled distances. $26.5 < I < 2369 \text{ kPa-ms/kg}^{1/3}$ ($3.27 < I < 264 \text{ psi-ms/lb}^{1/3}$)
Message:	<i>Z Outside Range for Free Air Burst or Air Burst.</i> $0.06 \leq Z \leq 11.9 \text{ m/kg}^{1/3}$
Description:	The available blast parameters for free air burst only exist for a range of scaled distances. $0.06 < Z < 11.9 \text{ m/kg}^{1/3}$ ($0.15 < Z < 30 \text{ ft/lb}^{1/3}$)
Message:	<i>Cannot calculate deflection angle.</i>

Description:	<i>Scaled Distance out of range.</i> In the process of iterating to calculate the angle of deflection, pressures are calculated corresponding to scaled distances. If the scaled distance at one point is out of range, the iteration is forced to stop and the deflection angle can't be calculated.
Message:	<i>Could not converge on a deflection angle.</i> <i>Geometry does not lend itself to regular reflection.</i> <i>Incident wave only.</i>
Description:	This is more of an indication as to what is occurring than an actual error. This simply indicates that the geometry between the blast location and a point on the surface of the structure will not be loaded by a ground reflected wave and only the incident wave will strike the location.

APPENDIX B EQUATIONS AND CURVES

B.1 Equations

B.1.1 Spherical Air Burst Parameters

Scaled Distance Z in $\text{ft/lb}^{1/3}$

Scaled Arrival Time, t_a^w ($\text{ms/lb}^{1/3}$)	
$5 < z \leq 30$	$t_a^w = -1.041 + 4.028 \times 10^{-1} z + 1.927 \times 10^{-2} z^2 - 1.832 \times 10^{-4} z^3 - 1.7759 \times 10^{-6} z^4$
$0.7 \leq z \leq 5$	$t_a^w = -2.252 \times 10^{-3} + 2.822 \times 10^{-2} z + 4.695 \times 10^{-2} z^2 + 1.677 \times 10^{-3} z^3 - 1.1550 \times 10^{-4} z^4$
$0.15 \leq z < 0.7$	$t_a^w = -1.6570 \times 10^{-2} + 1.6500 \times 10^{-1} z - 4.9260 \times 10^{-1} z^2 + 9.3120 \times 10^{-1} z^3 - 5.660 \times 10^{-4} z^4$
Side-on Overpressure, P_s^+ (psi)	
$9 \leq z \leq 30$	$P_s^+ = 13.88 \times e^{(-0.13 \times z)} + 1339 \times e^{(-0.72 \times z)} + 1.18$
$2 \leq z < 9$	$P_s^+ = 91.84 \times e^{(-0.3039 \times z)} + 2077 \times e^{(-1.174 \times z)} + 1.471$
$0.15 \leq z < 2$	$P_s^+ = 4175 \times e^{(-1.847 \times z)} + 7005 \times e^{(-5.31 \times z)} + 148.7$

Positive Scaled Duration, t_o^w (ms/lb^{1/3})	
$4.711 < z \leq 30$	$t_o^w = -5.414 \times 10^{-1} + (4.257 \times 10^{-1} \times z) + (-1.888 \times 10^{-2} \times z^2) + (3.849 \times 10^{-4} \times z^3) + (-2.9315 \times 10^{-6} \times z^4)$
$1.764 < z \leq 4.711$	$t_o^w = 1.447 + (-2.134 \times z) + (1.122 \times z^2) + (-0.2194 \times z^3) + (0.01567 \times z^4)$
$0.15 \leq z \leq 1.764$	$t_o^w = 3.995 \times 10^{-2} + (4.266 \times 10^{-3} \times z) + (3.898 \times 10^{-2} \times z^2) + (-2.762 \times 10^{-2} \times z^3) + (1.093 \times 10^{-2} \times z^4)$
Positive Scaled Side-On Impulse, i_o^w (psi-ms/lb^{1/3})	
$2.12 \leq z \leq 30$	$i_o^w = 7.739 \times e^{(-0.006992 \times z)} + 20.64 \times e^{(-0.191 \times z)} - 4.049$
$0.15 \leq z < 2.12$	$i_o^w = 13.49 \times e^{(-0.01364 \times z)} + 1406 \times e^{(-11.61 \times z)} + 4.282$
Shock Front Velocity, U (ft/s)	
$3.10 \leq z \leq 30$	$U = 25.85 \times e^{(-7.087 \times z)} + 13.77 \times e^{(-0.6661 \times z)} + 1.323$
$0.15 \leq z < 3.10$	$U = 1.825 \times e^{(-0.212 \times z)} + 11.670 \times e^{(-0.8218 \times z)} + 1.198$
Negative Side-on Overpressure, P_s^- (psi)	
$13 < z \leq 30$	$P_s^- = 0$
$8.81 < z \leq 13$	$P_s^- = \frac{1.43 - 1}{8.81 - 13} (8.81 - z) + 1$
$2.79 \leq z \leq 8.81$	$P_s^- = 1340.30263 \times e^{(-2.16967 \times z)} + 16.62046 \times e^{(-0.44246 \times z)} + 1.11225$
$0.15 \leq z < 2.79$	$P_s^- = 14.77214 + (9.26243 \times 10^{-1} \times z) + (-7.02374 \times 10^{-1} \times z^2) + (-1.27884 \times 10^{-1} \times z^3)$
Negative Scaled Side-On Impulse, i_s^{w-} (psi-ms/lb^{1/3})	
$13 < z \leq 30$	$i_s^{w-} = 0$
$2.70 \leq z \leq 13$	$i_s^{w-} = 12.97 \times e^{(-0.1057 \times z)} + 52.65 \times e^{(-0.5717 \times z)} + 1.274$
$0.15 \leq z < 2.70$	$i_s^{w-} = 54.42 + (12.42 \times z) + (-20.05 \times z^2) + (4.083 \times z^3)$
Normally Reflected Underpressure, P_m^- (psi)	
$25.2 < z \leq 30$	$P_m^- = \frac{-1.06}{(30 - 25.2)} (z - 25.2) + 1.06$

$1.85 < z \leq 25.2$	$P_{rn}^- = 3.537 \times e^{(-0.01393 \times z)} + 27.64 \times e^{(-0.4194 \times z)} - 1.426$
$0.15 < z \leq 1.82$	$P_{rn}^- = 15.34 + (-0.5191 \times z) + (1.871 \times z^2) + (-2.335 \times z^3)$
Normally Reflected Negative Scaled Impulse, i_{rn}^{w-} (psi-ms/lb^{1/3})	
$3.01 \leq z \leq 30$	$i_{rn}^{w-} = 16.69 \times e^{(-0.08252 \times z)} + 60.61 \times e^{(-0.4661 \times z)} + 2.342$
$0.15 \leq z < 3.01$	$i_{rn}^{w-} = 209.9 \times e^{(-0.6617 \times z)} - 168.5 \times e^{(-0.8891 \times z)} + 12.83$
Scaled Distance, z (ft/lb^{1/3}), from Normally Reflected Overpressure, P_{rn} (psi)	
$4000 \leq P_{rn} \leq 46000$	$z = 0.8628 \times e^{(-3.07 \times 10^{-5} \times P_{rn})} + 1.105 \times e^{(2.263 \times 10^{-4} \times P_{rn})} + 0.08716$
$52 \leq P_{rn} < 4000$	$z = 2.863 \times e^{(-8.63 \times 10^{-4} \times P_{rn})} + 4.41 \times e^{(-1.521 \times 10^{-2} \times P_{rn})} + 1.249$
$2.8 \leq P_{rn} < 52$	$z = 15.23 \times e^{(-9.165 \times 10^{-2} \times P_{rn})} + 56.5 \times e^{(0.5551 \times P_{rn})} + 6.14$
Scaled Distance, z (ft/lb^{1/3}), from Normally Reflected Scaled Impulse, i_{rn}^w (psi-ms/lb^{1/3})	
$157 \leq i_{rn}^w \leq 4570$	$z = 0.8945 \times e^{(-7.247 \times 10^{-4} \times i_{rn}^w)} + 2.561 \times e^{(7.221 \times 10^{-3} \times i_{rn}^w)} + 0.115$
$17.6 \leq i_{rn}^w < 157$	$z = 6.002 \times e^{(-0.01727 \times i_{rn}^w)} + 18.05 \times e^{(-0.1043 \times i_{rn}^w)} + 1.346$
$4.46 \leq i_{rn}^w < 17.6$	$z = 35.78 \times e^{(-0.1542 \times i_{rn}^w)} + 154.8 \times e^{(-0.7414 \times i_{rn}^w)} + 6.327$
Scaled Distance, z (ft/lb^{1/3}), from Incident Overpressure, P_s^+ (psi)	
$1.45 \leq P_s^+ \leq 47$	$z = \frac{-72.77 - 18.52 \times P_s^+ - 0.04527 \times P_s^{+2}}{1 - 2.895 \times P_s^+ - 0.05713 \times P_s^{+2}}$
$47 < P_s^+ \leq 6500$	$z = \frac{5.413 + 6.437 \times 10^{-3} \times P_s^+ - 2.56 \times 10^{-6} \times P_s^{+2} + 1.55 \times 10^{-10} \times P_s^{+3}}{1 + 9.601 \times 10^{-3} \times P_s^+ + 6.756 \times 10^{-7} \times P_s^{+2} - 7.788 \times 10^{-10} \times P_s^{+3}}$
Scaled Distance, z (ft/lb^{1/3}), from Scaled Incident Impulse, i_s^w (psi-ms/lb^{1/3})	
$17.63 \leq i_s^w \leq 312$	$z = \frac{0.3991 - 2.861 \times 10^{-2} \times i_s^w - 5.694 \times 10^{-5} \times i_s^{w2}}{1 - 4.775 \times 10^{-2} \times i_s^w - 8.874 \times 10^{-4} \times i_s^{w2}}$
$1.42 \leq i_s^w < 17.63$	$z = \frac{-412.3 + 26.28 \times i_s^w - 0.1797 \times i_s^{w2}}{1 - 6.485 \times i_s^w + 0.3493 \times i_s^{w2}}$

B.1.2 Hemispherical Surface Burst Parameters

Scaled Distance Z in ft/lb^{1/3}

Scaled Arrival Time, t_a^w (ms/lb^{1/3})	
$8.76 < z \leq 50$	$t_a^w = -7.1800 \times 10^{-1} + 2.5160 \times 10^{-1} z + 2.8010 \times 10^{-2} z^2 - 5.1070 \times 10^{-4} z^3 + 3.1810 \times 10^{-6} z^4$
$1.66 < z \leq 8.76$	$t_a^w = 3.0760 \times 10^{-2} - 7.1810 \times 10^{-3} z + 5.3970 \times 10^{-2} z^2 - 9.1630 \times 10^{-4} z^3 - 3.1125 \times 10^{-5} z^4$
$0.3 \leq z \leq 1.66$	$t_a^w = -1.4350 \times 10^{-2} + 8.1280 \times 10^{-2} z - 4.13140 \times 10^{-2} z^2 + 6.0320 \times 10^{-2} z^3 - 1.5230 \times 10^{-2} z^4$
Side-on Overpressure, P_s^+ (psi)	
$9.14 \leq z \leq 50$	$P_s^+ = 10.51 \times e^{(-0.08108 \times z)} + 1.214 \times 10^2 \times e^{(-0.3338 \times z)} + 0.7484$
$1.92 \leq z < 9.14$	$P_s^+ = 1.792 \times 10^2 \times e^{(-0.3608 \times z)} + 2.3510 \times 10^3 \times e^{(-1.1510 \times z)} + 5.0370$
$0.3 \leq z < 1.92$	$P_s^+ = 3.821 \times 10^3 \times e^{(-1.554 \times z)} + 1.0457 \times 10^4 \times e^{(-5.392 \times z)} + 1.611 \times 10^2$
Positive Scaled Duration, t_o^w (ms/lb^{1/3})	
$4.993 < z \leq 50$	$t_o^w = -6.527 \times 10^{-1} + (3.9810 \times 10^{-1} \times z) + (-1.3980 \times 10^{-2} \times z^2) + (2.299 \times 10^{-4} \times z^3) + (-1.3909 \times 10^{-6} \times z^4)$
$2.083 < z \leq 4.993$	$t_o^w = -4.3860 \times 10^{-1} + (8.964 \times 10^{-1} \times z) + (-5.59 \times 10^{-1} \times z^2) + (1.514 \times 10^{-1} \times z^3) + (-1.2880 \times 10^{-2} \times z^4)$
$0.3 \leq z \leq 2.083$	$t_o^w = 3.92 \times 10^{-2} + (3.3310 \times 10^{-2} \times z) + (-1.021 \times 10^{-2} \times z^2) + (7.011 \times 10^{-3} \times z^3)$
Positive Scaled Side-On Impulse, i_o^w (psi-ms/lb^{1/3})	
$2.334 \leq z \leq 50$	$i_o^w = 10.06 \times e^{(-0.003151 \times z)} + 24.46 \times e^{(-0.1267 \times z)} - 6.467$
$0.3 \leq z < 2.334$	$i_o^w = 145 \times e^{(-4.835 \times z)} + 10188 \times e^{(-15.76 \times z)} + 21.23$
Shock Front Velocity, U (ft/s)	
$1.78 \leq z \leq 50$	$U = 1.735 \times e^{(-0.1746 \times z)} + 13.91 \times e^{(-0.7973 \times z)} + 1.141$

$0.3 \leq z < 1.78$	$U = 13.89 \times e^{(-0.9868 \times z)} + 95.47 \times e^{(-11.17 \times z)} + 3.329$
Negative Side-on Overpressure, P_s^- (psi)	
$15.3 < z \leq 50$	$P_s^- = 0$
$3.83 < z \leq 15.3$	$P_s^- = 10.15 \times e^{(-0.272 \times z)} + 11320 \times e^{(-2.362 \times z)} + 0.8694$
$0.3 \leq z \leq 3.83$	$P_s^- = 14.88 + (0.338 \times z) + (-0.4953 \times z^2) + (-0.05664 \times z^3)$
Negative Scaled Side-On Impulse, i_s^{w-} (psi-ms/lb^{1/3})	
$16.3 < z \leq 50$	$i_s^{w-} = 5.615 \times e^{(-0.02169 \times z)} + 38.49 \times e^{(-0.1976 \times z)} + 0.08381$
$2.73 \leq z \leq 16.3$	$i_s^{w-} = 37.66 \times e^{(-0.204 \times z)} + 500.6 \times e^{(-1.455 \times z)} + 4.315$
$0.3 \leq z < 2.73$	$i_s^{w-} = 64.66 + (18.87 \times z) + (-20.41 \times z^2) + (3.499 \times z^3)$
Normally Reflected Underpressure, P_{rn}^- (psi)	
$25.2 < z \leq 50$	$P_{rn}^- = \frac{-1}{(50 - 28.8)}(z - 28.8) + 1$
$1.84 < z \leq 28.8$	$P_{rn}^- = 4.81 \times e^{(-0.01186 \times z)} + 23.35 \times e^{(0.3403 \times z)} - 2.3810$
$0.3 < z \leq 1.84$	$P_{rn}^- = 1.491 \times e^{(-1.32 \times z)} - 3.068 \times e^{(-2.04 \times z)} - 0.471$
Normally Reflected Negative Scaled Impulse, i_{rn}^{w-} (psi-ms/lb^{1/3})	
$1.43 < z \leq 30$	$i_{rn}^{w-} = 15.73 \times e^{(-0.0453 \times z)} + 73.69 \times e^{(-0.3177 \times z)} + 2.154$
$0.3 < z \leq 1.43$	$i_{rn}^{w-} = 1199 \times e^{(-0.07175 \times z)} - 437.7 \times e^{(-0.2039 \times z)} - 692.2$
Scaled Distance, z (ft/lb^{1/3}), from Normally Reflected Overpressure, P_r (psi)	
$2600 \leq P_r \leq 54100$	$z = 1.1210 \times e^{(-5.6301 \times 10^{-5} \times P_r)} + 1.792 \times e^{(-3.948 \times 10^{-4} \times P_r)} + 0.24950$
$44.60 \leq P_r < 2600$	$z = 2.914 \times e^{(-1.033 \times 10^{-3} \times P_r)} + 5.737 \times e^{(-1.227 \times 10^{-2} \times P_r)} + 1.685$
$1.84 \leq P_r < 44.6$	$z = 28.07 \times e^{(-0.12670 \times P_r)} + 125.90 \times e^{(-1.013 \times P_r)} + 8.172$
Scaled Distance, z (ft/lb^{1/3}), from Normally Reflected Scaled Impulse, i_{rn}^w (psi-ms/lb^{1/3})	

$60 < i_{rn}^w \leq 3430$	$z = 1.495 \times e^{(-1.107 \times 10^{-3} \times i_{rn}^w)} + 5.68 \times e^{(-0.01088 \times i_{rn}^w)} + 0.287$
$4.25 \leq i_{rn}^w \leq 60$	$z = 29.14 \times e^{(-0.06793 \times i_{rn}^w)} + 170.50 \times e^{(-0.4631 \times i_{rn}^w)} + 4.248$

B.1.3 Dynamic Pressure, Reflected Pressure, and Reflected Impulse

Dynamic Pressure, q (psi); (P_s^+ (psi))	
$1117.2 < P_s^+ \leq 10000$	$q = -8.914 \times 10^{-2} + (3.219 \times P_s^+) + (3.799 \times 10^{-4} \times P_s^{+2}) + (-3.2499 \times 10^{-8} \times P_s^{+3}) + (9.2141 \times 10^{-13} \times P_s^{+4})$
$90.45 < P_s^+ \leq 1117.2$	$q = -2.149 \times 10^1 + (1.03 \times P_s^+) + (3.656 \times 10^{-3} \times P_s^{+2}) + (-3.3113 \times 10^{-6} \times P_s^{+3}) + (1.3299 \times 10^{-9} \times P_s^{+4})$
$13.94 < P_s^+ \leq 90.45$	$q = 5.545 \times 10^{-1} + (-6.371 \times 10^{-2} \times P_s^+) + (2.417 \times 10^{-2} \times P_s^{+2}) + (-1.78 \times 10^{-4} \times P_s^{+3}) + (5.8404 \times 10^{-7} \times P_s^{+4})$
$2.52 \leq P_s^+ \leq 13.94$	$q = 7.519 \times 10^{-2} + (-5.969 \times 10^{-2} \times P_s^+) + (4.094 \times 10^{-2} \times P_s^{+2}) + (-2.187 \times 10^{-3} \times P_s^{+3}) + (6.7718 \times 10^{-5} \times P_s^{+4})$
$0 \leq P_s^+ < 2.52$	$q = 0$
Scaled Reflected Impulse, i_r^w (psi-ms/lb ^{1/3}); (P_s^+ (psi), β (°))	
$P_s^+ = 7000$	$i_r^w = 8159 + 14.25\beta - 3.316\beta^2 + 0.02439\beta^3$
$P_s^+ = 6000$	$i_r^w = 4903 + 7.598\beta - 1.897\beta^2 + 0.01366\beta^3$
$P_s^+ = 5000$	$i_r^w = 3194 - 1.255\beta - 1.097\beta^2 + 0.0081\beta^3$
$P_s^+ = 4000$	$i_r^w = 1959 + 0.2091\beta - 0.69477\beta^2 + 0.005088\beta^3$
$P_s^+ = 3000$	$i_r^w = 1106 - 0.3864\beta - 0.3756\beta^2 + 0.002752\beta^3$
$P_s^+ = 2000$	$i_r^w = 599.2 + 0.09814\beta - 0.2081\beta^2 + 0.001506\beta^3$
$P_s^+ = 1500$	$i_r^w = 399.6 + 0.556\beta - 0.1526\beta^2 + 0.001106\beta^3$
$P_s^+ = 1000$	$i_r^w = 253.3 - 0.03877\beta - 0.08333\beta^2 + 0.0006056\beta^3$
$P_s^+ = 700$	$i_r^w = 186.9 + 0.03405\beta - 0.06154\beta^2 + 0.0004437\beta^3$
$P_s^+ = 400$	$i_r^w = 119.7 + 0.1137\beta - 0.03538\beta^2 + 0.0002351\beta^3$

$P_s^+ = 200$	$i_r^w = 77.9 + 0.1123\beta - 0.01987\beta^2 + 0.0001321\beta^3$
$P_s^+ = 100$	$i_r^w = 50.63 + 0.06885\beta - 0.01046\beta^2 + 0.000063523\beta^3$
$P_s^+ = 50$	$i_r^w = 35.5 + 0.0166\beta - 0.005655\beta^2 + 0.000030623\beta^3$
$P_s^+ = 20$	$i_r^w = 23.3 - 0.03612\beta - 0.002144\beta^2 + 9.2674 \times 10^{-6} \beta^3$
$P_s^+ = 10$	$i_r^w = 14.95 + 0.008167\beta - 0.001855\beta^2 + 8.8695 \times 10^{-6} \beta^3$
$P_s^+ = 5$	$i_r^w = 9.765 + 0.01737\beta - 0.001037\beta^2 + 2.9314 \times 10^{-6} \beta^3$
$P_s^+ = 3$	$i_r^w = 7.058 - 0.004787\beta - 0.0002456\beta^2 - 1.194 \times 10^{-6} \beta^3$
$P_s^+ = 2$	$i_r^w = 5.236 - 0.01538\beta + 0.0001356\beta^2 - 2.76 \times 10^{-6} \beta^3$
$P_s^+ = 1.5$	$i_r^w = 4.317 - 0.009131\beta - 6.1761 \times 10^{-5} \beta^2 - 8.6306 \times 10^{-7} \beta^3$
$P_s^+ = 1$	$i_r^w = 2.953 - 0.0007995\beta - 1.1219 \times 10^{-4} \beta^2 - 2.4997 \times 10^{-7} \beta^3$
$P_s^+ = 0.7$	$i_r^w = 2.162 - 3.399 \times 10^{-4} \beta - 1.247 \times 10^{-4} \beta^2 - 3.3416 \times 10^{-7} \beta^3$
Reflection Coefficient, $C_{r\beta}$ (psi); (P_{so} (psi), β (°))	
$P_s^+ = 6500, 0 \leq \beta \leq 45$	$C_{r\beta} = 12.5 - 0.0634\beta + 1.19 \times 10^{-3} \beta^2 - 1.15 \times 10^{-4} \beta^3 + 1.50 \times 10^{-6} \beta^4$
$P_s^+ = 6500, 45 < \beta < 50$	$C_{r\beta} = -450 + 19.18\beta - 2.00 \times 10^{-1} \beta^2$
$P_s^+ = 6500, 50 \leq \beta \leq 90$	$C_{r\beta} = 657495 \times e^{(-0.2332 \times \beta)} + 54.49 \times e^{(-9.105 \times 10^{-4} \times \beta)} - 51.04$
$P_s^+ = 3000, 0 \leq \beta \leq 45$	$C_{r\beta} = 10.88 - 0.05592\beta + 5.0 \times 10^{-3} \beta^2 - 3.11 \times 10^{-4} \beta^3 + 4.23 \times 10^{-6} \beta^4$
$P_s^+ = 3000, 45 < \beta < 50$	$C_{r\beta} = -399.3 + 17.18\beta - 1.808 \times 10^{-1} \beta^2$
$P_s^+ = 3000, 50 \leq \beta \leq 90$	$C_{r\beta} = 9.428 \times e^{(0.01405 \times \beta)} + 108085 \times e^{(-0.2018 \times \beta)} - 1.649$
$P_s^+ = 2000, 0 \leq \beta \leq 45$	$C_{r\beta} = 10 - 0.03592\beta + 8.86 \times 10^{-3} \beta^2 - 2.69 \times 10^{-4} \beta^3 + 3.73 \times 10^{-6} \beta^4$
$P_s^+ = 2000, 45 < \beta < 60$	$C_{r\beta} = -1042 + 60.27\beta - 1.14\beta^2 - 7.15 \times 10^{-3} \beta^3$
$P_s^+ = 2000, 60 \leq \beta \leq 90$	$C_{r\beta} = 9.372 \times e^{(-0.01369 \times \beta)} + 95615 \times e^{(-0.1996 \times \beta)} - 1.723$

$P_s^+ = 1000, 0 \leq \beta \leq 40$	$C_{r\beta} = 8.56 - 0.01625\beta - 2.88 \times 10^{-3} \beta^2 + 9.25 \times 10^{-5} \beta^3 - 1.21 \times 10^{-6} \beta^4$
$P_s^+ = 1000, 40 < \beta < 50$	$C_{r\beta} = -109.6 + 5.21\beta - 5.79 \times 10^{-2} \beta^2$
$P_s^+ = 1000, 50 \leq \beta \leq 90$	$C_{r\beta} = 5211 \times e^{(-0.147 \times \beta)} + 8.118 \times e^{(-0.01677 \times \beta)} - 0.7925$
$P_s^+ = 500, 0 \leq \beta \leq 40$	$C_{r\beta} = 7.81 - 0.04417\beta + 1.48 \times 10^{-3} \beta^2 - 8.83 \times 10^{-5} \beta^3 + 1.17 \times 10^{-6} \beta^4$
$P_s^+ = 500, 40 < \beta < 50$	$C_{r\beta} = -76.72 + 3.699\beta - 4.091 \times 10^{-2} \beta^2$
$P_s^+ = 500, 50 \leq \beta \leq 90$	$C_{r\alpha} = 84.14 - 3.177\beta + 0.03945\beta^2 - 1.68 \times 10^{-4} \beta^3$
$P_s^+ = 400, 0 \leq \beta \leq 40$	$C_{r\beta} = 6.88 + 0.01117\beta - 1.68 \times 10^{-3} \beta^2 + 3.33 \times 10^{-6} \beta^3 + 2.5 \times 10^{-7} \beta^4$
$P_s^+ = 400, 40 < \beta \leq 50$	$C_{r\beta} = -591.4 + 38.21\beta - 8.09 \times 10^{-1} \beta^2 + 5.68 \times 10^{-3} \beta^3$
$P_s^+ = 400, 50 < \beta \leq 90$	$C_{r\beta} = 182.3 - 9.165\beta + 0.176\beta^2 - 1.51 \times 10^{-3} \beta^3 + 4.8589 \times 10^{-6} \beta^4$
$P_s^+ = 300, 0 \leq \beta \leq 40$	$C_{r\beta} = 6.69 - 0.03608\beta + 3.49 \times 10^{-3} \beta^2 - 2.09 \times 10^{-4} \beta^3 + 3.13 \times 10^{-6} \beta^4$
$P_s^+ = 300, 40 < \beta \leq 50$	$C_{r\beta} = -44.23 + 2.259\beta - 2.542 \times 10^{-2} \beta^2$
$P_s^+ = 300, 50 < \beta \leq 90$	$C_{r\beta} = -0.3834e^{(-0.08493\beta)} + 313.8e^{(-0.08622\beta)} + 0.962$
$P_s^+ = 200, 0 \leq \beta \leq 40$	$C_{r\beta} = 6.0 - 0.05125\beta + 5.57 \times 10^{-3} \beta^2 - 2.73 \times 10^{-4} \beta^3 + 3.79 \times 10^{-6} \beta^4$
$P_s^+ = 200, 40 < \beta \leq 47.5$	$C_{r\beta} = -25.59 + 1.429\beta - 1.65 \times 10^{-2} \beta^2$
$P_s^+ = 200, 47.5 < \beta \leq 90$	$C_{r\beta} = 87.19e^{(-0.06773\beta)} + 23.76e^{(-0.06984\beta)} + 0.766$
$P_s^+ = 150, 0 \leq \beta \leq 40$	$C_{r\beta} = 5.63 - 0.04083\beta + 4.11 \times 10^{-3} \beta^2 - 2.27 \times 10^{-4} \beta^3 + 3.42 \times 10^{-6} \beta^4$
$P_s^+ = 150, 40 < \beta \leq 47.5$	$C_{r\beta} = -15.83 + 0.9853\beta - 1.17 \times 10^{-2} \beta^2$
$P_s^+ = 150, 47.5 < \beta \leq 90$	$C_{r\beta} = 74.8e^{(-0.07006\beta)} + 12.42e^{(-0.05043\beta)} + 0.7312$
$P_s^+ = 100, 0 \leq \beta \leq 30$	$C_{r\beta} = 5.0 + 0.009833\beta - 1.90 \times 10^{-3} \beta^2 - 3.17 \times 10^{-5} \beta^3$
$P_s^+ = 100, 30 < \beta \leq 45$	$C_{r\beta} = -5.84 + 0.5907\beta - 0.00827\beta^2$
$P_s^+ = 100, 45 < \beta \leq 90$	$C_{r\beta} = 83.39e^{(-0.08007\beta)} + 5.213e^{(-0.00466\beta)} - 2.473$

$P_s^+ = 70, 0 \leq \beta \leq 30$	$C_{r\beta} = 4.50 + 0.01883\beta - 3.10 \times 10^{-3} \beta^2 + 6.17 \times 10^{-5} \beta^3$
$P_s^+ = 70, 30 < \beta \leq 45$	$C_{r\beta} = -8.23 + 0.6957\beta - 9.67 \times 10^{-3} \beta^2$
$P_s^+ = 70, 45 < \beta \leq 90$	$C_{r\beta} = 44.35e^{(-0.0695\beta)} + 4.037e^{(-0.00521\beta)} - 1.599$
$P_s^+ = 50, 0 \leq \beta \leq 30$	$C_{r\beta} = 4.0 + 0.002833\beta - 1.00 \times 10^{-3} \beta^2 + 1.17 \times 10^{-5} \beta^3$
$P_s^+ = 50, 30 < \beta \leq 45$	$C_{r\beta} = -11.62 + 0.84\beta - 1.112 \times 10^{-2} \beta^2$
$P_s^+ = 50, 45 < \beta \leq 90$	$C_{r\beta} = 67979e^{(-0.2687\beta)} + 16.02e^{(-0.04072\beta)} - 0.551$
$P_s^+ = 30, 0 \leq \beta \leq 30$	$C_{r\beta} = 3.5 - 0.04317\beta + 2.25 \times 10^{-3} \beta^2 - 4.33 \times 10^{-5} \beta^3$
$P_s^+ = 30, 30 < \beta \leq 45$	$C_{r\beta} = -5.32 + 0.4513\beta - 5.73 \times 10^{-3} \beta^2$
$P_s^+ = 30, 45 < \beta \leq 90$	$C_{r\beta} = 23.51e^{(-0.05679\beta)} + 10.48e^{(-0.05543\beta)} + 0.7494$
$P_s^+ = 20, 0 \leq \beta \leq 47.5$	$C_{r\beta} = 2.935 + 5.245 \times 10^{-3} \beta - 1.231 \times 10^{-3} \beta^2 + 4.2091 \times 10^{-5} \beta^3 - 3.2524 \times 10^{-7} \beta^4$
$P_s^+ = 20, 47.5 < \beta \leq 90$	$C_{r\beta} = 26.92 - 0.9431\beta + 0.01165\beta^2 + 4.8552 \times 10^{-5} \beta^3$
$P_s^+ = 10, 0 \leq \beta \leq 47.5$	$C_{r\beta} = 2.499 + 6.734 \times 10^{-3} \beta - 7.56 \times 10^{-4} \beta^2 + 1.08 \times 10^{-5} \beta^3 + 9.25 \times 10^{-8} \beta^4$
$P_s^+ = 10, 47.5 < \beta < 60$	$C_{r\beta} = -32.21 + 1.386\beta - 0.01368\beta^2$
$P_s^+ = 10, 60 \leq \beta \leq 90$	$C_{r\beta} = -7.264 + 0.4801\beta - 0.007914\beta^2 + 4.0 \times 10^{-5} \beta^3$
$P_s^+ = 5, 0 \leq \beta \leq 40$	$C_{r\beta} = 2.25$
$P_s^+ = 5, 40 < \beta \leq 50$	$C_{r\beta} = 14.92 - 0.6106\beta + 0.0073\beta^2$
$P_s^+ = 5, 50 < \beta \leq 90$	$C_{r\beta} = 24.91 + 0.84091\beta - 0.009897\beta^2 - 3.90 \times 10^{-5} \beta^3$
$P_s^+ = 2, 0 \leq \beta \leq 50$	$C_{r\beta} = 2$
$P_s^+ = 2, 50 < \beta \leq 90$	$C_{r\beta} = -63.18 + 2.839\beta - 0.03956\beta^2 + 1.77 \times 10^{-4} \beta^3$
$P_s^+ = 1, 0 \leq \beta \leq 60$	$C_{r\beta} = 2$
$P_s^+ = 1, 60 < \beta < 75$	$C_{r\beta} = -68.76 + 2.099\beta - 1.53 \times 10^{-2} \beta^2$

$P_s^+ = 1, 75 \leq \beta \leq 90$	$C_{r\beta} = -37.99 + 0.789\beta + 0.0042\beta^2$
$P_s^+ = 0.5, 0 \leq \beta \leq 60$	$C_{r\beta} = 2$
$P_s^+ = 0.5, 60 < \beta < 75$	$C_{r\beta} = 27.16 - 0.8113\beta + 6.53 \times 10^{-3} \beta^2$
$P_s^+ = 0.5, 75 \leq \beta \leq 90$	$C_{r\beta} = 46.21 - 0.9403\beta + 0.004867\beta^2$
$P_s^+ = 0.2, 0 \leq \beta \leq 60$	$C_{r\beta} = 2$
$P_s^+ = 0.2, 60 < \beta < 75$	$C_{r\beta} = 10.6 - 0.2713\beta + 2.13 \times 10^{-3} \beta^2$
$P_s^+ = 0.2, 75 \leq \beta \leq 90$	$C_{r\beta} = -157.1 + 3.965\beta - 0.02453\beta^2$

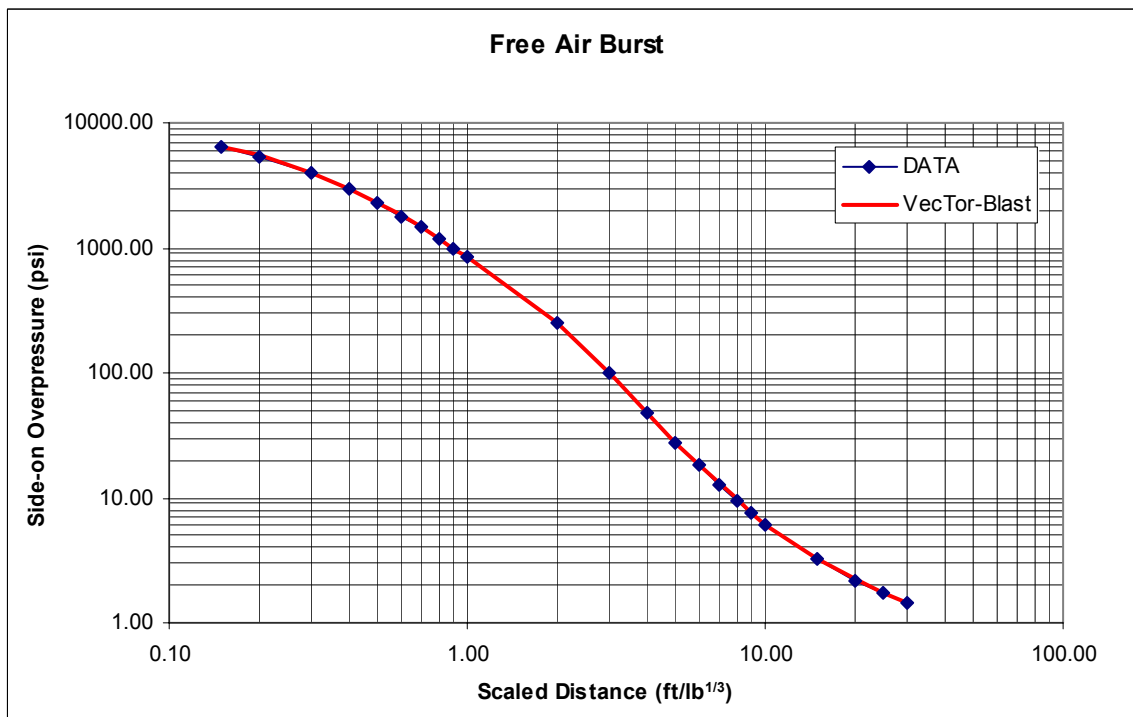
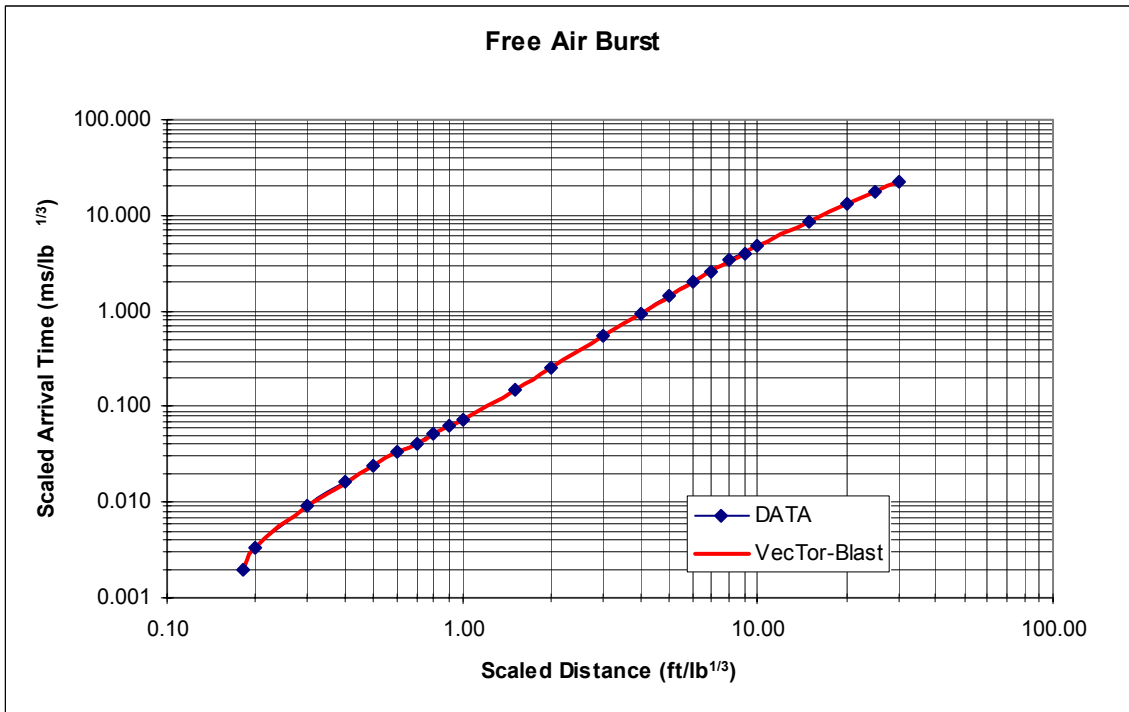
B.1.4 Mach Stem Formation

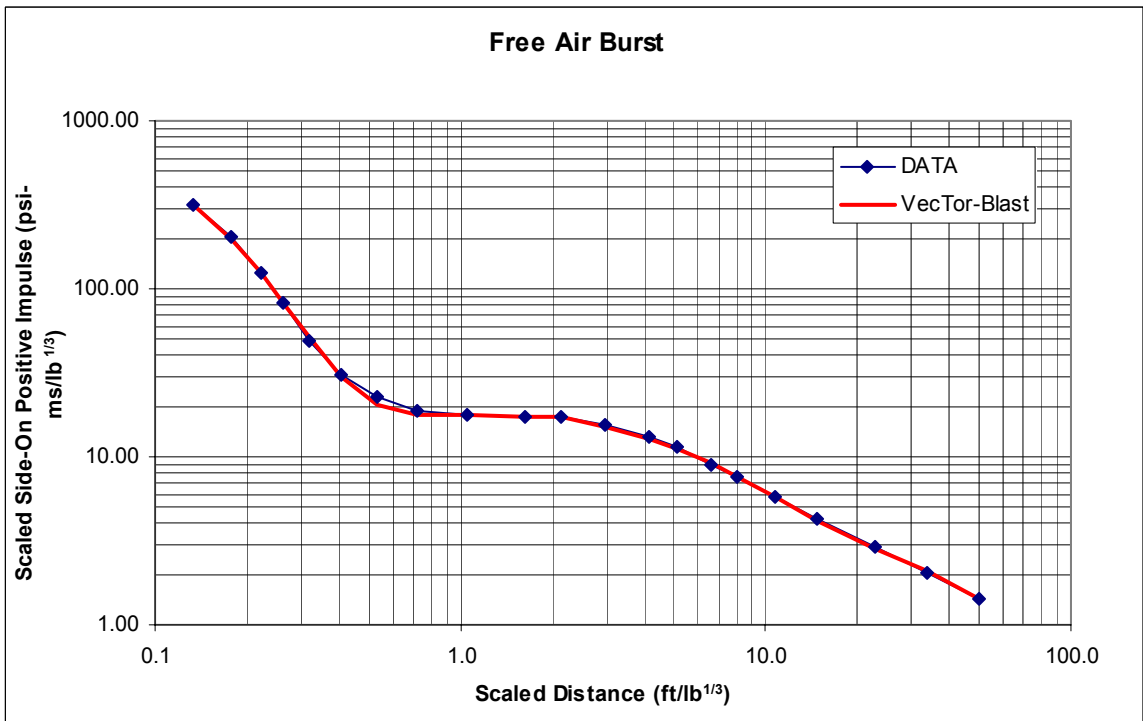
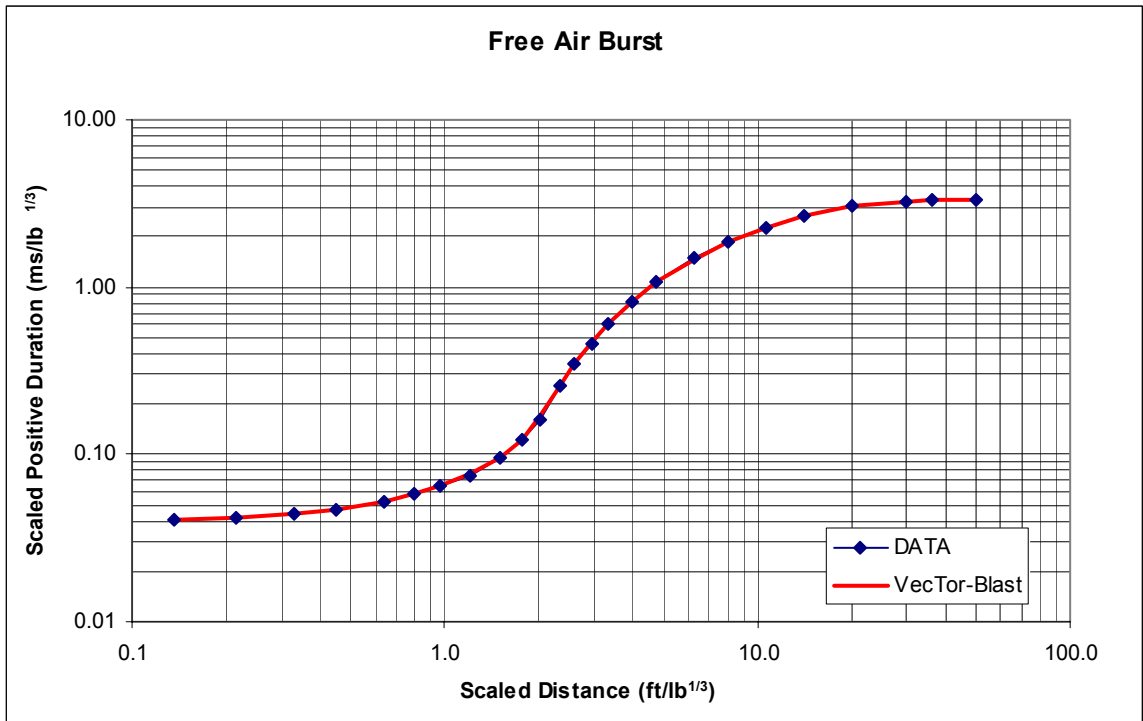
Scaled Distance Z in ft/lb^{1/3}

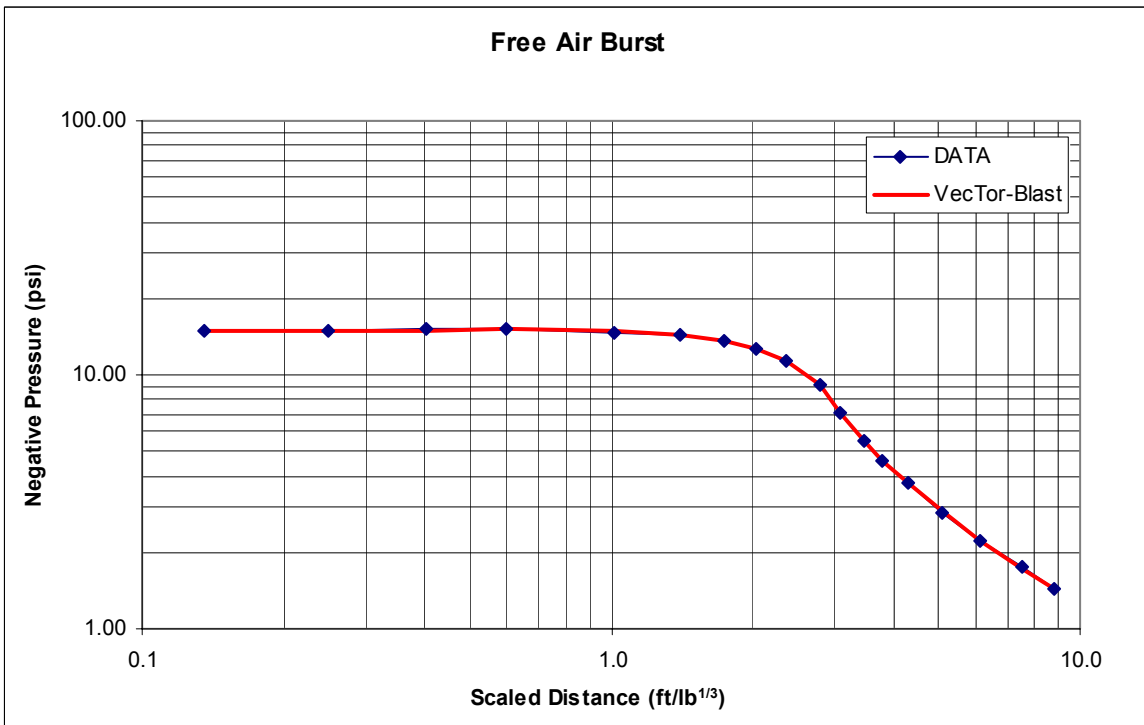
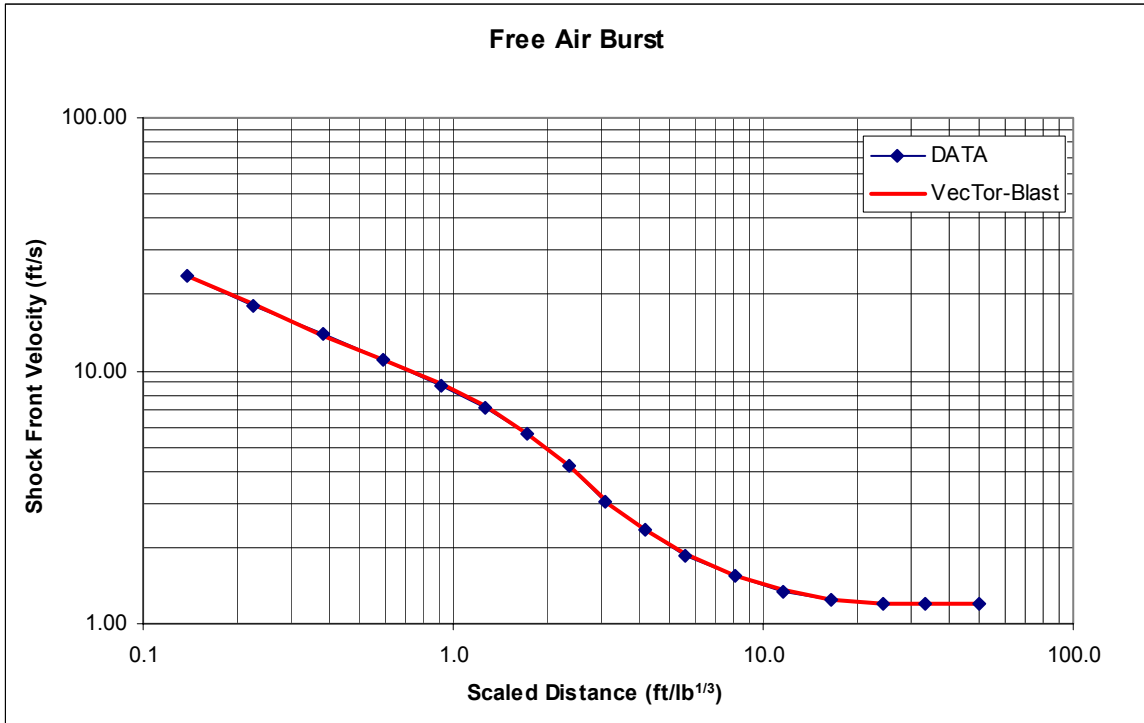
Minimum angle for Mach Stem formation, α_{crit} (deg)	
$0 \leq \varepsilon = \frac{P_o}{P_s^+ + P_o} \leq 1$	$\alpha_{crit} = \frac{40.02 - 76.81\varepsilon + 61.01\varepsilon^2 - 23.26\varepsilon^3}{1 - 1.79\varepsilon + 1.02\varepsilon^2 - 0.22\varepsilon^3}$
Scaled Triple Point Height, H_T^w (ft/lb ^{1/3}); (H_c^w (ft/lb ^{1/3}))	
$H_c^w = 1$	$H_T^w = -0.001z^4 + 0.0199z^3 + 0.0146z^2 + 0.1183z$
$H_c^w = 1.5$	$H_T^w = -7.0 \times 10^{-5} z^6 + 2.2 \times 10^{-3} z^5 - 0.0266z^4 + 0.1566z^3 - 0.3638z^2 + 0.3982z$
$H_c^w = 2$	$H_T^w = \frac{-5.513 \times 10^{-3} + 1.466 \times 10^{-2} z + 1.828 \times 10^{-2} z^2}{1 - 0.1273z + 1.068 \times 10^{-2} z^2 - 3.241 \times 10^{-4} z^3}$
$H_c^w = 2.5$	$H_T^w = \frac{-5.539 \times 10^{-3} + 5.889 \times 10^{-3} z + 3.692 \times 10^{-3} z^2 - 8.038 \times 10^{-5} z^3}{1 - 0.2982z + 3.927 \times 10^{-2} z^2 - 2.339 \times 10^{-3} z^3 + 5.167 \times 10^{-5} z^4}$
$H_c^w = 3$	$H_T^w = \frac{5.385 \times 10^{-4} - 0.2295z + 5.934 \times 10^{-2} z^2}{1 + 0.1211z - 3.345 \times 10^{-3} z^2}$
$H_c^w = 3.5$	$H_T^w = \frac{1.838 \times 10^{-3} + 1.524 \times 10^{-2} z + 1.379 \times 10^{-3} z^2}{1 - 0.156z + 1.002 \times 10^{-2} z^2 - 2.242 \times 10^{-4} z^3}$
$H_c^w = 4$	$H_T^w = \frac{-1.343 \times 10^{-3} - 1.075 \times 10^{-2} z + 5.559 \times 10^{-3} z^2}{1 - 0.07748z + 2.674 \times 10^{-3} z^2}$
$H_c^w = 5$	$H_T^w = \frac{-1.617 \times 10^{-3} + 2.83 \times 10^{-3} z + 1.433 \times 10^{-3} z^2}{1 - 0.08417z + 2.307 \times 10^{-3} z^2}$
$H_c^w = 6$	$H_T^w = \frac{-2.30 \times 10^{-3} + 9.116 \times 10^{-3} z - 8.267 \times 10^{-4} z^2}{1 - 0.1745z + 9.455 \times 10^{-3} z^2 - 1.734 \times 10^{-4} z^3}$

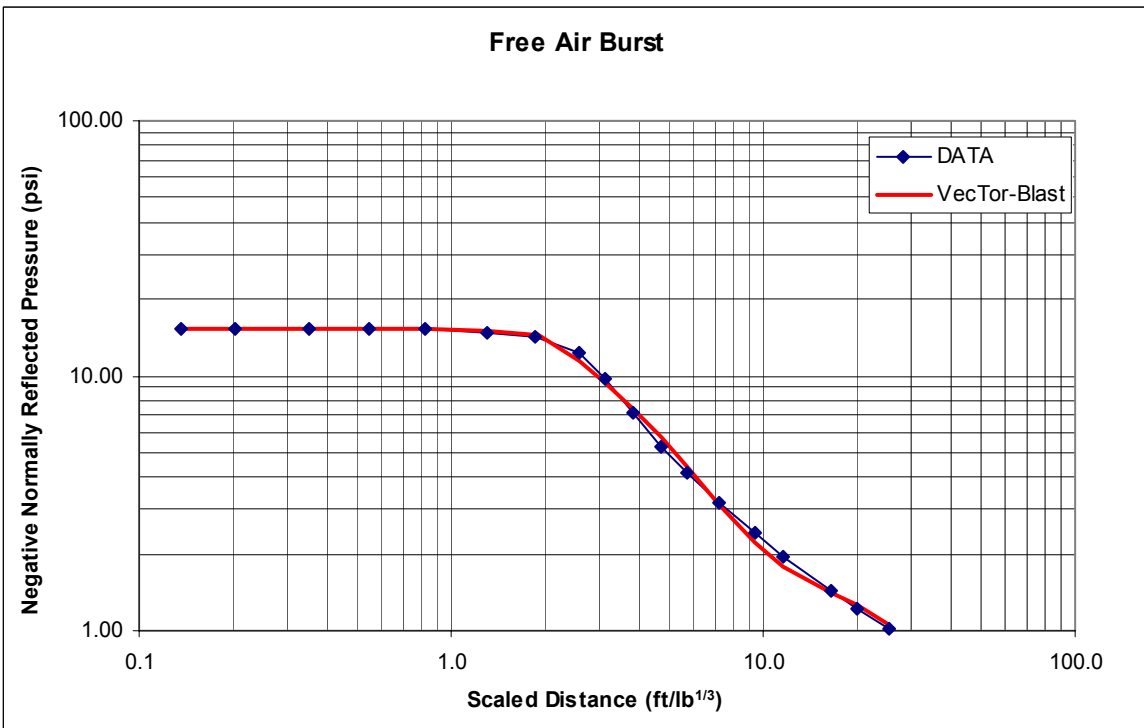
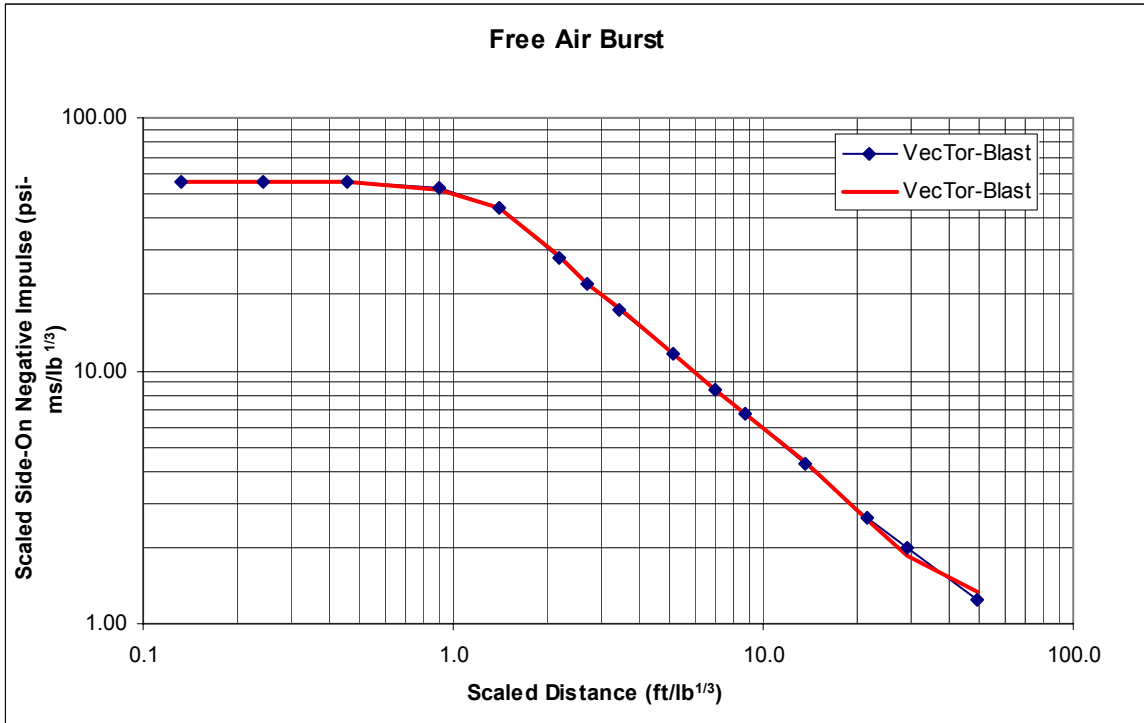
$H_c^w = 7$	$H_T^w = \frac{7.525 \times 10^{-4} + 8.725 \times 10^{-3} z - 7.177 \times 10^{-4} z^2}{1 - 0.1239z + 3.45 \times 10^{-3} z^2}$
Mach Pressure, P_{mach} (psi); (H_c^w (ft/lb^{1/3}), β_1 (°))	
$H_c^w = 0.8$	$P_{mach} = 11323 + 4.601\beta_1 - 8.718\beta_1^2 + 0.13\beta_1^3 - 5.469 \times 10^{-4} \beta_1^4$
$H_c^w = 1.9$	$P_{mach} = 1559 + 4.4\beta_1 - 1.609\beta_1^2 + 0.07331\beta_1^3 - 2.848 \times 10^{-3} \beta_1^4 - 6.67071 \times 10^{-5} \beta_1^5 - 8.729 \times 10^{-7} \beta_1^6 + 5.9304 \times 10^{-9} \beta_1^7 - 1.6574 \times 10^{-11} \beta_1^8$
$H_c^w = 3$	$P_{mach} = 483.5 - 11.39\beta_1 + 0.05746\beta_1^2 + 2.601 \times 10^{-4} \beta_1^3 - 1.704 \times 10^{-6} \beta_1^4$
$H_c^w = 5.3$	$P_{mach} = 72.48 + 0.7531\beta_1 - 0.04146\beta_1^2 + 1.862 \times 10^{-4} \beta_1^3 + 9.5714 \times 10^{-7} \beta_1^4$
$H_c^w = 7.2$	$P_{mach} = 34.86 + 0.6254\beta_1 - 4.35 \times 10^{-3} \beta_1^2 - 1.433 \times 10^{-4} \beta_1^3 + 1.5338 \times 10^{-6} \beta_1^4$
Mach Scaled Impulse, i_{mach} (psi-ms/lb^{1/3}); (H_c^w (ft/lb^{1/3}))	
$H_c^w = 0.8$	$i_{mach}^w = 316.4 - 2.947z - 0.1296z^2 + 2.474 \times 10^{-3} z^3 - 1.2237 \times 10^{-5} z^4$
$H_c^w = 1.9$	$i_{mach}^w = 92.46 - 0.6754z - 0.02238z^2 + 3.946 \times 10^{-4} z^3 - 2.1408 \times 10^{-6} z^4$
$H_c^w = 3$	$i_{mach}^w = 49.93 - 0.1927z - 0.0121z^2 + 1.481 \times 10^{-4} z^3 - 6.6732 \times 10^{-7} z^4$
$H_c^w = 5.3$	$i_{mach}^w = 24.9 - 0.05909z - 3.132 \times 10^{-4} z^2 - 8.221 \times 10^{-5} z^3 + 6.6493 \times 10^{-7} z^4$
$H_c^w = 7.2$	$i_{mach}^w = 17.09 - 0.0389z - 1.689 \times 10^{-3} z^2 - 4.0867 \times 10^{-5} z^3 + 3.3971 \times 10^{-7} z^4$

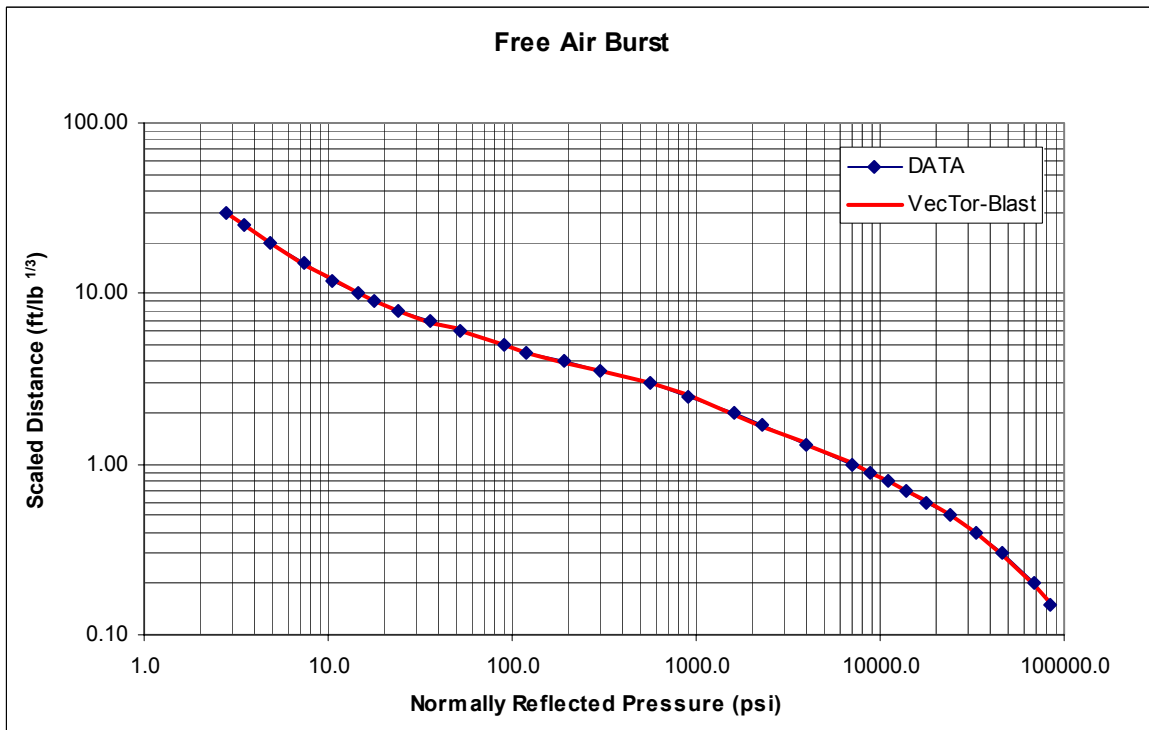
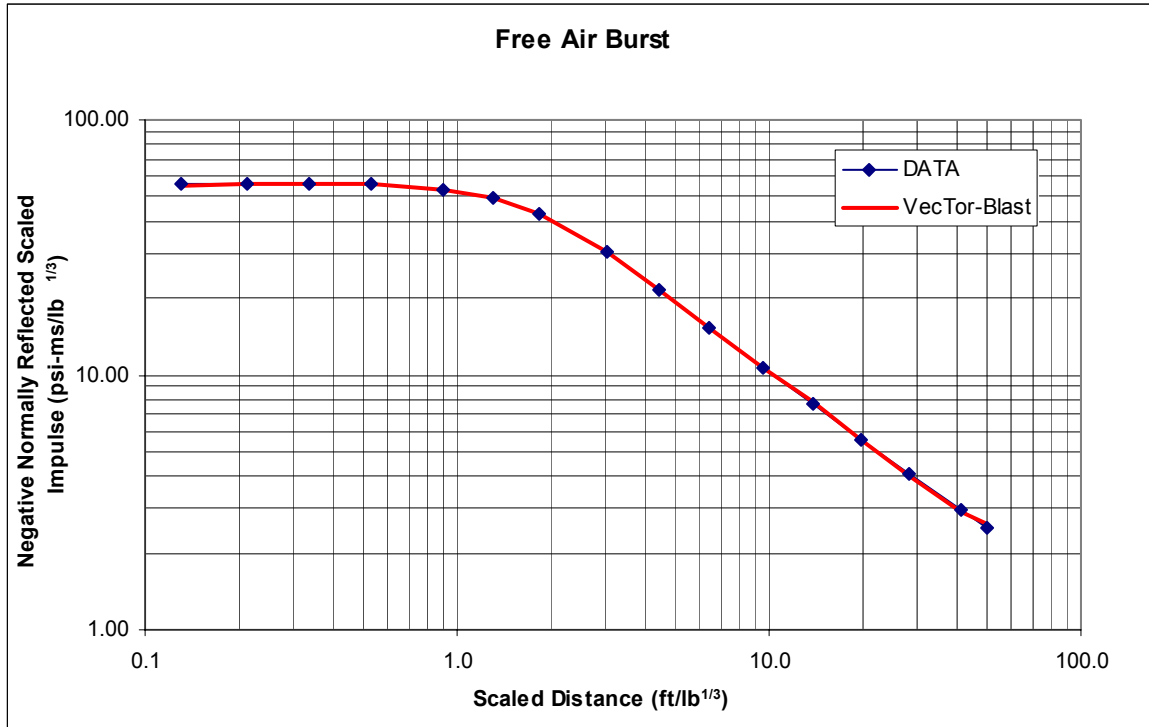
B.1 Curves

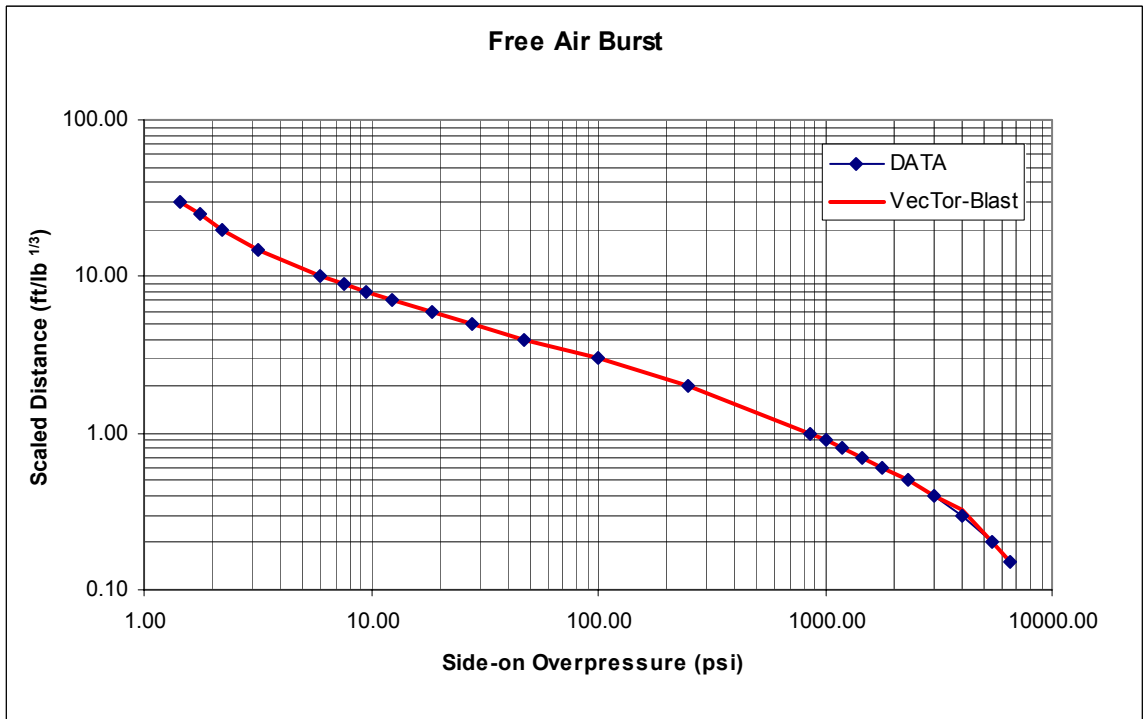
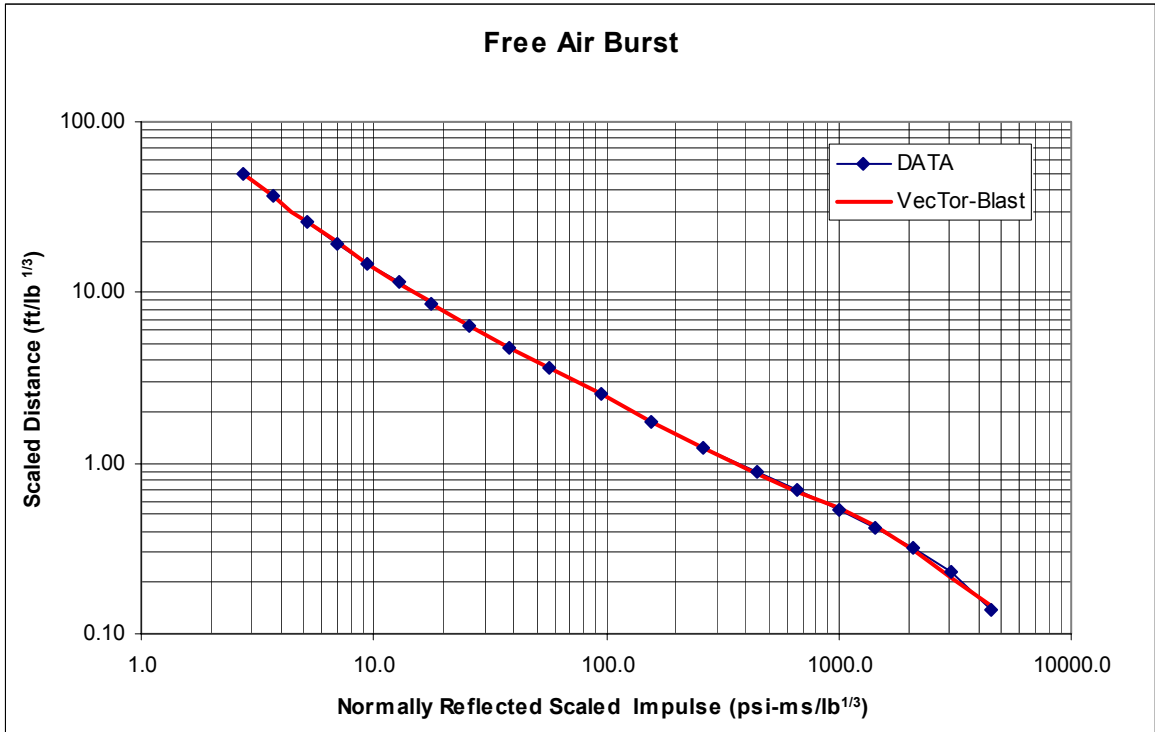


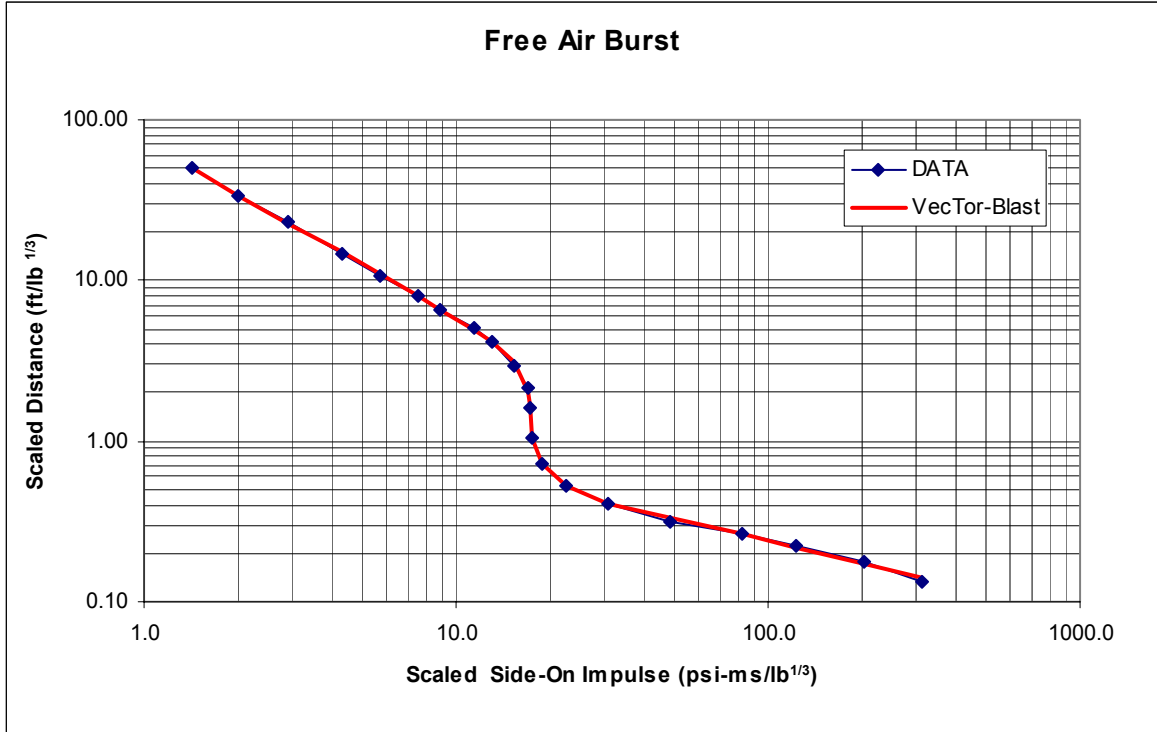


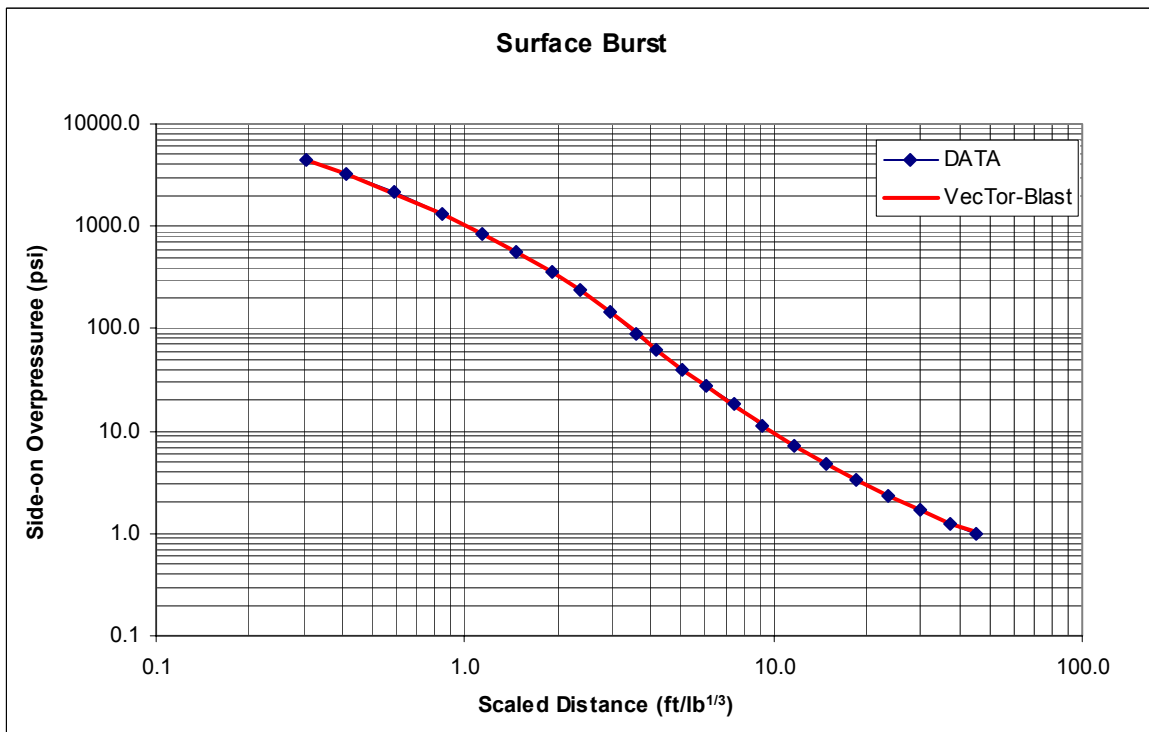
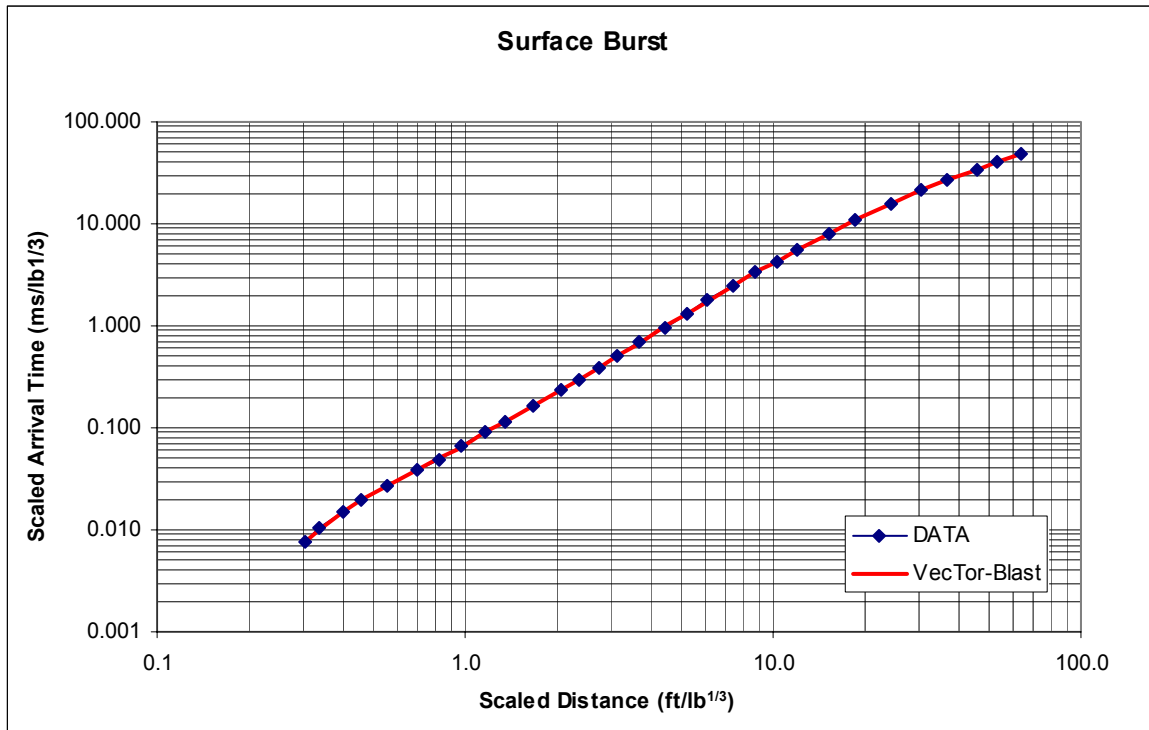


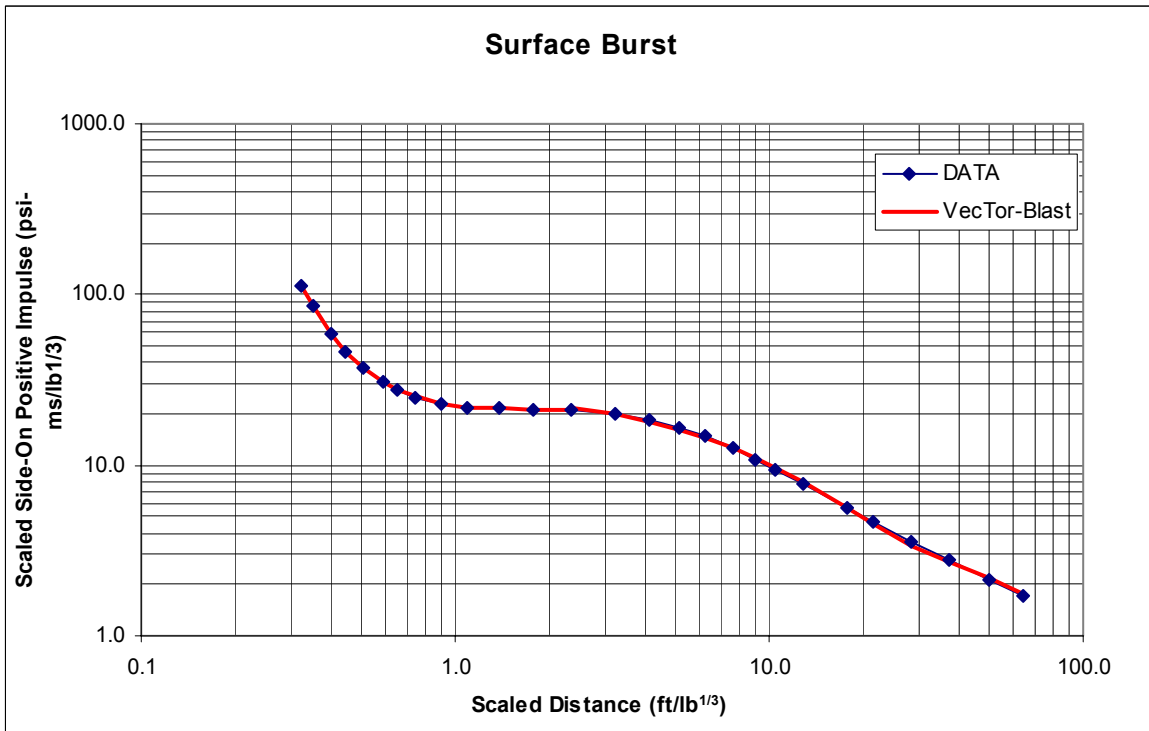
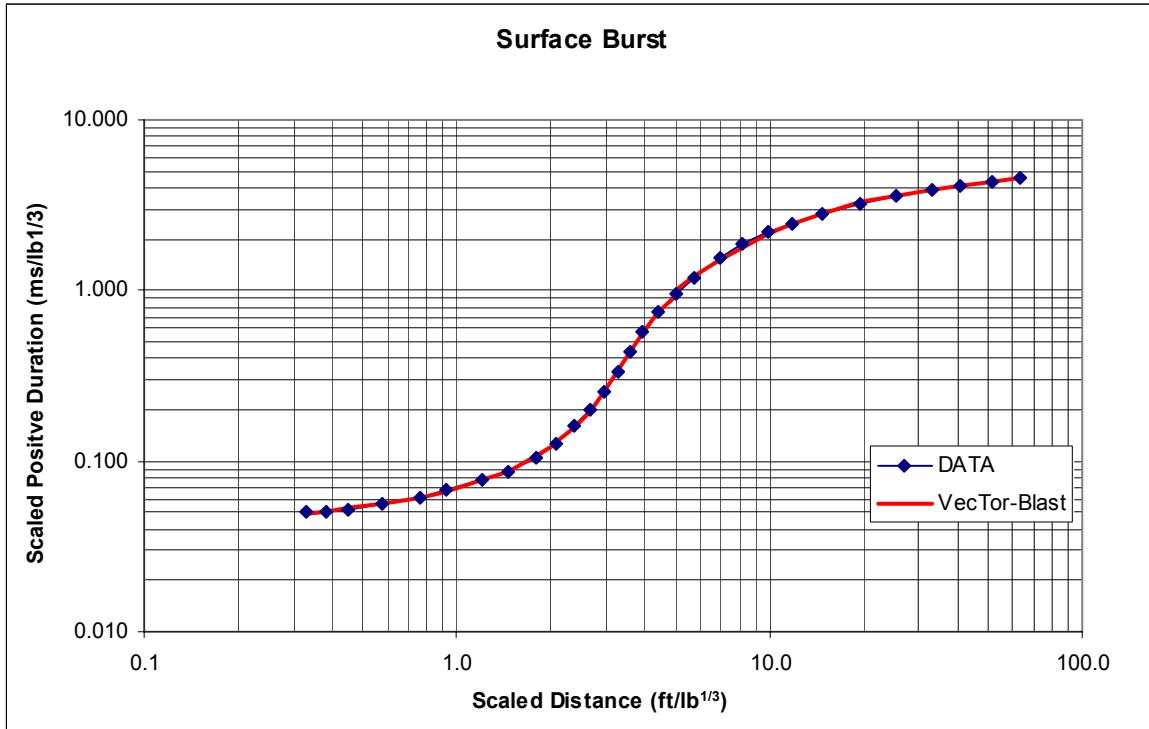


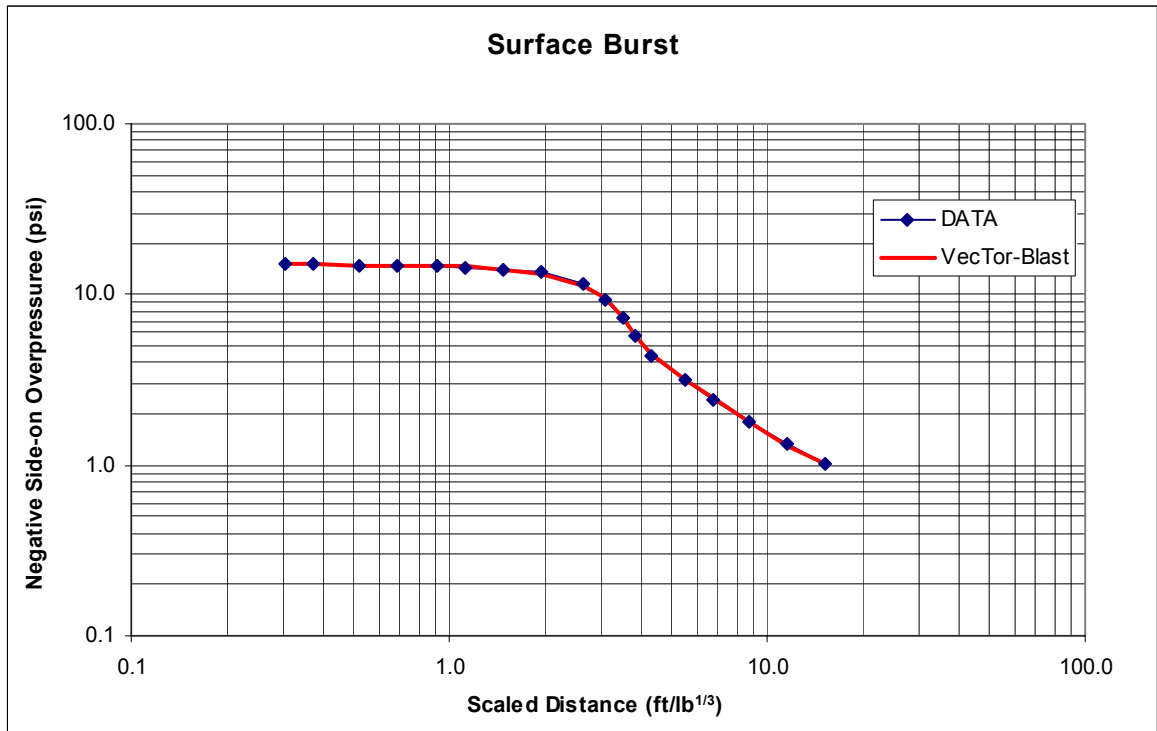
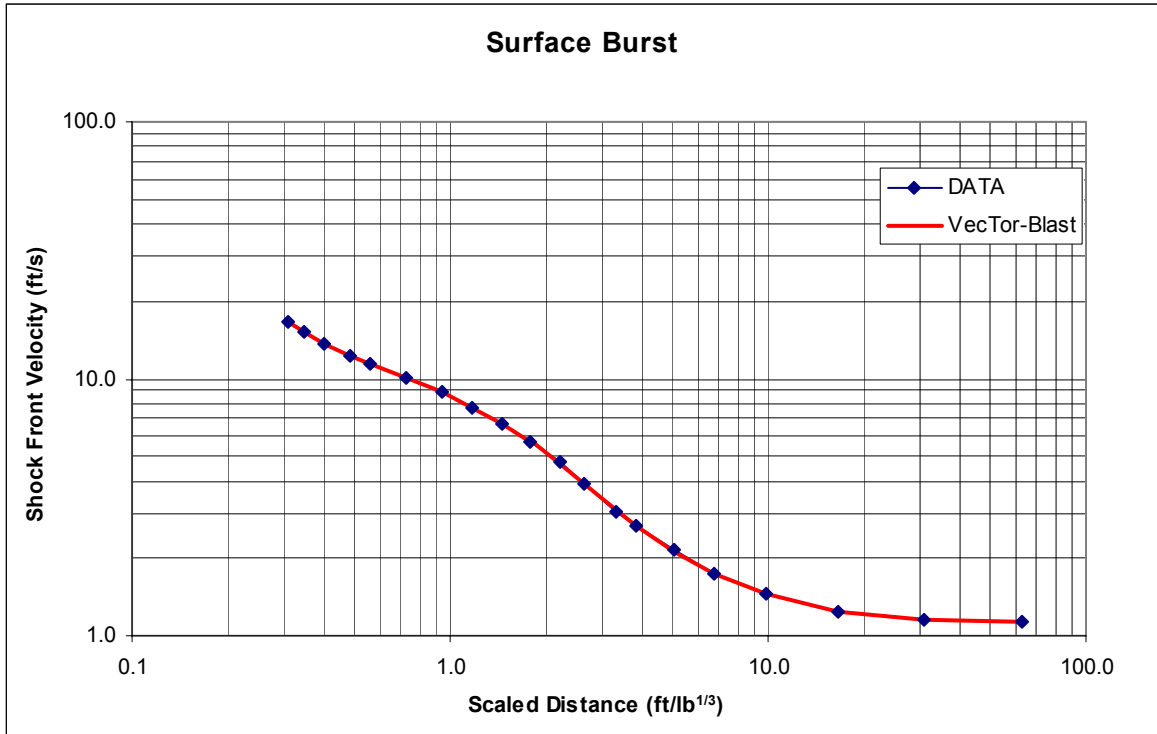


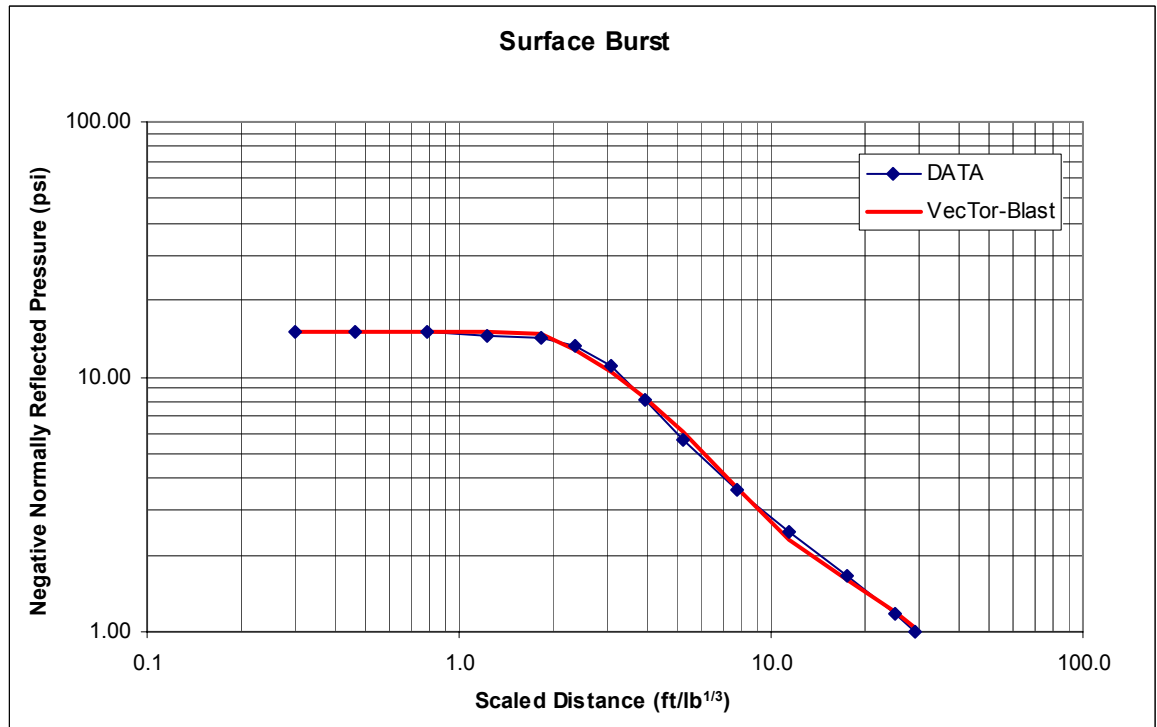
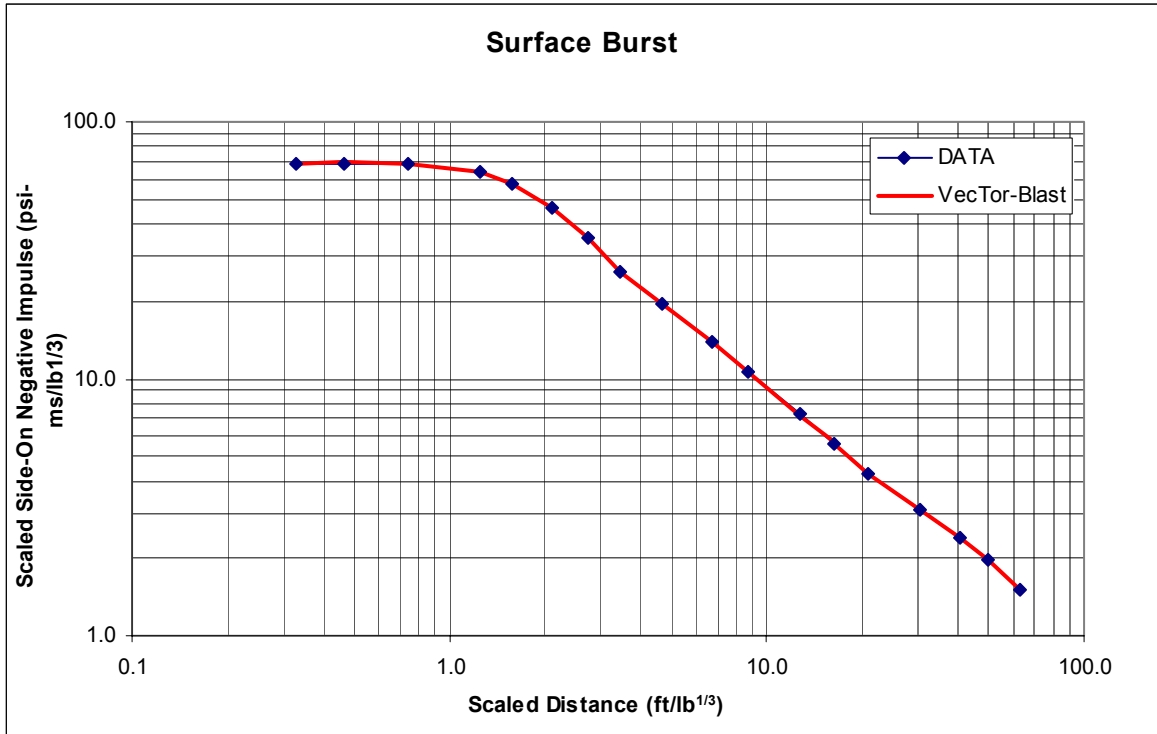


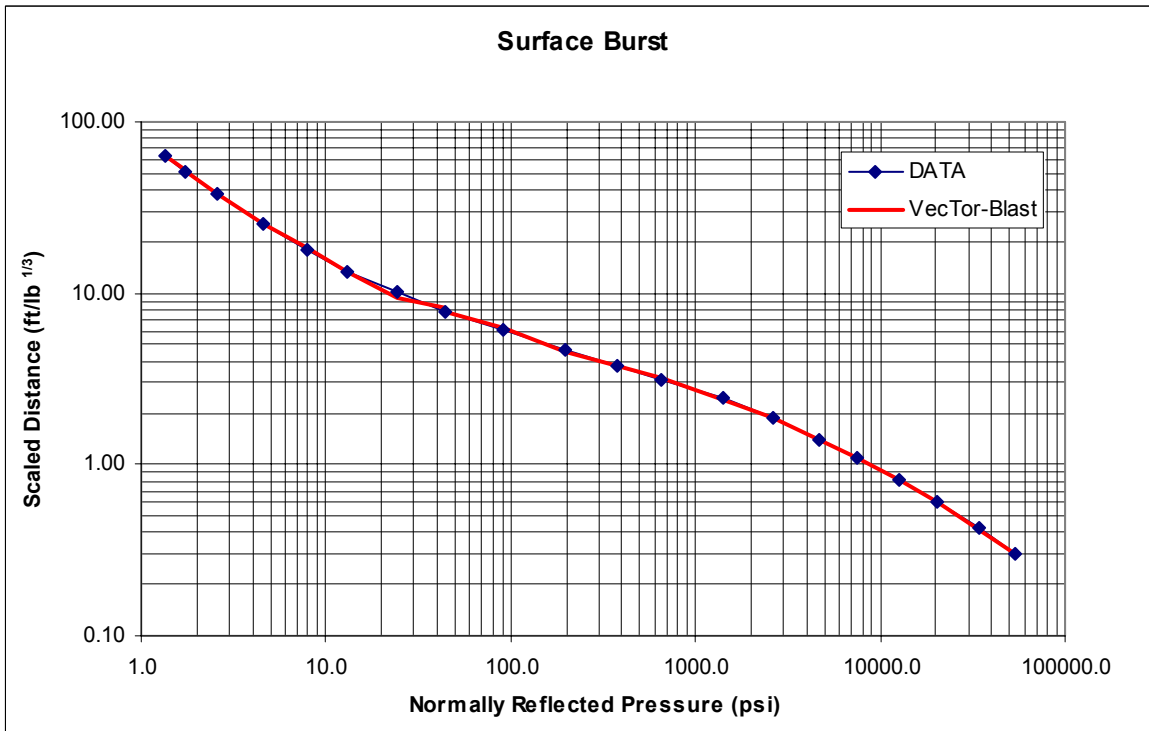
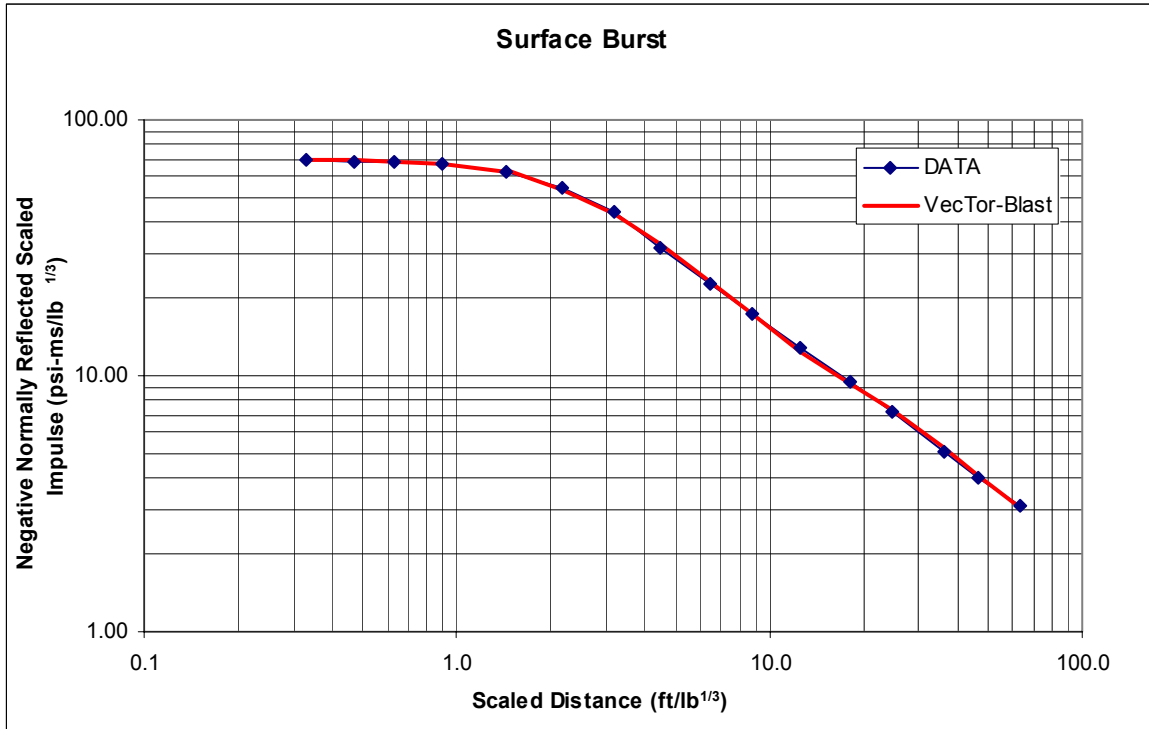


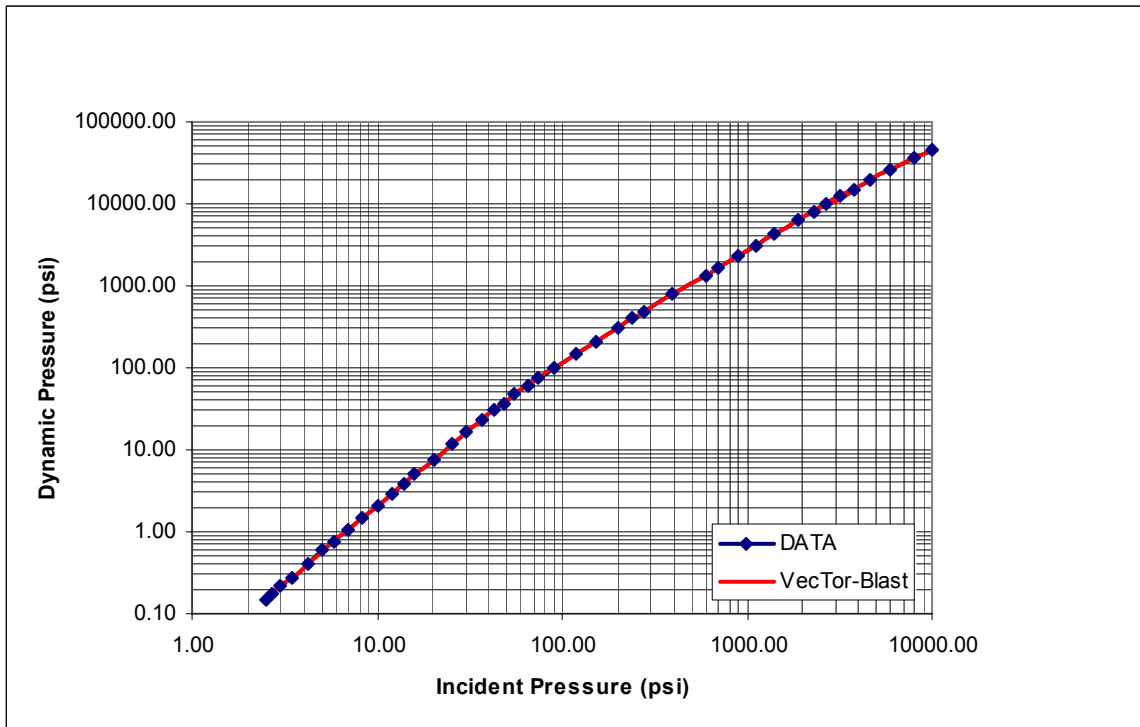
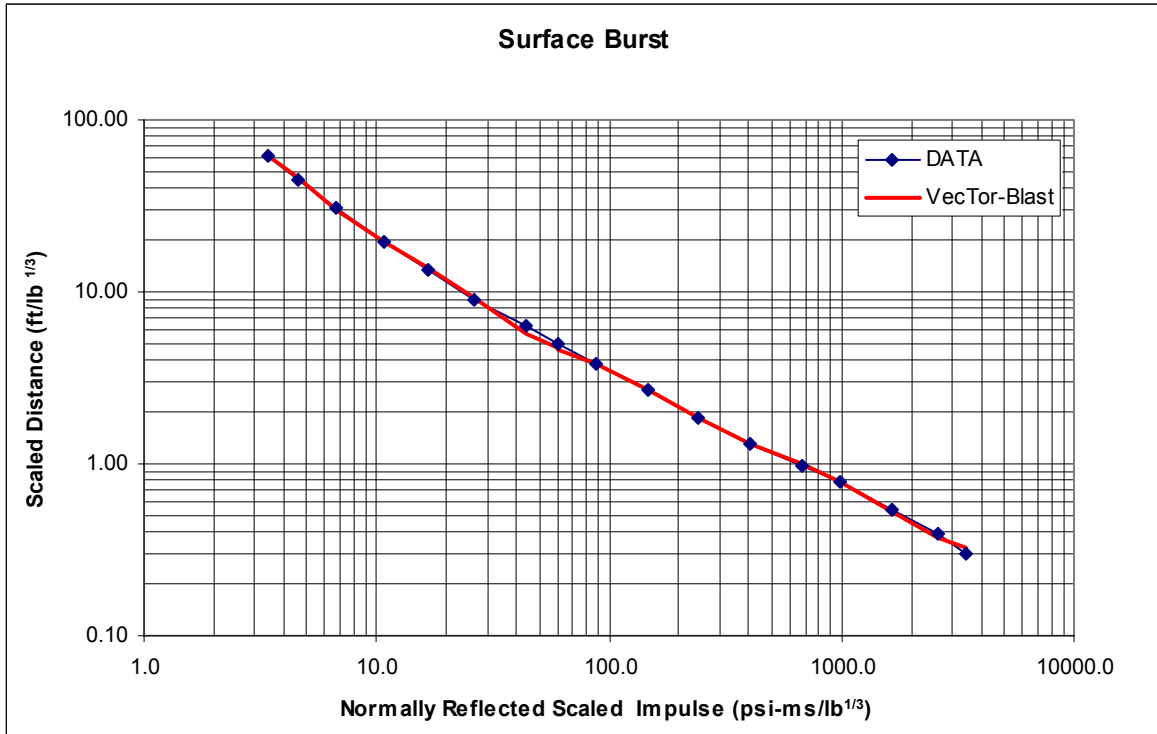


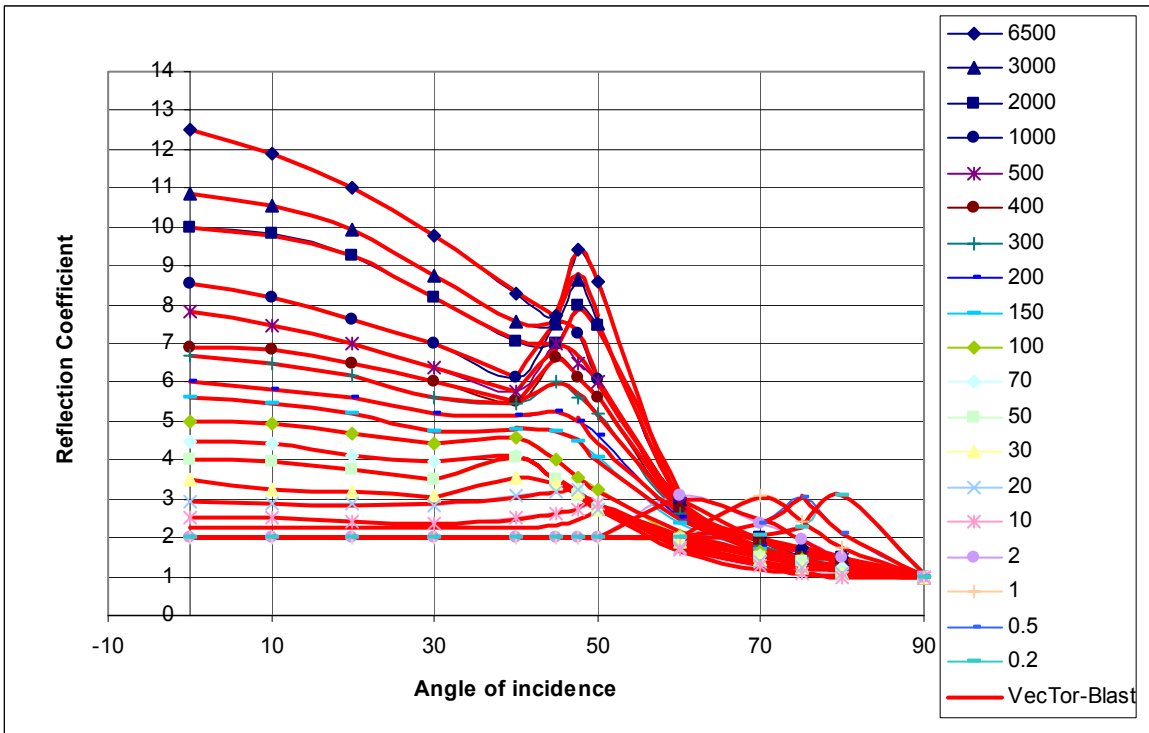
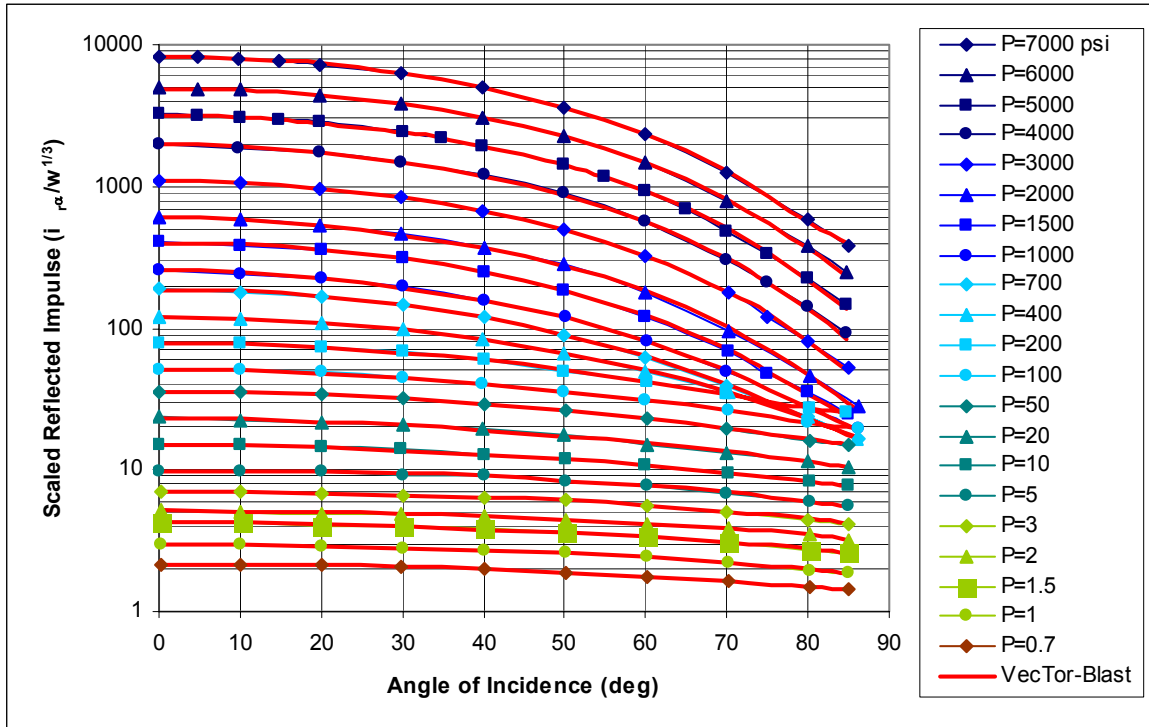


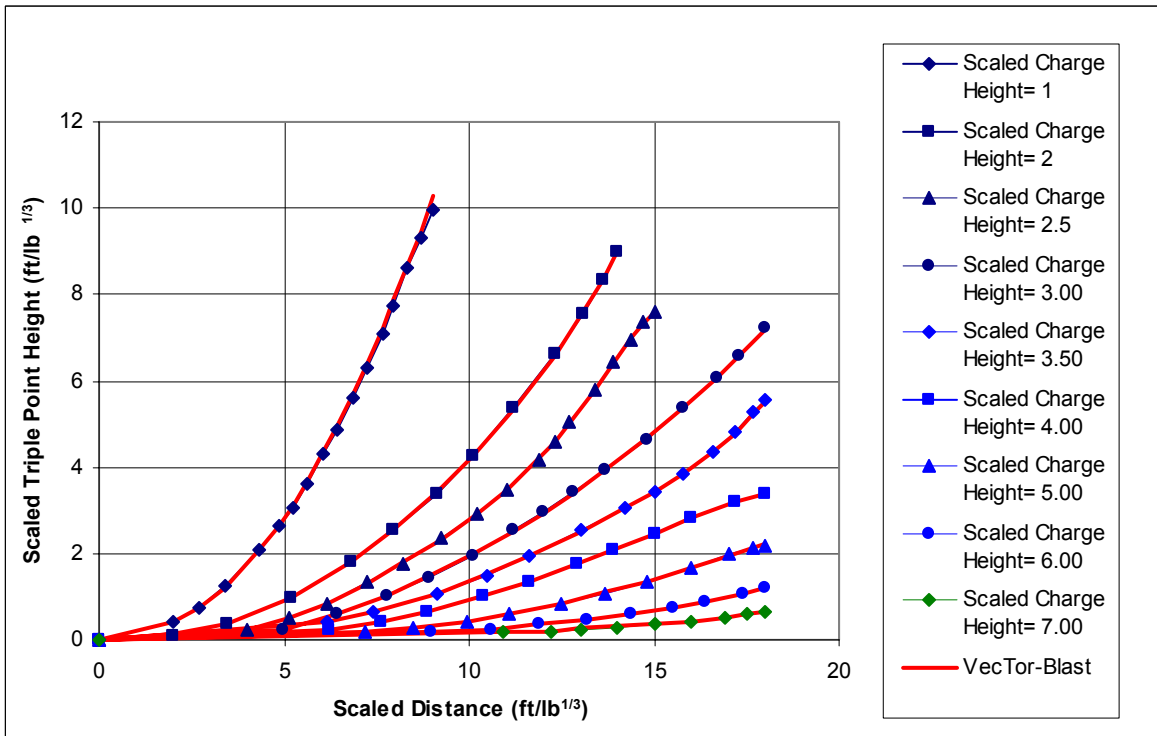
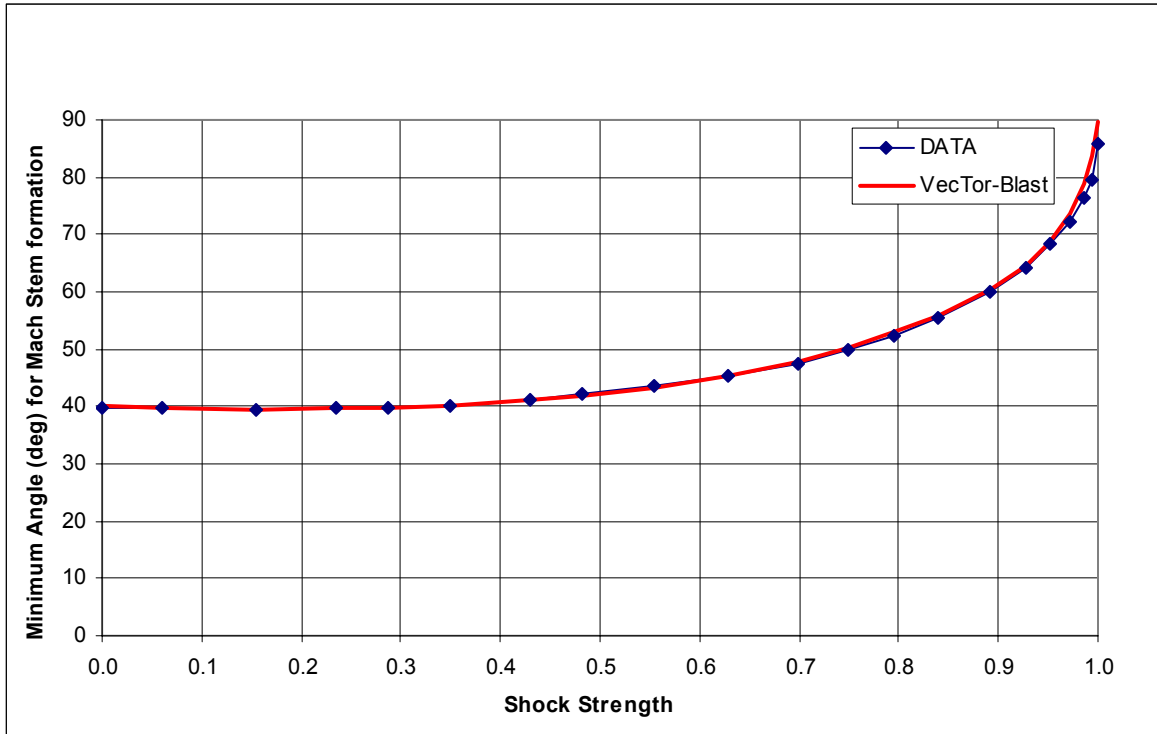


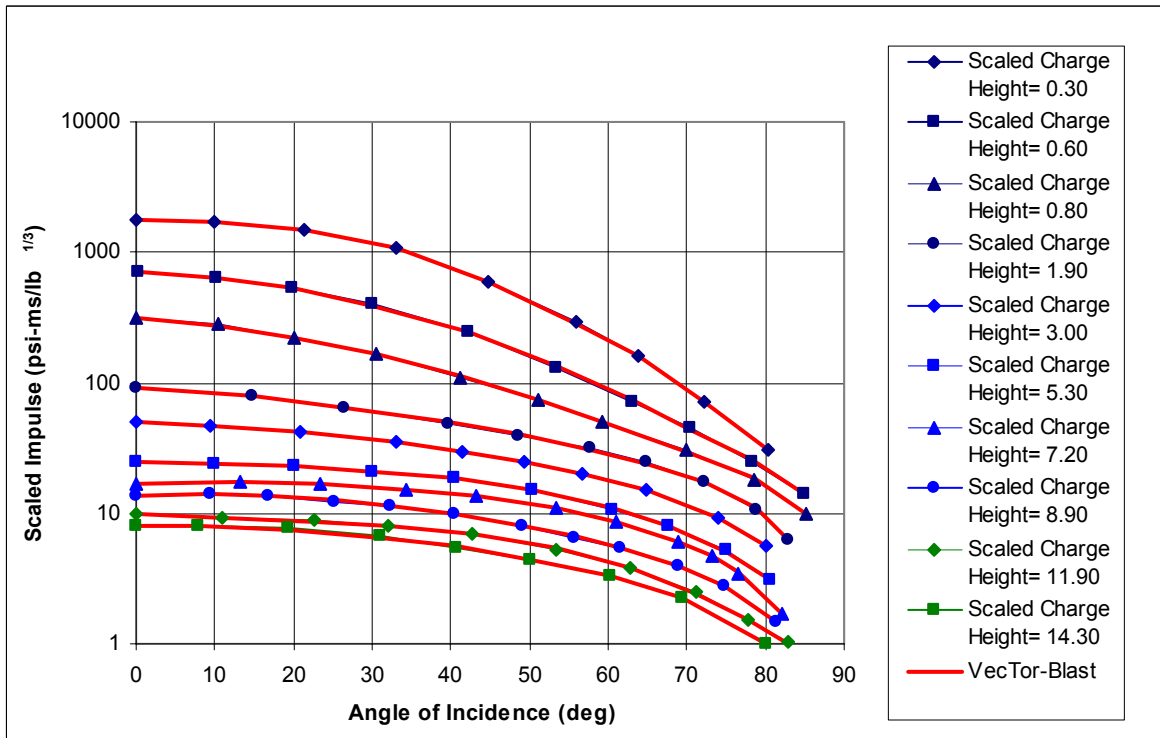
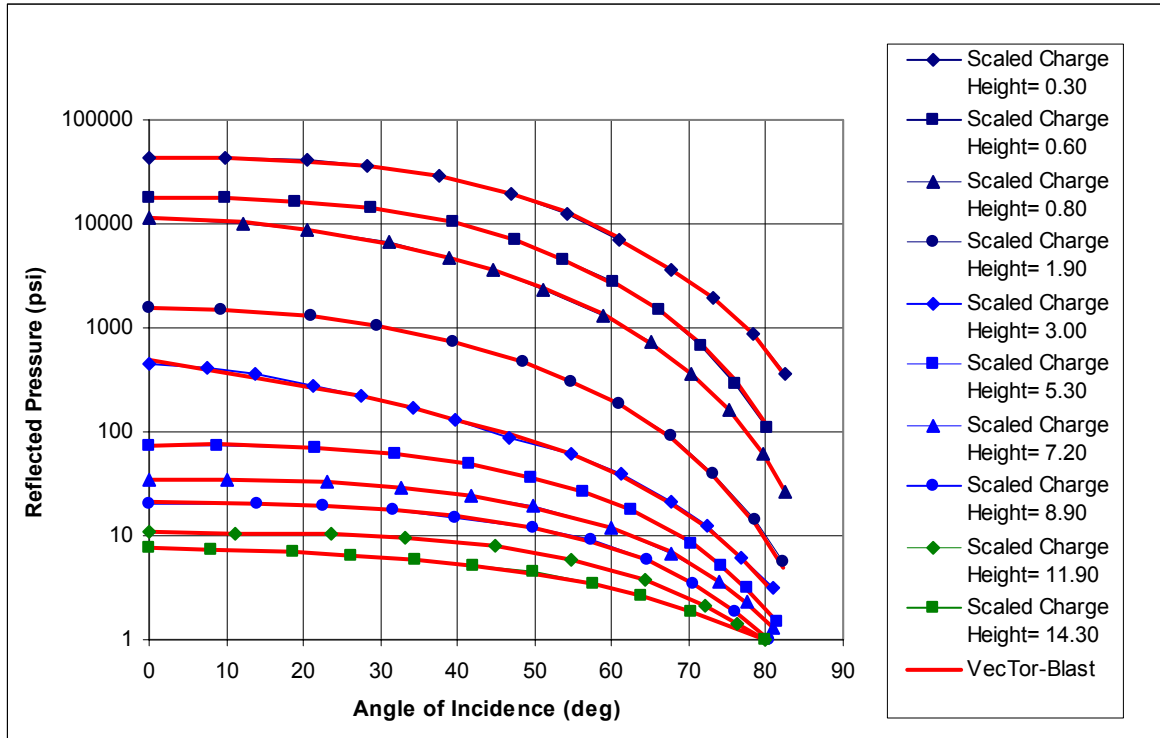












APPENDIX C *VECTOR-BLAST* PROGRAM

C.1 Introduction

VecTor-Blast is a single document interface (SDI) computer program created in Microsoft Visual c++.net for the Windows platform. It is a menu driven program where the user is able to make selections based on inputs, and results are displayed in a window. A data file is also generated to accompany the on-screen displays. *VecTor-Blast* is to be used as a pre-processor for finite element analysis of structures subjected to blast loading by providing an estimate of blast loads. The main role of *VecTor-Blast* is to provide a user interface for generating blast loads.

This chapter will describe the structure of *VecTor-Blast* and includes a flow chart of *VecTor-Blast*'s operations. *VecTor-Blast* can be broken down into a series of classes which run the entire program.

C.2 *VecTor-Blast* Flow Chart

The flow chart, in Figure C.1 and Figure C.2, shows the major operations in *VecTor-Blast*. The elliptical boxes represent the major classes while the major functions are shown in rectangular boxes with solid lines. The rectangular boxes with broken lines represent functions which are driven by menu selections in *VecTor-Blast*.

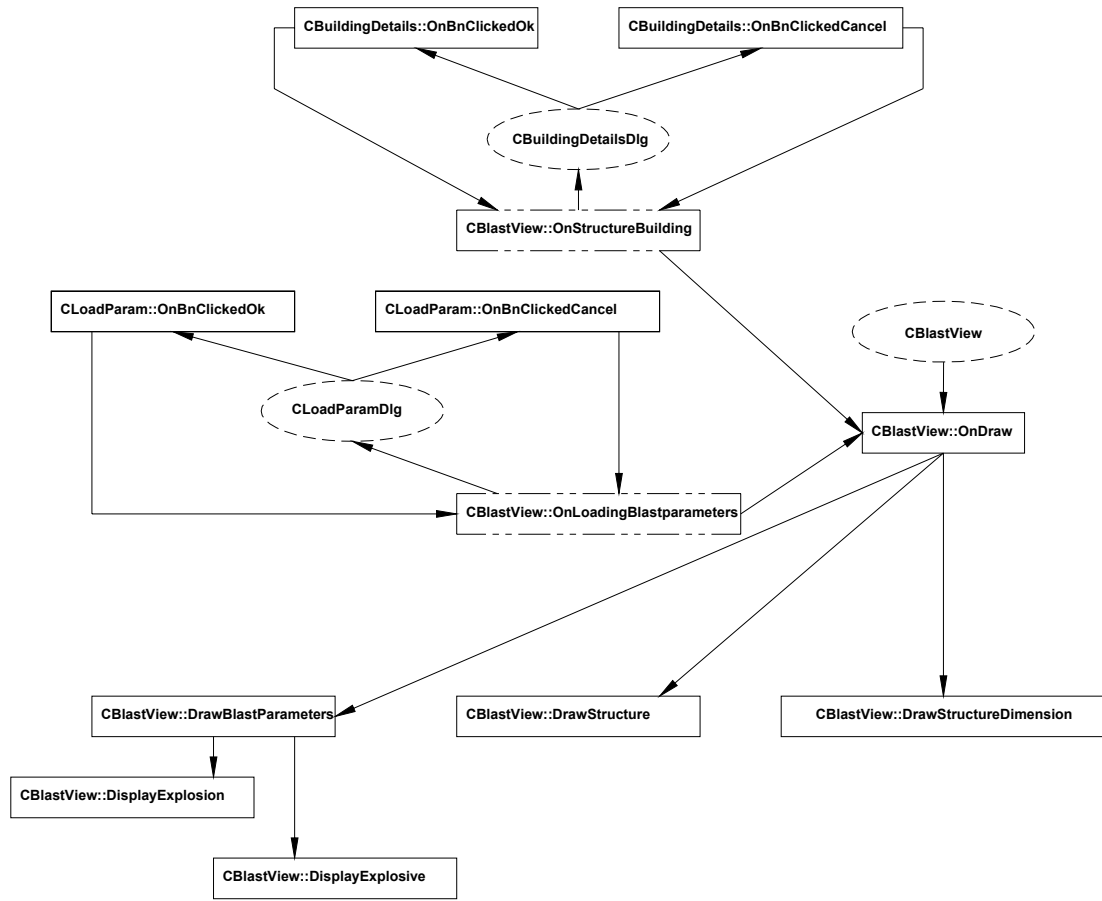


Figure C.1 Flow Chart of *VecTor-Blast*.

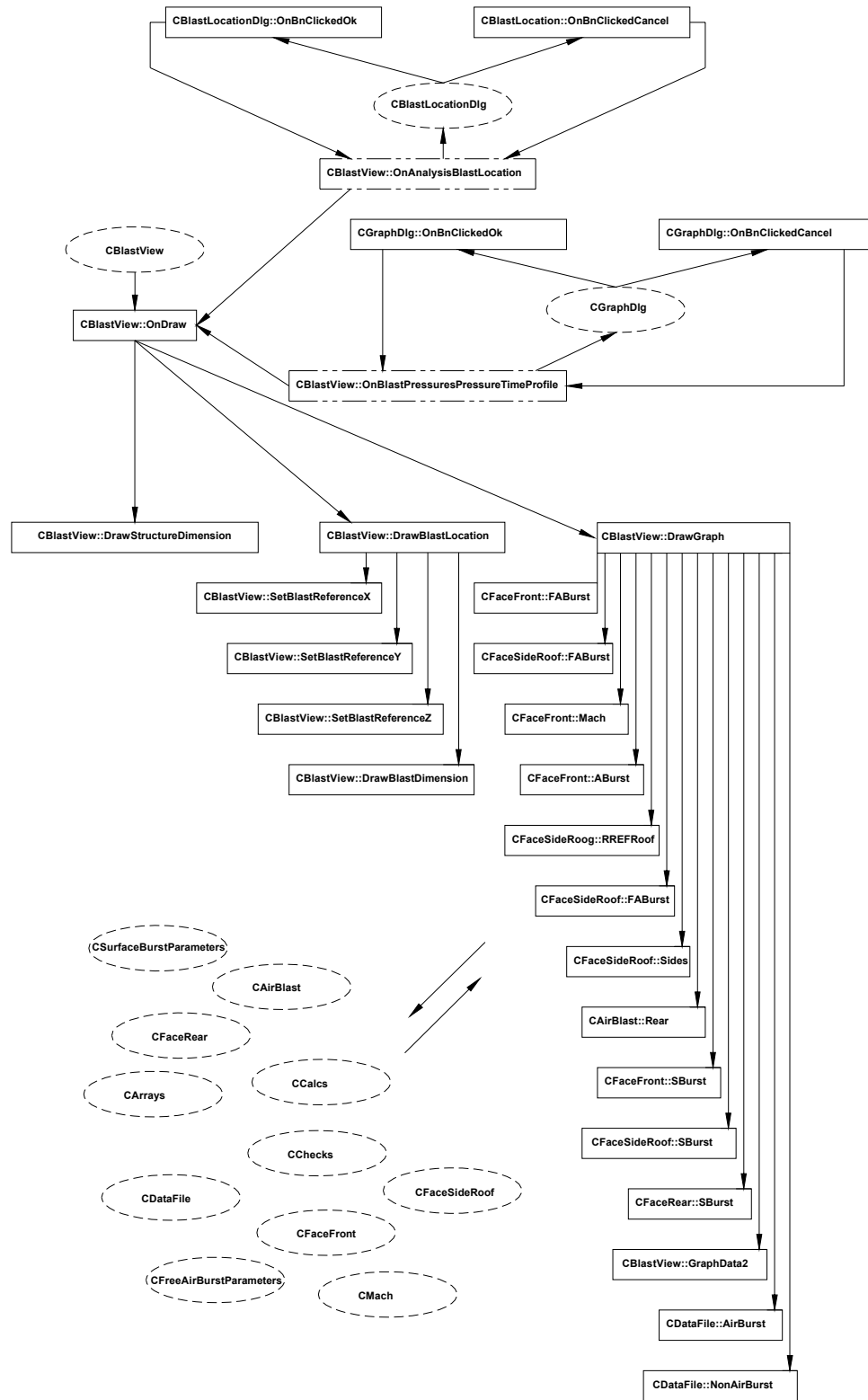


Figure C.2 Flow Chart of VecTor-Blast.

C.3 Classes and Functions

A listing of the classes and their respective functions are given below, as are a description of their operations.

AirBlast.cpp

Functions:

Name:	CAirBlast::Rear
Called By:	CBlastView::DrawGraph
Returns:	Arrays holding pressure-time histories for x, y, and z components on the rear face of the structure subjected to an airblast.
Description:	Calculates pressure-time histories from combining blast waves on the rear of the structure including mach waves, regularly reflected waves, and incident waves diffracting over the roof, front, and sides.

Arrays.cpp

Functions:

Name:	CArrays::ArrayNegative
Called By:	CBlastView::DrawGraph
Returns:	An array of pressure-time history points whose points are positive for overpressure and negative for underpressure.
Description:	Returns pressure-time history which is independent of direction in which its travelling relative to x, y, and z axis by checking the sign of the first pressure term such that overpressure is always positive (independent of direction).

Name:	CArrays::PoparrayABNONBLAST
Called By:	CBlastView::DrawGraph
Returns:	An array of pressure-time history points for an airburst with incident (side-on) components only.
Description:	Takes the all the pressures and times for incident (side-on) components and places them in an array in chronological order.

Name: **CArrays::Populatearray**
 Called By: CBlastView::DrawGraph
 Returns: An array of pressure-time history points for reflected (face-on) components.
 Description: Takes the pressures and times for reflected (face-on) components and places them in an array in chronological order.

Name: **CArrays::PopulateNonBlastFace**
 Called By: CBlastView::DrawGraph
 Returns: An array of pressure time-history points for a surface or free air burst for incident (side-on) components.
 Description: Takes the pressures and times for incident (side-on) components and places them in an array in chronological order.

Name: **CArrays::SortArray3AB**
 Called By: CBlastView::DrawGraph
 Returns: An array of times in chronological order and the number of time positions in that array.
 Description: Takes in three pressure-time history arrays, extracts all the times, and sorts them chronologically in a new array.

Name: **CArrays:: SortArray6**
 Called By: CAirBlast::Rear
 Returns: An array of times in chronological order and the number of time positions in that array.
 Description: Takes in six pressure-time history arrays, extracts all the times, and sorts them chronologically in a new array.

Name: **CArrays:: Superimpose3AB**
 Called By: CBlastView::DrawGraph
 Returns: An array of combined pressure-time histories, maximum and minimum pressure, and maximum time.
 Description: Takes in three pressure-time history arrays from an airburst and superimposes them into one array in chronological order.

Name: **CArrays:: Superimpose6**
 Called By: CAirBlast::Rear
 Returns: An array of combined pressure-time histories, maximum and minimum pressure, and maximum time.
 Description: Takes in six pressure-time history arrays and superimposes them

into one array in chronological order.

BlastDoc.cpp

Functions:

Name: **CBlastDoc::OnNewDocument**
 Called By: *File/New Menu
 Returns: True or false.
 Description: Resets variables for a new file.

* Built-in function

BlastLocationDlg.cpp

Called By: CBlastView::OnAnalysisBlastLocation

Functions:

Name: **CBlastLocationDlg::CheckInput**
 Called By: CBlastLocationDlg::OnBnClickedOk
 Returns: True or false.
 Description: Checks that appropriate dimensions are entered for the location of the explosion.

Name: **CBlastLocationDlg::OnBnClickedCancel**
 Called By: *Cancel button
 Returns: Receives message that Cancel has been clicked.
 Description: Closes dialog box and returns to
 CBlastView::OnAnalysisBlastLocation.

Name: **CBlastLocationDlg::OnBnClickedOk**
 Called By: *OK button
 Returns: Receives message that Ok has been clicked.
 Description: Based on the return of CBlastLocationDlg::CheckInput, closes the dialog box and returns to CBlastView::OnAnalysisBlastLocation or sends an error message asking the user to change the input.

* Built-in function

BlastDoc.cpp

Functions:

Name:	CBlastDoc::OnOpenDocument
Called By:	CBlastDoc
Returns:	True or false
Description:	Checks whether a file is being opened.

Name:	CBlastDoc::OnNewDocument
Called By:	CBlastDoc
Returns:	True or false
Description:	Checks whether a new file is being created and resets all the variables to their default values.

Name:	CBlastDoc::Serialize
Called By:	CBlastDoc
Returns:	True or false
Description:	Saves all variables to a file or reloads them if a file is being opened.

BlastView.cpp

Functions:

Name:	CBlastView::CheckFaceLocation
Called By:	CBlastView::DrawGraph
Returns:	True or false
Description:	Checks whether the new selected analysis point on the structure has the same coordinates as the previous one.

Name:	CBlastView::CheckMassStructureBlast
Called By:	CBlastView::DrawGraph
Returns:	True or false.
Description:	Checks whether any of newly entered coordinates of the structure, newly entered title, or newly entered mass of explosive changed compared to the previous entries.

Name:	CBlastView::DisplayExplosive
-------	-------------------------------------

Called By: CBlastView::DrawBlastParameters
 Returns: A string with the explosive type.
 Description: Converts the explosive type as an integer based on the value from CBlastView::OnLoadingBlastparameters to a string which can be displayed on the screen.

Name: **CBlastView::DisplayExplosion**
 Called By: CBlastView::DrawBlastParameters
 Returns: A string with the explosion type.
 Description: Converts the explosion type as an integer based on the value from CBlastView::OnLoadingBlastparameters to a string which can be displayed on the screen.

Name: **CBlastView::DrawBlastDimension**
 Called By: CBlastView::DrawBlastLocation
 Returns: Draws screen graphics.
 Description: Draws the dimensions of the blast location in the window.

Name: **CBlastView::DrawBlastLocation**
 Called By: CBlastView::OnDraw
 Returns: Draws screen graphics.
 Description: Controls the drawing of the explosion location in the window and draws the lines to the explosion.

Name: **CBlastView::DrawBlastParameters**
 Called By: CBlastView::OnDraw
 Returns: Draws screen graphics.
 Description: Displays the amount and description of the explosive based on values from CBlastView::OnLoadingBlastparameters.

Name: **CBlastView::DrawGraph**
 Called By: CBlastView::OnDraw
 Returns: Draws screen graphics.
 Description: Controls the drawing of the pressure-time history graph, all the calculations required to determine the pressure-time history, and the creation of the data file.

Name: **CBlastView::DrawGraphScaleButtons**
 Called By: CBlastView::OnDraw
 Returns: Draws screen graphics.
 Description: Controls the drawing of the scale buttons which can change the

	scale on the graph.
Name:	CBlastView::DrawStructure
Called By:	CBlastView::OnDraw
Returns:	Draws screen graphics.
Description:	Draws the structure.
Name:	CBlastView::DrawStructureDimension
Called By:	CBlastView::OnDraw
Returns:	Draws screen graphics.
Description:	Draws the dimensions of the structure based on values from CBlastView::OnStructureBuilding.
Name:	CBlastView::Fonts
Called By:	CBlastView::DrawStructureDimension, CBlastView::DrawBlastParameters, CBlastView::DrawBlastLocation, CBlastView::GraphLabels, CBlastView::GraphLinesx, CBlastView::GraphLinesy, CBlastView::OnDraw
Returns:	Text fonts.
Description:	Sets the font size of the text.
Name:	CBlastView::Graphdata2
Called By:	CBlastView::DrawGraph
Returns:	Draws screen graphics.
Description:	Takes in the final pressure-time history, graph window coordinates, maximum and minimum coordinates of the graph, and plots the points from the pressure-time history.
Name:	CBlastView::GraphIntervalX
Called By:	CBlastView::DrawGraph
Returns:	The size of intervals on the x-axis of the graph.
Description:	Calculates the size interval based on 10 intervals on the x-axis and the maximum time.
Name:	CBlastView::GraphIntervalY
Called By:	CBlastView::DrawGraph
Returns:	The size of intervals on the y-axis of the graph
Description:	Calculates the size interval based on the maximum and minimum pressure.
Name:	CBlastView:: GraphLabels
Called By:	CBlastView::OnDraw

Returns:	Draws screen graphics.
Description:	Adds the legend, chart title, and axis titles to the graph.
Name:	CBlastView::GraphLinesx
Called By:	CBlastView::OnDraw
Returns:	Draws screen graphics.
Description:	Draws the x gridlines of the graph based on the size of the y interval and the size of the graph.
Name:	CBlastView::GraphLinesy
Called By:	CBlastView::OnDraw
Returns:	Draws screen graphics.
Description:	Draws the y gridlines of the graph based on the size of the x interval and the size of the graph.
Name:	CBlastView::IntegertoString
Called By:	CBlastView::GraphLinesx
Returns:	A string variable.
Description:	Converts an integer variable to a string.
Name:	CBlastView::OnAnalysisBlastLocation
Called By:	Analysis/BlastLocation Menu
Returns:	Receives message that Blast Location dialog box is being accessed.
Description:	Allows access to results from CBlastLocationDlg. Results (variables) are transferred to variables in CBlastView.
Name:	CBlastView::OnBlastpressuresPressureTimeProfile
Called By:	Blastpressures/PressureTimeProfile Menu
Returns:	Receives message that the Graph Pressure dialog box is being accessed.
Description:	Allows access to results from CGraphDlg. Results (variables) are transferred to variables in CBlastView.
Name:	CBlastView::OnDraw
Called By:	*, CBlastView::OnAnalysisBlastLocation, CBlastView::OnBlastpressuresPressureTimeProfile, CBlastView::OnLoadingBlastparameters, CBlastDoc::OnNewDocument**, CBlastView::OnStructureBuilding
Returns:	Draws screen graphics.
Description:	Main function which controls drawing in the window including the layout of the window and where items are drawn and placed.

Name:	CBlastView::OnLButtonDown
Called By:	CBlastView
Returns:	Coordinates of left mouse click.
Description:	Checks whether the user has clicked on the axis modification buttons.

Name:	CBlastView::OnLButtonUp
Called By:	CBlastView
Returns:	Coordinates of left mouse click.
Description:	Checks whether the user has let go of the left click of the mouse.

Name:	CBlastView::OnLoadingBlastparameters
Called By:	Loading/Blastparameters Menu
Returns:	Receives message that the Blast Load Parameters dialog box is being accessed.
Description:	Allows access to results from CLoadParamDlg Results (variables) are transferred to variables in CBlastView.

Name:	CBlastView::OnStructureBuilding
Called By:	Structure/Building Menu
Returns:	Receives message that the Building Details dialog box is being accessed.
Description:	Allows access to results from CBuildingDetailsDlg Results (variables) are transferred to variables in CBlastView.

Name:	CBlastView::OnUpdateAnalysisBlastLocation
Called By:	*
Returns:	Sends message to update the Analysis/ BlastLocation Menu.
Description:	Enables or disables the Analysis/ BlastLocation Menu.

Name:	CBlastView::OnUpdateLoadingBlastparameters
Called By:	*
Returns:	Sends message to update the Loading/Blastparameters Menu.
Description:	Enables or disables the Loading/Blastparameters Menu.

Name:	CBlastView::OnUpdateBlastpressuresPressureTimeProfile
Called By:	*
Returns:	Sends message to update the Blastpressures/PressureTimeProfile Menu.
Description:	Enables or disables the Blastpressures/PressureTimeProfile Menu.

Name:	CBlastView::OnUpdateStructureBuilding
-------	--

Called By:	*
Returns:	Sends message to update the Structure/Building Menu.
Description:	Enables or disables the Structure/Building Menu.
Name:	CBlastView::Orderfastest
Called By:	CBlastView::DrawGraph
Returns:	Two arrays; array1 starting before array2.
Description:	Takes in two pressure-time history arrays and determines which one occurs first based on their arrival times.
Name:	CBlastView::Orderfastest3
Called By:	CBlastView::DrawGraph
Returns:	Three arrays; array1 starting before array2, array2 starting before array3.
Description:	Takes in three pressure-time history arrays and determines which occurs first, second, and third based on their arrival times.
Name:	CBlastView::SetBlastReferenceX
Called By:	CBlastView::DrawBlastLocation
Returns:	The x coordinate of the origin.
Description:	The x coordinate of the origin is returned based on the location of the explosion.
Name:	CBlastView::SetBlastReferenceY
Called By:	CBlastView::DrawBlastLocation
Returns:	The y coordinate of the origin.
Description:	The y coordinate of the origin is returned based on the location of the explosion.
Name:	CBlastView::SetBlastReferenceZ
Called By:	CBlastView::DrawBlastLocation
Returns:	The z coordinate of the origin.
Description:	The z coordinate of the origin is returned based on the location of the explosion.
Name:	CBlastView::SortArray
Called By:	CBlastView::DrawGraph
Returns:	An array of times in chronological order and the number of time positions in that array.
Description:	Takes in two pressure-time history arrays, extracts all the times, and sorts them chronologically in a new array.

Name: **CBlastView::SortArray3**
 Called By: CBlastView::DrawGraph
 Returns: An array of times in chronological order and the number of time positions in that array.
 Description: Takes in three pressure-time history arrays, extracts all the times, and sorts them chronologically in a new array.

Name: **CBlastView::Superimpose2**
 Called By: CBlastView::DrawGraph
 Returns: An array of combined pressure-time histories, maximum and minimum pressure, maximum time, and the net direction of the pressure.
 Description: Takes in two pressure-time history arrays and superimposes them into one array in chronological order.

Name: **CBlastView::Superimpose3**
 Called By: CBlastView::DrawGraph
 Returns: An array of combined pressure-time histories, maximum and minimum pressure, maximum time, and the net direction of the pressure.
 Description: Takes in three pressure-time history arrays and superimposes them into one array in chronological order.

* Built-in function

**Called indirectly

BuildingDetailsDlg.cpp

Called By: CBlastView::OnStructureBuilding

Functions:

Name: **CBuildingDetailsDlg::OnBnClickedCancel**
 Called By: *Cancel button
 Returns: Receives message that Cancel has been clicked.
 Description: Closes dialog box and returns to CBlastView::OnStructureBuilding.

Name: **CBuildingDetailsDlg::OnBnClickedOk**
 Called By: *OK button

Returns: Receives message that Ok has been clicked.
 Description: Closes dialog box accepting the input parameters and returns to
 CBlastView::OnStructureBuilding.

* Built-in function

Calcs.cpp

Functions:

Name: **CCalcs::CalcAngleofIncidence**
 Called By: CFaceFront::ABurst, CFaceFront::FABurst, CFaceFront::SBurst
 Returns: Angle of incidence.
 Description: Calculates angle of incidence of the ray path based on the
 geometry.

Name: **CCalcs::CalculateCr**
 Called By: CCalcs::ClearingTime
 Returns: The speed of sound in the reflected medium.
 Description: Calculates the value of the speed of sound in the reflected medium
 based on incident (side-on) overpressure.

Name: **CCalcs::Calculated**
 Called By: CCalcs::ClearingTime
 Returns: A geometrical parameter in the Kinney (Kinney, 1985) clearing time
 formula.
 Description: Calculates the distance from the analysis point to the nearest edge
 of the face.

Name: **CCalcs::CalculateS**
 Called By: CCalcs::ClearingTime
 Returns: A geometrical parameter in the Kinney (Kinney, 1985) and in TM 5-
 1300 (1969, 1990) clearing time formula.
 Description: Determines the smallest distance out of the half breadth or height
 of the face for surface burst or airburst. For a free-air burst, the
 function determines the smallest distance out of the half breadth or
 half width of the face.

Name: **CCalcs::CalculateR**
 Called By: CCalcs::ClearingTime
 Returns: A geometrical parameter in the army manual (TM 5-1300, 1990)

clearing time formula.

Description: R is the ratio of S/G where S is determined in CCalcs::CalculateS. G is the largest distance out of half breadth or height of the face for surface burst or airburst. For a free-air burst, G is the largest distance out of the half breadth or half width of the face.

Name: **CCalcs::CalculateDeflection**

Called By: CBlastView::DrawGraph, CFaceRear::REGRoof, CFaceRear::REGSide, CFaceSideRoof::REGRoof, CFaceSideRoof::REGSides

Returns: Angle of deflection.

Description: Calculates angle of deflection based on the geometry and the mass of explosive.

Name: **CCalcs::ClearingTime**

Called By: CFaceFront::ABurst, CFaceFront::FABurst, CFaceFront::Mach, CFaceFront::SBurst

Returns: Clearing time.

Description: Calculates clearing time based on geometry of blast face and the wave speed.

Name: **CCalcs::Direction**

Called By: CFaceFront::ABurst, CFaceFront::FABurst, CFaceFront::Mach, CFaceFront::SBurst

Returns: +1 or -1 (Positive along axis, +1, Negative along axis, -1)

Description: Determines the direction of the x, y, and z components based on direction cosines.

Name: **CCalcs::DoubletoString**

Called By: CBlastView::DrawBlastParameters, CBlastView::DrawBlastDimension, CBlastView::DrawStructureDimension

Returns: A string variable.

Description: Converts a double variable to a string (2 decimals).

Name: **CCalcs::DoubletoString2**

Called By: CGraphDlg::OnBnClickedFace1, CGraphDlg::OnBnClickedFace2, CGraphDlg::OnBnClickedFace3, CGraphDlg::OnBnClickedFace4, CGraphDlg::OnBnClickedFace5

Returns: A string variable.

Description: Converts a double variable to a string (5 decimals).

Name: **CCalcs::FictDuration**

Called By: CFaceFront::ABurst, CFaceFront::FABurst, CFaceFront::Mach,
 CFaceFront::SBurst, CFaceRear::MachRoof,
 CFaceRear::MachSides, CFaceRear::REGRoof,
 CFaceRear::REGSide, CFaceRear::SBurst,
 CFaceSideRoof::FABurst, CFaceSideRoof::FABurst2,
 CFaceSideRoof::MachRoof, CFaceSideRoof::MachSides,
 CFaceSideRoof::REGRoof, CFaceSideRoof::REGSides,
 CFaceSideRoof::SBurst,

Returns: Fictitious duration.

Description: Calculates the fictitious duration based on pressure and impulse.

Name: **CCalcs::FloattoString**

Called By: CBlastView::GraphLinesx, CBlastView::GraphLinesy

Returns: A string variable.

Description: Converts a float variable to a string (user specifies the number of decimals).

Name: **CCalcs::MultiplyAbsoluteValue**

Called By: CFaceFront::ABurst, CFaceFront::FABurst, CFaceFront::Mach,
 CFaceFront::SBurst

Returns: Absolute value of a number.

Description: Calculates the absolute value based on the direction of and the value of a vector component.

Name: **CCalcs::R**

Called By: CBlastView::DrawGraph, CFaceRear::REGRoof,
 CFaceSideRoof::REGRoof, CFaceSideRoof::REGSides,

Returns: The distance from the explosion to the analysis point.

Description: Calculates the distance from the explosion to the analysis point using geometry only (not used for ground reflection).

Name: **CCalcs::RProj**

Called By: CCalcs::R

Returns: The length of a straight line projected on two perpendicular surfaces.

Description: Calculates coordinates on the corner of two perpendicular surfaces

projected by a straight line passing through both surfaces. Those coordinates are then used to calculate a distance around the corner.

Name: **CCalcs::RRear**
 Called By: CBlastView::DrawGraph, CFaceRear::REGRoof, CFaceRear::REGSide,
 Returns: The distance from the explosion to the analysis point.
 Description: Calculates the distance from the explosion to the analysis point on the rear face using geometry only (not used for ground reflection).

Name: **CCalcs::ReflectedImpulse**
 Called By: CFaceFront::ABurst, CFaceFront::FABurst, CFaceFront::SBurst
 Returns: Reflected impulse.
 Description: Calculates the reflected impulse based on incident (side-on) overpressure and angle of incidence.

Name: **CCalcs::ReflectedOverpressure**
 Called By: CBlastView::DrawGraph, CFaceFront::ABurst, CFaceFront::FABurst, CFaceFront::Mach, CFaceFront::SBurst, CFaceRear::REGRoof, CFaceRear::REGSide, CFaceSideRoof::REGRoof, CFaceSideRoof::REGSides
 Returns: Reflected overpressure.
 Description: Calculates the reflected overpressure based on incident (side-on) overpressure and angle of incidence.

Name: **CCalcs::yzforRRegRef**
 Called By: CFaceRear::REGRoof, CFaceRear::REGSide, CFaceSideRoof::REGRoof, CFaceSideRoof::REGSides
 Returns: Y and z coordinates by reference.
 Description: Calculates coordinates on the corner of two perpendicular surfaces projected by a straight line passing through both surfaces.

Checks.cpp

Functions:

Name:	CChecks::CheckArea
Called By:	CBlastView::DrawGraph
Returns:	1 or 2 which represents a graph type.
Description:	Calculates the area under the reflected impulse curve and the cleared impulse curve and compares them. Returns the number corresponding to the smallest area where 1 is the first curve and 2 is the second curve.

Name:	CChecks::CheckArea2
Called By:	CBlastView::DrawGraph
Returns:	1 or 2, representing a graph type.
Description:	Calculates the area under the reflected impulse curve and the cleared impulse curve for two combining waves and compares them. Returns the number corresponding to the smallest area where 1 is the first curve and 2 is the second curve.

Name:	CChecks::CheckHc
Called By:	CMach::MachFormMachZone
Returns:	True or false.
Description:	Checks whether the scaled charge height is within data range.

Name:	CChecks::CheckPandi
Called By:	CBlastView::DrawGraph, CFaceRear::MachSides, CFaceRear::MachRoof, CFaceSideRoof::MachRoof, CFaceSideRoof::MachSides,
Returns:	True or false.
Description:	Checks whether Mach pressure and impulse are within limitations of scaled distance

Name:	CChecks::CheckZ
Called By:	CBlastView::DrawGraph, CCalcs::CalculateDeflection, CFaceRear::MachSide, CFaceRear::REGRoof, CFaceRear::REGSide, CFaceSideRoof::REGRoof, CFaceSideRoof::REGSides,
Returns:	True or false.

Description: Checks whether the scaled distance is within the data range for free airburst and surface burst parameters.

Name: **CChecks::CheckZg**

Called By: CMach::MachFormMachZone

Returns: True or false.

Description: Checks whether the scaled distance is within the range of scaled height of charge data.

Name: **CChecks::DataCheck**

Called By: CDataFile::Airburst, CDataFile::NonAirburst

Returns: True or false.

Description: Checks whether the difference between the value in array position n+1 and the value in array position n is almost 0.

DataFile.cpp

Functions:

Name: **CDataFile::Airburst**

Called By: CBlastView::DrawGraph

Returns: Data file to desktop.

Description: Takes in all airburst blast parameter data including the pressure-time histories and prints them to a data file.

Name: **CDataFile::NonAirburst**

Called By: CBlastView::DrawGraph

Returns: Data file to desktop.

Description: Takes in all non airburst blast parameter data including the pressure-time histories and prints them to a data file.

FaceFront.cpp

Functions:

Name: **CFaceFront::ABurst**

Called By: CBlastView::DrawGraph

Returns: Blast parameters by reference.

Description: Function containing all the calculations for airburst parameters on the blast face.

Name: **CFaceFront::FABurst**
 Called By: CBlastView::DrawGraph, CFaceSideRoof::REGRoof
 Returns: Blast parameters by reference.
 Description: Function containing all the calculations for free airburst parameters on the blast face.

Name: **CFaceFront::Mach**
 Called By: CBlastView::DrawGraph
 Returns: Blast parameters by reference.
 Description: Function containing all the calculations for Mach wave parameters on the blast face.

Name: **CFaceFront::SBurst**
 Called By: CBlastView::DrawGraph
 Returns: Blast parameters by reference.
 Description: Function containing all the calculations for surface burst parameters on the blast face.

FaceRear.cpp

Functions:

Name: **CFaceRear::AirBurstRoof**
 Called By: CAirBlast::Rear
 Returns: Blast parameters by reference.
 Description: Function containing all the calculations for airburst parameters for waves coming over the roof and diffracting on the rear face.

Name: **CFaceRear::AirBurstSides**
 Called By: CAirBlast::Rear
 Returns: Blast parameters by reference.
 Description: Function containing all the calculations for airburst parameters for waves coming over the sides and diffracting on the rear face.

Name: **CFaceRear::MachRoof**
 Called By: CFaceRear::AirBurstRoof
 Returns: Scaled distance corresponding to mach pressure and blast parameters by reference.
 Description: Function containing all the calculations for mach blast parameters on the roof.

Name: **CFaceRear::MachSides**
 Called By: CFaceRear::AirBurstSides
 Returns: Blast parameters by reference.
 Description: Function containing all the calculations for mach blast parameters on the sides.

Name: **CFaceRear::REGRoof**
 Called By: CFaceRear::AirBurstRoof
 Returns: Blast parameters by reference.
 Description: Function contains all the calculations for ground reflected waves and incident waves diffracting over the roof and on to the rear face.

Name: **CFaceRear::REGSide**
 Called By: CFaceRear::AirBurstRoof
 Returns: Blast parameters by reference.
 Description: Function contains all the blast parameter calculations for ground reflected waves and incident waves diffracting over the sides and on to the rear face.

FaceSideRoof.cpp

Functions:

Name: **CFaceSideRoof::FABurst**
 Called By: CBlastView::DrawGraph
 Returns: Blast parameters by reference.
 Description: Function containing all calculations for blast parameters for a free air burst diffracting over the sides.

Name: **CFaceSideRoof::FABurst2**
 Called By: CBlastView::DrawGraph
 Returns: Blast parameters by reference.
 Description: Function containing all calculations for blast parameters for a free air burst diffracting over the sides in array format.

Name: **CFaceSideRoof::MachRoof**
 Called By: CFaceSideRoof::RREFRoof
 Returns: Scaled distance corresponding to mach pressure and blast parameters by reference..
 Description: Function containing all the calculations for mach blast parameters

	diffracting on to the roof.
--	-----------------------------

Name:	CFaceSideRoof::MachSides
Called By:	CFaceSideRoof::Sides
Returns:	Scaled distance corresponding to mach pressure.
Description:	Function containing all the calculations for mach blast parameters diffracting on to the sides.

Name:	CFaceSideRoof::REGRoof
Called By:	CFaceSideRoof::RREFRoof
Returns:	Blast parameters by reference.
Description:	Function containing all the calculations for regularly ground reflected waves and incident waves diffracting on to the roof.

Name:	CFaceSideRoof::REGSides
Called By:	CFaceSideRoof::Sides
Returns:	Blast parameters by reference.
Description:	Function containing all the blast parameter calculations for regularly ground reflected waves and incident waves diffracting on to the sides.

Name:	CFaceSideRoof::RREFRoof
Called By:	CBlastView::DrawGraph
Returns:	Blast parameters by reference.
Description:	Function containing all calculations for blast parameters for an airburst burst diffracting over the roof.

Name:	CFaceSideRoof::SBurst
Called By:	CBlastView::DrawGraph
Returns:	Blast parameters by reference.
Description:	Function containing all calculations for blast parameters for a surface burst diffracting over the sides.

Name:	CFaceSideRoof::Sides
Called By:	CBlastView::DrawGraph
Returns:	Blast parameters by reference.
Description:	Function containing all calculations for blast parameters for waves diffracting over the sides.

FreeAirBurstParameters.cpp

Functions:

Name:	CFreeAirBurstParameters::ArrivalTime
Called By:	CFaceFront::ABurst, CFaceFront::FABurst, CFaceFront::Mach, CFaceRear::MachRoof, CFaceRear::MachSides, CFaceRear::REGRoof, CFaceRear::REGSide, CFaceSideRoof::FABurst, CFaceSideRoof::FABurst2, CFaceSideRoof::MachRoof, CFaceSideRoof::MachSides, CFaceSideRoof::REGRoof, CFaceSideRoof::REGSides
Returns:	Arrival time.
Description:	Calculates arrival time based on scaled distance for a free air burst.

Name:	CFreeAirBurstParameters::DragCoefficient
Called By:	CFaceFront::ABurst, CFaceFront::FABurst, CFaceFront::Mach, CFaceRear::MachRoof, CFaceRear::MachSides, CFaceRear::REGRoof, CFaceRear::REGSide, CFaceSideRoof::FABurst, CFaceSideRoof::FABurst2, CFaceSideRoof::MachRoof, CFaceSideRoof::MachSides, CFaceSideRoof::REGRoof, CFaceSideRoof::REGSides
Returns:	Drag coefficient.
Description:	Calculates the drag coefficient based on dynamic pressure and the loaded face.

Name:	CFreeAirBurstParameters::DynamicPressure
Called By:	CFaceFront::ABurst, CFaceFront::FABurst, CFaceFront::Mach, CFaceFront::SBurst, CFaceRear::MachRoof, CFaceRear::MachSides, CFaceRear::REGRoof, CFaceRear::REGSide, CFaceRear::SBurst, CFaceSideRoof::FABurst, CFaceSideRoof::FABurst2, CFaceSideRoof::MachRoof, CFaceSideRoof::MachSides, CFaceSideRoof::REGRoof, CFaceSideRoof::REGSides, CFaceSideRoof::SBurst
Returns:	Dynamic pressure.

Description: Calculates dynamic pressure based on incident (side-on) pressure.

Name: **CFreeAirBurstParameters::IncidentOverpressure**

Called By: CFaceFront::ABurst, CFaceFront::FABurst,
 CFaceFront::Mach, CFaceRear::MachRoof, CFaceRear::MachSides,
 CFaceRear::REGRoof,
 CFaceRear::REGSide, CFaceSideRoof::FABurst,
 CFaceSideRoof::FABurst2, CFaceSideRoof::MachRoof,
 CFaceSideRoof::MachSides, CFaceSideRoof::REGRoof,
 CFaceSideRoof::REGSides, CMach::MachFormMachZone

Returns: Incident (side-on) overpressure.

Description: Calculates incident (side-on) overpressure based on scaled distance for a free air burst.

Name: **CFreeAirBurstParameters::IncidentUnderpressure**

Called By: CFaceFront::ABurst, CFaceFront::FABurst,
 CFaceFront::Mach, CFaceRear::MachRoof, CFaceRear::MachSides,
 CFaceRear::REGRoof,
 CFaceRear::REGSide, CFaceSideRoof::FABurst,
 CFaceSideRoof::FABurst2, CFaceSideRoof::MachRoof,
 CFaceSideRoof::MachSides, CFaceSideRoof::REGRoof,
 CFaceSideRoof::REGSides

Returns: Incident (side-on) underpressure.

Description: Calculates incident (side-on) underpressure based on scaled distance for a free air burst.

Name: **CFreeAirBurstParameters::NegativeIncidentImpulse**

Called By: CFaceFront::ABurst, CFaceFront::FABurst,
 CFaceFront::Mach, CFaceRear::MachRoof, CFaceRear::MachSides,
 CFaceRear::REGRoof,
 CFaceRear::REGSide, CFaceSideRoof::FABurst,
 CFaceSideRoof::FABurst2, CFaceSideRoof::MachRoof,
 CFaceSideRoof::MachSides, CFaceSideRoof::REGRoof,
 CFaceSideRoof::REGSides

Returns: Incident (side-on) negative impulse.

Description: Calculates incident (side-on) negative impulse based on scaled distance and scaled mass of explosive for a free air burst.

Name: **CFreeAirBurstParameters::NegativeReflectedImpulse**

Called By: CFaceFront::ABurst, CFaceFront::FABurst, CFaceFront::Mach
 Returns: Negative reflected (face-on) impulse.
 Description: Calculates negative reflected (face-on) impulse based on scaled distance and scaled mass of explosive for a free air burst.

Name: **CFreeAirBurstParameters::NegativeReflectedPressure**
 Called By: CFaceFront::ABurst, CFaceFront::FABurst, CFaceFront::Mach
 Returns: Negative reflected (face-on) pressure.
 Description: Calculates negative reflected (face-on) pressure based on scaled distance for a free air burst.

Name: **CFreeAirBurstParameters::PositiveDuration**
 Called By: CFaceFront::ABurst, CFaceFront::FABurst,
 CFaceFront::Mach, CFaceRear::MachRoof, CFaceRear::MachSides,
 CFaceRear::REGRoof,
 CFaceRear::REGSide, CFaceSideRoof::FABurst,
 CFaceSideRoof::FABurst2, CFaceSideRoof::MachRoof,
 CFaceSideRoof::MachSides, CFaceSideRoof::REGRoof,
 CFaceSideRoof::REGSides
 Returns: Positive duration.
 Description: Calculates positive duration based on scaled distance and scaled mass of explosive for a free air burst.

Name: **CFreeAirBurstParameters::PositiveIncidentImpulse**
 Called By: CFaceFront::ABurst, CFaceFront::FABurst,
 CFaceFront::Mach, CFaceRear::MachRoof, CFaceRear::MachSides,
 CFaceRear::REGRoof,
 CFaceRear::REGSide, CFaceSideRoof::FABurst,
 CFaceSideRoof::FABurst2, CFaceSideRoof::MachRoof,
 CFaceSideRoof::MachSides, CFaceSideRoof::REGRoof,
 CFaceSideRoof::REGSides
 Returns: Incident (side-on) positive impulse.
 Description: Calculates incident (side-on) positive impulse based on scaled distance and scaled mass of explosive for a free air burst.

Name: **CFreeAirBurstParameters::ShockFrontVelocity**
 Called By: CFaceFront::ABurst, CFaceFront::FABurst, CFaceFront::Mach
 Returns: Shock front velocity.
 Description: Calculates shock front velocity based on scaled distance for a free air

burst.

Name: **CFreeAirBurstParameters::Zfromposlr**
 Called By: CFaceFront::ABurst, CFaceFront::FABurst, CFaceFront::Mach
 Returns: Scaled distance.
 Description: Calculates the scaled distance corresponding to a positive normally reflected impulse for a free air burst.

Name: **CFreeAirBurstParameters::ZfromposPr**
 Called By: CFaceFront::ABurst, CFaceFront::FABurst, CFaceFront::Mach
 Returns: Scaled distance.
 Description: Calculates the scaled distance corresponding to a positive normally reflected pressure for a free air burst.

GraphDlg.cpp

Called By: CBlastView::OnBlastPressuresPressureTimeProfile

Functions:

Name: **CGraphDlg::AssignLimit**
 Called By: CGraphDlg::OnBnClickedOk
 Returns: Assigns values to member variables representing limits.
 Description: Assigns the structure's edges as limits based on the face selected within which the analysis point must be chosen.

Name: **CGraphDlg::enableORdisableLoc**
 Called By: CGraphDlg::OnBnClickedFace1, CGraphDlg::OnBnClickedFace2, CGraphDlg::OnBnClickedFace3, CGraphDlg::OnBnClickedFace4, CGraphDlg::OnBnClickedFace5
 Returns: Sends message to enable or disable specific windows.
 Description: Enables and disables certain coordinate boxes of the analysis point based on the face selected.

Name: **CGraphDlg::LimitCheck**
 Called By: CGraphDlg::OnBnClickedOk
 Returns: True or false.
 Description: Checks the coordinates of the entered analysis point against the limits assigned in CGraphDlg::AssignLimit.

Name: **CGraphDlg::OnBnClickedCancel**

Called By: *Cancel button
 Returns: Receives message that Cancel has been clicked.
 Description: Closes dialog box and returns to
 CBlastView::OnBlastpressuresPressureTimeProfile.

Name: **CGraphDlg::OnBnClickedFace1**
 Called By: *Clicking Face 1
 Returns: Receives message that Face1 has been clicked.
 Description: Defines which coordinate boxes of the analysis point should be disabled and enabled.

Name: **CGraphDlg::OnBnClickedFace2**
 Called By: *Clicking Face 2
 Returns: Receives message that Face2 has been clicked.
 Description: Defines which coordinate boxes of the analysis point should be disabled and enabled.

Name: **CGraphDlg::OnBnClickedFace3**
 Called By: *Clicking Face 3
 Returns: Receives message that Face3 has been clicked.
 Description: Defines which coordinate boxes of the analysis point should be disabled and enabled.

Name: **CGraphDlg::OnBnClickedFace4**
 Called By: *Clicking Face 4
 Returns: Receives message that Face4 has been clicked.
 Description: Defines which coordinate boxes of the analysis point should be disabled and enabled.

Name: **CGraphDlg::OnBnClickedFace5**
 Called By: *Clicking Face 5
 Returns: Receives message that Face5 has been clicked.
 Description: Defines which coordinate boxes of the analysis point should be disabled and enabled.

Name: **CGraphDlg::OnBnClickedOk**
 Called By: *OK button
 Returns: Receives message that OK has been clicked.
 Description: Based on the return of CGraphDlg::LimitCheck, closes the dialog box and returns to
 CBlastView::OnBlastpressuresPressureTimeProfile or sends an

error message asking the user to change the input.

* Built-in function

LoadParamDlg.cpp

Called By: CBlastView::OnLoadingBlastparameters

Functions:

Name: **CLoadParamDlg::ClearNotEnabled**

Called By: CLoadParamDlg::OnBnClickedExbuiltin,
CLoadParamDlg::OnBnClickedExcustom

Returns: Sends message to clear text in the windows.

Description: Clears data out of disables input boxes.

Name: **CLoadParamDlg::CustomEnergy**

Called By: CLoadParamDlg::OnBnClickedOk

Returns: Assigns a value to member variable representing equivalent mass.

Description: Calculates the TNT equivalent mass if a custom explosive is selected.

Name: **CLoadParamDlg::enableORdisableCustom**

Called By: CLoadParamDlg::OnBnClickedExbuiltin,
CLoadParamDlg::OnBnClickedExcustom

Returns: Sends message regarding the accessibility of the window.

Description: Enables or disables the custom explosive boxes.

Name: **CLoadParamDlg::MassEnergy**

Called By: CLoadParamDlg::OnBnClickedOk

Returns: Assigns a value to member variable representing equivalent mass.

Description: Calculates the TNT equivalent mass if a built-in explosive is selected.

Name: **CLoadParamDlg::OnBnClickedCancel**

Called By: *Cancel button

Returns: Receives message that Cancel has been clicked.

Description: Closes dialog box and returns to
CBlastView::OnLoadingBlastparameters.

Name: **CLoadParamDlg::OnBnClickedExbuiltin**

Called By: *Clicking Built-in Explosive

Returns: Receives message that Built-in Explosive has been clicked.
 Description: Defines which custom explosive parameters are disabled and which built-in parameters are enabled.

Name: **CLoadParamDlg::OnBnClickedExcustom**
 Called By: *Clicking Custom Explosive
 Returns: Receives message that Custom Explosive has been clicked.
 Description: Defines which custom explosive parameters are enabled and which built-in parameters are disabled.

Name: **CLoadParamDlg::OnBnClickedOk**
 Called By: *OK button
 Returns: Receives message that Ok has been clicked.
 Description: Based on whether Custom Explosive is clicked or Built-in Explosive is clicked; calls either CLoadParamDlg::MassEnergy or CLoadParamDlg::CustomEnergy, closes the dialog box, and returns to CBlastView::OnLoadingBlastparameters.

* Built-in function

Mach.cpp

Function:

Name: **CMach::HeightofTriplePoint**
 Called By: CMach::MachFormMachZone
 Returns: Height of the triple point.
 Description: Calculates the height of the triple point based on scaled charge height, scaled distance, and scaled mass of explosive.

Name: **CMach::MachAngle**
 Called By: CMach::MachFormMachZone
 Returns: Minimum angle of incidence necessary for mach stem formation.
 Description: Calculates the angle of incidence necessary for mach stem formation based on incident pressure.

Name: **CMach::MachFormMachZone**
 Called By: CBlastView::DrawGraph,
 CFaceRear::AirBurstRoof, CFaceRear::AirBurstSides,
 CFaceSideRoof::RREFRoof, CFaceSideRoof::Sides
 Returns: Mach stem parameters by reference.

Description:	Determines if the analysis point is in a mach stem.
--------------	---

Name:	CMach::MachImpulse
Called By:	CBlastView::DrawGraph, CFaceRear::MachRoof, CFaceRear::MachSides, CFaceSideRoof::MachRoof, CFaceSideRoof::MachSides
Returns:	Incident impulse.
Description:	Calculates the impulse from a mach wave based on scaled height of charge, angle of incidence, and scaled mass of explosive.

Name:	CMach::MachPressure
Called By:	CBlastView::DrawGraph, CFaceRear::MachRoof, CFaceRear::MachSides, CFaceSideRoof::MachRoof, CFaceSideRoof::MachSides
Returns:	Incident mach pressure.
Description:	Calculates the pressure from a mach wave based on scaled height of charge and angle of incidence.

Name:	CMach::Zfromincidentimpulse
Called By:	CBlastView::DrawGraph, CFaceRear::MachRoof, CFaceRear::MachSides, CFaceSideRoof::MachRoof, CFaceSideRoof::MachSides
Returns:	Scaled distance.
Description:	Calculates the scaled distance corresponding to a positive incident impulse.

Name:	CMach::Zfromincidentpressure
Called By:	CBlastView::DrawGraph, CFaceRear::MachRoof, CFaceRear::MachSides, CFaceRear::REGRoof, CFaceRear::REGSide, CFaceSideRoof::MachRoof, CFaceSideRoof::MachSides, CFaceSideRoof::REGRoof, CFaceSideRoof::REGSides
Returns:	Scaled distance.
Description:	Calculates the scaled distance corresponding to a positive incident pressure.

SurfaceBurstParameters.cpp

Functions:

Name:	CSurfaceBurstParameters::ArrivalTime
Called By:	CFaceFront::SBurst, CFaceRear::SBurst, CFaceSideRoof::SBurst
Returns:	Arrival time.
Description:	Calculates arrival time based on scaled distance for a surface burst.

Name:	CSurfaceBurstParameters::DragCoefficient
Called By:	CFaceFront::SBurst, CFaceRear::SBurst, CFaceSideRoof::SBurst
Returns:	Drag coefficient.
Description:	Calculates the drag coefficient based on dynamic pressure and the loaded face.

Name:	CSurfaceBurstParameters::IncidentOverpressure
Called By:	CFaceFront::SBurst, CFaceRear::SBurst, CFaceSideRoof::SBurst
Returns:	Incident (side-on) overpressure.
Description:	Calculates incident (side-on) overpressure based on scaled distance for a surface burst.

Name:	CSurfaceBurstParameters::IncidentUnderpressure
Called By:	CFaceFront::SBurst, CFaceRear::SBurst, CFaceSideRoof::SBurst
Returns:	Incident (side-on) underpressure.
Description:	Calculates incident (side-on) underpressure based on scaled distance for a surface burst.

Name:	CSurfaceBurstParameters::NegativeIncidentImpulse
Called By:	CFaceFront::SBurst, CFaceRear::SBurst, CFaceSideRoof::SBurst
Returns:	Incident (side-on) negative impulse.
Description:	Calculates incident (side-on) negative impulse based on scaled distance and scaled mass of explosive for a surface burst.

Name:	CSurfaceBurstParameters::NegativeReflectedImpulse
Called By:	CFaceFront::SBurst
Returns:	Negative reflected (face-on) impulse.
Description:	Calculates negative reflected (face-on) impulse based on scaled distance and scaled mass of explosive for a surface burst.

Name:	CSurfaceBurstParameters::NegativeReflectedPressure
Called By:	CFaceFront::SBurst
Returns:	Negative reflected (face-on) pressure.
Description:	Calculates negative reflected (face-on) pressure based on scaled distance for a surface burst.

Name:	CSurfaceBurstParameters::PositiveDuration
-------	--

Called By: CFaceFront::SBurst, CFaceRear::SBurst, CFaceSideRoof::SBurst
 Returns: Positive duration.
 Description: Calculates positive duration based on scaled distance and scaled mass of explosive for a surface burst.

Name: **CSurfaceBurstParameters::PositiveIncidentImpulse**
 Called By: CFaceFront::SBurst, CFaceRear::SBurst, CFaceSideRoof::SBurst
 Returns: Incident (side-on) positive impulse.
 Description: Calculates incident (side-on) positive impulse based on scaled distance and scaled mass of explosive for a surface burst.

Name: **CSurfaceBurstParameters::ShockFrontVelocity**
 Called By: CFaceFront::SBurst
 Returns: Shock front velocity.
 Description: Calculates shock front velocity based on scaled distance for a surface burst.

Name: **CSurfaceBurstParameters::Zfromposlr**
 Called By: CFaceFront::SBurst
 Returns: Scaled distance.
 Description: Calculates the scaled distance corresponding to a positive normally reflected impulse for a surface burst.

Name: **CSurfaceBurstParameters::ZfromposPr**
 Called By: CFaceFront::SBurst
 Returns: Scaled distance.
 Description: Calculates the scaled distance corresponding to a positive normally reflected pressure for a surface burst.

APPENDIX D SAMPLE PROBLEMS

D.1 Introduction

Sample calculations are outlined here to help the user better understand *VecTor-Blast's* computations.

D.2 Blast Loads From A Surface Burst

D.2.1 Problem

Determine the pressure-time history at the points A, B, and C on the structure shown in Figure D.1. The explosive used is Pentolite 50/50 with a mass of 40 kg.

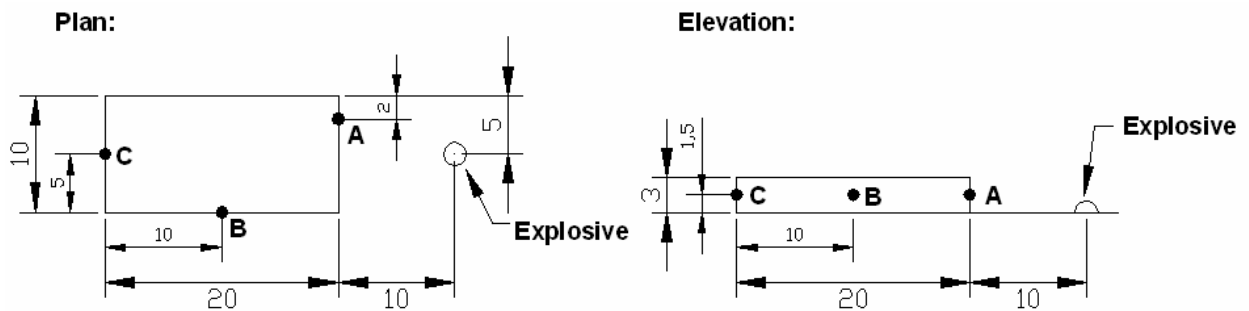


Figure D.1 Structure loaded by a surface burst.

Step 1: Determine the TNT equivalency:

Mass specific energy of Pentolite 50/50: 5110 kJ/mol

Mass specific energy of TNT: 4520 kJ/mol

$$w_{TNT} = \frac{H_{PENT}}{H_{TNT}} w_{PENT} = \left(\frac{5110 \text{ kJ/mol}}{4520 \text{ kJ/mol}} \right) \times (40 \text{ kg}) = 45.22 \text{ kg} = 99.70 \text{ lb}$$

D.2.2 Point A

Step 2: Determine the distance to point A:

$$R = \sqrt{10^2 + 1.5^2 + (5-2)^2} = 10.55 \text{ m}$$

Step 3: Determine the free-field blast parameters from Figure 2.7

a. Scaled Distance:

$$Z = \frac{R}{w^{\frac{1}{3}}} = \frac{10.55 \text{ m}}{(45.22 \text{ kg})^{\frac{1}{3}}} = 2.96 \text{ m/kg}^{\frac{1}{3}} = 7.46 \text{ ft/lb}^{\frac{1}{3}}$$

b. Total Incident Overpressure:

$$P_s^+ = 17.61 \text{ psi} = 121.39 \text{ kPa}$$

c. Angles of Incidence:

$$\beta_{xyz} = \tan^{-1} \left(\frac{\sqrt{(3-1.5)^2 + (5-2)^2}}{(30-20)} \right) = 18.54^\circ$$

$$\beta_{yz} = \tan^{-1} \left(\frac{5-2}{1.5-0} \right) = 63.43^\circ$$

d. Pressure:

$$\text{x-comp: } P_{sx}^+ = 121.39 \times \cos(18.54^\circ) = 115.09 \text{ kPa} = 16.69 \text{ psi}$$

$$\text{y-comp: } P_{sy}^+ = 121.39 \times \sin(18.54^\circ) \times \cos(63.43^\circ) = 17.26 \text{ kPa} = 2.50 \text{ psi}$$

$$\text{z-comp: } P_{sz}^+ = 121.39 \times \sin(18.54^\circ) \times \sin(63.43^\circ) = 34.52 \text{ kPa} = 5.01 \text{ psi}$$

e. Arrival Time:

Scaled Arrival Time:

$$t_a^w = 2.51 \text{ ms/lb}^{\frac{1}{3}}$$

Arrival Time:

$$t_a = 2.51 \text{ ms} / \text{lb}^{\frac{1}{3}} \times (99.07 \text{ lb})^{\frac{1}{3}} = 11.63 \text{ ms}$$

f. Positive Duration:

Scaled Positive Duration:

$$t_0^w = 1.63 \text{ ms} / \text{lb}^{\frac{1}{3}}$$

Positive Duration:

$$t_0^+ = 1.63 \text{ ms} / \text{lb}^{\frac{1}{3}} \times (99.70 \text{ lb})^{\frac{1}{3}} = 7.56 \text{ ms}$$

g. Positive Incident Impulse:

Scaled Positive Impulse:

$$i_s^w = 12.86 \text{ psi} \cdot \text{ms} / \text{lb}^{\frac{1}{3}}$$

Positive Impulse:

$$i_s^+ = 12.86 \text{ psi} \cdot \text{ms} / \text{lb}^{\frac{1}{3}} \times (99.70 \text{ lb})^{\frac{1}{3}} = 59.64 \text{ psi} \cdot \text{ms} = 411.17 \text{ kPa} \cdot \text{ms}$$

x-component:

$$i_{sx}^+ = 411.17 \times \cos(18.54^\circ) = 389.83 \text{ kPa} \cdot \text{ms}$$

y-component:

$$i_{sy}^+ = 411.17 \times \sin(18.54^\circ) \times \cos(63.43^\circ) = 58.48 \text{ kPa} \cdot \text{ms}$$

z-component:

$$i_{sz}^+ = 411.17 \times \sin(18.54^\circ) \times \sin(63.43^\circ) = 116.93 \text{ kPa} \cdot \text{ms}$$

h. Shock Front Velocity

$$U = 1.65 \text{ ft} / \text{ms} = 0.50 \text{ m} / \text{ms}$$

i. Dynamic Pressure from Appendix B.

$$P_{sx}^+ = 16.69 \text{ psi}, q_x = 5.44 \text{ psi} = 37.53 \text{ kPa}$$

$$P_{sy}^+ = 2.50 \text{ psi}, q_y = 0 \text{ psi} = 0 \text{ kPa}$$

$$P_{sz}^+ = 5.01 \text{ psi}, q_z = 0.57 \text{ psi} = 3.94 \text{ kPa}$$

j. Dynamic Pressure Coefficient, C_d (Table 3.4)x-component: $C_d = 1$ y-component: $q = 0 \text{ psi}$, $C_d = 0$ z-component: $q = 0.57 \text{ psi}$, $C_d = -0.4$

Step 4: Determine reflected pressure and impulse

a. Read $C_{r\beta}$ for $P_s^+ = 17.61 \text{ psi}$ and $\beta = 18.54^\circ$ from Figure 2.10

$$C_{r\beta} = 2.74, \quad P_r^+ = C_{r\beta} \times P_s^+ = 2.74 \times 17.61 \text{ psi} = 48.25 = 333.14 \text{ kPa}$$

b. Read i_r^w for $P_s^+ = 17.61 \text{ psi}$ and $\beta = 18.54^\circ$ from Appendix B

$$i_r^w = 20.17 \text{ psi} \cdot \text{ms} / \text{lb}^{\frac{1}{3}}$$

$$i_r^+ = 20.17 \text{ psi} \cdot \text{ms} / \text{lb}^{\frac{1}{3}} \times (99.70 \text{ lb})^{\frac{1}{3}} = 93.54 \text{ psi} \cdot \text{ms} = 644.95 \text{ kPa} \cdot \text{ms}$$

Step 5: Positive Times

a. Fictitious positive duration

x-component:

$$t_{ofx}^+ = \frac{2i_{sx}^+}{P_{sx}^+} = \frac{2 \times 389.83 \text{ kPa} \cdot \text{ms}}{115.09 \text{ kPa}} = 6.77 \text{ ms}$$

y-component:

$$t_{ofy}^+ = \frac{2i_{sy}^+}{P_{sy}^+} = \frac{2 \times 58.47 \text{ kPa} \cdot \text{ms}}{17.26 \text{ kPa}} = 6.77 \text{ ms}$$

z-component:

$$t_{ofz}^+ = \frac{2i_{sz}^+}{P_{sz}^+} = \frac{2 \times 116.93 \text{ kPa} \cdot \text{ms}}{34.52 \text{ kPa}} = 6.77 \text{ ms}$$

b. Clearing Time (x-component only)

$$P_s^+ = 121.39 \text{ kPa} = 17.61 \text{ psi}, \quad C_r = 1.39 \text{ ft} / \text{ms} = 0.42 \text{ m} / \text{ms}$$

(Appendix B)

$$S = 3 < \frac{10}{2} \text{ m}$$

$$G = \frac{10}{2} > 3 \text{ m}, \quad R_c = \frac{S}{G} = \frac{3 \text{ m}}{5 \text{ m}} = 0.6 \text{ m}$$

$$t_c = \frac{4S}{(1 + R_c)C_r} = \frac{(4 \times 3 \text{ m})}{(1 + 0.6) \times 0.42} = 17.86 \text{ ms} > 6.77 \text{ ms}$$

clearing does not occur

c. Reflected Positive Duration (x-component only)

$$t_r = \frac{2i_r^+}{P_r^+} = \frac{2 \times 644.95 \text{ kPa} \cdot \text{ms}}{333.14 \text{ kPa}} = 3.87 \text{ ms}$$

Step 6: Negative Pressures and Impulse (y and z components) from Fig 2.7

a. Negative Pressure

$$Z = 7.46 \text{ ft} / \text{lb}^{\frac{1}{3}}, \quad P_s^- = 2.20 \text{ psi} = 15.18 \text{ kPa}$$

y-component:

$$P_{sy}^- = 15.18 \times \sin(18.54^\circ) \times \cos(63.43^\circ) = 2.16 \text{ kPa}$$

z-component:

$$P_{sz}^- = 15.18 \times \sin(18.54^\circ) \times \sin(63.43^\circ) = 4.32 \text{ kPa}$$

b. Negative Impulse

$$Z = 7.46 \text{ ft} / \text{lb}^{\frac{1}{3}}, \quad i_s^{w-} = 12.54 \text{ psi} \cdot \text{ms} / \text{lb}^{\frac{1}{3}}$$

$$i_s^- = 58.15 \text{ psi} \cdot \text{ms} = 400.95 \text{ kPa} \cdot \text{ms}$$

y-component:

$$i_{sy}^- = 400.95 \times \sin(18.54^\circ) \times \cos(63.43^\circ) = 57.02 \text{ kPa} \cdot \text{ms}$$

z-component:

$$i_{sz}^- = 400.95 \times \sin(18.54^\circ) \times \sin(63.43^\circ) = 114.02 \text{ kPa} \cdot \text{ms}$$

Step 7: Negative Reflected Pressure and Impulse (x-component)

a. Read value of Z corresponding to P_r^+ and i_r^+ on Fig 2.7

$$P_r^+ = 48.25 \text{ psi}, Z(P_r^+) = 7.62 \text{ ft/lb}^{\frac{1}{3}} = 3.03 \text{ m/kg}^{\frac{1}{3}}$$

$$i_r^+ = 93.54 \text{ psi} \cdot \text{ms}, Z(i_r^+) = 11.66 \text{ ft/lb}^{\frac{1}{3}} = 4.63 \text{ m/kg}^{\frac{1}{3}}$$

b. Read values of P_m^- and i_m^- from Z values found in part a on Fig 2.7

$$P_m^-(7.63) = 3.75 \text{ psi} = 25.89 \text{ kPa}$$

$$i_m^{w-}(11.66) = 13.23 \text{ psi} \cdot \text{ms/lb}^{\frac{1}{3}}$$

$$i_m^- = 61.38 \text{ psi} \cdot \text{ms} = 423.21 \text{ kPa} \cdot \text{ms}$$

Step 8: Negative Durations

a. Fictitious Negative Duration

x-component:

$$t_{fnegx} = \frac{2i_m^-}{P_m^-} = \frac{2(423.21 \text{ kPa} \cdot \text{ms})}{25.89 \text{ kPa}} = 32.69 \text{ ms}$$

y-component:

$$t_{fnegy} = \frac{2i_{sy}^-}{P_{sy}^-} = \frac{2(57.02 \text{ kPa} \cdot \text{ms})}{2.16 \text{ kPa}} = 52.79 \text{ ms}$$

z-component:

$$t_{fnegz} = \frac{2i_{sz}^-}{P_{sz}^-} = \frac{2(114.02 \text{ kPa} \cdot \text{ms})}{4.32 \text{ kPa}} = 52.79 \text{ ms}$$

b. Negative Rise Times

x-component:

$$t_{risex} = 0.27t_{fnegx} = 0.27 \times 32.69 \text{ ms} = 8.83 \text{ ms}$$

y-component:

$$t_{risey} = 0.27t_{fnegy} = 0.27 \times 52.79 \text{ ms} = 14.25 \text{ ms}$$

z-component:

$$t_{risez} = 0.27t_{fnegz} = 0.27 \times 52.79 \text{ ms} = 14.25 \text{ ms}$$

Step 9: Construct Pressure-Time Curve

Note: The reflected pressure time curve is used since the reflecting

impulse is less than the impulse produced by the clearing time.

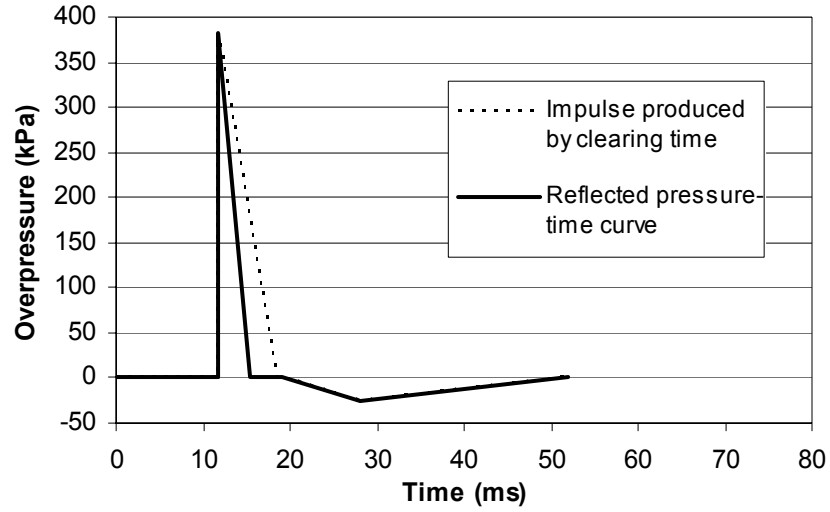


Figure D.2 Example 1.1 x-component pressure-time history at point A.

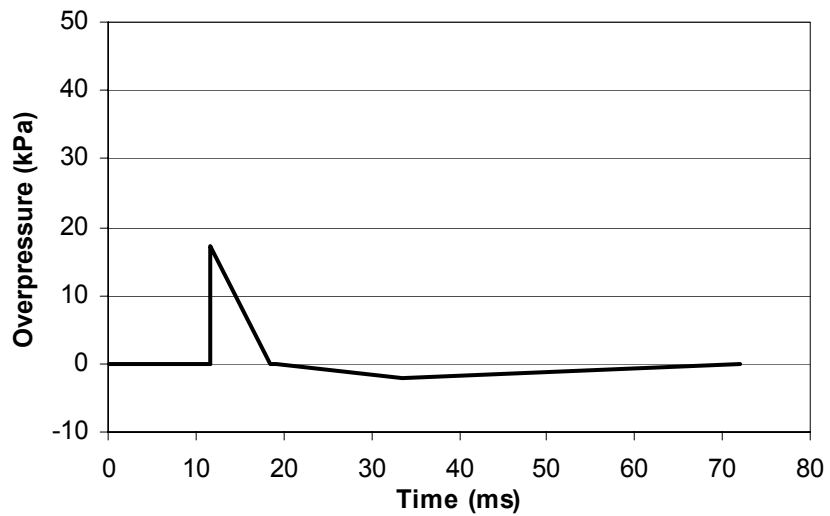


Figure D.3 Example 1.1 y-component pressure-time history at point A.

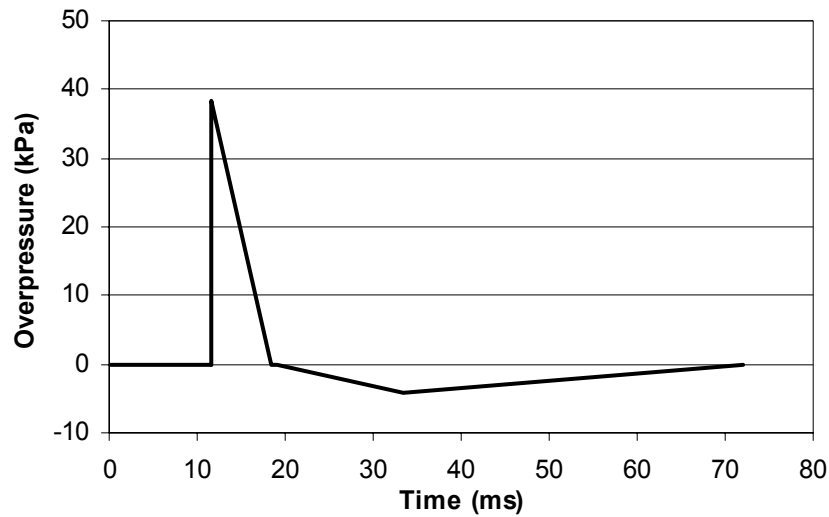


Figure D.4 Example 1.1 z-component pressure-time history at point A.

D.2.3 Point B

Only the z-component will have a pressure-time history since the overpressure is acting normal to point B.

Wave diffracts around one corner. Therefore the diffraction factor, $D_f=1.0$.

Step 10: Determine the distance to point B:

Method 1:

(All distances in m.)

$$X_b = 30 \quad X_{AP} = 10 \quad X' = 20$$

$$Z_b = 5 \quad Z_{AP} = 10 \quad Z'' = 10$$

$$Y_b = 0 \quad Y_{AP} = 1.5$$

$$\frac{X_b - X_{AP}}{X' - X_{AP}} = \frac{Y_b - Y'}{Y_b - Y_{AP}}$$

$$Y' = Y_b - \frac{(X_b - X')(Y_b - Y_{AP})}{(X_b - X_{AP})} = 0 - \frac{(30 - 20)(0 - 1.5)}{(30 - 10)}$$

$$Y' = 0.75$$

$$R_1 = \sqrt{((X_b - X')^2 + (Y_b - Y')^2 + (Z_b - Z')^2)}$$

$$R_1 = \sqrt{((30 - 20)^2 + (0 - 0.75)^2 + (5 - 10)^2)}$$

$$R_1 = 11.21$$

$$R_2 = \sqrt{((X' - X_{AP})^2 + (Y' - Y_{AP})^2 + (Z' - Z_{AP})^2)}$$

$$R_2 = \sqrt{((20 - 10)^2 + (0.75 - 1.5)^2 + (10 - 5)^2)}$$

$$R_2 = 10.03$$

$$R = R_1 + R_2 = 21.24$$

Method 2:

(All distances in m.)

$$X_b = 30 \quad X_{AP} = 10 \quad X' = 20$$

$$Z_b = 5 \quad Z_{AP} = 10 \quad Z' = 10$$

$$Y_b = 0 \quad Y_{AP} = 1.5 \quad Y' = 1.5$$

$$R_1 = \sqrt{((X_b - X')^2 + (Y_b - Y')^2 + (Z_b - Z')^2)}$$

$$R_1 = \sqrt{((30 - 20)^2 + (0 - 1.5)^2 + (5 - 10)^2)}$$

$$R_1 = 11.28$$

$$R_2 = \sqrt{((X' - X_{AP})^2 + (Y' - Y_{AP})^2 + (Z' - Z_{AP})^2)}$$

$$R_2 = \sqrt{((20 - 10)^2 + (1.5 - 1.5)^2 + (10 - 10)^2)}$$

$$R_2 = 10$$

$$R = R_1 + R_2 = 21.28$$

The shortest distance is therefore 21.24 m.

Step 11: Determine the free-field blast parameters from Figure 2.7

a. Scaled Distance:

$$Z = \frac{R}{w^{\frac{1}{3}}} = \frac{21.24 \text{ m}}{(45.22 \text{ kg})^{\frac{1}{3}}} = 5.96 \text{ m/kg}^{\frac{1}{3}} = 15.02 \text{ ft/lb}^{\frac{1}{3}}$$

b. Total Incident Overpressure:

$$P_s^+ = 4.66 \text{ psi} \times D_f = 4.66 \text{ psi} \times 1.0 = 4.66 \text{ psi} = 32.15 \text{ kPa}$$

c. Arrival Time:

Scaled Arrival Time:

$$t_a^w = 7.18 \text{ ms/lb}^{\frac{1}{3}}$$

Arrival Time:

$$t_a = 7.18 \text{ ms/lb}^{\frac{1}{3}} \times (99.07 \text{ lb})^{\frac{1}{3}} = 33.24 \text{ ms}$$

f. Positive Duration:

Scaled Positive Duration:

$$t_0^w = 2.88 \text{ ms/lb}^{\frac{1}{3}}$$

Positive Duration:

$$t_0^+ = 2.88 \text{ ms/lb}^{\frac{1}{3}} \times (99.70 \text{ lb})^{\frac{1}{3}} = 13.36 \text{ ms}$$

g. Positive Incident Impulse:

$$i_s^w = 6.77 \text{ psi} \cdot \text{ms/lb}^{\frac{1}{3}} \times D_f = 6.77 \text{ psi} \cdot \text{ms/lb}^{\frac{1}{3}} \times 1 = 6.77 \text{ psi} \cdot \text{ms/lb}^{\frac{1}{3}}$$

$$i_s^+ = 6.77 \text{ psi} \cdot \text{ms/lb}^{\frac{1}{3}} \times (99.70 \text{ lb})^{\frac{1}{3}} = 31.41 \text{ psi} \cdot \text{ms} = 216.55 \text{ kPa} \cdot \text{ms}$$

h. Total Incident Underpressure:

$$P_s^- = 1.04 \text{ psi} = 7.17 \text{ kPa}$$

i. Negative Incident Impulse:

$$i_s^{w-} = 6.09 \text{ psi} \cdot \text{ms/lb}^{\frac{1}{3}}$$

$$i_s^- = 6.09 \text{ psi} \cdot \text{ms/lb}^{\frac{1}{3}} \times (99.70 \text{ lb})^{\frac{1}{3}} = 28.16 \text{ psi} \cdot \text{ms} = 194.13 \text{ kPa} \cdot \text{ms}$$

j. Dynamic Pressure from Appendix B.

$$P_s^+ = 4.66 \text{ psi}, \quad q = 0.45 \text{ psi} = 3.43 \text{ kPa}$$

k. Dynamic Pressure Coefficient, C_d (Table 3.4)

$$q = 0.45 \text{ psi} \quad C_d = -0.4$$

Step 12: Positive Durations

a. Fictitious positive duration

$$t_{of}^+ = \frac{2i_s^+}{P_s^+} = \frac{2 \times 216.55 \text{ kPa} \cdot \text{ms}}{32.15 \text{ kPa}} = 13.47 \text{ ms}$$

Step 13: Negative Durations

a. Fictitious Negative Duration

$$t_{fneg} = \frac{2i_s^-}{P_s^-} = \frac{2(194.13 \text{ kPa} \cdot \text{ms})}{7.17 \text{ kPa}} = 54.15 \text{ ms}$$

b. Negative Rise Times

$$t_{fneg} = 0.27t_{fneg} = 0.27 \times 54.15 \text{ ms} = 14.62 \text{ ms}$$

Step 14: Construct Pressure-Time Curve

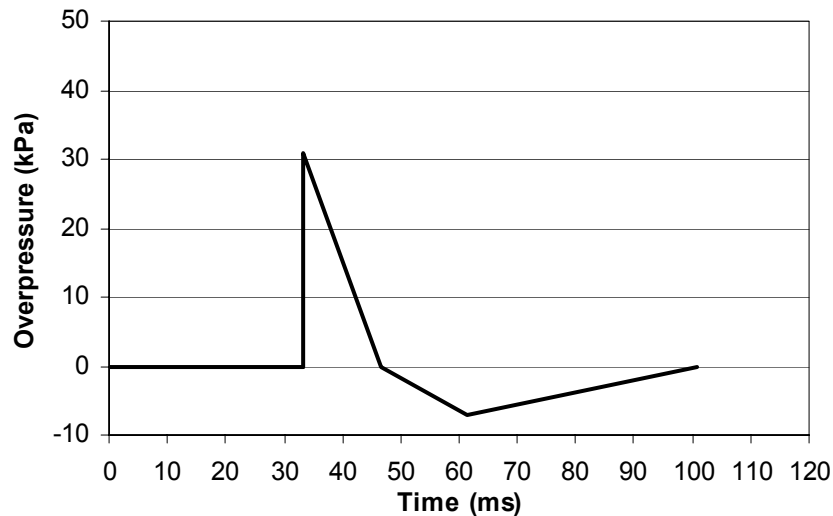


Figure D.5 Example 1.1 pressure-time history at point B

D.2.4 Point C

Only the x-component will have a pressure-time history.

Three diffracted wave rays will combine on the rear wall at point C; one coming over the roof, and the other two coming around from both sides.

R_N will represent the wave ray coming over the north side in plan view.

R_R will represent the wave ray coming over the roof.

R_S will represent the wave ray coming over the south side in plan view.

The blast wave diffracts around two corners.

Therefore the diffraction factor, $D_f = 0.35^n = 0.35^2 = 0.1225$.

Step 15: Determine the distances to point B:

a. R_S

Method 1:

(All distances in m.)

$$X_b = 30 \quad X_{AP} = 0 \quad X' = 20 \quad X'' = 0$$

$$Z_b = 5 \quad Z_{AP} = 5 \quad Z' = 10 \quad Z'' = 10$$

$$Y_b = 0 \quad Y_{AP} = 1.5 \quad Y'' = 1.5$$

$$\frac{X_b - X_{AP}}{X' - X_{AP}} = \frac{Y_b - Y'}{Y_b - Y_{AP}}$$

$$Y' = Y_b - \frac{(X_b - X')(Y_b - Y_{AP})}{(X_b - X_{AP})} = 0 - \frac{(30 - 20)(0 - 1.5)}{(30 - 0)}$$

$$Y' = 0.5$$

$$R_1 = \sqrt{((X_b - X')^2 + (Y_b - Y')^2 + (Z_b - Z')^2)}$$

$$R_1 = \sqrt{((30 - 20)^2 + (0 - 0.5)^2 + (5 - 10)^2)}$$

$$R_1 = 11.19$$

$$R_2 = \sqrt{((X' - X'')^2 + (Y' - Y'')^2 + (Z' - Z'')^2)}$$

$$R_2 = \sqrt{((20-0)^2 + (0.5-1.5)^2 + (10-10)^2)}$$

$$R_2 = 20.03$$

$$R_3 = \sqrt{((X''-X_{AP})^2 + (Y''-Y_{AP})^2 + (Z''-Z_{AP})^2)}$$

$$R_3 = \sqrt{((0-0)^2 + (1.5-1.5)^2 + (10-5)^2)}$$

$$R_3 = 5.00$$

$$R = R_1 + R_2 + R_3 = 36.22$$

Method 2:

(All distances in m.)

$$X_b = 30 \quad X_{AP} = 0 \quad X' = 20 \quad X'' = 0$$

$$Z_b = 5 \quad Z_{AP} = 5 \quad Z' = 10 \quad Z'' = 10$$

$$Y_b = 0 \quad Y_{AP} = 1.5 \quad Y' = 1.5 \quad Y'' = 1.5$$

$$R_1 = \sqrt{((X_b - X')^2 + (Y_b - Y')^2 + (Z_b - Z')^2)}$$

$$R_1 = \sqrt{((30-20)^2 + (0-1.5)^2 + (5-10)^2)}$$

$$R_1 = 11.28$$

$$R_2 = \sqrt{((X' - X'')^2 + (Y' - Y'')^2 + (Z' - Z'')^2)}$$

$$R_2 = \sqrt{((20-0)^2 + (1.5-1.5)^2 + (10-10)^2)}$$

$$R_2 = 20.00$$

$$R_3 = \sqrt{((X'' - X_{AP})^2 + (Y'' - Y_{AP})^2 + (Z'' - Z_{AP})^2)}$$

$$R_3 = \sqrt{((0-0)^2 + (1.5-1.5)^2 + (10-5)^2)}$$

$$R_3 = 5.00$$

$$R = R_1 + R_2 + R_3 = 36.28$$

The shortest distance is therefore 36.22 m.

b. R_R

Method 1:

(All distances in m.)

$$X_b = 30 \quad X_{AP} = 0 \quad X' = 20 \quad X'' = 0$$

$$Z_b = 5 \quad Z_{AP} = 5 \quad Z'' = 5$$

$$Y_b = 0 \quad Y_{AP} = 1.5 \quad Y' = 3 \quad Y'' = 3$$

$$\frac{X_b - X_{AP}}{X' - X_{AP}} = \frac{Z_b - Z'}{Z_b - Z_{AP}}$$

$$Z' = Z_b - \frac{(X_b - X')(Z_b - Z_{AP})}{(X_b - X_{AP})} = 5 - \frac{(30 - 20)(5 - 5)}{(30 - 0)}$$

$$Z' = 5$$

$$R_1 = \sqrt{((X_b - X')^2 + (Y_b - Y')^2 + (Z_b - Z')^2)}$$

$$R_1 = \sqrt{((30 - 20)^2 + (0 - 3)^2 + (5 - 5)^2)}$$

$$R_1 = 10.44$$

$$R_2 = \sqrt{((X' - X'')^2 + (Y' - Y'')^2 + (Z' - Z'')^2)}$$

$$R_2 = \sqrt{((20 - 0)^2 + (3 - 3)^2 + (5 - 5)^2)}$$

$$R_2 = 20.00$$

$$R_3 = \sqrt{((X'' - X_{AP})^2 + (Y'' - Y_{AP})^2 + (Z'' - Z_{AP})^2)}$$

$$R_3 = \sqrt{((0 - 0)^2 + (3 - 1.5)^2 + (5 - 5)^2)}$$

$$R_3 = 1.5$$

$$R = R_1 + R_2 + R_3 = 31.94$$

Method 2:

(All distances in m.)

$$X_b = 30 \quad X_{AP} = 0 \quad X' = 20 \quad X'' = 0$$

$$Z_b = 5 \quad Z_{AP} = 5 \quad Z' = 5 \quad Z'' = 5$$

$$Y_b = 0 \quad Y_{AP} = 1.5 \quad Y' = 3 \quad Y'' = 3$$

$$R_1 = \sqrt{((X_b - X')^2 + (Y_b - Y')^2 + (Z_b - Z')^2)}$$

$$R_1 = \sqrt{((30 - 20)^2 + (0 - 3)^2 + (5 - 5)^2)}$$

$$R_1 = 10.44$$

$$R_2 = \sqrt{((X' - X'')^2 + (Y' - Y'')^2 + (Z' - Z'')^2)}$$

$$R_2 = \sqrt{((20 - 0)^2 + (3 - 3)^2 + (5 - 5)^2)}$$

$$R_2 = 20.00$$

$$R_3 = \sqrt{((X'' - X_{AP})^2 + (Y'' - Y_{AP})^2 + (Z'' - Z_{AP})^2)}$$

$$R_3 = \sqrt{((0 - 0)^2 + (3 - 1.5)^2 + (5 - 5)^2)}$$

$$R_3 = 1.5$$

$$R = R_1 + R_2 + R_3 = 31.94$$

The shortest distance is therefore 31.94 m.

c. R_N

Method 1:

$$X_b = 30 \quad X_{AP} = 0 \quad X' = 20 \quad X'' = 0$$

$$Z_b = 5 \quad Z_{AP} = 5 \quad Z' = 0 \quad Z'' = 0$$

$$Y_b = 0 \quad Y_{AP} = 1.5 \quad Y'' = 1.5$$

$$\frac{X_b - X_{AP}}{X' - X_{AP}} = \frac{Y_b - Y'}{Y_b - Y_{AP}}$$

$$Y' = Y_b - \frac{(X_b - X')(Y_b - Y_{AP})}{(X_b - X_{AP})} = 0 - \frac{(30 - 20)(0 - 1.5)}{(30 - 0)}$$

$$Y' = 0.5$$

$$R_1 = \sqrt{((X_b - X')^2 + (Y_b - Y')^2 + (Z_b - Z')^2)}$$

$$R_1 = \sqrt{((30 - 20)^2 + (0 - 0.5)^2 + (5 - 0)^2)}$$

$$R_1 = 11.19$$

$$R_2 = \sqrt{((X' - X'')^2 + (Y' - Y'')^2 + (Z' - Z'')^2)}$$

$$R_2 = \sqrt{((20 - 0)^2 + (0.5 - 1.5)^2 + (0 - 0)^2)}$$

$$R_2 = 20.03$$

$$R_3 = \sqrt{((X'' - X_{AP})^2 + (Y'' - Y_{AP})^2 + (Z'' - Z_{AP})^2)}$$

$$R_3 = \sqrt{((0 - 0)^2 + (1.5 - 1.5)^2 + (0 - 5)^2)}$$

$$R_3 = 5.00$$

$$R = R_1 + R_2 + R_3 = 36.22$$

Method 2:

(All distances in m.)

$$X_b = 30 \quad X_{AP} = 0 \quad X' = 20 \quad X'' = 0$$

$$Z_b = 5 \quad Z_{AP} = 5 \quad Z' = 0 \quad Z'' = 0$$

$$Y_b = 0 \quad Y_{AP} = 1.5 \quad Y' = 1.5 \quad Y'' = 1.5$$

$$R_1 = \sqrt{((X_b - X')^2 + (Y_b - Y')^2 + (Z_b - Z')^2)}$$

$$R_1 = \sqrt{((30 - 20)^2 + (0 - 1.5)^2 + (5 - 0)^2)}$$

$$R_1 = 11.28$$

$$R_2 = \sqrt{((X' - X'')^2 + (Y' - Y'')^2 + (Z' - Z'')^2)}$$

$$R_2 = \sqrt{((20 - 0)^2 + (1.5 - 1.5)^2 + (10 - 10)^2)}$$

$$R_2 = 20.00$$

$$R_3 = \sqrt{\left((X'' - X_{AP})^2 + (Y'' - Y_{AP})^2 + (Z'' - Z_{AP})^2\right)}$$

$$R_3 = \sqrt{\left((0 - 0)^2 + (1.5 - 1.5)^2 + (0 - 5)^2\right)}$$

$$R_3 = 5.00$$

$$R = R_1 + R_2 + R_3 = 36.28$$

The shortest distance is therefore 36.22 m.

Step 16: Determine the free-field blast parameters from figure 2.7

a. Scaled Distance:

R_S:

$$Z_S = \frac{R}{w^{\frac{1}{3}}} = \frac{36.22 \text{ m}}{(45.22 \text{ kg})^{\frac{1}{3}}} = 10.17 \text{ m/kg}^{\frac{1}{3}} = 25.63 \text{ ft/lb}^{\frac{1}{3}}$$

R_R:

$$Z_R = \frac{R}{w^{\frac{1}{3}}} = \frac{31.94 \text{ m}}{(45.22 \text{ kg})^{\frac{1}{3}}} = 8.97 \text{ m/kg}^{\frac{1}{3}} = 22.60 \text{ ft/lb}^{\frac{1}{3}}$$

R_N:

$$Z_N = \frac{R}{w^{\frac{1}{3}}} = \frac{36.22 \text{ m}}{(45.22 \text{ kg})^{\frac{1}{3}}} = 10.17 \text{ m/kg}^{\frac{1}{3}} = 25.63 \text{ ft/lb}^{\frac{1}{3}}$$

b. Total Incident Overpressure:

R_S:

$$P_{sS}^+ = 2.09 \text{ psi} \times D_f = 2.09 \text{ psi} \times 0.1225 = 0.26 \text{ psi} = 1.76 \text{ kPa}$$

R_R:

$$P_{sR}^+ = 2.49 \text{ psi} \times D_f = 2.49 \text{ psi} \times 0.1225 = 0.31 \text{ psi} = 2.11 \text{ kPa}$$

R_N:

$$P_{sN}^+ = 2.09 \text{ psi} \times D_f = 2.09 \text{ psi} \times 0.1225 = 0.26 \text{ psi} = 1.76 \text{ kPa}$$

c. Arrival Time:

Scaled Arrival Time:

R_S:

$$t_{aS}^w = 16.90 \text{ ms} / \text{lb}^{\frac{1}{3}}$$

R_R:

$$t_{aR}^w = 14.21 \text{ ms} / \text{lb}^{\frac{1}{3}}$$

R_N:

$$t_{aN}^w = 16.90 \text{ ms} / \text{lb}^{\frac{1}{3}}$$

Arrival Time:

R_S:

$$t_a = 16.90 \text{ ms} / \text{lb}^{\frac{1}{3}} \times (99.07 \text{ lb})^{\frac{1}{3}} = 78.36 \text{ ms}$$

R_R:

$$t_a = 14.21 \text{ ms} / \text{lb}^{\frac{1}{3}} \times (99.07 \text{ lb})^{\frac{1}{3}} = 65.88 \text{ ms}$$

R_N:

$$t_a = 16.90 \text{ ms} / \text{lb}^{\frac{1}{3}} \times (99.07 \text{ lb})^{\frac{1}{3}} = 78.36 \text{ ms}$$

f. Positive Duration:

R_S:

$$t_{oS}^w = 3.64 \text{ ms} / \text{lb}^{\frac{1}{3}}$$

$$t_{oS}^+ = 3.64 \text{ ms} / \text{lb}^{\frac{1}{3}} \times (99.70 \text{ lb})^{\frac{1}{3}} = 16.87 \text{ ms}$$

R_R:

$$t_{oR}^w = 3.50 \text{ ms} / \text{lb}^{\frac{1}{3}}$$

$$t_{oR}^+ = 3.50 \text{ ms} / \text{lb}^{\frac{1}{3}} \times (99.70 \text{ lb})^{\frac{1}{3}} = 16.21 \text{ ms}$$

R_N:

$$t_{oN}^w = 3.64 \text{ ms} / \text{lb}^{\frac{1}{3}}$$

$$t_{oN}^+ = 3.64 \text{ ms} / \text{lb}^{\frac{1}{3}} \times (99.70 \text{ lb})^{\frac{1}{3}} = 16.87 \text{ ms}$$

g. Positive Incident Impulse:

Scaled Positive Impulse:

 R_S :

$$i_{sS}^w = 3.76 \text{ psi} \cdot \text{ms} / \text{lb}^{\frac{1}{3}} \times D_f = 3.76 \text{ psi} \cdot \text{ms} / \text{lb}^{\frac{1}{3}} \times 0.1225$$

$$i_{sS}^w = 0.46 \text{ psi} \cdot \text{ms} / \text{lb}^{\frac{1}{3}}$$

$$i_{sS}^+ = 0.46 \text{ psi} \cdot \text{ms} / \text{lb}^{\frac{1}{3}} \times (99.70 \text{ lb})^{\frac{1}{3}} = 2.14 \text{ psi} \cdot \text{ms} = 14.74 \text{ kPa} \cdot \text{ms}$$

 R_R :

$$i_{sR}^w = 4.30 \text{ psi} \cdot \text{ms} / \text{lb}^{\frac{1}{3}} \times D_f = 4.30 \text{ psi} \cdot \text{ms} / \text{lb}^{\frac{1}{3}} \times 0.1225$$

$$i_{sR}^w = 0.53 \text{ psi} \cdot \text{ms} / \text{lb}^{\frac{1}{3}}$$

$$i_{sR}^+ = 0.53 \text{ psi} \cdot \text{ms} / \text{lb}^{\frac{1}{3}} \times (99.70 \text{ lb})^{\frac{1}{3}} = 2.44 \text{ psi} \cdot \text{ms} = 16.83 \text{ kPa} \cdot \text{ms}$$

 R_N :

$$i_{sN}^w = 3.76 \text{ psi} \cdot \text{ms} / \text{lb}^{\frac{1}{3}} \times D_f = 3.76 \text{ psi} \cdot \text{ms} / \text{lb}^{\frac{1}{3}} \times 0.1225$$

$$i_{sN}^w = 0.46 \text{ psi} \cdot \text{ms} / \text{lb}^{\frac{1}{3}}$$

$$i_{sN}^+ = 0.46 \text{ psi} \cdot \text{ms} / \text{lb}^{\frac{1}{3}} \times (99.70 \text{ lb})^{\frac{1}{3}} = 2.14 \text{ psi} \cdot \text{ms} = 14.74 \text{ kPa} \cdot \text{ms}$$

h. Total Incident Underpressure:

 R_S :

$$P_{sS}^- = 0 \text{ psi} = 0 \text{ kPa}$$

 R_R :

$$P_{sR}^- = 0 \text{ psi} = 0 \text{ kPa}$$

 R_N :

$$P_{sN}^- = 0 \text{ psi} = 0 \text{ kPa}$$

i. Negative Incident Impulse:

R_S:

$$i_{sS}^{w-} = 3.76 \text{ psi} \cdot \text{ms} / \text{lb}^{\frac{1}{3}} \times D_f = 3.76 \text{ psi} \cdot \text{ms} / \text{lb}^{\frac{1}{3}} \times 0.1225$$

$$i_{sS}^{w-} = 0.46 \text{ psi} \cdot \text{ms} / \text{lb}^{\frac{1}{3}}$$

$$i_{sS}^- = 0.46 \text{ psi} \cdot \text{ms} / \text{lb}^{\frac{1}{3}} \times (99.70 \text{ lb})^{\frac{1}{3}} = 2.14 \text{ psi} \cdot \text{ms} = 14.74 \text{ kPa} \cdot \text{ms}$$

R_R:

$$i_{sR}^{w-} = 4.30 \text{ psi} \cdot \text{ms} / \text{lb}^{\frac{1}{3}} \times D_f = 4.30 \text{ psi} \cdot \text{ms} / \text{lb}^{\frac{1}{3}} \times 0.1225$$

$$i_{sR}^{w-} = 0.53 \text{ psi} \cdot \text{ms} / \text{lb}^{\frac{1}{3}}$$

$$i_{sR}^- = 0.53 \text{ psi} \cdot \text{ms} / \text{lb}^{\frac{1}{3}} \times (99.70 \text{ lb})^{\frac{1}{3}} = 2.44 \text{ psi} \cdot \text{ms} = 16.83 \text{ kPa} \cdot \text{ms}$$

R_N:

$$i_{sN}^{w-} = 3.76 \text{ psi} \cdot \text{ms} / \text{lb}^{\frac{1}{3}} \times D_f = 3.76 \text{ psi} \cdot \text{ms} / \text{lb}^{\frac{1}{3}} \times 0.1225$$

$$i_{sN}^{w-} = 0.46 \text{ psi} \cdot \text{ms} / \text{lb}^{\frac{1}{3}}$$

$$i_{sN}^- = 0.46 \text{ psi} \cdot \text{ms} / \text{lb}^{\frac{1}{3}} \times (99.70 \text{ lb})^{\frac{1}{3}} = 2.14 \text{ psi} \cdot \text{ms} = 14.74 \text{ kPa} \cdot \text{ms}$$

j. Dynamic Pressure from Appendix B.

R_S:

$$P_{sS}^+ = 0.26 \text{ psi}, q = 0 \text{ psi} = 0 \text{ kPa}$$

R_R:

$$P_{sR}^+ = 0.31 \text{ psi}, q = 0 \text{ psi} = 0 \text{ kPa}$$

R_N:

$$P_{sN}^+ = 0.26 \text{ psi}, q = 0 \text{ psi} = 0 \text{ kPa}$$

k. Dynamic Pressure Coefficient, C_d (Table 3.4)

R_S:

$$q = 0 \text{ psi} \quad C_d = 0$$

R_R:

$$q = 0 \text{ psi} \quad C_d = 0$$

R_N :

$$q = 0 \text{ psi} \quad C_d = 0$$

Step 17: Positive Durations

a. Fictitious positive duration

R_S :

$$t_{ofS}^+ = \frac{2i_{sS}^+}{P_{sS}^+} = \frac{2 \times 14.74 \text{ kPa} \cdot \text{ms}}{1.76 \text{ kPa}} = 16.72 \text{ ms}$$

R_R :

$$t_{ofR}^+ = \frac{2i_{sR}^+}{P_{sR}^+} = \frac{2 \times 16.3 \text{ kPa} \cdot \text{ms}}{2.11 \text{ kPa}} = 15.98 \text{ ms}$$

R_N :

$$t_{ofS}^+ = \frac{2i_{sN}^+}{P_{sN}^+} = \frac{2 \times 14.74 \text{ kPa} \cdot \text{ms}}{1.76 \text{ kPa}} = 16.72 \text{ ms}$$

Step 18: Negative Durations

a. Fictitious Negative Duration

R_S :

$$t_{fnegS} = \frac{2i_{sS}^-}{P_{sS}^-}, \quad P_{sS}^- = 0, \quad \therefore t_{fnegS} = 0 \text{ ms}$$

R_R :

$$t_{fnegR} = \frac{2i_{sR}^-}{P_{sR}^-}, \quad P_{sR}^- = 0, \quad \therefore t_{fnegR} = 0 \text{ ms}$$

R_N :

$$t_{fnegN} = \frac{2i_{sN}^-}{P_{sN}^-}, \quad P_{sN}^- = 0, \quad \therefore t_{fnegN} = 0 \text{ ms}$$

b. Negative Rise Times

R_S :

$$t_{riseS} = 0.27t_{fneg} = 0.27 \times 0 \text{ ms} = 0 \text{ ms}$$

R_R :

$$t_{riseR} = 0.27t_{fneg} = 0.27 \times 0 \text{ ms} = 0 \text{ ms}$$

R_N :

$$t_{riseN} = 0.27t_{fneg} = 0.27 \times 0 \text{ ms} = 0 \text{ ms}$$

Step 19: Construct Pressure-Time Curve

Note: The individual pressure-time curves, shown first, are superimposed to create the final pressure time curve.

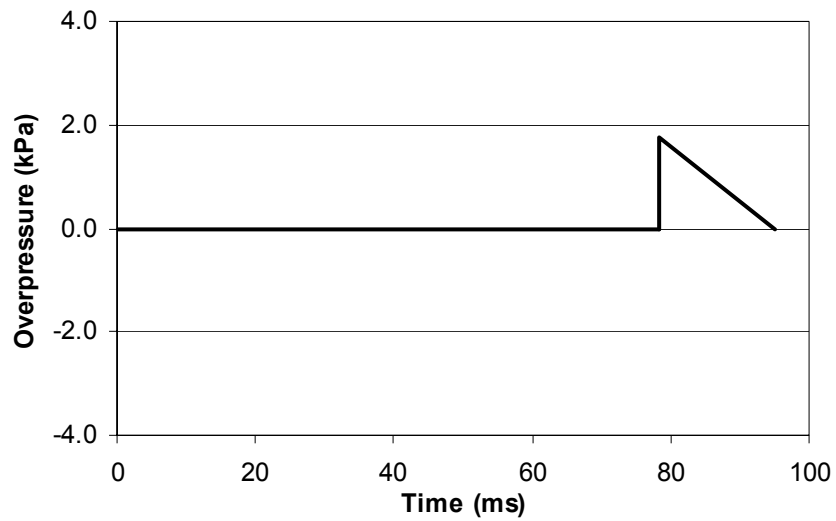


Figure D.6 Example 1.1 pressure time history from R_S .

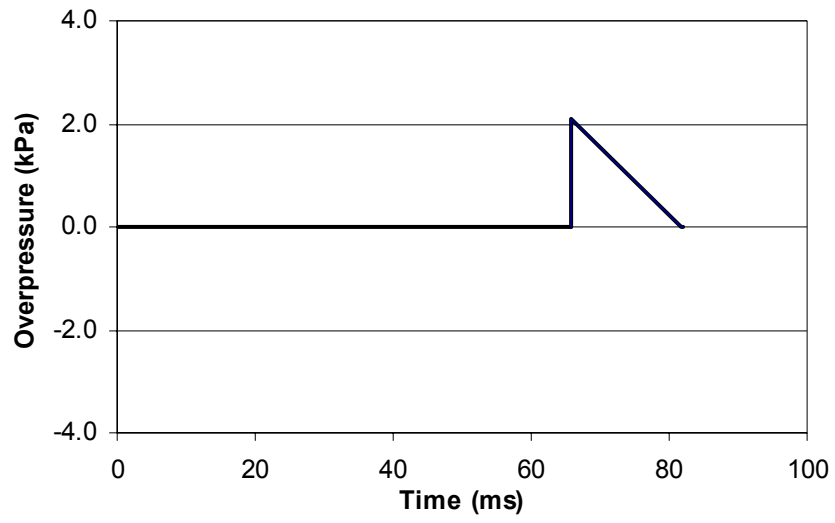


Figure D.7 Example 1.1 pressure time history from R_R .

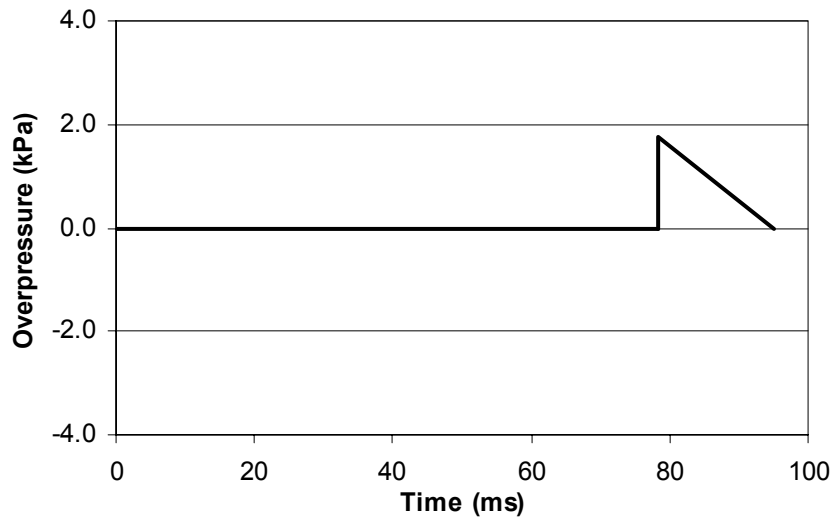


Figure D.8 Example 1.1 pressure time history from R_N .

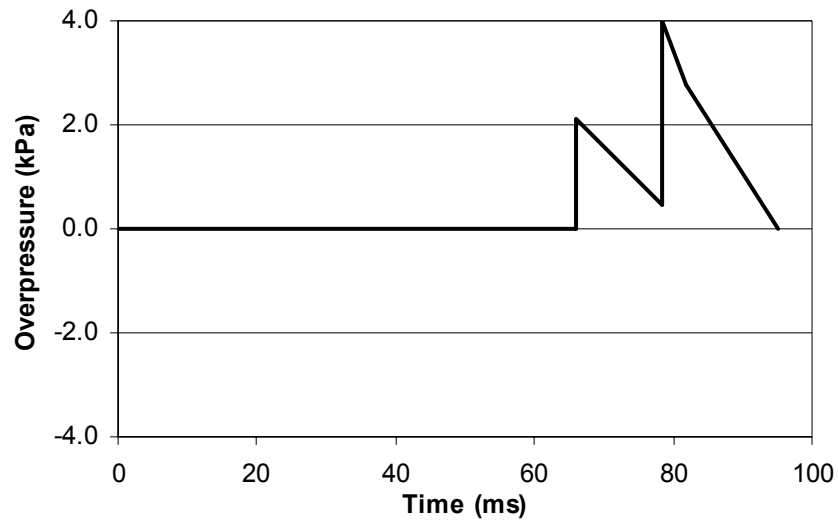


Figure D.9 Example 1.1 pressure-time history at point C.

D.3 Blast Loads From An Air Burst

D.3.1 Problem

Determine the pressure-time history at the point A on the structure shown in Figure D.10. The explosive used is Lead Azide with a mass of 50 kg.

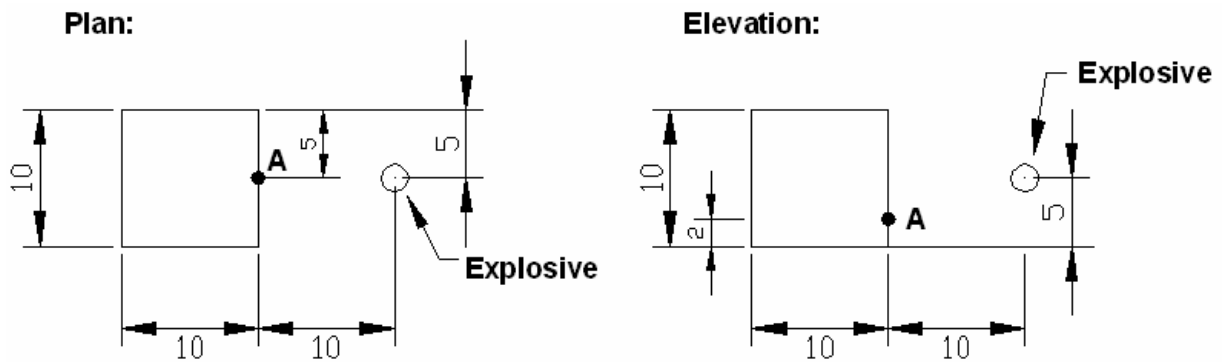


Figure D.10 Structure loaded by an air burst.

D.3.2 Point A

Step 1: Determine the angle made with the base of the structure, the distance to the base of the structure:

$$\beta_1 = \tan^{-1}\left(\frac{20 \text{ m} - 10 \text{ m}}{5 \text{ m}}\right) = 63.43^\circ$$

$$R = \sqrt{(20 - 10)^2 + (5 - 0)^2 + (5 - 5)^2} = 11.18 \text{ m}$$

Step 2: Determine the TNT equivalency:

Mass specific energy of Lead Azide: 1540 kJ/mol

Mass specific energy of TNT: 4520 kJ/mol

$$w_{TNT} = \frac{H_{LEAD}}{H_{TNT}} w_{LEAD} = \left(\frac{1540 \text{ kJ/mol}}{4520 \text{ kJ/mol}}\right) \times (50 \text{ kg}) = 17.04 \text{ kg} = 37.56 \text{ lb}$$

$$Z = \frac{R}{w^{\frac{1}{3}}} = \frac{11.18 \text{ m}}{(17.04 \text{ kg})^{\frac{1}{3}}} = 4.34 \text{ m/kg}^{\frac{1}{3}} = 10.94 \text{ ft/lb}^{\frac{1}{3}}$$

Step 3: Determine if a mach stem loads point A:

a. Overpressure at the base of the structure from Fig. 2.6

$$P_s^+ = 34.65 \text{ kPa} = 5.03 \text{ psi}$$

b. Determine the minimum angle for Mach stem formation from Fig.

2.9.

$$\varepsilon = \frac{101.35 \text{ kPa}}{34.65 \text{ kPa} + 101.35 \text{ kPa}} = 0.74$$

$$\alpha_{crit} = 49.74^\circ$$

$$\alpha_{crit} < \beta_1$$

Therefore a mach stem forms.

d. Determine the height of the triple point from Appendix B:

$$H_c^w = \frac{5 \text{ m}}{(17.04 \text{ kg})^{\frac{1}{3}}} = 1.94 \text{ m/kg}^{\frac{1}{3}} = 4.90 \text{ ft/lb}^{\frac{1}{3}}$$

$$R_g = 10 \text{ m}$$

$$\therefore H_T^w = 0.813 \text{ ft/lb}^{\frac{1}{3}}$$

$$H_T = 0.813 \text{ ft/lb}^{\frac{1}{3}} \times (37.56 \text{ lb})^{\frac{1}{3}} = 2.72 \text{ ft} = 0.83 \text{ m}$$

$$H_T < 2 \text{ m}$$

Triple point does not reach point A. Mach stem does not load point A.

Step 4: Determine if reflected waves reach point A (See Fig. 3.5):

This is an iterative process.

a. Initial Conditions

$$\alpha_{crit} < \beta_1, \beta_{max} = \beta_1 = 63.43^\circ$$

$$\beta_{min} = 0.06^\circ$$

$$d = \sqrt{(20-10)^2 + (5-5)^2} = 10.00 \text{ m}$$

Iteration 1 begins.

b. Determine the Mach number in Region I:

$$\beta = \frac{\beta_{max} + \beta_{min}}{2} = \frac{63.43^\circ + 0.06^\circ}{2} = 31.75^\circ$$

$$D_{2a} = Y_b \times \tan \beta = (5 \text{ m}) \times \tan(31.75^\circ) = 3.09 \text{ m}$$

$$D_{2b} = d - D_{2a} = 10 \text{ m} - 3.09 \text{ m} = 6.91 \text{ m}$$

$$R_{2a} = \sqrt{Y_b^2 + D_{2a}^2} = \sqrt{5^2 + 3.09^2} = 5.88 \text{ m}$$

$$Z = \frac{5.88 \text{ m}}{(17.04 \text{ kg})^{\frac{1}{3}}} = 2.28 \text{ m/kg}^{\frac{1}{3}} = 5.76 \text{ ft/lb}^{\frac{1}{3}}$$

$$P_s^+ = 136.68 \text{ kPa} = 19.82 \text{ psi}$$

$$M_x = 1 + \frac{6P_s^+}{7 \times (101.35 \text{ kPa})} = 1 + \frac{6 \times (136.68 \text{ kPa})}{7 \times (101.35 \text{ kPa})} = 2.16$$

$$M_1 = \frac{M_x}{\sin \beta} = \frac{2.16}{\sin(31.75^\circ)} = 4.10$$

c. Determine the Mach number in Region II:

$$\phi = \beta - \tan^{-1} \left(\tan \beta \times \frac{(5 + (M_1 \sin \beta)^2)}{(6 \times (M_1 \sin \beta)^2)} \right)$$

$$\phi = 31.75^\circ - \tan^{-1} \left(\tan(31.75^\circ) \times \frac{(5 + (4.10 \times \sin(31.75^\circ))^2)}{(6 \times (4.10 \times \sin(31.75^\circ))^2)} \right)$$

$$\phi = 19.68^\circ$$

$$M_2 = \frac{\sqrt{\frac{(5 + (M_1 \sin \beta)^2)}{(6 \times (M_1 \sin \beta)^2)}}}{\sin(\beta - \phi)} = \frac{\sqrt{\frac{(5 + (4.10 \times \sin(31.75^\circ))^2)}{(6 \times (4.10 \times \sin(31.75^\circ))^2)}}}{\sin(31.75^\circ - 19.68^\circ)}$$

$$M_2 = 2.64$$

d. Determine the angle of deflection:

Iteration 2 begins.

i. Initial Conditions:

$$\min = \beta = 31.75^\circ$$

$$\max = 90^\circ$$

ii. Determine β_2 :

$$\beta_2 = \frac{\max + \min}{2} = \frac{31.75^\circ + 90^\circ}{2} = 60.88^\circ$$

iii. Determine C_1 and C_2 :

$$C_1 = \frac{\tan(\beta_2 - \phi)}{\tan \beta_2} = \frac{\tan(60.88^\circ - 19.68^\circ)}{\tan(60.88^\circ)} = 0.48$$

$$C_2 = \frac{(5 + (M_2 \sin \beta_2)^2)}{(6 \times (M_2 \sin \beta_2)^2)} = \frac{(5 + (2.64 \times \sin(60.88^\circ))^2)}{(6 \times (2.64 \times \sin(60.88^\circ))^2)} = 0.32$$

iv. Compare C_1 and C_2 :

$$C_2 - C_1 = 0.32 - 0.48 = -0.16 \neq 0$$

Repeat steps d.ii to d.iv until $(C_1 - C_2) \approx 0$

Since $(C_2 - C_1) < 0$, $\max = \beta_2 = 60.88^\circ$

v. Value making $(C_1 - C_2) \approx 0$

$$\beta_2 = 40.71^\circ$$

vi. Angle of deflection:

$$\alpha = \beta_2 - \phi = 40.71^\circ - 19.68^\circ = 21.03^\circ$$

e. Check height reached by deflected wave:

$$\text{height} = D_{2b} \tan \alpha = (6.91 \text{ m}) \times \tan(21.03^\circ) = 2.66 \text{ m}$$

$$Y_{AP} - \text{height} = 2 - 2.66 = -0.66 \text{ m} \neq 0$$

Repeat steps b through e until $Y_{AP} - \text{height} \approx 0$

Since $(Y_{AP} - \text{height}) < 0$, $\beta_{\max} = \beta_1 = 31.75^\circ$

Step 5: Values for deflection angle:

$$\beta = 26.58^\circ$$

$$\beta_2 = 32.14^\circ$$

$$\therefore \alpha = 14.94^\circ$$

$$D_{2a} = 2.50 \text{ m}$$

$$D_{2b} = 7.50 \text{ m}$$

Step 6: Determine distances from explosion to ground to AP:

$$R_{2a} = \sqrt{D_{2a}^2 + Y_b^2} = \sqrt{(2.50)^2 + (5)^2} = 5.59 \text{ m}$$

$$R_{2b} = \sqrt{D_{2b}^2 + Y_{AP}^2} = \sqrt{(7.50)^2 + (2)^2} = 7.76 \text{ m}$$

Step 7: Determine the equivalent scaled distance weight and equivalent TNT weight:

$$Z_1 = \frac{R_{2a}}{w_0^{\frac{1}{3}}} = \frac{5.59 \text{ m}}{(17.04 \text{ kg})^{\frac{1}{3}}} = 2.17 \text{ m/kg}^{\frac{1}{3}} = 5.48 \text{ ft/lb}^{\frac{1}{3}}$$

$$P_s^+ = 153.05 \text{ kPa} = 22.20 \text{ psi (Fig 2.6)}$$

$$P_m(P_s^+, \beta) = 443.53 \text{ kPa} = 64.33 \text{ psi (Fig. 2.10)}$$

$$P_r = \sqrt{(P_m)^2 + (P_s^+ \sin \beta)^2} = \sqrt{(443.53)^2 + (153.05 \times \sin(26.58^\circ))^2}$$

$$P_r = 448.79 \text{ kPa}$$

$$Z_2(P_r) = 1.42 \text{ m/kg}^{\frac{1}{3}} = 3.58 \text{ ft/lb}^{\frac{1}{3}} \text{ (Appendix B)}$$

$$w_1 = \left(\frac{R_{2a}}{Z_2} \right)^3 = \left(\frac{5.59 \text{ m}}{1.42 \text{ m/kg}^{\frac{1}{3}}} \right)^3 = 61.23 \text{ kg} = 134.99 \text{ lb}$$

$$Z_3 = \frac{R_{2a} + R_{2b}}{w_1^{\frac{1}{3}}} = \frac{5.59 \text{ m} + 7.76 \text{ m}}{(62.23 \text{ kg})^{\frac{1}{3}}} = 3.37 \text{ m/kg}^{\frac{1}{3}} = 8.51 \text{ ft/lb}^{\frac{1}{3}}$$

Scaled distance for ground reflected wave:

$$Z_r = Z_3 = 3.37 \text{ m/kg}^{\frac{1}{3}} = 8.51 \text{ ft/lb}^{\frac{1}{3}}$$

Step 8: Determine the scaled distance of incident wave:

$$R = \sqrt{(20-10)^2 + (5-2)^2 + (5-5)^2} = 10.44 \text{ m}$$

$$Z_i = \frac{R}{w^{\frac{1}{3}}} = \frac{10.44 \text{ m}}{(17.04 \text{ kg})^{\frac{1}{3}}} = 4.06 \text{ m/kg}^{\frac{1}{3}} = 10.25 \text{ ft/lb}^{\frac{1}{3}}$$

Step 9: Determine the free-field blast parameters from Figure 2.7

i - represents the incident wave

r - represents the ground reflected wave

a. Total Incident Overpressure:

$$i: P_s^+ = 5.70 \text{ psi} = 39.30 \text{ kPa}$$

$$r: P_s^+ = 8.42 \text{ psi} = 58.05 \text{ kPa}$$

c. Angles of Incidence:

$$i: \beta_{xyz} = \tan^{-1} \left(\frac{\sqrt{(5-2)^2 + (5-5)^2}}{(30-20)} \right) = 16.70^\circ$$

$$\beta_{zy} = \tan^{-1} \left(\frac{5-5}{2-5} \right) = 0.00^\circ$$

$$r: \beta_{xyz} = \alpha = 14.94^\circ$$

$$\beta_{zy} = \tan^{-1} \left(\frac{5-5}{2-0} \right) = 0.00^\circ$$

d. Pressure:

i: x-component

$$P_{sx}^+ = 39.30 \times \cos(16.70^\circ) = 37.64 \text{ kPa} = 5.46 \text{ psi}$$

y-component

$$P_{sy}^+ = 39.30 \times \sin(16.70^\circ) \times \cos(0.00^\circ) = 11.29 \text{ kPa} = 1.64 \text{ psi}$$

z-component

$$P_{sz}^+ = 39.30 \times \sin(16.70^\circ) \times \sin(0.00^\circ) = 0 \text{ kPa} = 0 \text{ psi}$$

r: x-component

$$P_{sx}^+ = 58.05 \times \cos(14.94^\circ) = 56.09 \text{ kPa} = 8.13 \text{ psi}$$

y-component

$$P_{sy}^+ = 58.05 \times \sin(14.94^\circ) \times \cos(0.00^\circ) = 14.96 \text{ kPa} = 2.17 \text{ psi}$$

z-component

$$P_{sz}^+ = 58.05 \times \sin(14.94^\circ) \times \sin(0.00^\circ) = 0 \text{ kPa} = 0 \text{ psi}$$

e. Arrival Time:

Scaled Arrival Time:

$$i: t_a^w = 4.88 \text{ ms} / \text{lb}^{\frac{1}{3}}$$

$$r: t_a^w = 3.68 \text{ ms} / \text{lb}^{\frac{1}{3}}$$

Arrival Time:

$$i: t_a = 4.88 \text{ ms/lb}^{\frac{1}{3}} \times (37.56 \text{ lb})^{\frac{1}{3}} = 16.34 \text{ ms}$$

$$r: t_a = 3.68 \text{ ms/lb}^{\frac{1}{3}} \times (134.99 \text{ lb})^{\frac{1}{3}} = 18.88 \text{ ms}$$

f. Positive Duration:

Scaled Positive Duration:

$$i: t_0^w = 2.22 \text{ ms/lb}^{\frac{1}{3}}$$

$$r: t_0^w = 1.94 \text{ ms/lb}^{\frac{1}{3}}$$

Positive Duration:

$$i: t_0^+ = 2.22 \text{ ms/lb}^{\frac{1}{3}} \times (37.56 \text{ lb})^{\frac{1}{3}} = 7.43 \text{ ms}$$

$$r: t_0^+ = 1.94 \text{ ms/lb}^{\frac{1}{3}} \times (134.99 \text{ lb})^{\frac{1}{3}} = 9.96 \text{ ms}$$

g. Positive Incident Impulse:

Scaled Positive Impulse:

$$i: i_s^w = 6.08 \text{ psi} \cdot \text{ms/lb}^{\frac{1}{3}}$$

$$r: i_s^w = 7.28 \text{ psi} \cdot \text{ms/lb}^{\frac{1}{3}}$$

Positive Impulse:

$$i: i_s^+ = 6.08 \text{ psi} \cdot \text{ms/lb}^{\frac{1}{3}} \times (37.56 \text{ lb})^{\frac{1}{3}} = 20.37 \text{ psi} \cdot \text{ms} = 140.43 \text{ kPa} \cdot \text{ms}$$

$$r: i_s^+ = 7.28 \text{ psi} \cdot \text{ms/lb}^{\frac{1}{3}} \times (134.99 \text{ lb})^{\frac{1}{3}} = 37.35 \text{ psi} \cdot \text{ms} = 257.55 \text{ kPa} \cdot \text{ms}$$

i: x-component

$$i_{sx}^+ = 140.43 \times \cos(16.70^\circ) = 37.64 \text{ kPa} = 134.50 \text{ psi}$$

y-component

$$i_{sy}^+ = 140.43 \times \sin(16.70^\circ) \times \cos(0.00^\circ) = 40.35 \text{ kPa} \cdot \text{ms}$$

z-component

$$i_{sz}^+ = 140.43 \times \sin(16.70^\circ) \times \sin(0.00^\circ) = 0 \text{ kPa} \cdot \text{ms}$$

r: x-component

$$i_{sx}^+ = 257.55 \times \cos(14.94^\circ) = 248.85 \text{ kPa} \cdot \text{ms}$$

y-component

$$i_{sy}^+ = 257.55 \times \sin(14.94^\circ) \times \cos(0.00^\circ) = 66.40 \text{ kPa} \cdot \text{ms}$$

z-component

$$i_{sz}^+ = 257.55 \times \sin(14.94^\circ) \times \sin(0.00^\circ) = 0 \text{ kPa} \cdot \text{ms}$$

h. Shock Front Velocity

$$i: U = 1.34 \text{ ft/ms} = 0.41 \text{ m/ms}$$

$$r: U = 1.37 \text{ ft/ms} = 0.42 \text{ m/ms}$$

i. Dynamic Pressure from Appendix B.

$$i: P_{sx}^+ = 5.46 \text{ psi}, q_x = 1.15 \text{ psi} = 7.90 \text{ kPa}$$

$$P_{sy}^+ = 1.64 \text{ psi}, q_y = 0 \text{ psi} = 0 \text{ kPa}$$

$$P_{sz}^+ = 0 \text{ psi}, q_z = 0 \text{ psi} = 0 \text{ kPa}$$

$$r: P_{sx}^+ = 8.13 \text{ psi}, q_x = 1.42 \text{ psi} = 9.77 \text{ kPa}$$

$$P_{sy}^+ = 2.17 \text{ psi}, q_y = 0 \text{ psi} = 0 \text{ kPa}$$

$$P_{sz}^+ = 0 \text{ psi}, q_z = 0 \text{ psi} = 0 \text{ kPa}$$

j. Dynamic Pressure Coefficient, C_d (Table 3.4)

$$i: \text{x-component: } C_d = 1$$

$$\text{y-component: } q = 0 \text{ psi}, C_d = 0$$

$$\text{z-component: } q = 0 \text{ psi}, C_d = 0$$

$$r: \text{x-component: } C_d = 1$$

$$\text{y-component: } q = 0 \text{ psi}, C_d = 0$$

$$\text{z-component: } q = 0 \text{ psi}, C_d = 0$$

Step 10: Determine reflected pressure and impulse

a. i: Read $C_{r\beta}$ for $P_s^+ = 5.46$ psi and $\beta = 16.70^\circ$ from Figure 2.10

$$C_{r\beta} = 2.28, P_r^+ = C_{r\beta} \times P_s^+ = 2.28 \times 5.70 \text{ psi} = 12.99 = 89.58 \text{ kPa}$$

r: Read $C_{r\beta}$ for $P_s^+ = 8.42$ psi and $\beta = 14.94^\circ$ from Figure 2.10

$$C_{r\beta} = 2.40, P_r^+ = C_{r\beta} \times P_s^+ = 2.40 \times 8.42 \text{ psi} = 19.51 = 139.39 \text{ kPa}$$

b. i: Read i_r^w for $P_s^+ = 5.70$ psi and $\beta = 16.70^\circ$ from Appendix B

$$i_r^w = 10.46 \text{ psi} \cdot \text{ms} / \text{lb}^{\frac{1}{3}}$$

$$i_r^+ = 10.46 \text{ psi} \cdot \text{ms} / \text{lb}^{\frac{1}{3}} \times (37.56 \text{ lb})^{\frac{1}{3}} = 35.02 \text{ psi} \cdot \text{ms} = 241.43 \text{ kPa} \cdot \text{ms}$$

r: Read i_r^w for $P_s^+ = 8.42$ psi and $\beta = 14.94^\circ$ from Appendix B

$$i_r^w = 13.14 \text{ psi} \cdot \text{ms} / \text{lb}^{\frac{1}{3}}$$

$$i_r^+ = 13.14 \text{ psi} \cdot \text{ms} / \text{lb}^{\frac{1}{3}} \times (134.99 \text{ lb})^{\frac{1}{3}} = 67.42 \text{ psi} \cdot \text{ms} = 464.85 \text{ kPa} \cdot \text{ms}$$

Step 11: Positive Times

a. Fictitious positive duration

i: x-component

$$t_{ofx}^+ = \frac{2i_{sx}^+}{P_{sx}^+} = \frac{2 \times 134.50 \text{ kPa} \cdot \text{ms}}{37.64 \text{ kPa}} = 7.15 \text{ ms}$$

y-component

$$t_{ofy}^+ = \frac{2i_{sy}^+}{P_{sy}^+} = \frac{2 \times 40.35 \text{ kPa} \cdot \text{ms}}{11.29 \text{ kPa}} = 7.15 \text{ ms}$$

z-component

$$t_{ofz}^+ = 0, \because i_{sz}^+ = 0$$

r: x-component

$$t_{ofx}^+ = \frac{2i_{sx}^+}{P_{sx}^+} = \frac{2 \times 248.85 \text{ kPa} \cdot \text{ms}}{56.08 \text{ kPa}} = 8.88 \text{ ms}$$

y-component

$$t_{ofy}^+ = \frac{2i_{sy}^+}{P_{sy}^+} = \frac{2 \times 66.40 \text{ kPa} \cdot \text{ms}}{14.96 \text{ kPa}} = 8.88 \text{ ms}$$

z-component

$$t_{ofz}^+ = 0, \because i_{sz}^+ = 0$$

b. Clearing Time (x-component only)

$$\text{i: } P_s^+ = 39.30 \text{ kPa} = 5.70 \text{ psi}, C_r = 1.22 \text{ ft/ms} = 0.37 \text{ m/ms}$$

$$\text{r: } P_s^+ = 58.05 \text{ kPa} = 8.42 \text{ psi}, C_r = 1.26 \text{ ft/ms} = 0.38 \text{ m/ms}$$

(Appendix B)

$$\text{i: } S = \frac{10}{2} < 10 \text{ m}$$

$$G = 10 > \frac{10}{2} \text{ m}, R_c = \frac{S}{G} = \frac{5 \text{ m}}{10 \text{ m}} = 0.5 \text{ m}$$

$$t_c = \frac{4S}{(1+R_c)C_r} = \frac{(4 \times 5 \text{ m})}{(1+0.5) \times 0.37} = 35.99 \text{ ms} > 7.43 \text{ ms}$$

clearing does not occur

$$\text{r: } S = \frac{10}{2} < 10 \text{ m}$$

$$G = 10 > \frac{10}{2} \text{ m}, R_c = \frac{S}{G} = \frac{5 \text{ m}}{10 \text{ m}} = 0.5 \text{ m}$$

$$t_c = \frac{4S}{(1+R_c)C_r} = \frac{(4 \times 5 \text{ m})}{(1+0.5) \times 0.38} = 35.09 \text{ ms} > 9.96 \text{ ms}$$

clearing does not occur

c. Reflected Positive Duration (x-component only)

$$\text{i: } t_r = \frac{2i_r^+}{P_r^+} = \frac{2 \times 241.43 \text{ kPa} \cdot \text{ms}}{89.58 \text{ kPa}} = 5.39 \text{ ms}$$

$$\text{r: } t_r = \frac{2i_r^+}{P_r^+} = \frac{2 \times 464.85 \text{ kPa} \cdot \text{ms}}{139.39 \text{ kPa}} = 6.67 \text{ ms}$$

Step 12: Negative Pressures and Impulse (y and z components) from Fig 2.7

a. Negative Pressure

$$i: Z = 10.23 \text{ ft} / \text{lb}^{\frac{1}{3}}, P_s^- = 1.15 \text{ psi} = 7.90 \text{ kPa}$$

y-component:

$$P_{sy}^- = 7.90 \times \sin(16.70^\circ) \times \cos(0.00^\circ) = 2.27 \text{ kPa}$$

z-component:

$$P_{sz}^- = 7.90 \times \sin(16.70^\circ) \times \sin(0.00^\circ) = 0 \text{ kPa}$$

$$r: Z = 8.54 \text{ ft} / \text{lb}^{\frac{1}{3}}, P_s^- = 1.49 \text{ psi} = 10.29 \text{ kPa}$$

y-component:

$$P_{sy}^- = 10.29 \times \sin(14.94^\circ) \times \cos(0.00^\circ) = 2.65 \text{ kPa} \cdot \text{ms}$$

z-component:

$$P_{sz}^- = 10.29 \times \sin(14.94^\circ) \times \sin(0.00^\circ) = 0 \text{ kPa} \cdot \text{ms}$$

b. Negative Impulse

$$i: Z = 10.23 \text{ ft} / \text{lb}^{\frac{1}{3}}, i_s^{w-} = 5.82 \text{ psi} \cdot \text{ms} / \text{lb}^{\frac{1}{3}}$$

$$i_s^- = 19.50 \text{ psi} \cdot \text{ms} = 134.51 \text{ kPa} \cdot \text{ms}$$

y-component:

$$i_{sy}^- = 134.51 \times \sin(16.70^\circ) \times \cos(0.00^\circ) = 38.65 \text{ kPa} \cdot \text{ms}$$

z-component:

$$i_{sz}^- = 134.51 \times \sin(16.70^\circ) \times \sin(0.00^\circ) = 114.02 \text{ kPa} \cdot \text{ms}$$

$$r: Z = 8.54 \text{ ft} / \text{lb}^{\frac{1}{3}}, i_s^{w-} = 6.93 \text{ psi} \cdot \text{ms} / \text{lb}^{\frac{1}{3}}$$

$$i_s^- = 35.57 \text{ psi} \cdot \text{ms} = 245.21 \text{ kPa} \cdot \text{ms}$$

y-component:

$$i_{sy}^- = 400.95 \times \sin(18.54^\circ) \times \cos(63.43^\circ) = 57.02 \text{ kPa} \cdot \text{ms}$$

z-component:

$$i_{sz}^- = 400.95 \times \sin(18.54^\circ) \times \sin(63.43^\circ) = 114.02 \text{ kPa} \cdot \text{ms}$$

Step 13: Negative Reflected Pressure and Impulse (x-component)

a. i: Read value of Z corresponding to P_r^+ and i_r^+ on Fig 2.7

$$P_r^+ = 12.99 \text{ psi}, Z(P_r^+) = 10.81 \text{ ft} / \text{lb}^{\frac{1}{3}} = 4.29 \text{ m} / \text{kg}^{\frac{1}{3}}$$

$$i_r^+ = 35.02 \text{ psi} \cdot \text{ms}, Z(i_r^+) = 13.53 \text{ ft} / \text{lb}^{\frac{1}{3}} = 5.37 \text{ m} / \text{kg}^{\frac{1}{3}}$$

r: Read value of Z corresponding to P_r^+ and i_r^+ on Fig 2.7

$$P_r^+ = 20.21 \text{ psi}, Z(P_r^+) = 8.53 \text{ ft} / \text{lb}^{\frac{1}{3}} = 3.38 \text{ m} / \text{kg}^{\frac{1}{3}}$$

$$i_r^+ = 67.42 \text{ psi} \cdot \text{ms}, Z(i_r^+) = 11.05 \text{ ft} / \text{lb}^{\frac{1}{3}} = 4.38 \text{ m} / \text{kg}^{\frac{1}{3}}$$

b. i: Read values of P_{rn}^- and i_{rn}^- from Z values found in part (a) on Fig 2.7.

$$P_{rn}^-(10.81) = 1.91 \text{ psi} = 13.19 \text{ kPa}$$

$$i_{rn}^{w-}(13.53) = 7.92 \text{ psi} \cdot \text{ms} / \text{lb}^{\frac{1}{3}}$$

$$i_{rn}^- = 26.52 \text{ psi} \cdot \text{ms} = 182.82 \text{ kPa} \cdot \text{ms}$$

r: Read values of P_{rn}^- and i_{rn}^- from Z values found in part a on Fig. 2.7

$$P_{rn}^-(8.53) = 2.49 \text{ psi} = 17.15 \text{ kPa}$$

$$i_{rn}^{w-}(11.05) = 8.23 \text{ psi} \cdot \text{ms} / \text{lb}^{\frac{1}{3}}$$

$$i_{rn}^- = 42.21 \text{ psi} \cdot \text{ms} = 332.41 \text{ kPa} \cdot \text{ms}$$

Step 14: Negative Durations

a. Fictitious Negative Duration

i: x-component:

$$t_{fnegx} = \frac{2i_{rn}^-}{P_{rn}^-} = \frac{2(182.82 \text{ kPa} \cdot \text{ms})}{13.19 \text{ kPa}} = 27.72 \text{ ms}$$

y-component:

$$t_{fnegy} = \frac{2i_{sy}^-}{P_{sy}^-} = \frac{2(38.65 \text{ kPa} \cdot \text{ms})}{2.27 \text{ kPa}} = 34.06 \text{ ms}$$

z-component:

$$t_{fnegz} = 0, \quad i_{sz}^- = 0$$

r: x-component:

$$t_{fnegx} = \frac{2i_{rn}^-}{P_{rn}^-} = \frac{2(332.41 \text{ kPa} \cdot \text{ms})}{17.15 \text{ kPa}} = 38.76 \text{ ms}$$

y-component:

$$t_{fnegy} = \frac{2i_{sy}^-}{P_{sy}^-} = \frac{2(63.20 \text{ kPa} \cdot \text{ms})}{2.65 \text{ kPa}} = 47.67 \text{ ms}$$

z-component:

$$t_{fnegz} = 0, \quad i_{sz}^- = 0$$

b. Negative Rise Times

i: x-component:

$$t_{risex} = 0.27t_{fnegx} = 0.27 \times 27.72 \text{ ms} = 7.48 \text{ ms}$$

y-component:

$$t_{risey} = 0.27t_{fnegy} = 0.27 \times 34.06 \text{ ms} = 9.20 \text{ ms}$$

z-component:

$$t_{risez} = 0.27t_{fnegz} = 0 \text{ ms}$$

r: x-component:

$$t_{risex} = 0.27t_{fnegx} = 0.27 \times 38.76 \text{ ms} = 10.47 \text{ ms}$$

y-component:

$$t_{risey} = 0.27t_{fnegy} = 0.27 \times 47.67 \text{ ms} = 12.87 \text{ ms}$$

z-component:

$$t_{fnegz} = 0, \quad i_{sz}^- = 0$$

Step 15: Construct Pressure-Time Curve

Note: The reflected pressure time curve is used since the reflecting impulse is less than the impulse produced by the clearing time.

Adopting the sign convention shown in Fig. 3.1 not all components are traveling in the same direction. The y-components of the incident and reflected wave are traveling in opposite directions.

The individual pressure-time curves, shown first, are superimposed to create the final pressure time curves.

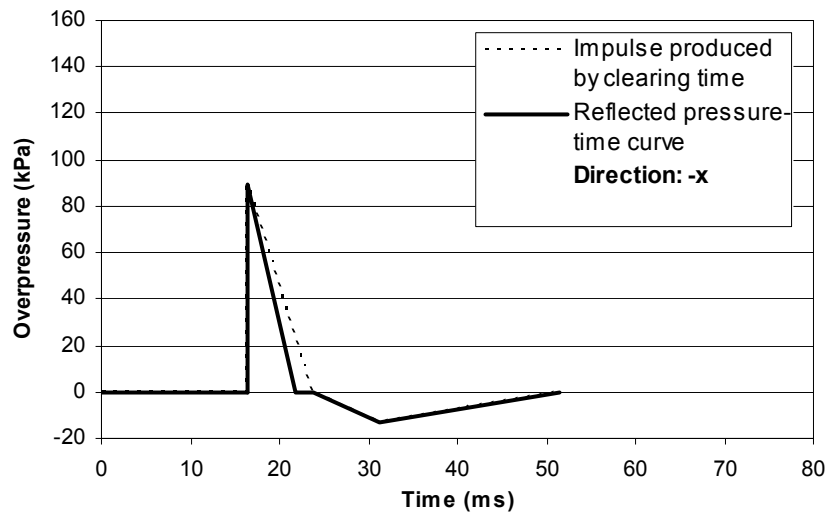


Figure D.11 Example 1.2 x-component pressure-time history at point A (incident wave).

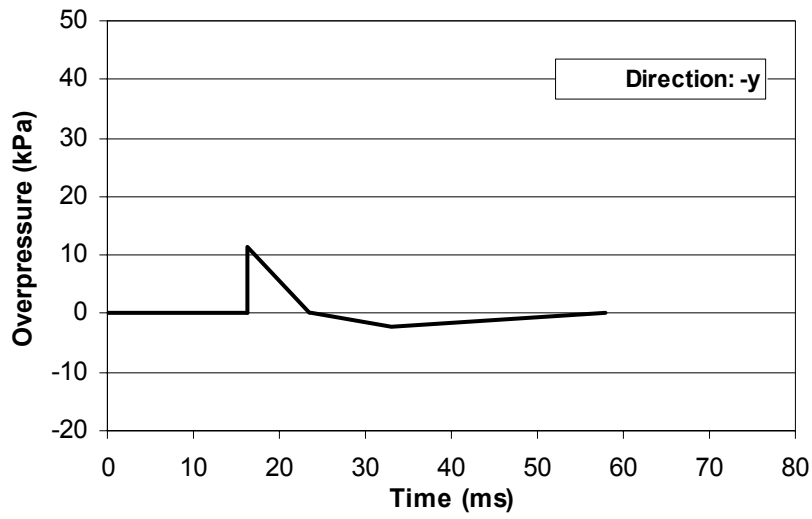


Figure D.12 Example 1.2 y-component pressure-time history at point A (incident wave).

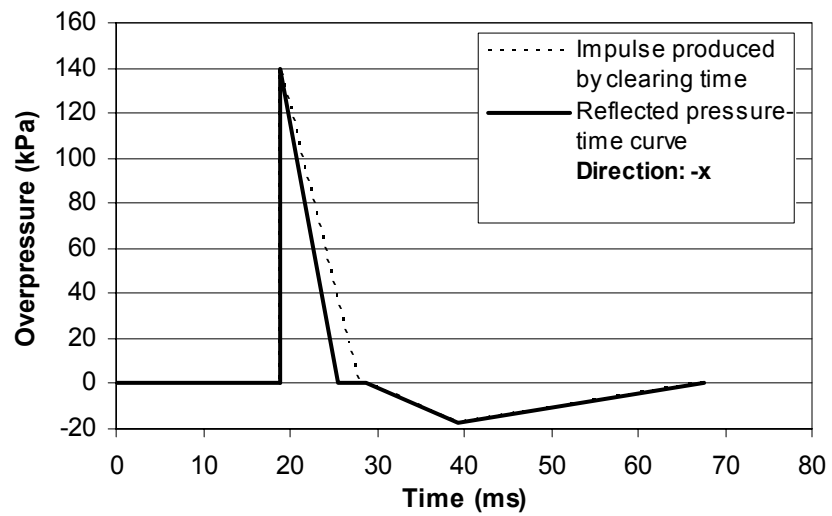


Figure D.13 Example 1.2 x-component pressure-time history at point A (reflected wave).

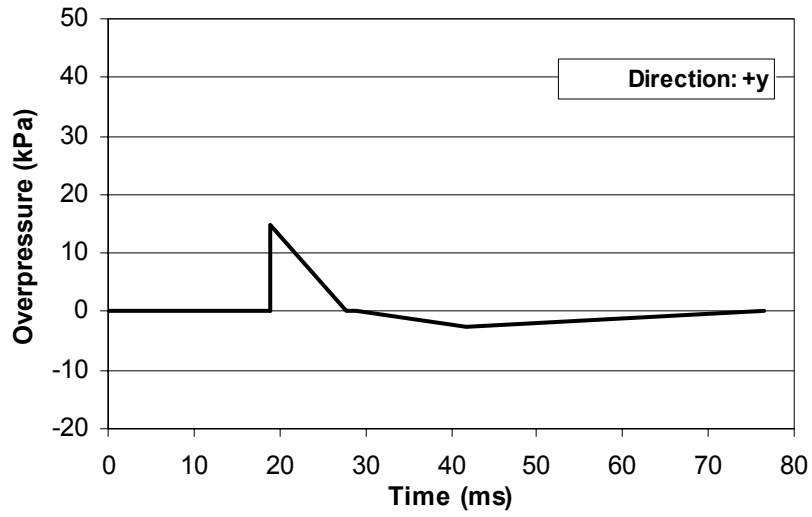


Figure D.14 Example 1.2 y-component pressure-time history at point A (reflected wave).

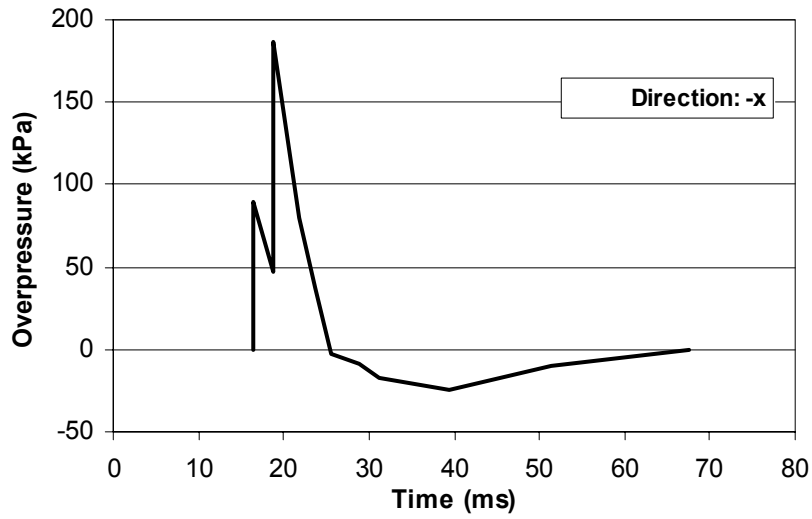


Figure D.15 Example 1.2 combined x-component pressure-time history at point A.

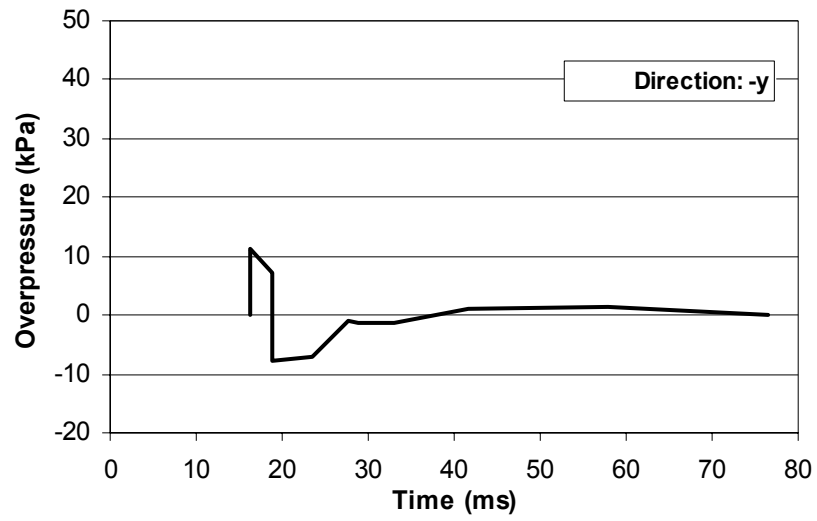


Figure D.16 Example 1.2 combined y-component pressure-time history at point A.

APPENDIX E SAMPLE INPUTS/OUTPUTS

E.1 Introduction

The inputs and outputs pertain to the Armstrong analysis (see Chapter 4) where it was necessary to determine the pressure-time history on the front face of the structure at points along the centreline. The output includes what the *VecTor-Blast* data file would contain.

E.2 Inputs

Explosive: PBX-9407

Mass: 73g

Structure Dimensions (mm):

x: 336

y: 457.5

z: 336

Blast Location (mm):

x: 480

y: 0

z: 168

Points (mm):

x: 336

y: 50, 100, 150, 200, 250, 300, 350, 400, 450

z: 168

E.2 Outputs

Title: Armstrong Analysis Front Face
 Analysis By: Phil Miller
 Job File: Job

BLAST PARAMATERS

Explosive: PBX-9407
 Mass(kg): 0.073
 Equivalent
 TNT Mass(kg): 0.092
 Explosion Type: SURFACE BURST

STRUCTURAL PARAMATERS

	x(m)	y(m)	z(m)
Structure	0.34	0.46	0.34
Blast Location	0.48	0.00	0.17
Analysis Point	0.34	0.05	0.17
Face:	2		
Distance(m):	0.152		
Scaled			
Distance(m/kg ^{1/3}):	0.337		
alphaxyz(deg):	19.15		
alphayz(deg):	-0.00		

WAVE PARAMETERS

	Arrival Time(ms)	Pso+ (kPa)	Dynamic Pres.(kPa)	Drag Coeff	Impulse+ (kPa-msec)
X-Compt	0.03	8379.6	24308.5	1.0	90.4
Y-Compt	0.03	2909.6	5912.7	-0.2	31.4
Z-Compt	0.00	0.0	0.0	0.0	0.0
	Ref. Imp.+ (kPa-msec)	Pr+ (kPa)	Clearing Time(ms)	Fict. Pos. Dur.(ms)	Ref. Pos. Dur.(ms)
X-Compt	1232.7	77001.6	0.04	0.02	0.03
Y-Compt	31.4	2909.6	0.00	0.02	0.02
Z-Compt	0.0	0.0	0.00	0.0	0.00
	Positive Dur.(ms)	Pso- (kPa)	Pr- (kPa)	Neg. Rise Time(ms)	Negative Dur.(ms)
X-Compt	0.04	101.8	25.6	5.26	19.50
Y-Compt	0.04	33.4	33.4	1.46	5.42
Z-Compt	0.00	0.0	0.0	0.00	0.00

Pressure-Time Results

	Pressure (kPa)	Time (ms)
X-Component		
Direction: -x		
	0.000	0.031
	77001.602	0.031
	0.000	0.063
	0.000	0.069
	-25.645	5.333
	0.000	19.564
Y-Component		
Direction: +y		
	0.000	0.031
	1727.033	0.031
	0.000	0.053
	0.000	0.069
	-33.413	1.532
	0.000	5.489
Z-Component		
Direction: -z		
	0.000	0.000

	x(m)	y(m)	z(m)
Analysis Point	0.34	0.10	0.17
Face:	2		
Distance(m):	0.175		
Scaled			
Distance(m/kg ^{1/3}):	0.388		
alphaxyz(deg):	34.78		
alphayz(deg):	-0.00		

WAVE PARAMETERS

	Arrival Time(ms)	Pso+ (kPa)	Dynamic Pres.(kPa)	Drag Coeff.	Impulse+ (kPa-msec)
X-Compt	0.04	5947.0	15155.5	1.0	75.0
Y-Compt	0.04	4129.9	9423.5	-0.2	52.1
Z-Compt	0.00	0.0	0.0	0.0	0.0
	Ref. Imp.+ (kPa-msec)	Pr+ (kPa)	Clearing Time(ms)	Fict. Pos. Dur.(ms)	Ref. Pos. Dur.(ms)
X-Compt	758.4	50552.1	0.04	0.03	0.03
Y-Compt	52.1	4129.9	0.00	0.03	0.03

	Z-Compt	0.0	0.0	0.00	0.00	0.00
		Positive Dur.(ms)	Pso- (kPa)	Pr- (kPa)	Neg. Rise Time(ms)	Negative Dur.(ms)
X-Compt	0.04	100.6	18.7	6.15	22.77	
Y-Compt	0.04	57.7	57.7	1.45	5.35	
Z-Compt	0.00	0.0	0.0	0.00	0.00	

Pressure-Time Results

	Pressure (kPa)	Time (ms)
X-Component		
Direction: -x		
	0.000	0.039
	50552.117	0.039
	0.000	0.069
	0.000	0.079
	-18.686	6.228
	0.000	22.852
Y-Component		
Direction: +y		
	0.000	0.039
	2245.181	0.039
	0.000	0.064
	0.000	0.079
	-57.747	1.525
	0.000	5.434
Z-Component		
Direction: -z		
	0.000	0.000

	x(m)	y(m)	z(m)
Analysis Point	0.34	0.15	0.17
Face:	2		
Distance(m):	0.208		
Scaled Distance(m/kg ^(1/3)):	0.460		
alphaxyz(deg):	46.17		
alphayz(deg):	-0.00		

WAVE PARAMETERS

	Arrival Time(ms)	Pso+ (kPa)	Dynamic Pres.(kPa)	Drag Coeff.	Impulse+ (kPa-msec)
X-Compt	0.05	3871.6	8657.1	1.0	61.1

Y-Compt	0.05	4032.9	9134.5	-0.2	63.6
Z-Compt	0.00	0.0	0.0	0.0	0.0
	Ref. Imp.+ (kPa-msec)	Pr+ (kPa)	Clearing Time(ms)	Fict. Pos. Dur.(ms)	Ref. Pos. Dur.(ms)
X-Compt	458.0	40644.7	0.04	0.03	0.02
Y-Compt	63.6	4032.9	0.00	0.03	0.03
Z-Compt	0.0	0.0	0.00	0.00	0.00
	Positive Dur.(ms)	Pso- (kPa)	Pr- (kPa)	Neg. Rise Time(ms)	Negative Dur.(ms)
X-Compt	0.04	99.6	15.2	6.02	22.31
Y-Compt	0.04	72.2	72.2	1.41	5.23
Z-Compt	0.00	0.0	0.0	0.00	0.00

Pressure-Time Results

	Pressure (kPa)	Time (ms)
X-Component		
Direction: -x		
	0.000	0.052
	40644.719	0.052
	0.000	0.075
	0.000	0.096
	-15.193	6.121
	0.000	22.410
Y-Component		
Direction: +y		
	0.000	0.052
	2206.037	0.052
	0.000	0.084
	0.000	0.096
	-72.204	1.508
	0.000	5.324
Z-Component		
Direction: -z		
	0.000	0.000

	x(m)	y(m)	z(m)
Analysis Point	0.34	0.20	0.17
Face:	2		
Distance(m):	0.246		
Scaled			
Distance(m/kg ^{1/3}):	0.546		
alphaxyz(deg):	54.25		
alphayz(deg):	-0.00		

WAVE PARAMETERS

	Arrival Time(ms)	Pso+ (kPa)	Dynamic Pres.(kPa)	Drag Coeff.	Impulse+ (kPa-msec)
X-Compt	0.07	2490.9	4787.1	1.0	50.7
Y-Compt	0.07	3459.6	7458.6	-0.2	70.5
Z-Compt	0.00	0.0	0.0	0.0	0.0
	Ref. Imp.+ (kPa-msec)	Pr+ (kPa)	Clearing Time(ms)	Fict. Pos. Dur.(ms)	Ref. Pos. Dur.(ms)
X-Compt	297.0	18381.0	0.05	0.04	0.03
Y-Compt	70.5	3459.6	0.00	0.04	0.04
Z-Compt	0.0	0.0	0.00	0.00	0.00
	Positive Dur.(ms)	Pso- (kPa)	Pr- (kPa)	Neg. Rise Time(ms)	Negative Dur.(ms)
X-Compt	0.05	92.9	5.2	14.41	53.37
Y-Compt	0.05	79.8	79.8	1.36	5.04
Z-Compt	0.00	0.0	0.0	0.00	0.00

Pressure-Time Results

	Pressure (kPa)	Time (ms)
X-Component		
Direction: -x		
	0.000	0.070
	18381.016	0.070
	0.000	0.102
	0.000	0.119
	-5.225	14.529
	0.000	53.490
Y-Component		
Direction: +y		
	0.000	0.070
	1967.828	0.070
	0.000	0.110
	0.000	0.119
	-79.794	1.479
	0.000	5.158
Z-Component		
Direction: -z		
	0.000	0.000

	x(m)	y(m)	z(m)
Analysis Point	0.34	0.25	0.17
Face:	2		
Distance(m):	0.289		
Scaled			
Distance(m/kg ^{1/3}):	0.639		
alphaxyz(deg):	60.06		
alphayz(deg):	-0.00		

WAVE PARAMETERS

	Arrival Time(ms)	Pso+ (kPa)	Dynamic Pres.(kPa)	Drag Coeff.	Impulse+ (kPa-msec)
X-Compt	0.09	1638.0	2684.7	1.0	43.1
Y-Compt	0.09	2843.7	5732.4	-0.2	74.8
Z-Compt	0.00	0.0	0.0	0.0	0.0
	Ref. Imp.+ (kPa-msec)	Pr+ (kPa)	Clearing Time(ms)	Fict. Pos. Dur.(ms)	Ref. Pos. Dur.(ms)
X-Compt	215.7	9291.9	0.06	0.05	0.05
Y-Compt	74.8	2843.7	0.00	0.05	0.05
Z-Compt	0.0	0.0	0.00	0.00	0.00
	Positive Dur. (ms)	Pso- (kPa)	Pr- (kPa)	Neg. Rise Time(ms)	Negative Dur.(ms)
X-Compt	0.06	82.9	86.7	0.75	2.76
Y-Compt	0.06	83.1	83.1	1.30	4.80
Z-Compt	0.00	0.0	0.0	0.00	0.00

Pressure-Time Results

	Pressure (kPa)	Time (ms)
X-Component		
Direction: -x		
	0.000	0.091
	9291.888	0.091
	0.000	0.137
	0.000	0.147
	-86.729	0.893
	0.000	2.911
Y-Component		
Direction: +y		
	0.000	0.091
	1697.239	0.091
	0.000	0.143
	0.000	0.147
	-83.071	1.442
	0.000	4.946

Z-Component
 Direction: -z
 0.000 0.000

	x(m)	y(m)	z(m)
Analysis Point	0.34	0.30	0.17
Face:	2		
Distance(m):	0.333		
Scaled			
Distance(m/kg^(1/3)):	0.737		
alphaxyz(deg):	64.36		
alphayz(deg):	-0.00		

WAVE PARAMETERS

	Arrival Time(ms)	Pso+ (kPa)	Dynamic Pres.(kPa)	Drag Coeff.	Impulse+ (kPa-msec)
X-Compt	0.12	1118.4	1576.0	1.0	37.3
Y-Compt	0.12	2330.1	4369.2	-0.2	77.7
Z-Compt	0.00	0.0	0.0	0.0	0.0
	Ref. Imp.+ (kPa-msec)	Pr+ (kPa)	Clearing Time(ms)	Fict. Pos. Dur.(ms)	Ref. Pos. Dur.(ms)
X-Compt	172.3	5835.2	0.07	0.07	0.06
Y-Compt	77.7	2330.1	0.00	0.07	0.07
Z-Compt	0.0	0.0	0.00	0.00	0.00
	Positive Dur.(ms)	Pso- (kPa)	Pr- (kPa)	Neg. Rise Time(ms)	Negative Dur.(ms)
X-Compt	0.07	71.1	75.6	0.74	2.75
Y-Compt	0.07	83.5	83.5	1.22	4.53
Z-Compt	0.00	0.0	0.0	0.00	0.00

Pressure-Time Results

	Pressure (kPa)	Time (ms)
X-Component		
Direction: -x		
	0.000	0.116
	5835.231	0.116
	0.000	0.175
	0.000	0.181
	-75.618	0.923
	0.000	2.928

Y-Component

Direction: +y

0.000	0.116
1456.260	0.116
0.000	0.183
0.000	0.181
-83.523	1.403
0.000	4.708

Z-Component

Direction: -z

0.000	0.000
-------	-------

	x(m)	y(m)	z(m)
Analysis Point	0.34	0.35	0.17
Face:	2		
Distance(m):	0.378		
Scaled			
Distance(m/kg ^(1/3)):	0.838		
alphaxyz(deg):	67.64		
alphayz(deg):	-0.00		

WAVE PARAMETERS

	Arrival Time(ms)	Pso+ (kPa)	Dynamic Pres.(kPa)	Drag Coeff.	Impulse+ (kPa-msec)
X-Compt	0.15	775.2	938.0	1.0	32.8
Y-Compt	0.15	1884.2	3260.2	-0.2	79.6
Z-Compt	0.00	0.0	0.0	0.0	0.0
	Ref. Imp.+ (kPa-msec)	Pr+ (kPa)	Clearing Time(ms)	Fict. Pos. Dur.(ms)	Ref. Pos. Dur.(ms)
X-Compt	149.4	3831.9	0.08	0.08	0.08
Y-Compt	79.6	1884.2	0.00	0.08	0.08
Z-Compt	0.0	0.0	0.00	0.00	0.00
	Positive Dur.(ms)	Pso- (kPa)	Pr- (kPa)	Neg. Rise Time(ms)	Negative Dur.(ms)
X-Compt	0.08	58.	67.3	0.74	2.74
Y-Compt	0.08	81.9	81.9	1.15	4.25
Z-Compt	0.00	0.0	0.0	0.00	0.00

Pressure-Time Results

	Pressure (kPa)	Time (ms)
X-Component		
Direction: -x		
	0.000	0.145
	3831.889	0.145
	0.000	0.223
	-67.259	0.963
	0.000	2.967
Y-Component		
Direction: +y		
	0.000	0.145
	1232.129	0.145
	0.000	0.230
	0.000	0.222
	-81.943	1.370
	0.000	4.472
Z-Component		
Direction: -z		
	0.000	0.000

	x(m)	y(m)	z(m)
Analysis Point	0.34	0.40	0.17
Face:	2		
Distance(m):	0.425		
Scaled			
Distance(m/kg^(1/3)):	0.941		
alphaxyz(deg):	70.20		
alphayz(deg):	-0.00		

WAVE PARAMETERS

	Arrival Time(ms)	Pso+ (kPa)	Dynamic Pres.(kPa)	Drag Coeff.	Impulse+ (kPa-msec)
X-Compt	0.18	547.5	565.4	1.0	29.7
Y-Compt	0.18	1520.9	2421.5	-0.2	82.5
Z-Compt	0.00	0.0	0.0	0.0	0.0
	Ref. Imp.+ (kPa-msec)	Pr+ (kPa)	Clearing Time(ms)	Fict. Pos Dur.(ms)	Ref. Pos. Dur.(ms)
X-Compt	137.1	2740.1	0.09	0.11	0.10
Y-Compt	82.5	1520.9	0.00	0.11	0.11
Z-Compt	0.0	0.0	0.00	0.00	0.00

	Positive Dur.(ms)	Pso- (kPa)	Pr- (kPa)	Neg. Rise Time(ms)	Negative Dur.(ms)
X-Compt	0.09	46.2	61.6	0.75	2.77
Y-Compt	0.09	78.7	78.7	1.08	4.00
Z-Compt	0.00	0.0	0.0	0.00	0.00

Pressure-Time Results

	Pressure (kPa)	Time (ms)
X-Component		
Direction: -x		
	0.000	0.179
	2740.082	0.179
	175.824	0.270
	0.000	0.287
	0.000	0.270
	-61.646	1.018
	0.000	3.040

Y-Component		
Direction: +y		
	0.000	0.179
	1036.561	0.179
	0.000	0.287
	0.00	0.270
	-78.744	1.350
	0.000	4.269

Z-Component		
Direction: -z		
	0.000	0.000

	x(m)	y(m)	z(m)
Analysis Point	0.34	0.45	0.17
Face:	2		
Distance(m):	0.472		
Scaled			
Distance(m/kg ^{1/3}):	1.046		
alphaxyz(deg):	72.26		
alphayz(deg):	-0.00		

WAVE PARAMETERS

	Arrival Time(ms)	Pso+ (kPa)	Dynamic Pres.(kPa)	Drag Coeff.	Impulse+ (kPa-msec)
X-Compt	0.22	393.6	336.3	1.0	26.0

Y-Compt	0.22	1230.1	1800.9	-0.2	81.2
Z-Compt	0.00	0.0	0.0	0.0	0.0
	Ref. Imp.+ (kPa-msec)	Pr+ (kPa)	Clearing Time(ms)	Fict. Pos. Dur.(ms)	Ref. Pos. Dur.(ms)
X-Compt	126.8	2016.6	0.11	0.13	0.13
Y-Compt	81.2	1230.1	0.00	0.13	0.13
Z-Compt	0.0	0.0	0.00	0.00	0.00
	Positive Dur.(ms)	Pso- (kPa)	Pr- (kPa)	Neg. Rise Time(ms)	Negative Dur.(ms)
X-Compt	0.11	35.8	56.5	0.76	2.81
Y-Compt	0.11	74.1	74.1	1.03	3.82
Z-Compt	0.00	0.0	0.0	0.00	0.00

Pressure-Time Results

	Pressure (kPa)	Time (ms)
X-Component		
Direction: -x		
	0.000	0.217
	2016.629	0.217
	107.560	0.329
	0.000	0.349
	0.000	0.329
	-56.516	1.087
	0.000	3.136
Y-Component		
Direction: +y		
	0.000	0.217
	869.962	0.217
	0.000	0.349
	0.000	0.329
	-74.141	1.360
	0.0001	4.148
Z-Component		
Direction: -z		
	0.000	0.000
